Chiral Phospha[*n*]ferrocenophanes:

New Metallopolymers through Ring-Opening Polymerizations

A Thesis Submitted to the College of

Graduate and Postdoctoral Studies

in Partial Fulfilment of the Requirements

for the Degree of Doctor of Philosophy

in the Department of Chemistry

University of Saskatchewan

Saskatoon

by

PHAN THUY MY CAO

PERMISSION TO USE

In presenting this dissertation in partial fulfilment of the requirements for a postgraduate degree from the University of Saskatchewan, I agree that the libraries of this university may make it freely available for inspection. I further agree that permission for copying of this dissertation in any manner, in whole or in part, for scholarly purposes may be granted by Professor Jens Müller who supervised my dissertation work or, in his absence, by the Head of Department or the Dean of the College in which my thesis work was done. It is understood that any copying or publication or use of this dissertation or parts of thereof for financial gain shall not be allowed without my written permission. It is also understood that due recognition shall be given to me and to the University of Saskatchewan in any scholarly use which may be made of any material in my dissertation.

Request for permission to copy or to make other uses of materials in this dissertation in whole or part should be addressed to:

Head of the Chemistry Department
165-110 Science Place
University of Saskatchewan
Saskatoon, Saskatchewan S7N 5C9
Canada

OR

Dean
College of Graduate and Postdoctoral Studies
University of Saskatchewan
116 Thorvaldson Building, 110 Science Place
Saskatoon, Saskatchewan S7N 5C9
Canada

ABSTRACT

Chiral polymers have many important applications, including separation of racemic compounds and catalysts in asymmetric syntheses. There are many examples of chiral natural polymers, such as proteins, DNA, or cellulose. However, synthetic chiral polymers are rather rare. On the other hand, the incorporation of metal centers into synthetic polymer chains allows the preparation of new functional materials with unique properties that complement those of organic macromolecular materials. Recently, Müller's group developed a synthetic route to strained ferrocenophanes (FCPs) with planar chirality, and via ring-opening polymerization (ROP), new chiral metallopolymers were obtained. In this thesis, the syntheses of new chiral phospha[*n*]FCPs are described, as well as their behaviors towards ROP.

New enantiomerically pure phospha[*n*]FCPs (*n* = 1, 2) equipped with two *i*Pr groups in α positions were prepared. The molecular structure of diphospha[2]FCP (S_p,S_p,*R*,*R*)-**90**$^{\mathbf{CH2SiMe3}}$ was determined by single-crystal X-ray analysis showing a tilt angle α = 12.2°. Furthermore, the new chiral (S_p,S_p,*S*,*S*)-1,1′-(N*i*Pr$_2$)$_2$fc$^{i\mathrm{Pr}}$ **88**$^{\mathbf{NiPr2}}$ (fc$^{i\mathrm{Pr}}$ = (S_p,S_p)-[(Me$_2$CH)–(C$_5$H$_3$)]$_2$Fe) was also selectively synthesized and isolated, which gave suitable crystals for single-crystal X-ray analysis.

Attempted anionic ROPs were performed on phospha[1]FCPs, however, no polymeric materials could be obtained from these reactions. Detailed studies on phospha[1]FCPs with different substituents on phosphorus atom were carried out, showing that the initiation step in the anionic ROP worked, but the ring-propagation did not occur. In attempts to perform this type of reaction, one of the phospha[1]FCP (S_p,S_p)-**20**$^{\mathbf{Ph}}$ showed the ability to be cleanly ring-opened when using 1 equiv of *n*BuLi and afforded a 3 to 1 diastereomeric mixture of products. This mixture was sulfurized and a single isomer, (S_p,*R*)-**95**$^{\mathbf{S}}$, was isolated and characterized by single-

crystal X-ray analysis. In addition, based on the clean anionic ring-opening reaction of the compound (S_p,S_p)-**20**$^{\mathbf{Ph}}$ with 1 equiv of *n*BuLi, the new chiral ferrocene-based phosphine ligand (S_p,*S*)-**99** was successfully synthesized.

In order to measure the amount of strain in [1]FCPs, differential scanning calorimetry (DSC) studies were performed on a series of phospha[1]FCPs having different substituent groups. On the other hand, thermal ROP of compound (S_p,S_p)-**21**$^{\mathbf{Ph}}$ afforded both linear polymer **102**$_{\mathbf{n}}$ and cyclic oligomers **103**. Gel permeation chromatography (GPC) of the sulfurized polymer resulted in a molecular weight of 19 kDa (M_w) and a dispersity of 1.3 ($Đ$). Mass spectroscopic analysis of the oligomers showed the presence of cyclic species from dimers to hexamers. After sulfurization, preparative thin layer chromatography (PTLC) led to the separation of five isomeric dimers. Structural characterization of one of the dimers (*syn*-C_2-**103**$^{\mathbf{S}}$-**3**) by single-crystal X-ray analysis revealed that Fe–Cp bond broke during the thermal ROP process.

ACKNOWLEDEMENTS

First of all, my deepest acknowledge goes to my supervisor, Dr. Jens Müller, for the patient guidance, encouragement and advice he has provided throughout my time as his student. I have been lucky to have a supervisor who cared so much about my work, and who responded to my questions and queries so promptly.

I would like to thank the former and current members of my advisory committee: Dr. Dale Ward, Dr. Suzanne Abrams, Dr. Richard Bowles, Dr. Timothy Lewis Kelly, Dr. Jonathan Dimmock, and Dr. Brian Sterenberg, for their insightful comments and encouragement, but also for the hard questions which incented me to widen my research from various perspectives.

I would like to thank the Department of Chemistry and the College of Graduate Studies and Postdoctoral Studies, University of Saskatchewan for financial support and scholarships. I am grateful for the assistance of the staff at the Saskatchewan Structural Science Center: Dr. Keith C. Brown, Dr. Wilson J. Quail, Dr. Jianfeng Zhu, Ken Thoms and Dr. Ramaswami Sammynaiken. My sincere thanks also go to Dr. Valerie MacKenzie and Dr. Pia Wennek for their help with laboratory instruments.

I would like to acknowledge the support and encouragement from former and current members of the Müller's Research group. It was a joy to work with you all in the last five years, and I wish you all the best with your future career.

I must express my gratitude to Huy, my husband, for his continued and unfailing love and understanding all of the ups and downs of my research life. Last but not least, I am very grateful to my loving parents, as well as my sister, for their endless love, support, and encouragement throughout my life. Their support and encouragement made this dissertation possible.

TABLE OF CONTENTS

LIST OF ABBREVIATIONS

ΔH ..... enthalpy change

CBS ..... Corey-Bakshi-Shibata

CHN analysis ..... elemental analysis

cod 1,5-cyclooctadiene

conf ..... configuration

Cp ..... cyclopentadienyl

$Đ$ ..... dispersity

d ..... doublet

DCM ..... dichloromethane

de ..... diastereomeric excess

DFT ..... density functional theory

DLS ..... dynamic light scattering

ds ..... diastereoselectivity

DSC ..... differential scanning calorimetry

dt ..... doublet of triplets

ee ..... enantiomeric excess

equiv ..... equivalent

fc ..... $(C_5H_4)_2Fe$

FCC ..... flash column chromatography

fc^{iPr} ..... (S_p,S_p)-2,2'-$[(Me_2CH)$-$(C_5H_3)]_2Fe$

FCP ..... ferrocenophane

FD ..... field desorption

GPC ..... gel permeation chromatography

J ..... coupling constant

m ..... multiplet

MALDI TOF ..... matrix assisted laser desorption ionization-time of flight

MCP ..... metallocenophane

M_n ..... number average molecular weight

M_p ..... peak molecular weight

MS ..... mass spectrometry

M_w ..... weight average molecular weight

M_z ..... z-average molecular weight

nbd ..... norbornadiene

NMR ..... nuclear magnetic resonance

PFP ..... polyferrocenylphosphine

PFS ..... polyferrocenylsilane

PI ..... polyisoprene

ppm ..... parts per million

pst ..... pseudo triplet

PTLC ..... preparative thin layer chromatography

q ..... quartet

r.b. ..... round bottom

r.t. ..... room temperature

ROP ..... ring-opening polymerization

s ..... singlet

t .....triplet

thf ..... tetrahydrofuran

tmeda.....N,N,N′,N′-tetramethylethylenediamine

tmp 2,2,6,6-tetramethylpiperidine

XRD ..... X-ray diffraction

LIST OF FIGURES

LIST OF SCHEMES

LIST OF TABLES

CHAPTER 1. INTRODUCTION

The field of synthetic polymers grew extensively over the last century and had a long lasting impact on society.[1–3] These types of polymers have been used for a wide range of applications – from textiles to coatings, adhesives to packaging materials – and have been produced in massive quantities to fulfil global demand. The larger part of these materials is carbon-based organic polymers, which can be synthesized via step-growth and chain-growth polymerization, respectively. Ring-opening polymerization (ROP) is one form of chain-growth polymerization, which has also been used to prepare organic polymers, starting from strained cyclic organic compounds. In comparison, the use of strained organometallic compounds to prepare polymers with transition-metal centres in the backbone, so called metallopolymers, have been less explored. The main reason was due to some preparative problems, such as synthetic procedures, purification aspects, and a lack of readily available starting materials. However, this field of study has been developing rapidly over the last few decades, and continues to attract much attention.[4,5,6–9,10]

Metallocyclophanes are a class of strained cyclic organometallic compounds with a transition metal complex. In these compounds, two π-hydrocarbon rings of a sandwich complex are linked together by *n* atoms in the bridging position. Due to the interesting structure of these compounds, a wide variety of metallocyclophanes with varying transition metals, π-hydrocarbon rings, and bridging elements were prepared. [*n*]Metallocenophanes (**1**; Figure 1-1),[11] [*n*]metalloarenophanes (**2**; Figure 1-1),[12] [*n*]metalloarenocenophanes (**3**; Figure 1-1),[13–15] and *ansa*-cycloheptatrienyl–cyclopentadienyl complexes of type **4** (Figure 1-1)[16,17] are just some of many examples of metallocyclophanes that have been reported.

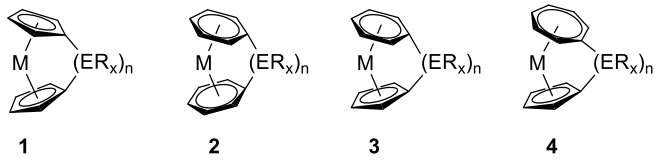

Figure 1-1. Metallocyclophanes.

Among the many metallocyclophanes, [*n*]metallocenophanes ([*n*]MCPs; **1**) are the largest class of strained cyclic organometallic compounds. [*n*]MCPs are compounds that contain two η^5-cyclopentadienyl (Cp) rings that sandwich a transition metal M through π-, σ-, and δ-bonds, and are connected together by *n* bridging elements through σ- bonds. The strained MCPs have interesting structures and the ability to undergo ROP (Scheme 1-1), resulting in high-molecular-weight polymers.

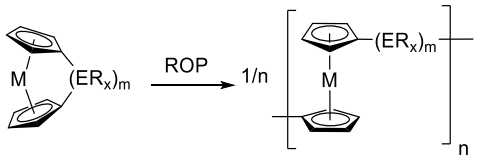

Scheme 1-1. Ring-opening polymerization of metallocenophanes.

1.1 [*n*]Metallocenophanes and ring-opening polymerization of strained metallocenophanes

The first reported example of an [*n*]MCP is the [3]ferrocenophane ([3]FCP) (**5**; Figure 1-2), which was prepared in 1957 by Rinehart *et al.*[18] Shortly after this discovery, the same group reported the synthesis of a [2]FCP with a C_2Me_4 bridge (**6**; Figure 1-2).[19] Fifteen years later, Osborne and co-worker prepared the first two [1]FCPs with a silicon bridge (**7** and **8**; Figure 1-2).[20]

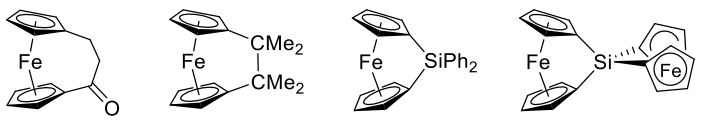

5 **6** **7** **8**

Figure 1-2. The first reported examples of [*n*]FCPs.

To date, there are two well-known methods to prepare strained [*n*]FCPs: the "flytrap" route and the "salt-metathesis" reaction (Scheme 1-2). The "flytrap" route requires the preparation of a dianionic compound, which consists of two cyclopentadienide rings linked together by a bridging moiety. The dianionic compound reacts with an appropriate metal(II) dihalide to give the targeted [*n*]FCP. This method is typically used to prepare [*n*]MCPs with n ≥ 2; e.g., the dicarba[2]FCP (**6**) was obtained through this pathway.[19] However, the salt-metathesis reaction is the most commonly employed method and is usually applied to prepare [*n*]FCPs. The salt-metathesis method involves the reaction of a dilithioferrocene(tmeda) and an element dihalide to yield the targeted strained FCP. Several strained [1]FCPs, including those with bridging elements from group 13 (B, Al, Ga, In),[21] group 14 (Si, Ge, Sn),[11] group 15 (P, As),[11,22–25] group 16 (S, Se), and others have been prepared by the salt-metathesis method.[26]

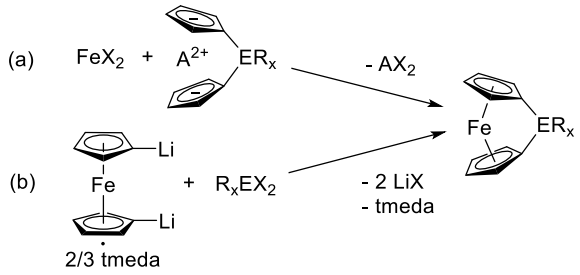

Scheme 1-2. Synthetic pathways for [*n*]FCPs via (a) a "flytrap" route, or (b) the salt-metathesis route.

In ferrocene, two Cp rings are parallel to each other. The introduction of short ansa[*n*] bridges (*n* = 1, 2) causes the Cp rings to tilt, thus generating strain in the ferrocene system.[11,27] The dihedral angle between the two Cp planes in an [*n*]FCP is known as tilt angle α, which is a measure of the degree of ring tilt.[11,26] In addition to the α angle, the β ($Cp_{centroid}$–Cp_{ipso}–E), the θ (C_{ipso}–E–C'_{ipso}), the δ ($Cp_{centroid}$–M–$Cp'_{centroid}$), and the τ angles also help to describe the ring-tilted structure of [*n*]FCPs (Figure 1-3).[28]

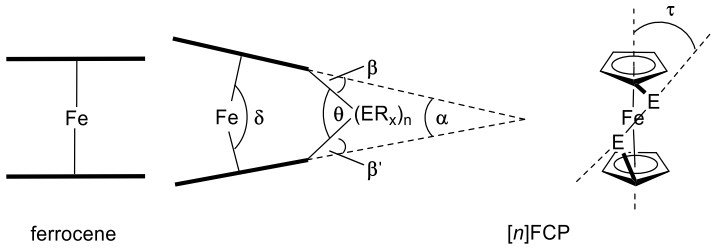

Figure 1-3. Representation of ferrocene and geometric parameters α, β, δ, θ, and τ in an [*n*]FCP.

The tilt angle α is inversely proportional to the size of the bridging element: the smaller the bridging element, the larger the α angle is. For example, a sila[1]FCP (**9**$^{\mathbf{R}}$; Figure 1-4) has a tilt angle α of approximately 18–22°,[29,30] whereas a bora[1]FCP (**10**) has a larger tilt angle (α ~ 31–32°).[31] Furthermore, increasing the number of atoms in the FCP bridging moiety decreases the tilt angle α.[28] For instance, the phospha[1]FCP **11**$^{t\mathbf{Bu}}$ has a larger tilt angle (α ~ 27°)[32] compared to that of the diphospha[2]FCP **26**$^{t\mathbf{Bu}}$ (α ~ 13°).[33]

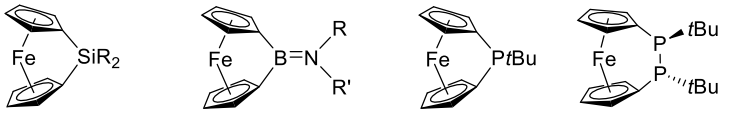

9$^{\mathbf{R}}$ (R = Ph or Me) **10a** (R = R' = $SiMe_3$) **10b** (R = R' = *i*Pr) **11**$^{t\mathbf{Bu}}$ **26**$^{t\mathbf{Bu}}$

Figure 1-4. [*n*]FCPs with varying bridging elements.

The first reported metal-containing polymer is polyvinylferrocene, which was prepared by Arimoto and Haven at DuPont Co. in the 1950s.[34] However, the synthetic difficulties associated with lack of characterization methods were main problems during the early development of the metallopolymers field. More specifically, the polymerization led to undesirable side reactions giving low-molecular-weight polymers that are often insoluble and poorly characterized. Until the mid-1990s, many of the key obstacles to the preparation of high-molecular-weight and soluble metallopolymers had been overcome through the development of new synthetic pathways. The synthesis of high-molecular-weight poly(ferrocenylsilane)s (PFSs), which was reported by Manners and co-workers in 1992 (Scheme 1-3),[35] was a milestone in this development. Since this key discovery, a wide variety of strained [1]FCPs incorporating group 13 (B, Ga, Al), group 14 (Si, Ge, Sn), group 15 (P, As) and group 16 (S, Se) elements have all been shown to undergo ROP reactions.[35–39,11,40,41]

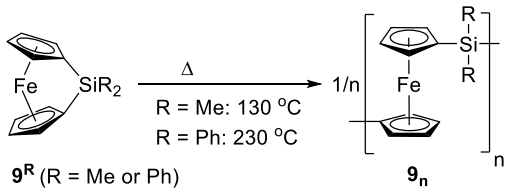

Scheme 1-3. Synthesis of poly(ferrocenylsilane)s via thermal ROP of sila[1]FCPs.

Phosphorus, a unique element which plays important roles in both organic and inorganic chemistry, was selected as the main element for this thesis's topic. Due to the relatively small radius of phosphorus, phosphorus-bridged [1]FCPs are highly strained species that have the ability to undergo ROP.[37–39,42] The following sections describe the preparation of phospha[*n*]FCPs and their behavior towards ROP.

1.2 Phosphorus-bridged [*n*]ferrocenophanes and poly(ferrocenylphosphine)s

Phosphines are a very important class of ligands, especially in asymmetric catalysis. Many catalysts contain phosphines, and many catalytic reactions use chiral phosphines.[43–45] In addition, the incorporation of phosphorus into the polymer backbone led to materials with novel applications.[46–48] Phosphorus-containing polymers are of particular interest, because they can offer either monodentate or multidentate sites for coordination of a metal fragment. Therefore, these phosphorus-containing polymers can be used as sensors, and as polymer-supported ligands for transition-metal complexes in organic transformation.[44,49,50]

Phospha[1]FCPs are among a few groups of strained sandwich compounds that can be polymerized with controlled molecular weight and molecular weight distribution.[39,42,51,37,38,52–55] Poly(ferrocenylphosphine)s (PFPs) also show possible applications as polymer-supported ligands in catalysis.[24,56] This is due to the presence of phosphorus centers in the main chain, which allows for the incorporation of metal complexes. In addition, the unusually high refractive indices of PFPs make them promising materials for a range of photonic applications.[57,39] Manners and co-workers investigated the optical properties of polyferrocenes with Si and P as the bridging elements.[57,58] Both of these polymers showed exceptionally high refractive indices (RI) with relative low optical dispersion. On the other hand, comparing to materials containing group 14 elements (such as, PFSs), PFPs have higher RIs. This can be explained by the P-valency of phosphorus compounds. The P-center in PFPs is trivalent with a non-bonding pair of electrons. Therefore, it was assumed that for phosphorus, a higher molar value of refraction indicated the higher tendency of nonbonding electrons to be polarized by an applied field.[58] Another interesting and useful property of PFPs is their micellization behavior.[56] A diblock copolymer of poly(isoprene-*b*-ferrocenylphenylphosphine) formed micellar aggregates in hexane

with a dense PFP core. Furthermore, additional metal atoms can be introduced into the micelle core via the coordination with phosphine groups. These self-assembled metal-containing micelles offer possible applications in catalysis or as precursors to magnetic nanostructures.[56,59,60]

1.2.1 Phosphorus-bridged [1]ferrocenophanes

The synthesis of phospha[1]FCPs was first reported in 1980 by Osborne *et al.* (**11^{Ph}**; Scheme 1-4)[61] and by Seyferth and Withers (**11^{Ph}** and **11^{Me}**)[62]. After these first reports, many phospha[1]FCPs with various substituents (**11^{R}**; Scheme 1-4) were also synthesized by typical salt-metathesis methods using dilithioferrocene(tmeda).[25,39,37,32]

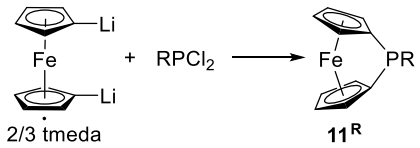

R = Ph, Me, *t*Bu, p-*t*BuC$_6$H$_4$, CH$_2$C(CH$_3$)$_3$, Cl, N*i*Pr$_2$, CH$_2$SiMe$_3$, tmp

Scheme 1-4. Synthesis of phospha[1]FCPs via the salt-metathesis reaction.

In 1983, a further significant contribution to this area was reported by Cullen *et al*., with the synthesis of the first planar-chiral phospha[1]FCPs (**12–14**; Scheme 1-5a), which were prepared as racemates.[32] Later, Manners and co-workers reported the synthesis of other planar-chiral phospha[1]FCPs (**15** and **16**; respectively; Scheme 1-5b), with the compound **15** was obtained as a mixture of four racemates.[37]

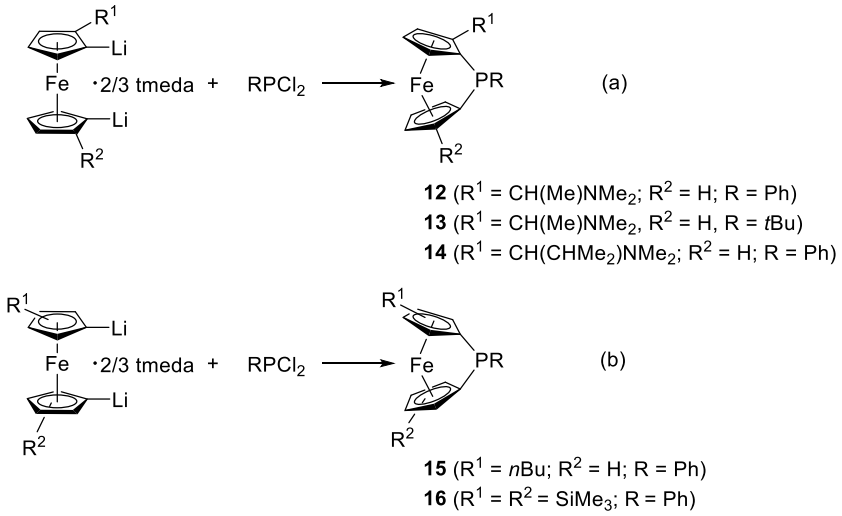

Scheme 1-5. Synthesis of racemic, planar-chiral phospha[1]FCPs.

Brunner *et al*. first reported the synthesis of chiral phospha[1]FCPs having chiral substituents on phosphorus atoms (**17** and **18**; Scheme 1-6).[24] The compound **17** as well as its polymeric derivative from thermal ROP were used as chiral ligands in the Rh-catalyzed diastereoselective hydrogenation of folic acid.[24]

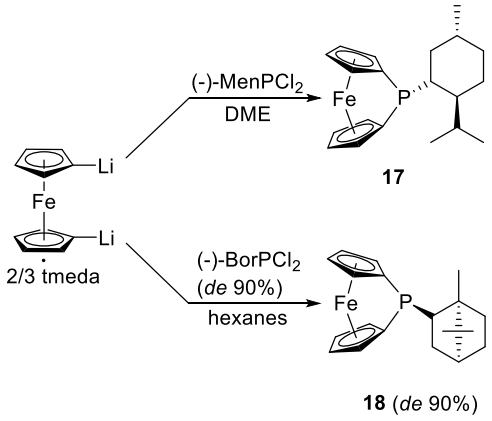

Scheme 1-6. Synthesis of chiral phospha[1]FCPs.

Recently, Müller and co-workers reported the synthesis of chiral phospha[1]FCPs starting from an enantiomerically pure dibromoferrocene (S_p,S_p)-**19**, which was equipped with

alkyl groups on both Cp rings [(S_p,S_p)-**20**$^{\mathbf{R}}$ and (S_p,S_p)-**21**; Scheme 1-7].[63,64] Later, the same group synthesized a racemate of planar-chiral phospha[1]FCP, having one *i*Pr group on the ferrocene moiety (*rac*-**22**).

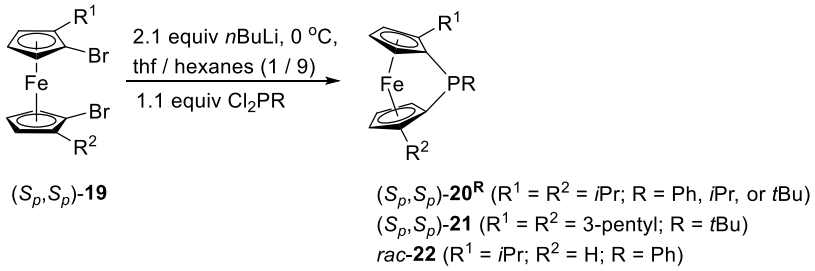

(S_p,S_p)-**19**

(S_p,S_p)-**20**$^{\mathbf{R}}$ (R^1 = R^2 = *i*Pr; R = Ph, *i*Pr, or *t*Bu)
(S_p,S_p)-**21** (R^1 = R^2 = 3-pentyl; R = *t*Bu)
rac-**22** (R^1 = *i*Pr; R^2 = H; R = Ph)

Scheme 1-7. Synthesis of chiral phospha[1]FCPs having alkyl substituted Cp rings.

1.2.2 Diphospha[2]ferrocenophanes

In [2]FCPs, the common angles α, β, δ, and θ are defined in a similar manner as those in [1]FCPs. In addition, the angle τ is also introduced in the [2]FCP system, which is the angle between the least-squares plane $Cp_{centroid}$–Fe–$Cp_{centroid}$ and the E–E bridging bond vector (Figure 1-5).[11] In general, the introduction of an additional bond into the bridge of [2]FCPs leads to a decrease in the tilt angle α comparing to that of the [1]FCPs, therefore diminishes the ring strain.

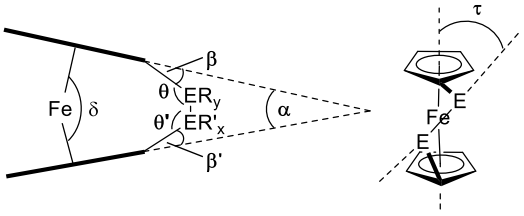

Figure 1-5. Common angles to characterize distortions in [2]FCPs.

While there are many reports on the preparation of phospha[1]FCPs as well as their polymerization behaviors,[37–39,42,63] diphospha[2]FCPs have not been extensively studied so far. The first diphospha[2]FCP is the bis(triphosphazene)-bridged [2]FCP (**23**; Figure 1-6), which

was reported by Allcock in 1984.[65] Compound **23** was isolated in a trace amount from the mixture obtained from the reaction of dilithioferrocene(tmeda) with an excess of hexachlorotriphosphazene $(NPCl_2)_3$. The phosphorus centres of species **23** reacted with nucleophiles like CF_3CH_2ONa or $LiEt_3BH$ to give ring-opened products.[65] Later, Pietschnig *et al*. reported the preparation of a diphospha[2]FCP with trivalent and pentavalent phosphorus atoms in the *ansa* bridge (**24**), using a water-induced P–P bond formation reaction.[66]

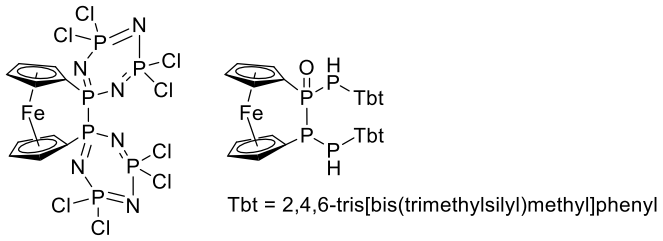

23 **24**

Figure 1-6. Diphospha[2]FCPs having pentavalent phosphorus centers.

Recently, Mizuta and co-workers isolated the first diphospha[2]FCP containing *t*Bu groups on trivalent diphosphine units (**26**$^{t\mathbf{Bu}}$; Scheme 1-8), through a reductive coupling with magnesium turnings.[33] Later, the same group also reported the synthesis and isolation of the diphospha[2]FCP with NEt_2 substituents on the two trivalent phosphorus atoms (**26**$^{\mathbf{NEt2}}$).[67] The X-ray crystallographic measurement of compound **26**$^{\mathbf{NEt2}}$ showed a tilt angle of 12.6°, which is 1° smaller than that of the previously diphospha[2]FCP (**26**$^{t\mathbf{Bu}}$, α = 13.6°).[33]

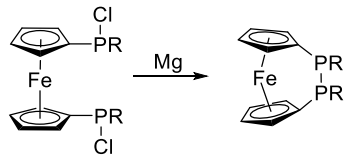

25$^{\mathbf{R}}$ (R = *t*Bu, NEt_2) **26**$^{\mathbf{R}}$ (R = *t*Bu, NEt_2)

Scheme 1-8. Synthesis of diphospha[2]FCPs through a reductive coupling with magnesium turnings.

Others [2]FCPs contained phosphorus as one of the bridging elements were also successfully synthesized (**27**–**30**; Figure 1-7).[68,54] Due to the significant Cp ring tilt of **27** and **28** (α = 14.9° and 18.2°; respectively), both compounds could be thermally polymerized.[54] Later, Müller and co-workers reported the first example of [2]FCP bridged by nitrogen and phosphorus atom (**29**; Figure 1-7).[68] In addition, in the purification of compound **29** by column chromatography, its desilylated counterpart was also isolated (**30**).

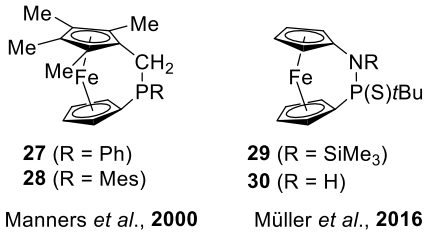

Figure 1-7. [2]FCPs with phosphorus in bridging positions.

To date, there are no reports on the polymerization activities of the diphospha[2]FCPs. The currently known application of diphospha[2]FCPs as diphosphine ligands is the coordination reactions with [(W(CO)$_5$] and [Cr(CO)$_5$] metal fragments (Scheme 1-9).[33,67]

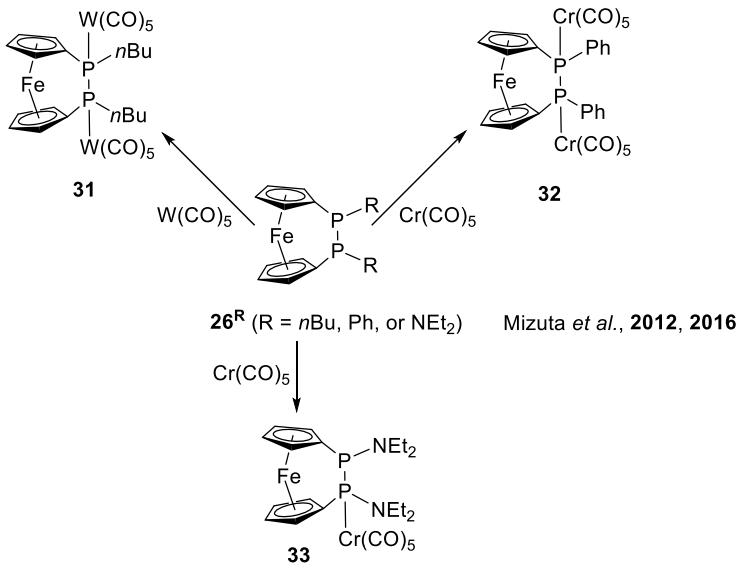

Scheme 1-9. Synthesis of metal complexes of diphospha[2]FCPs.

1.2.3 Other phosphorus-bridged [*n*]ferrocenophanes

The first [3]FCP where phosphorus is included in a carbon tether (**34**; Figure 1-8) was reported by Hey-Hawkins and co-workers.[69] After that, Pietschnig *et al.* reported the synthesis of [3]FCP with NPN bridge (**35**),[70] and recently, they also prepared a series of [3]FCPs with P–Si–P motifs (**36**).[71]

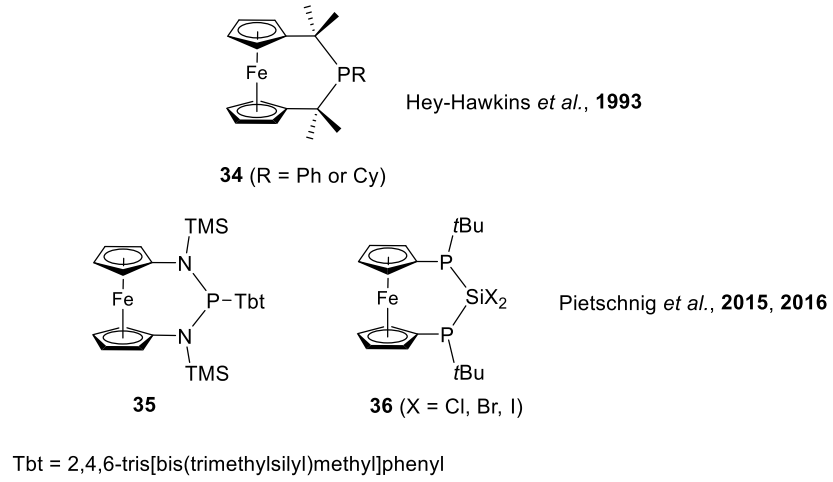

Figure 1-8. [3]FCPs with phosphorus in the heterobridge.

Marinetti and co-workers synthesized 2-phospha[3]FCPs derivatives with either stereogenic carbons (**37**; Figure 1-9) or planar chirality (**38**).[72,73] The planar chiral [3]FCPs **38** were used as catalysts for a [3 + 2] cyclization reaction, between ethyl 2,3-butadienoate and diethyl fumarate. Especially, the chiral compound with a cyclohexyl (Cy) group on phosphorus, $\mathbf{38^{Cy}}$, showed both high yield (70%) and high enantioselectivity (90%) in this type of cyclization reaction.[72]

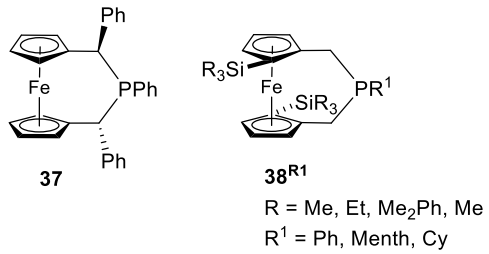

Figure 1-9. Chiral 2-phospha[3]FCPs.

Osborne and co-workers reported the synthesis of the first triphospha[3]FCPs (**39**; Figure 1-10), using the reaction of 1,1′-dibromoferrocene and LiP(Ph)-P(Ph)-P(Ph)Li.[74] Recently, Pietschnig *et al.* synthesized a series of triphospha[3]FCPs with various substituents on phosphorus atoms (**40**–**43**).[75] All of these [3]FCPs are basically unstrained as the Cp rings deviate only slightly from coplanarity (interplanar angles α = 1.2–4°).[74,75]

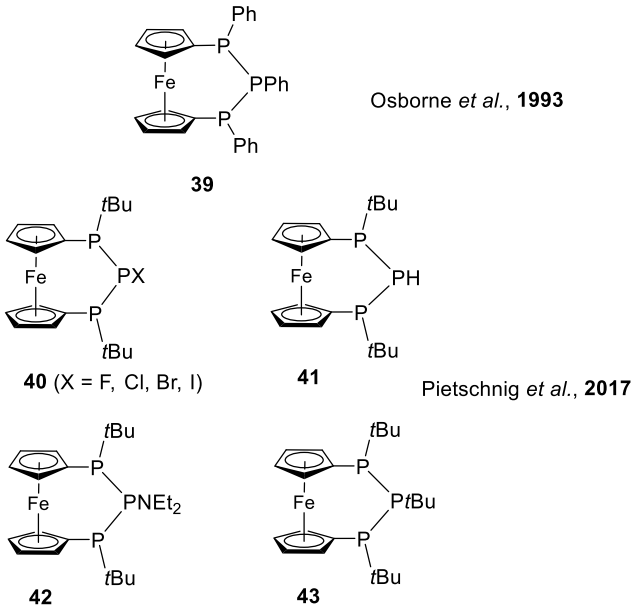

Figure 1-10. Triphospha[3]FCPs.

1.2.4 Poly(ferrocenylphosphine)s via ring-opening polymerization of phospha[*n*]ferrocenophanes

In the early 1980s, Seyferth and co-workers isolated high-molecular-weight PFPs (M_w = 161 kDa) via a polycondensation reaction when treating 1,1-dilithio ferrocene with $PhPCl_2$ (Scheme 1-10).[22] For a polycondensation reaction, such a large molecular weight is unexpected due to the difficulties in achieve both high purity levels of the reactive organometallic species, and the precise stoichiometry between the monomers. Therefore, polycondensation reactions normally lead to the formation of only low-molecular-weight products. The authors did not speculate about this unexpected high value of the molecular weight.

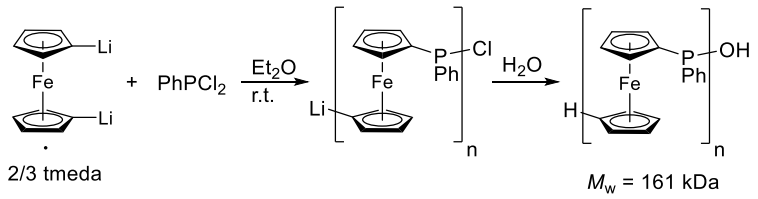

Scheme 1-10. Synthesis of poly(ferrocenylphosphine)s via polycondensation reaction.

Also in the same work, attempted anionic ROP was performed by reacting the phospha[1]FCP **11**^{Ph} with phenyllithium in ethereal solvents (Scheme 1-11).[22] This led to the formation of oligo(ferrocenylphosphine)s with 2–5 repeating units.

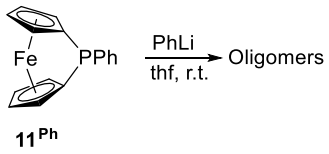

Scheme 1-11. Attempted anionic ROP of the phospha[1]FCP **11**^{Ph}.

In 1995, Manners successfully produced high-molecular-weight PFPs via thermal ROP of the phospha[1]FCP **11^{Ph}**.[37] Ring-opening polymerization, one form of chain-growth polymerization, is an efficient way for the formation of high-molecular-weight polymers. The driving force for the ROP is the release of ring strain of metallocenophanes. The following sections describe different types of ROP methods applied for phospha[1]FCPs.

1.2.4.1 Thermal ring-opening polymerizations

Thermal ROP of metallocenophanes is one of the most convenient and simplest method to obtain metallopolymers. However, with this method molecular weight and molecular weight distributions cannot be controlled. Manners *et al*. first reported the successful thermal ROP of phospha[1]FCPs having different substituents on the Cp rings (**11^{Ph}**, **15**, and **16**; Scheme 1-12) to afford polymers **11$_n^{Ph}$**, **15$_n$** and **16$_n$**, respectively.[37] The resulting polymers were reacted with elemental sulfur in order to be analyzed by Gel Permeation Chromatography (GPC). The sulfurized polymers possessed molecular weights from 18,000–65,000, and molecular weight distributions from 1.5–2.3.[37] In contrast, direct thermal ROP of a phosphine sulfide bridged [1]FCP (**11^{Ph}-S**) resulted in partial decomposition of the products, and generation of insoluble materials that cannot be analyzed.[37]

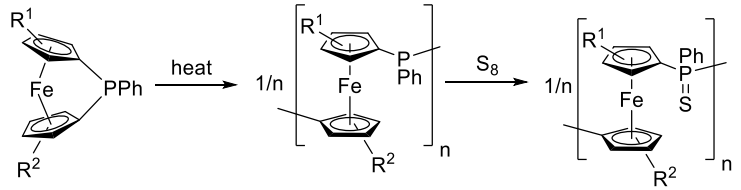

Scheme 1-12. Thermal ROP of substituted phospha[1]FCPs and sulfurization of resulting PFPs.

Later, Manners and co-workers conducted the thermal ROP of a phosphonium-bridged [1]FCPs (**44**; Scheme 1-13) to yield polymer $\mathbf{44_n}$.[52] The molecular weight as well as the molecular weight distribution of polymer $\mathbf{44_n}$ could not be determined by GPC, due to the interaction between the cationic polymer backbone and the column material. Dynamic light scattering (DLS) studies showed that the polymer $\mathbf{44_n}$ possessed hydrodynamic radii in the range of 30–45 nm, suggesting that the compound was polymeric rather than oligomeric.[52]

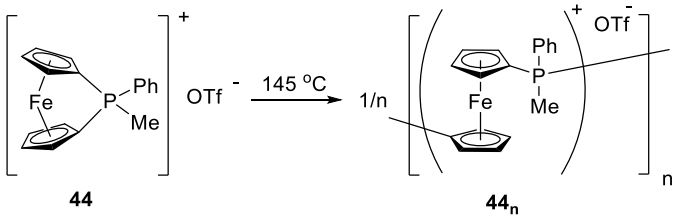

44 **44_n**

Scheme 1-13. Thermal ROP of the phosphonium-bridged [1]FCP **44**.

Brunner *et al*. thermally polymerized the chiral phospha[1]FCPs **17** and **18**, which afforded oligomeric products $\mathbf{17_n}$ and $\mathbf{18_n}$ with up to 8 repeating units (Scheme 1-14).[24] The rhodium complexes of **17** and its oligomeric product $\mathbf{17_n}$ were both used as catalysts for asymmetric hydrogenation of folic acid, however, low diastereomeric excesses were achieved (2.1–20%).[24]

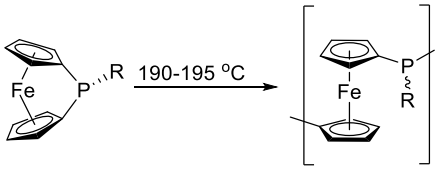

17 (R = menthol)
18 (R = borneol)

$\mathbf{17_n}$
$\mathbf{18_n}$

Scheme 1-14. Thermal ROP of the chiral phospha[1]FCPs **17** and **18**.

The first thermal ROP of phospha[2]FCP was reported by Manners and co-worker.[54] Compound **27** was thermally polymerized at 250 °C to afford polymer $\mathbf{27_n}$, which was then

reacted with elemental sulfur in order to be analyzed by GPC (Scheme 1-15). The sulfurized polymer **27$_n$-S** possessed a molecular weight M_w of 1.2 x 10^4 g/mol and a dispersity $Đ$ of 1.6.

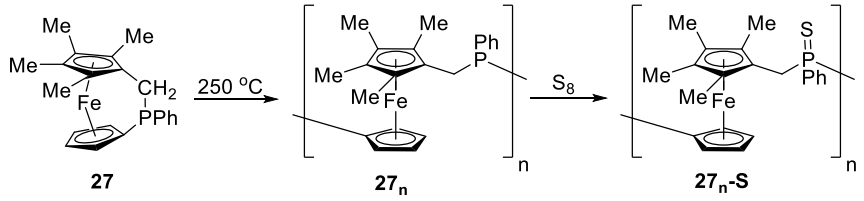

Scheme 1-15. Thermal ROP of compound **27**.

Recently, Müller and co-workers reported on a thermal ROP of a planar-chiral phospha[1]FCP having one *i*Pr group on the ferrocene moiety (Scheme 1-16).[51] This polymerization led to the formation of polymer **22$_n$** and cyclic oligomers of type **45**. MS data of the cyclic oligomers showed the presence of a range of cyclic species, from dimers to heptamers. Structure characterization of one of the isolated cyclic dimers (*anti*-**45**) led to the conclusion that the Fe–Cp bond breaks during the thermal ROP process.

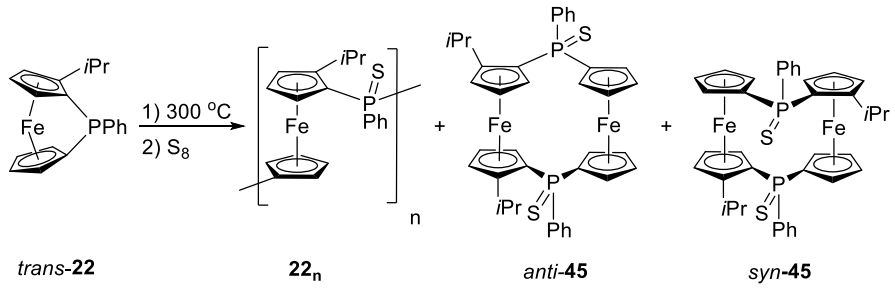

Scheme 1-16. Thermal ROP of the planar-chiral [1]FCP *trans*-**22**.

1.2.4.2 Living anionic ring-opening polymerizations

Living anionic ROP provides several advantages over other polymerization methods, such as control of molecular weight, and narrow molecular weight distribution of polymers. Anionic ROP of metallocenophanes initiated by organolithium reagents involves a cleavage of a Cp–P

bond in the monomer. The living anionic ROP of phospha[1]FCP **11^{Ph}** using *n*BuLi as initiator was reported by Manners *et al*. (Scheme 1-17).[38,42] After sulfurization, depending on monomer to initiator ratios (11:1 to 100:1), the resulting polymer **46$_n$-S** possessed molecular weights ranging from 36,000 to 32,000, respectively.

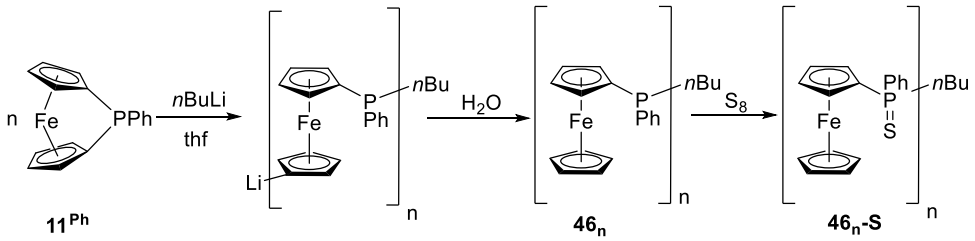

Scheme 1-17. Living anionic ROP of compound **11^{Ph}**.

Also in the same work, a block copolymer prepared by living anionic ROP of species **11^{Ph}** with hexamethylcyclotrisiloxane (**47$_n$**; Scheme 1-18) reacted with either Pd(1,5-cod)Cl_2 or $Fe_2(CO)_9$, resulting in polymers **48$_n$**.[38] In both cases, the amount of coordination to phosphine groups was estimated to be about 20–22% based on ^{31}P NMR spectroscopy.

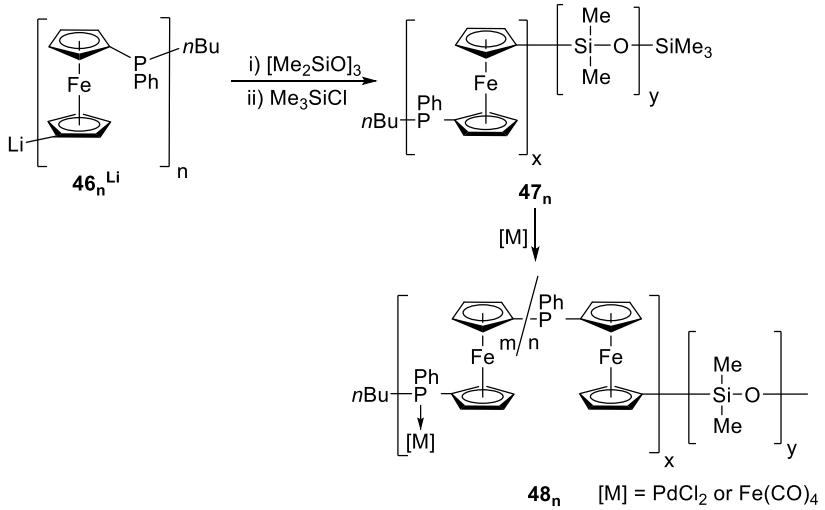

Scheme 1-18. Synthesis of diblock copolymer **47$_n$** and metal coordination reaction of the block copolymer **47$_n$** with Pd(1,5-cod)Cl_2 and $Fe_2(CO)_9$.

The diblock copolymer poly(isoprene-*b*-ferrocenylphosphine)s (PI-*b*-PFP) $\mathbf{49_n}$ was synthesized via a living anionic ROP (Scheme 1-19).[56] Micellization of PI-*b*-PFP with different block ratios was studied by transmission electron microscopy (TEM) and DLS measurements. These block copolymers formed star-shaped spherical micelles in hexanes, with a dense PFP core surrounded by a corona of PI chains. In addition, the phosphorus sites in the block copolymer backbone were reacted with Au(CO)Cl to produce the corresponding gold-modified block copolymers.[56]

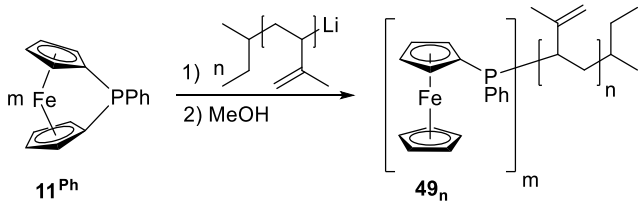

$\mathbf{11^{Ph}}$ $\mathbf{49_n}$

Scheme 1-19. Synthesis of poly(isoprene-*b*-ferrocenylphosphine)s $\mathbf{49_n}$.

1.2.4.3 Photolytic ring-opening polymerizations

Photolytic ROP is the most recent method that was developed to obtain well-defined high-molecular-weight polyferrocenes. Miyoshi and co-workers first reported the photolytic ROP of phospha[1]FCP $\mathbf{11^{Ph}}$ to yield in polymer $\mathbf{50_n}$ with $M_n = 1.9 \times 10^3$ Da (Scheme 1-20).[53] The authors also found the formation of cyclic dimers **51** as minor products when the compound $\mathbf{11^{Ph}}$ was irradiated under ultraviolet-visible (UV-Vis) light.[76] Both *syn* and *anti* isomers of the cyclic dimers **51** were isolated, and their molecular structures were solved by single-crystal X-ray analysis.[76]

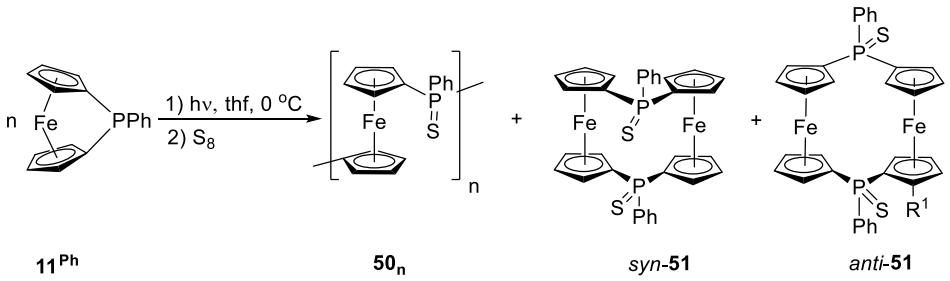

Scheme 1-20. Photolytic ROP of compound $\mathbf{11^{Ph}}$.

In the same work, the photolytic ROP of phosphorus-bridged [1]FCPs coordinated to a transition metal moiety (**52**; Scheme 1-21) afforded highly metallized polymer $\mathbf{53_n}$ with M_n = 1.8 × 10^4 Da and $Đ$ = 1.67.[53] Since the pendant group is present in every repeating unit, the final polymer $\mathbf{53_n}$ has a well-defined structure.

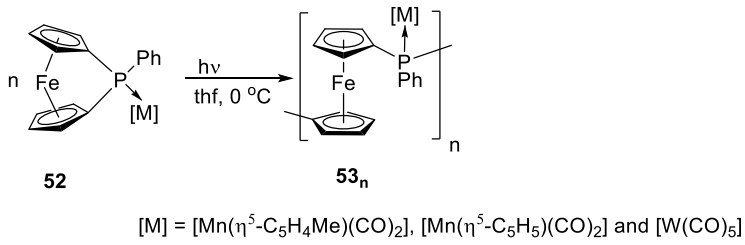

Scheme 1-21. Photolytic ROP of phospha[1]FCPs coordinated to a metal fragment.

In order to understand the mechanism of this photolytic ROP, Miyoshi and co-workers carried out the photolysis of phospha[1]FCP $\mathbf{11^{Ph}}$**-S** in the presence of $P(OMe)_3$ or PMe_3.[55] When being irradiated with a large excess of $P(OMe_3)$, compound $\mathbf{11^{Ph}}$**-S** was transformed into species **54**. Single-crystal X-ray analysis of this compound showed that one Cp ring underwent a haptotropic shift from η^5 to η^1. Thermal ROP of **54** yielded polymer $\mathbf{50_n}$, indicating that the structural feature of this compound is suitable for polymerization.

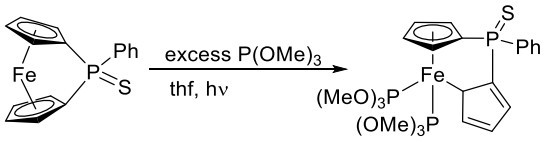

11^{Ph}-S **54**

Scheme 1-22. Photolysis of compound **11^{Ph}-S** in the presence of $P(OMe)_3$.

In contrast, if $P(OMe_3)$ was replaced by stronger coordinating ligand PMe_3, the ring-opened product **55** was formed. NMR spectroscopic data revealed that one Cp ring completely dissociated from the iron centre.

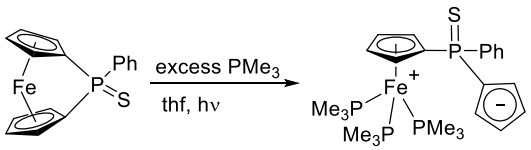

11^{Ph}-S **55**

Scheme 1-23. Photolysis of compound **11^{Ph}-S** in the presence of PMe_3.

These results strongly support that the mechanism of photolytic ROP proceeds through a cleavage of the Fe–Cp bond (Scheme 1-24). First, the UV-Vis irradiation of monomer **11^{Ph}-S** weakens the Fe–Cp bond and facilitates a nucleophilic attack at the Fe center. A η^5-to-η^1 haptotropic shift occurs, leaving two vacant coordination sites on the Fe center, which are occupied by two thf molecules. This ring slippage leads to the formation of intermediate **56**. The compound **56** further reacts with another monomer **11^{Ph}-S**, thereby propagating the molecule chain.

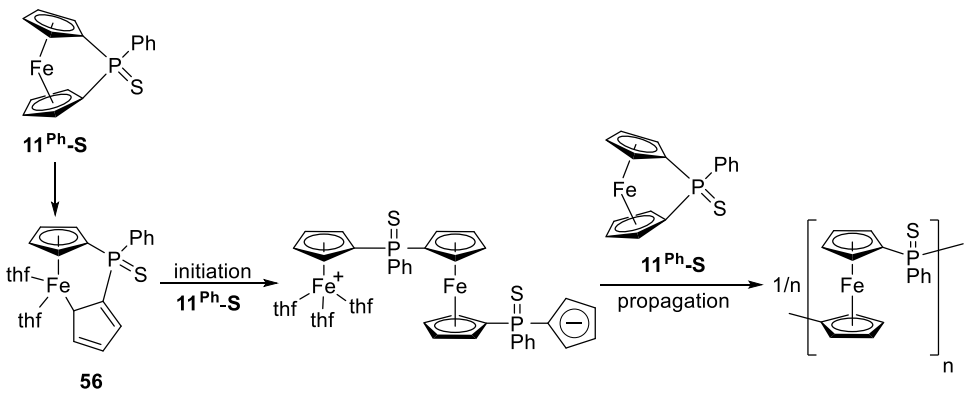

Scheme 1-24. Proposed mechanism for the photolytic ROP of compound **11^{Ph}-S**. For the intermediate **56**, only one of many feasible isomers is shown. These isomers differ with respect to the position of the allylic proton on the η^1 bound Cp ring.

In recent years, Manners and co-workers synthesized homopolymers and diblock-copolymers of PFPs via a photolytic living anionic ROP of phospha[1]FCPs **57$_n$** and **58$_n$** (Scheme 1-25).[39] This type of living polymerization provides the same advantages as anionic ROP, such as control over molecular weight, and deliver of narrow molecular weight distribution. Furthermore, it can also allow for the preparation of block copolymers. In addition, the use of a milder initiator like NaC_5H_5 makes this polymerization method easier to perform in practice than that where conventional organolithium reagents (like *n*BuLi) are required.

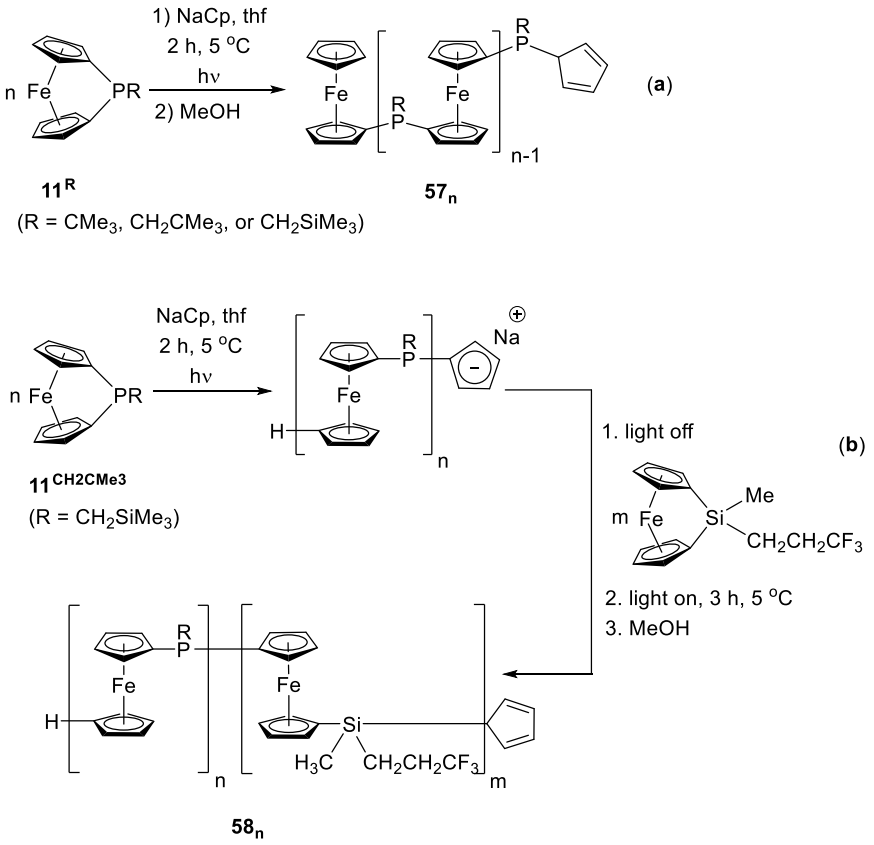

Scheme 1-25. Synthesis of (a) poly(ferrocenylphosphine)s homopolymers $\mathbf{57_n}$ and (b) diblock copolymer $\mathbf{58_n}$ through photolytic living anionic ROP. For the polymer $\mathbf{57_n}$ and $\mathbf{58_n}$, only one specific isomer was shown, with respect to the Cp ring.

The living anionic ROP initiated by organolithium reagents occurs through a cleavage of Cp–P bond. By contrast, the photolytic living anionic ROP proceeds through photoactivation and subsequent cleavage of the Fe–Cp bond of the monomer. The mechanism of this photolytic living anionic ROP (Scheme 1-26) is similar to that of the previously mentioned photolytic ROP of compound $\mathbf{11^{Ph}}$**-S** (Scheme 1-24).

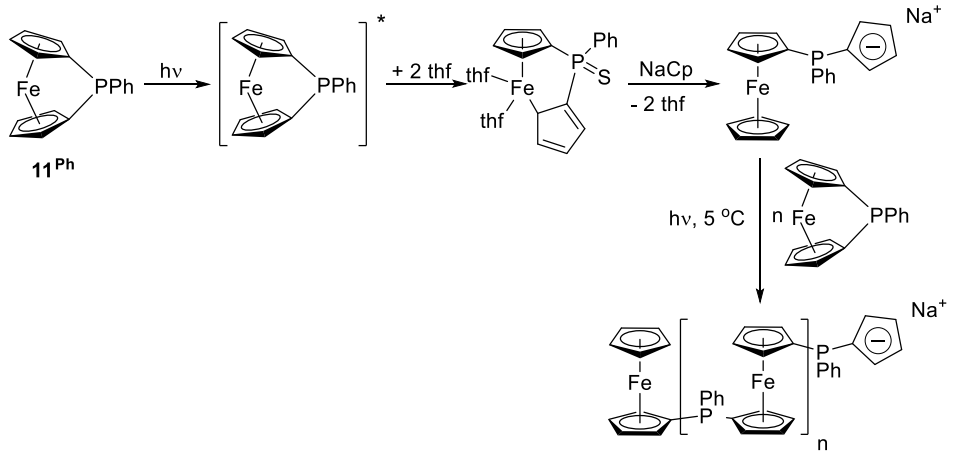

Scheme 1-26. Proposed mechanism for the photolytic living anionic ROP of compound **11^{Ph}**.

1.2.4.4 Transition-metal-catalyzed ring-opening polymerizations

Phospha[1]FCPs have also been shown to have the ability to undergo transition-metal-catalyzed ROP.[52,77] However, trivalent phosphines do not undergo ROP under these conditions due to the poisoning of the employed catalysts by coordination to phosphorus centers.[77] Reaction of the phospha[1]FCP **11^{Ph}** with methyl triflate led to a phosphonium-bridged [1]FCP **44** that could be converted into polymeric material by transition-metal-catalyzed ROP (Scheme 1-27).[52] In addition to the polymer **59$_n$**, other unidentified products were found. The authors speculated that these byproducts are likely *cis* and *trans* conformers of cyclic dimers.[52]

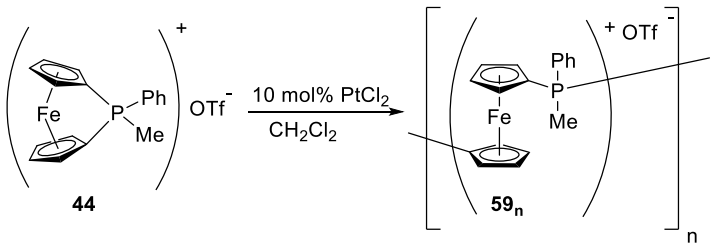

Scheme 1-27. Transition-metal-catalyzed ROP of the phosphonium-bridged [1]FCP **44**.

The reaction of compound **11^{Ph}** with boron trichloride resulted in a borane adduct (**60**; Scheme 1-28) of the phosphorus-bridged [1]FCP. The adduct **60** was found to undergo transition-metal-catalyzed ROP with a platinum catalyst,[77] resulting in the insoluble polymer **60$_n$**, which could not be analyzed by GPC. However, solid-state NMR spectroscopy and pyrolysis-mass spectrometry confirmed that **60$_n$** is poly(ferrocenylphenylphosphine trichloroborane).[77]

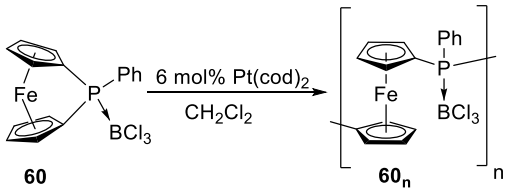

60 **60$_n$**

Scheme 1-28. Transition-metal-catalyzed ROP of the borane adduct **60** of phospha[1]FCP.

1.3 Ferrocene-based P-chiral phosphine ligands

1.3.1 Planar-chiral ferrocenes

Electrophilic substitutions on the Cp ring of a ferrocene unit can break its plane of symmetry, thus creating a planar-chiral ferrocene. In this thesis, the nomenclature "R_p" and "S_p" proposed by Schlögl[78] is used to indicate the planar chirality of substituted ferrocene derivatives (Figure 1-11). According to this rule, when a molecule is viewed from above, a *R* or *S* configuration indicates a clockwise or anticlockwise sequence of groups of decreasing priority, respectively.

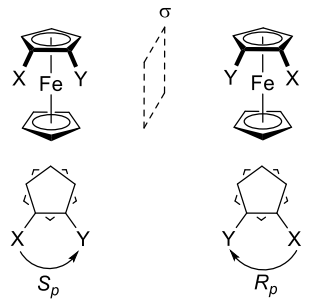

Figure 1-11. Assigning planar chirality for 1,2-heterodisubstituted ferrocenes using the S_p and R_p stereodescriptors, as defined by Schlögl,[78] where X has a higher priority than Y.

Planar-chiral ferrocenes are very important compounds that are commonly applied in asymmetric catalysis. A remarkable example of the use of a chiral ferrocene ligand in the chemical industry is the synthesis of a precursor of the herbicide (*S*)-metolachlor, by an Ir-Xyliphos-catalyzed asymmetric hydrogenation reaction (Scheme 1-29).[79] This is an extremely efficient process and is the largest-scale enantioselective catalytic process in industry with turnover numbers (TONs) of 2,000,000 and turnover frequencies (TOFs) of around 600,000 h^{-1}, producing more than 10,000 tons per annum. The following section describes the preparation of chiral ferrocene-based phosphine ligands and their application in asymmetric catalysis.

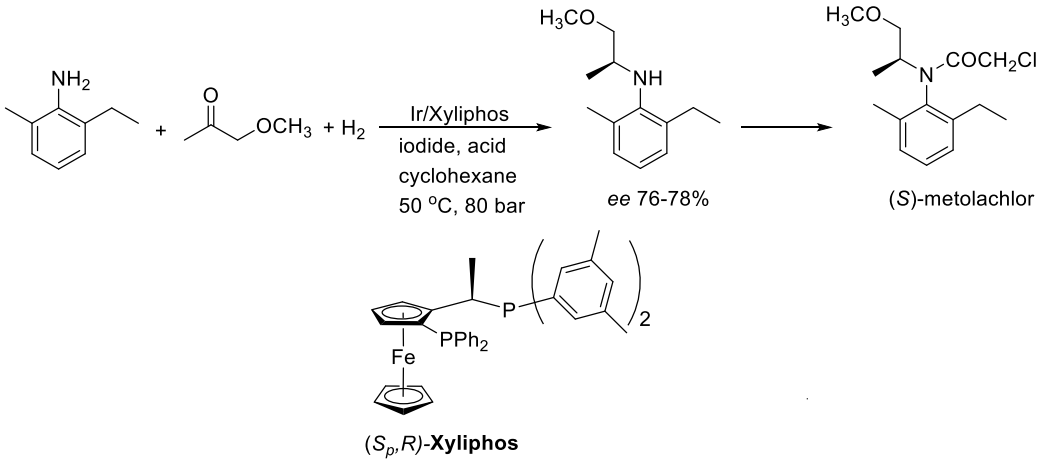

Scheme 1-29. Enantioselective synthesis of (*S*)-metolachlor.

1.3.2 Structural variety of ferrocene-based P-chiral phosphine ligands

The first example of an enantiopure planar-chiral ferrocenylphosphine is ppfa (**68**; Figure 1-12), which was synthesized by Hayashi and Kumada in 1974 via a diastereoselective *ortho*-lithiation of Ugi's amine.[80] This ligand is an efficient chiral ligand in some transition-metal-mediated reactions, and since this early discovery, a variety of chiral ferrocene ligands have been developed and used in asymmetric catalysis (Figure 1-12).[81–83]

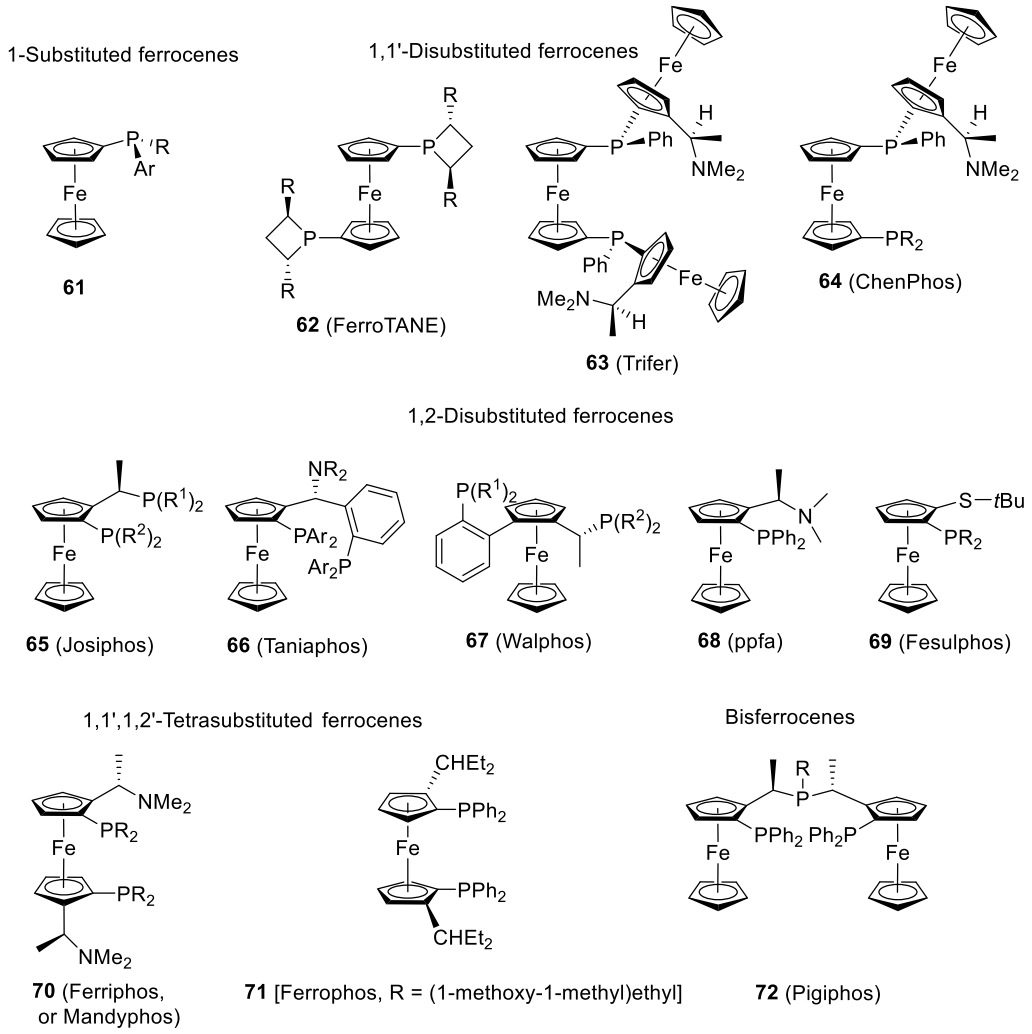

Figure 1-12. Representative families of chiral ferrocene ligands with various applications in asymmetric catalysis.

The Ugi amine method is the most widely used strategy to synthesize chiral ferrocene-based ligands, especially 1,2-disubstituted derivatives. Some specific ligands derived from Ugi's amine are Josiphos (**65**),[84] Taniaphos (**66**),[85,86] Walphos (**67**),[87] and Pigiphos (**72**).[88] For the Josiphos-type ligand (**65**), after the diasteroselective *ortho*-lithiation, the dimethylamino group in the Ugi amine is substituted using a secondary phosphine (R_2PH) or pyrazole in polar solvents (Scheme 1-30a).[84] The synthesis of the Walphos-type ligand (**67**) following Ugi amine method is also illustrated in Scheme 1-30b.

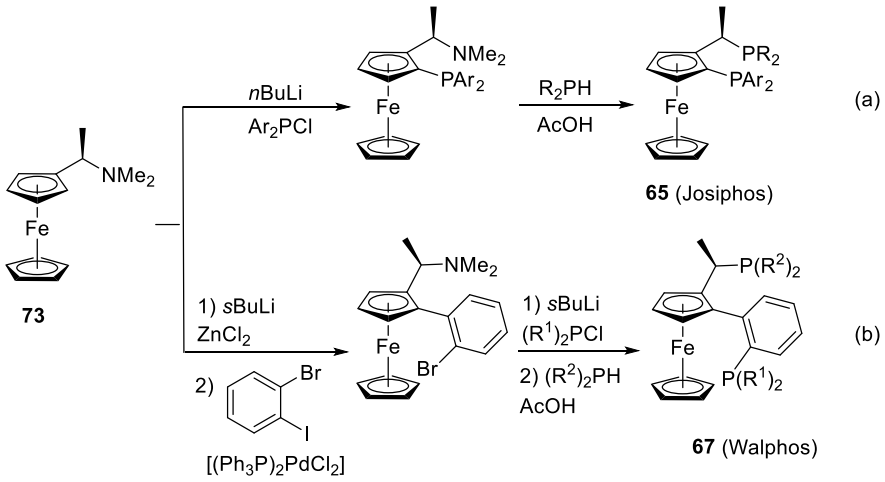

Scheme 1-30. Examples of syntheses of 1,2-disubstituted ferrocene ligands (Josiphos and Walphos) from Ugi's amine.

In recent years, a wide variety of 1,2-disubstituted ferrocene ligands have also been synthesized by a sulfoxide approach, including ligands with planar chirality only (for example, the Fesulphos **69** [89,90] or Taniaphos-type ligand (**66**; Scheme 1-31).[91] In this method, the chiral sulfoxide was first employed via the diastereoselective *ortho*-lithiation step.[89,90,91] After that, the *ortho*-directing group can be reduced to a metal-coordinating thioether (Fesulphos; **69**),[89,90] or it can act as a leaving group by a *t*BuLi-mediated C–S cleavage, and further react with an appropriate electrophile (Taniaphos; **66**).[91]

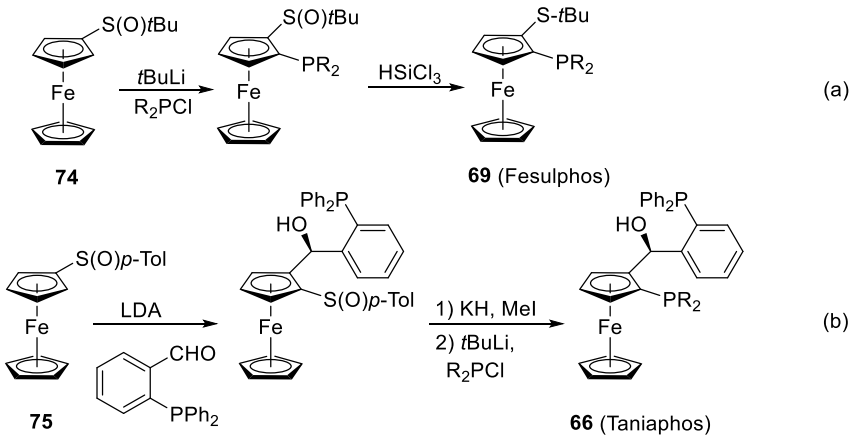

Scheme 1-31. Sulfoxide approach for the synthesis of 1,2-disubstituted ferrocene ligands Taniaphos and Fesulphos.

Another notable contribution to this area is the preparation of a new class of ligands called "Ferriphos" with a 1,1',2,2'-tetrasubstituted ferrocenyl pattern, and later one type of Ferriphos ligand was renamed as Mandyphos by Degusaa.[92,93] These ligands were developed from the Corey-Bakshi-Shibata (CBS) reduction of a 1,1'-diacetylferrocene to the corresponding diol, followed by a nucleophilic substitution reaction (Scheme 1-32). A worthy note about this method is the retention of configuration (*R*,*R*-central chirality) on the ferrocene unit during the formation of product. Kang and co-workers have independently reported the C_2-symmetric bisphosphine Ferrophos ligand with similar structural features (**71**; Figure 1-12).[94]

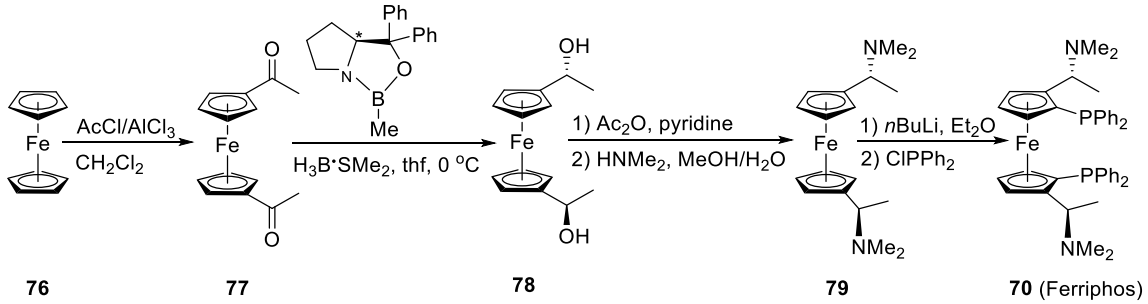

Scheme 1-32. Synthesis of C_2-symmetrical Ferriphos ligand.

Burk *et al*. reported the synthesis of the 1,1'-disubstituted ferrocenyl phosphine FerroTANE (**62**; Figure 1-12) achieved by attaching two phosphetanyl fragments to the ferrocene moiety.[95] In accordance with the interest in C_2-symmetric ferrocenyl ligands, Marinetti and co-workers also isolated some rhodium and ruthenium complexes of FerroTANE-type ligand (**62**; Figure 1-12).[96,97] In recent years, Chen and co-workers synthesized a new class of chiral diphosphine ligand called Trifer (**63**; Figure 1-12), which combines carbon- and phosphorus-centered chirality and planar chirality.[98] Later, the same group reported the synthesis of another C_1-symmetric P-chiral diphosphine ligand, ChenPhos (**64**; Figure 1-12) which was also developed from the Ugi amine method.[99]

1.3.3 Applications of chiral ferrocene-based phosphine ligands in asymmetric catalysis

Many chiral ferrocene-based phosphine ligands with outstanding applications in asymmetric catalysis have been developed (Figure 1-12). Among those, many impressive results have been achieved with members of the Josiphos (**65**), Ferriphos (**70**), Taniaphos (**66**), and FerroTANE (**62**) families. For instance, the Josiphos-type ligands (**65**) have taken the lead in many industrial applications of asymmetric catalysis. One of the notable industrial applications of Josiphos ligands is the Rh-catalyzed asymmetric synthesis of (+)-Biotin (Scheme 1-33).[100] The Josiphos-type ligand **65**$^{t\mathbf{Bu}}$, containing bulky *t*Bu group, was found to afford a very high diastereoselectivity in the synthesis of intermediate **80**.

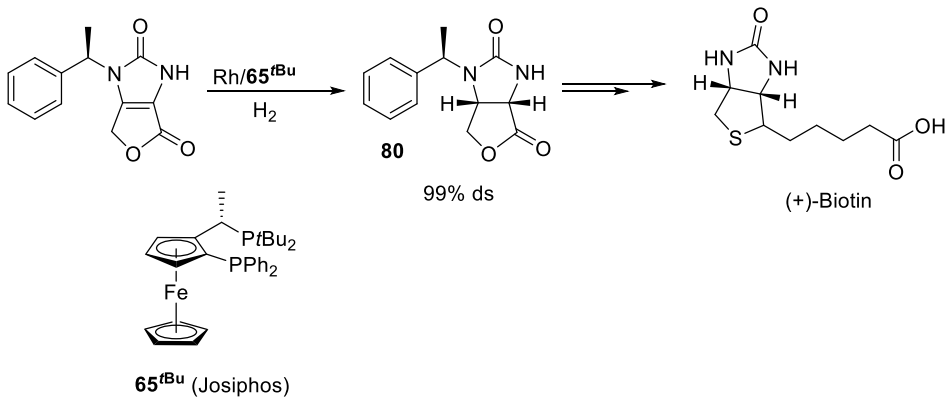

Scheme 1-33. Rh-catalyzed synthesis of (+)-Biotin intermediate using the Josiphos-type ligand **65**$^{t\mathbf{Bu}}$.

A group at Takeda Chemical Industries studied the Rh-catalyzed asymmetric hydrogenation of a β,β-diaryl-substituted α,β-unsaturated acid (Scheme 1-34).[101] Among many ligands used for test reactions, the Josiphos-type ligand **65**$^{\mathbf{Cy}}$ provided the corresponding substituted propanoic acid (**81**) in 93% *ee*. This product is a key intermediate for synthesizing naphthoquinone derivative **II**, which is a potential therapeutic drug for neurodegenerative disease.

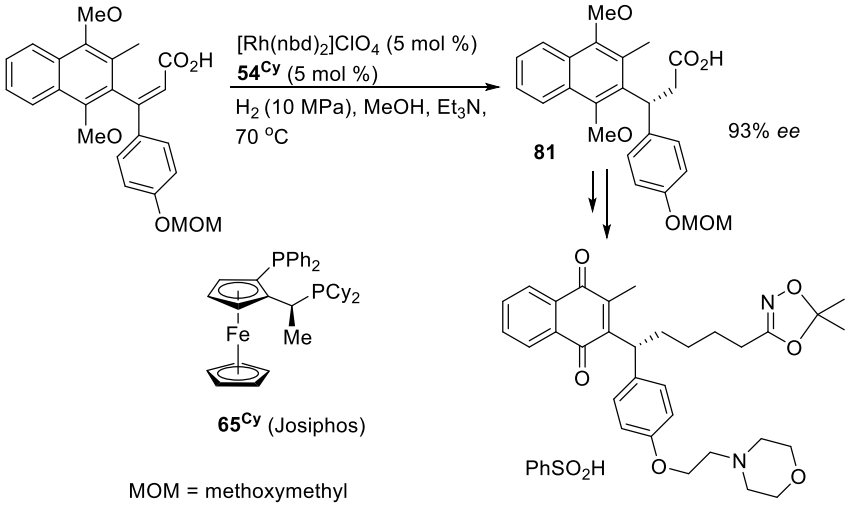

Scheme 1-34. Josiphos/Rh-catalyzed asymmetric hydrogenation of a β,β-diaryl-substituted α,β-unsaturated acid drug precursor.

In addition to the above industrial applications, chiral ferrocene-based phosphine ligands also have found their applications on laboratory scale. A C_2-symmetric ferrocene-based phosphine ligand FerroPhos (**71**) developed by Kang *et al*. was found to be efficient for Rh-catalyzed hydrogenations of α-dehydroamino acid derivatives (98% *ee*).[94,102] The Mandyphos-type ligand **70** also provided excellent enantioselectivities in asymmetric hydrogenation of α-dehydroamino acid derivatives (up to > 99.5% *ee*) (Scheme 1-35).[85] Rh- or Ru-complexes equipped with Taniaphos-type ligand **66**,[86,103] have shown the high efficiency in asymmetric hydrogenations. Especially, the Taniaphos-type ligand having a MeO group at the chiral carbon center (**66**$^{\mathbf{MeO}}$), showed good to outstanding performances in hydrogenation of several olefin and ketone substrates (up to 99% *ee*) (Scheme 1-35).[85]

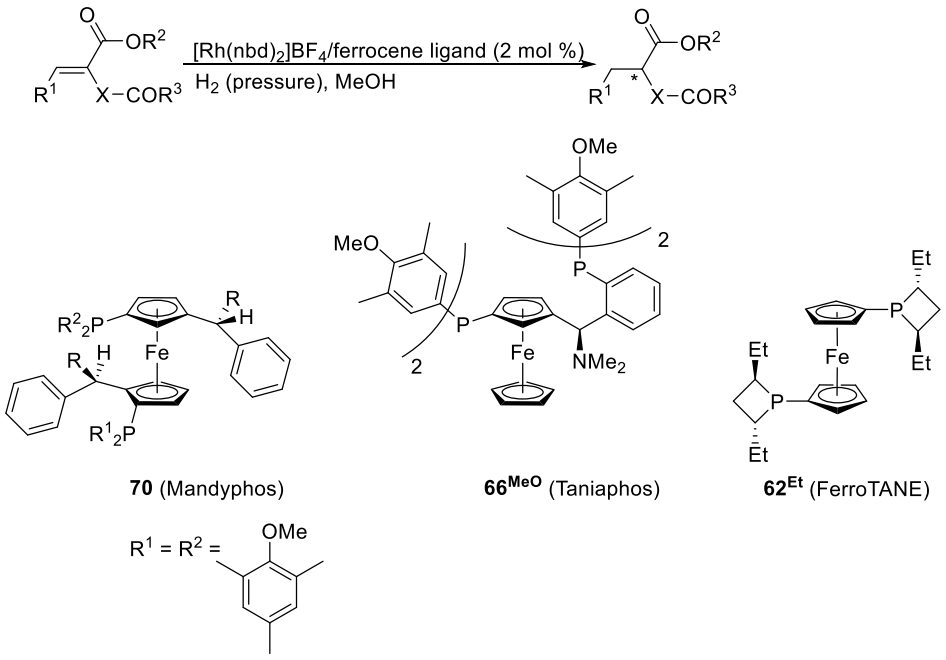

Scheme 1-35. Rh-catalyzed asymmetric hydrogenation of dehydro-α-amino acids and itaconic acid derivatives.

The synthesis of FerroTANE-type ligands was reported independently by Marinetti[96,97] and Burk.[95] The FerroTANE-type ligand **62**$^{\mathbf{Et}}$ has been successfully applied in Rh-catalyzed

hydrogenation of itaconates, which showed outstanding results in term of rate as well as enantioselectivity (98% *ee*) (Scheme 1-35).[95] These types of catalysts were also used in the Rh-catalyzed hydrogenation of β-keto esters, and showed moderate to high enantioselectivities (Scheme 1-36).[96]

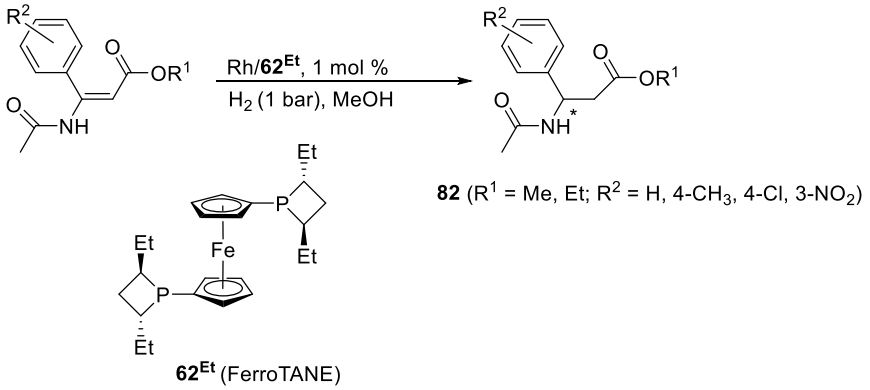

Scheme 1-36. Rh-catalyzed asymmetric hydrogenation of α,β-unsaturated (E)-β-acylamino esters.

1.4 Research objectives

The main objective of my PhD thesis was to synthesize new chiral phosphorus-containing polymers, more specifically, poly(ferrocenylphosphine)s (PFPs). In order to achieve the main goal, it was intended to prepare a family of monomers for ROPs. As mentioned in section 1.2, phospha[1]FCPs are among a few groups of strained organometallic compounds that can undergo ROP with control over molecular weight and molecular weight distribution. Although phospha[1]FCPs are well-documented in literature,[22,24,25,61,62,39,32] chiral phospha[1]FCPs are comparatively less explored.[32,24,37] On the other hand, diphospha[2]FCPs have not been thoroughly studied to date,[28,33,65,66,104] and no attempts to polymerize these compounds have been reported. Therefore, new enantiomerically pure phospha[*n*]FCPs (*n* = 1, 2) with different

substituents on phosphorus were prepared. Once synthesized, the polymerization behaviour of these new species was explored.

Thermal ROP was chosen to polymerize these strained compounds (section 2.3), as it is one of the most convenient methods to obtain well-defined metallopolymers. However, with this method molecular weight and molecular weight distribution cannot be controlled. Therefore, the use of another advanced technique was selected. As discussed in section 1.2.4.2, anionic ROP provides the preparation of polymers with control of major structural factors that affect polymer properties. In addition to the polymerization, alkyl groups on the ferrocene moiety could be used as markers to investigate the mechanistic insights into the unknown mechanism of thermal ROP.

CHAPTER 2. RESULTS AND DISCUSSION

2.1 Synthesis of chiral phospha[*n*]ferrocenophanes

2.1.1 Synthesis of (S_p,S_p)-1,1′-dibromo-2,2′-di(isopropyl)ferrocene

The synthesis of the starting material of key importance for the thesis at hand, the dibromoferrocene (S_p,S_p)-**19**, was successfully performed by following the published procedure (Scheme 2-1).[105,92] The key step in the multistep synthesis is the asymmetric CBS reduction of 1,1'-diacetylferrocene **77** to the *R,R*-isomer of the diol **78**, which was transformed into amine **79** with retention of configuration.[105,92] Compound **79** was stereospecifically lithiated and then brominated with 1,2-dibromotetrachloroethane to yield species **84**. In this last step of Scheme 2-1, the central chirality was removed to give the final compound (S_p,S_p)-**19** with planar chirality (S_p,S_p-isomer; C_2 symmetry).[102,105]

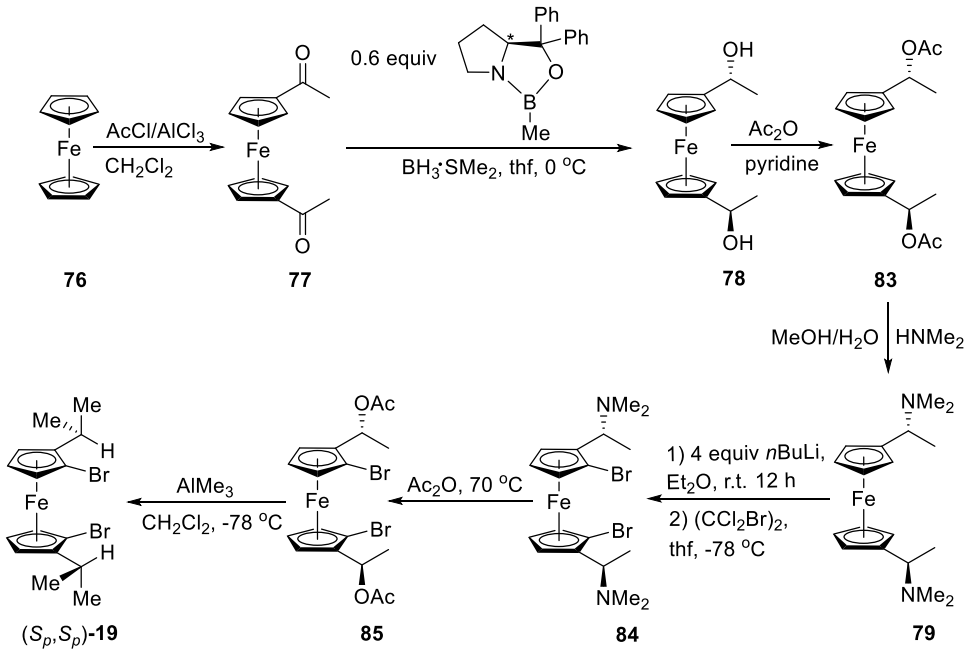

Scheme 2-1. Synthesis of the known chiral dibromoferrocene (S_p,S_p)-**19**.

The reported single-crystal X-ray analysis data of the dibromoferrocene (S_p,S_p)-**19** showed that one of the methyl groups of *i*Pr is approximately in the same plane as a Cp ring, whereas the second methyl group is oriented away from iron and nearly perpendicular to the Cp ring.[105] It is interesting to note that a recent study revealed that the alkyl group, which is oriented approximately perpendicular to the Cp ring, affects the outcome of the salt-metathesis reaction.[106]

2.1.2 Synthesis and characterization of the chiral phospha[1]ferrocenophane (S_p,S_p)-**86**^{CH2SiMe3}

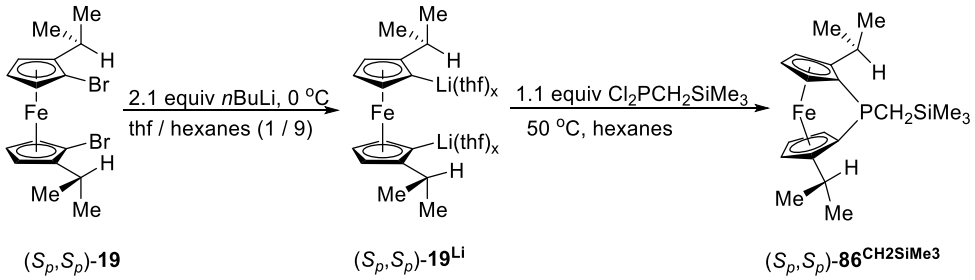

(S_p,S_p)-**19** (S_p,S_p)-**19**^{Li} (S_p,S_p)-**86**^{CH2SiMe3}

Scheme 2-2. Synthesis of the chiral phospha[1]FCP (S_p,S_p)-**86**^{CH2SiMe3}.

Due to the moderate steric bulk of -CH_2SiMe_3 group, the targeted phospha[1]FCP **86**^{CH2SiMe3} was expected to be stable enough to be isolated. The known compound $Cl_2PCH_2SiMe_3$ (**87**; Scheme 2-3) was synthesized using the reaction of phosphorus trichloride with an organocadmium reagent.[39] The latter species was prepared in situ by a transmetallation of the Grignard reagent (trimethylsilyl methyl magnesium chloride) with anhydrous cadmium chloride at a low temperature (0 °C). Repeated flask-to-flask condensation at reduced pressure yielded species **87** as a clear oil, which shows one signal at δ = 205.5 ppm in the ^{31}P NMR spectrum (reported value: δ = 205.8 ppm).[39]

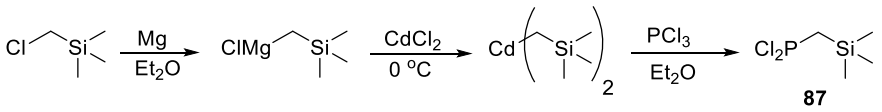

Scheme 2-3. Synthesis of the phosphorus reagent **87**.

Addition of Cl_2PSiMe_3 afforded the targeted phospha[1]FCP (S_p,S_p)-**86**^{CH2SiMe3} (Scheme 2-2), which could be clearly identified in the reaction mixture by its distinct pattern of six Cp signals in ^{1}H NMR spectra. This could also be observed by a distinctive color change from orange to dark-red. The compound (S_p,S_p)-**86**^{CH2SiMe3} was isolated by vacuum sublimation at 80 °C, to yield a mixture of a dark-red oil and a solid. The mixture was further purified by crystallization in hexanes at –80 °C, and the final product was obtained in a form of dark-red crystals (50% isolated yield).

As expected for a C_1-symmetric compound, ^{1}H NMR spectroscopic data of the isolated species show 6 equally intense peaks in the Cp range at δ = 4.41, 4.25, 4.22, 4.18, 4.04, and 3.96 ppm (Figure 2-1). This is similar to the ^{1}H NMR pattern of Cp range of the related chiral phospha[1]FCPs (S_p,S_p)-**20**^{R}, which were previously synthesized by the former group member Saeid Sadeh (Figure 2-2).[64] Compared to the ^{1}H NMR spectrum of the known non-alkylated phospha[1]FCP (**11**^{CH2SiMe3}) which showed four signals in the Cp range (δ = 4.42, 4.35, 4.29 and 4.22 ppm), an unusually low δ value (3.96 ppm) in one of the Cp protons signal of (S_p,S_p)-**86**^{CH2SiMe3} was observed. The signal at δ = 3.96 ppm is assigned to one of the α-H, which is in the proximity of *i*Pr group on the neighboring Cp ring. The methine protons of *i*Pr groups resonate at δ = 3.10 and 3.43 ppm. The signal difference in the chemical shift is likely caused by the CH_2SiMe_3 group, which shields one of the methine proton. On the other hand, the two methine signals show different patterns in ^{1}H NMR spectrum, for example, a septet at δ = 3.10 ppm and a septet of doublets at δ = 3.43 ppm. As the methine protons of the *i*Pr groups of the

precursor (S_p,S_p)-**19** appear as septets, the additional coupling in compound (S_p,S_p)-**86**$^{\mathbf{CH2SiMe3}}$ at δ = 3.43 ppm must be caused by phosphorus (J_{PH} = 3.2 Hz). The fact that only one of the two methine protons shows coupling with phosphorus proves that it cannot occur through bonds, but through space.[107,108] The chiral species (S_p,S_p)-**86**$^{\mathbf{CH2SiMe3}}$ equipped with two *i*Pr groups adjacent to phosphorus is a unique species to exemplify the uncommon through-space nuclear ^{1}H-^{31}P coupling. This type of compound is an ideal example to differentiate between through-space and through-bond coupling mechanism in NMR spectroscopy.[107]

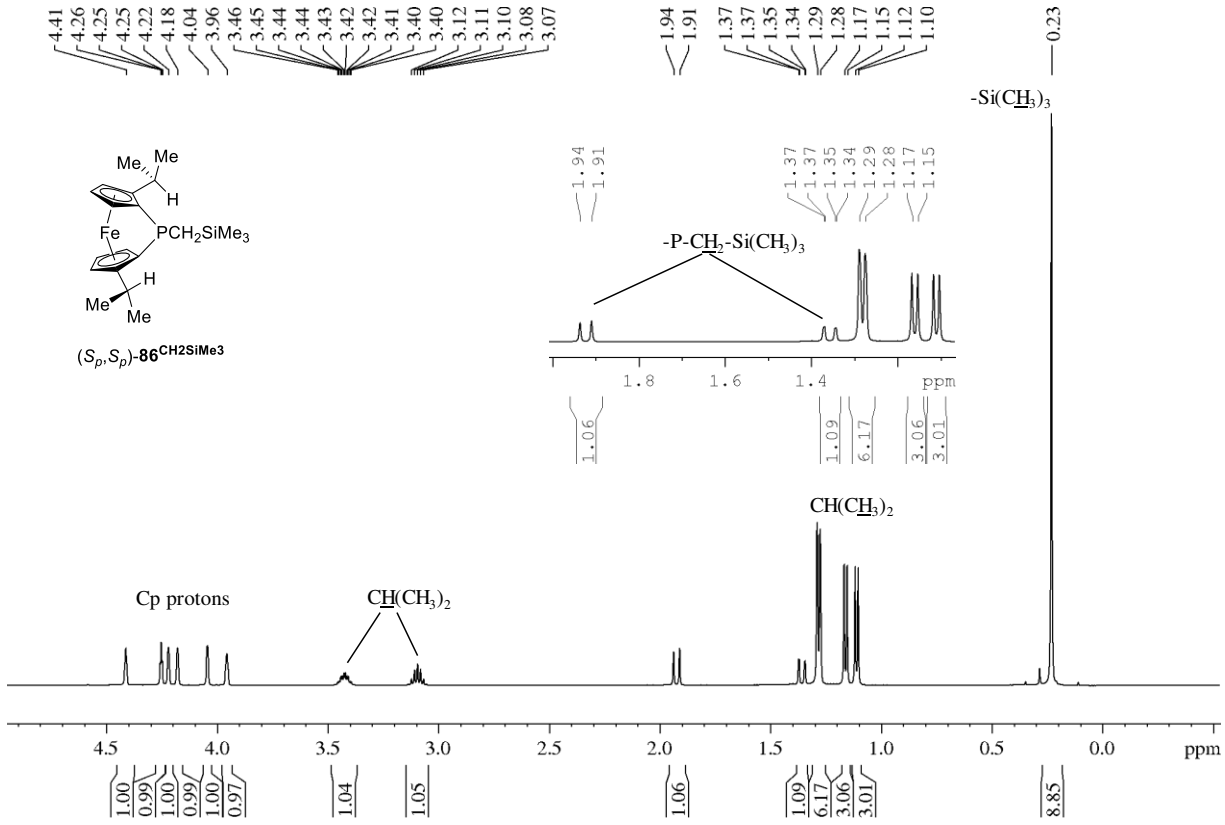

Figure 2-1. ^{1}H NMR spectrum (500 MHz) of the chiral phospha[1]FCP (S_p,S_p)-**86**$^{\mathbf{CH2SiMe3}}$.

The most distinguishable feature of the ^{13}C{^{1}H} NMR spectrum of (S_p,S_p)-**86**$^{\mathbf{CH2SiMe3}}$ is the upfield shifts of the two *ipso*-carbon atoms attached to the bridging P atom, which appear as two doublets at δ = 19.6 and 20.4 ppm (J_{PC} = 49 and 67 Hz; respectively). These values are close

to those of the known phospha[1]FCP with the same bridging moiety (**11**$^{\mathbf{CH2SiMe3}}$; δ = 20.8 ppm).[39] Two downfield resonances for the *ipso*-carbon atoms attached to *i*Pr groups at δ = 104.7 and 106.7 ppm, are also in the reported chemical shift range of chiral phospha[1]FCPs ((*S*$_p$,*S*$_p$)-**20**$^{\mathbf{R}}$ and (*S*$_p$,*S*$_p$)-**21**$^{\mathbf{tBu}}$; δ = 104–107 ppm).[109,51,64] The ^{31}P NMR spectrum of species (*S*$_p$,*S*$_p$)-**86**$^{\mathbf{CH2SiMe3}}$ shows a signal at δ = –4.2 ppm, which is quite close to the known non-alkylated species (**11**$^{\mathbf{CH2SiMe3}}$; δ = –7.1 ppm).[39]

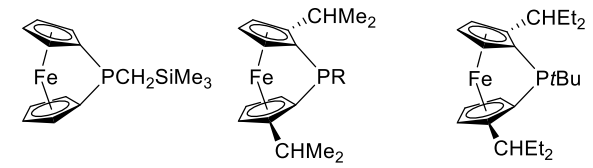

11$^{\mathbf{CH2SiMe3}}$ (*S*$_p$,*S*$_p$)-**20**$^{\mathbf{R}}$ R = Ph, *i*Pr, *t*Bu (*S*$_p$,*S*$_p$)-**21**$^{\mathbf{tBu}}$

Figure 2-2. Non-alkylated and alkylated phospha[1]FCPs.

2.1.3 Synthesis and characterization of the chiral phospha[1]ferrocenophane (*S*$_p$,*S*$_p$)-86$^{\mathbf{NiPr2}}$

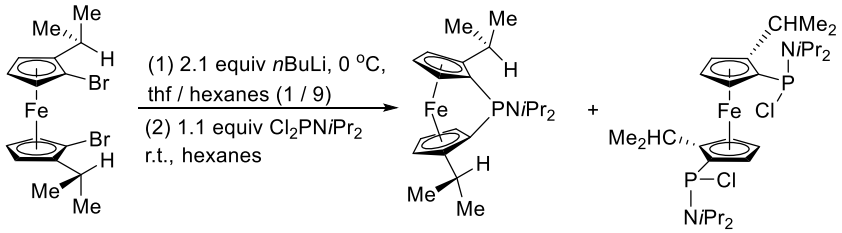

(*S*$_p$,*S*$_p$)-**19** (*S*$_p$,*S*$_p$)-**86**$^{\mathbf{NiPr2}}$ **88**$^{\mathbf{NiPr2}}$

Scheme 2-4. Synthesis of the chiral phospha[1]FCP (*S*$_p$,*S*$_p$)-**86**$^{\mathbf{NiPr2}}$, along with the formation of 1,1'-bis(phosphanyl)ferrocene **88**$^{\mathbf{NiPr2}}$.

The known aminodichlorophosphine **89** was prepared by a one-step synthesis from *i*Pr$_2$NH and PCl$_3$ at 0 °C in hexanes (Scheme 2-5).[110] The final product **89** was obtained as a colorless liquid by condensation under partial pressure (0.1 mbar). The ^{31}P NMR spectrum of compound **89** shows one signal at δ = 170.3 ppm, which is close to the reported ^{31}P chemical shift of the same

compound (δ = 170.2 ppm).[110] Since the N*i*Pr$_2$ group has a large steric bulk and works as a π-donate to phosphorus center, the resulted phopsha[1]FCP (S_p,S_p)-**86**$^{\mathbf{NiPr2}}$ was also expected to be stable enough for the isolation, like the previously synthesized (S_p,S_p)-**86**$^{\mathbf{CH2SiMe3}}$.

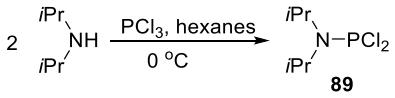

89

Scheme 2-5. Synthesis of the phosphorus reagent **89**.

As before, Li/Br exchange reaction was used to prepare (S_p,S_p)-**19**$^{\mathbf{Li}}$, followed by a dropwise addition of a *i*Pr$_2$NPCl$_2$ solution over a period of 10 min using a syringe pump (Scheme 2-4). The reaction mixture was then warmed up to r.t. and stirred at this temperature for 30 min. The ^{1}H NMR spectrum of the reaction mixture shows an approximate ratio of 1 to 1 between (S_p,S_p)-**86**$^{\mathbf{NiPr2}}$ and 1,1'-(N*i*Pr$_2$)$_2$fc$^{i\mathrm{Pr}}$ **88**$^{\mathbf{NiPr2}}$ (fc$^{i\mathrm{Pr}}$ = (S_p,S_p)-1,1'-[(Me$_2$CH)H$_3$C$_5$]$_2$Fe). The phospha[1]FCP (S_p,S_p)-**86**$^{\mathbf{NiPr2}}$ was isolated by a flask-to-flask condensation at reduced pressure, with temperature of 80 °C, and obtained as a dark-red oil (20% isolated yield). The compound was characterized with NMR spectroscopy, mass spectrometry, and CHN elemental analysis.

In the ^{1}H NMR spectrum of the isolated species, the lack of symmetry is clearly observed with four overlapping signals in the Cp range, corresponding to six Cp protons (δ = 4.45, 4.22, 4.15, and 3.91 ppm; Figure 2-3). Its ^{13}C{^{1}H} NMR spectrum shows two distinct doublets at δ = 105.9 and 104.3 ppm for two *ipso*-carbon atoms caused by coupling with ^{31}P atoms [J_{PC} = 10 Hz and 33 Hz], indicating the presence of a *non*-symmetrical compound. These ^{13}C chemical shifts are close to those of reported chiral P[1]FCPs ((S_p,S_p)-**20**$^{\mathbf{Ph}}$ and (S_p,S_p)-**21**$^{\mathbf{tBu}}$; Figure 2-2).[109,64]

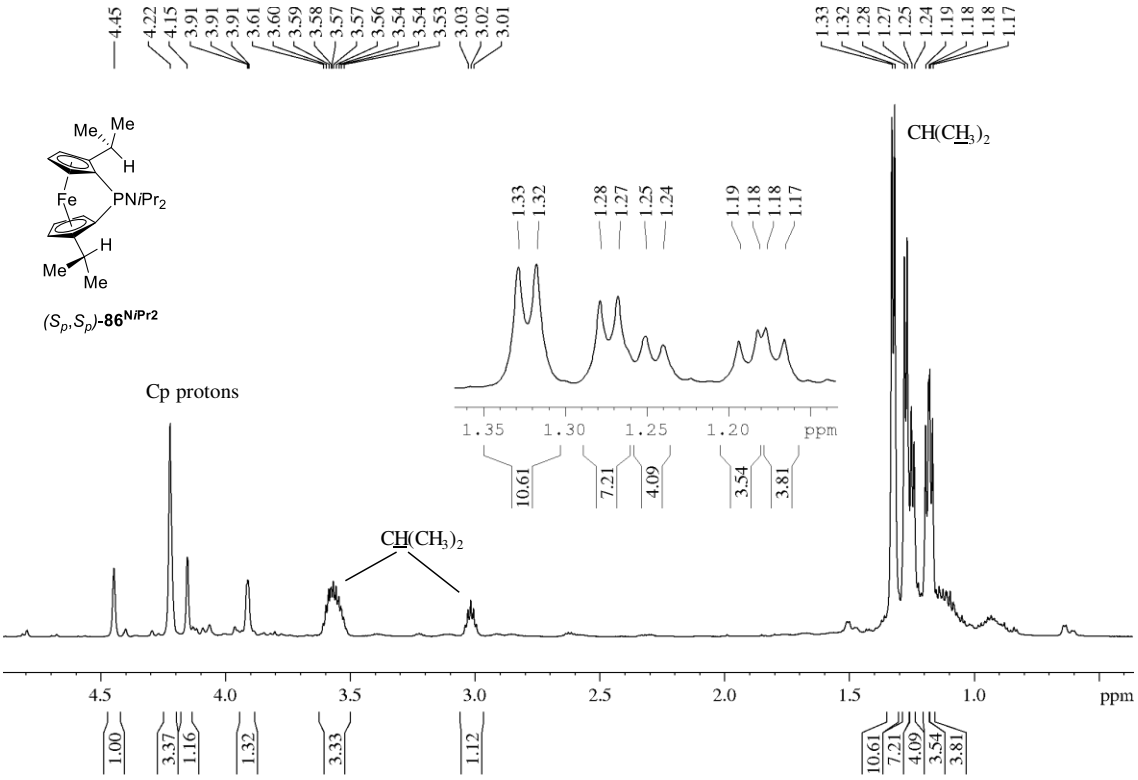

Figure 2-3. ^{1}H NMR spectrum (600 MHz) of the chiral phospha[1]FCP (S_p,S_p)-**86**$^{\mathbf{NiPr2}}$.

It was noticed that the difference in ^{31}P chemical shifts between the non-alkylated and alkylated phospha[1]FCPs having Ph [**11**$^{\mathbf{Ph}}$ and (S_p,S_p)-**20**$^{\mathbf{Ph}}$] or CH_2SiMe_3 [**11**$^{\mathbf{CH2SiMe3}}$ and (S_p,S_p)-**86**$^{\mathbf{CH2SiMe3}}$] substituents on phosphorus was approximately 3 ppm.[38,39] By contrast, the non-alkylated and alkylated phospha[1]FCPs with N*i*Pr$_2$ substituents (**11**$^{\mathbf{NiPr2}}$ and (S_p,S_p)-**86**$^{\mathbf{NiPr2}}$; respectively), show a significant difference in ^{31}P chemical shift (δ = 31.1[25] and 49.7 ppm; respectively). So far, the reason for this is still unclear.

2.1.4 Synthesis and characterization of the 1,1'-bis(phosphanyl)ferrocene (S_p,S_p,S,S)-**88**$^{N\mathit{i}Pr2}$

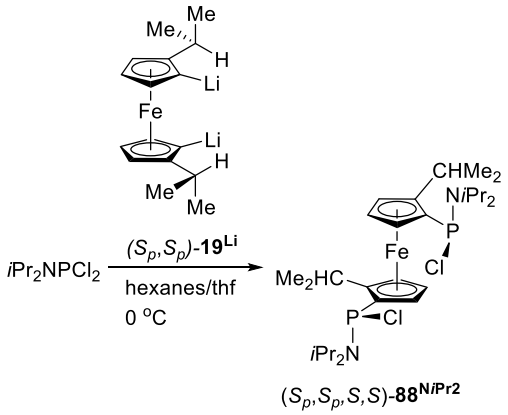

Scheme 2-6. Synthesis of the chiral bis(phosphanyl)ferrocene (S_p,S_p,S,S)-**88**$^{N\mathit{i}Pr2}$.

As mentioned above, the addition of iPr$_2$NPCl$_2$ solution to the dilithio ferrocene derivative (S_p,S_p)-**19**^{Li} gave a 1 to 1 mixture of phospha[1]FCP (S_p,S_p)-**86**$^{N\mathit{i}Pr2}$ and 1,1'-species **88**$^{N\mathit{i}Pr2}$. In order to fully characterize the 1,1'-bis(phosphonyl)ferrocene **88**$^{N\mathit{i}Pr2}$, this compound was synthesized selectively using the reverse order of addition that was used before. That means a solution of the dilithio species (S_p,S_p)-**19**^{Li} was added to the solution of 3 equivalents of iPr$_2$NPCl$_2$ within 10 min at 0 °C (Scheme 2-6). Due to phosphorus being a stereogenic atom, 3 diastereomers could possibly form in this reaction. However, the synthesis was very selective, as one of the isomers was found to be dominant. For example, the ^{31}P NMR spectroscopic data of this reaction mixture show signals in the range of δ = 131.1–123.0 ppm, with the major signal at δ = 123.2 ppm (Figure 2-4).

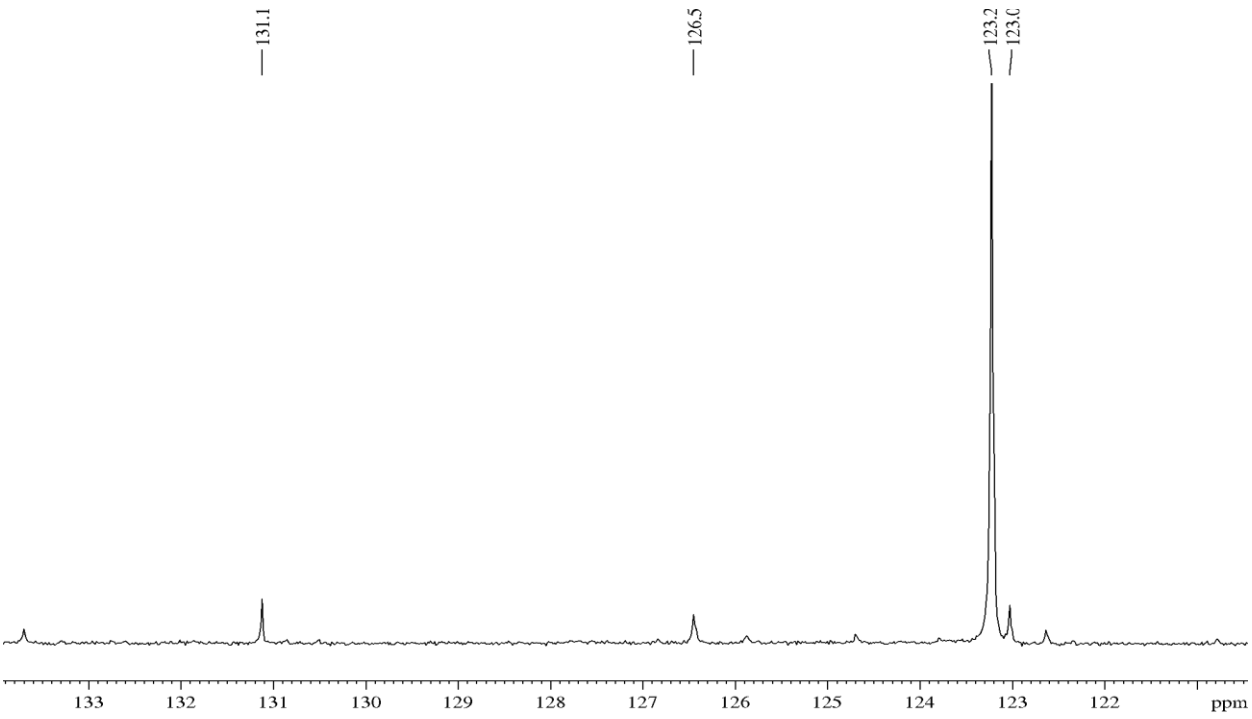

Figure 2-4. $^{31}P\{^{1}H\}$ NMR spectrum (500 MHz) of the reaction mixture.

The reaction mixture was purified by sublimation at reduced pressure, with a temperature of approximately 135 °C, resulting in a yellow solid (31% isolated yield). The yellow solid was crystallized in hexanes at –80 °C to yield yellow crystals that were used for single-crystal X-ray diffraction analysis. The crystal structure shows species **88**$^{\mathbf{NiPr2}}$ crystallized in a monoclinic space group C2 displaying a two-fold symmetry with both phosphorus atoms possessing *S*-configuration. On the other hand, the two bulky N*i*Pr$_2$ groups are oriented away from the ferrocene moieties to avoid steric repulsion with Fe atom.

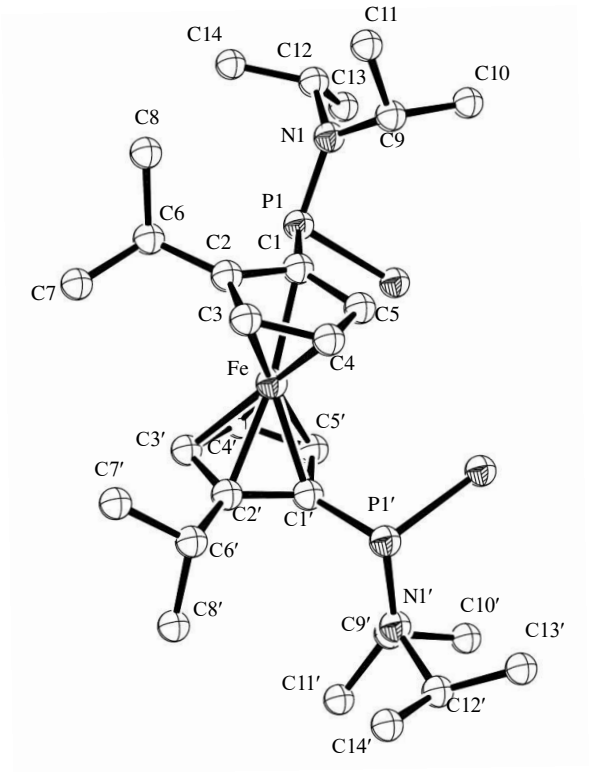

Figure 2-5. Molecular structure of (S_p,S_p,*S*,*S*)-**88**$^{Ni\mathbf{Pr2}}$ with thermal ellipsoids at the 50% probability level. Hydrogen atoms are omitted for clarity. Selected bond lengths [Å] and bond angles [°]: P1–C1 = 1.809(2); P1–Cl1 = 2.1539(8); P1–N1 = 1.668(2); C1–P1–Cl1 = 97.82(8); C2–P1–C1 = 122.20(18); N1–P1–C1 = 102.75(11); P1–N1–C12 = 116.52(16); C12–N1–C9 = 116.3(2); C9–N1–P1 = 124.21(16). For other bond lengths [Å] and angles [°] see Table 4–1.

The obtained crystals were characterized by CHN elemental analysis, mass spectrometry, and NMR spectroscopy. Both the ^{1}H and ^{13}C NMR spectra support the expectation that species (S_p,S_p,*S*,*S*)-**88**$^{Ni\mathbf{Pr2}}$ is a single diastereomer, having C_2-symmetry. Specifically, the ^{1}H NMR spectrum shows three Cp signals of equal intensity for six Cp protons (δ = 4.27, 4.69 and 5.19 ppm), and six doublets for twelve methyl groups (δ = 0.59, 1.05, 1.08, 1.22, 1.35 and 1.47 ppm). One of the most distinguished signals are those of methine protons of the *i*Pr groups on the two Cp rings (δ = 2.88 ppm), which is more upfield than that of the phospha[1]FCP (S_p,S_p)-**86**$^{Ni\mathbf{Pr2}}$ (δ = 3.57 and 3.02 ppm). Furthermore, the methine signal is a septet of doublets, which is caused

by additional coupling with phosphorus atom. The $^{13}C\{^{1}H\}$ NMR spectrum of species (S_p,S_p,S,S)-**88**$^{\mathbf{NiPr2}}$ shows two doublets at δ = 102.8 and 77.1 ppm for the *i*Pr-bound and the phosphorus-bound carbon atoms, respectively. Its ^{31}P NMR spectrum shows one signal at δ = 123.3 ppm, indicating the presence of a single diastereomer.

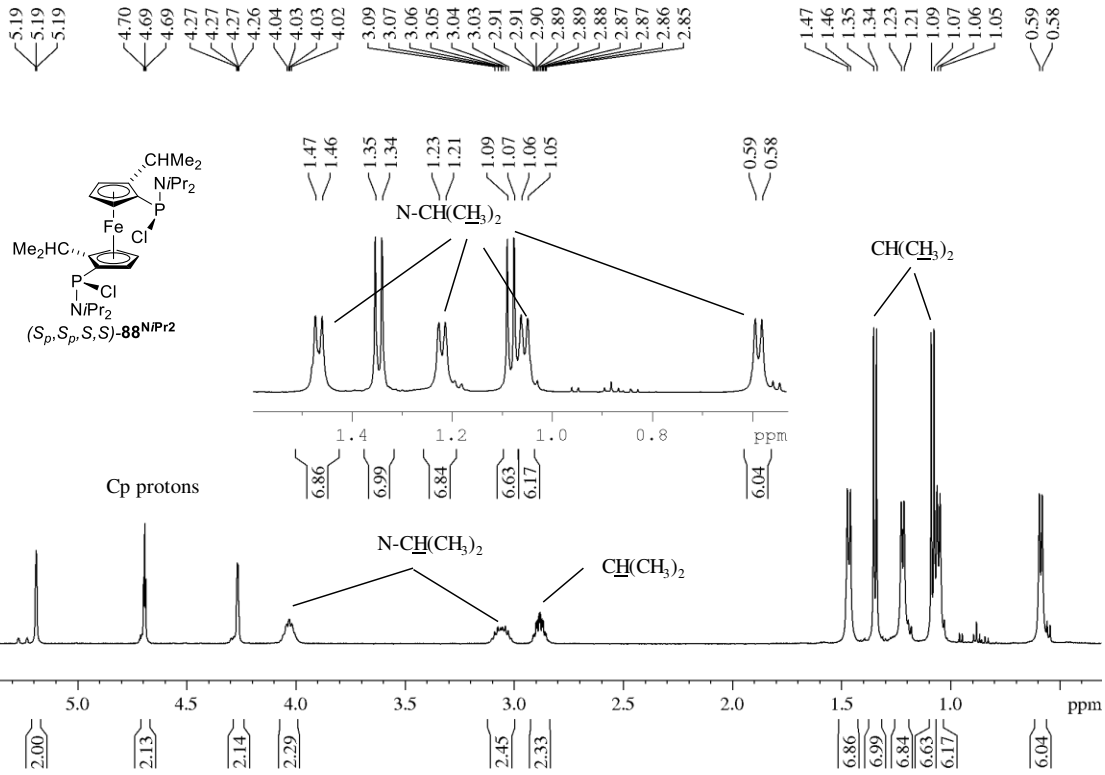

Figure 2-6. ^{1}H NMR spectrum (500 MHz) of the chiral 1,1'-bis(phosphanyl)ferrocene (S_p,S_p,S,S)-**88**$^{\mathbf{NiPr2}}$.

In general, three possible isomers can be obtained in this reaction, which are shown in Figure 2-7. The formation of these isomers can be explained based on a S_N2-like nucleophilic substitution mechanism.[111,112] Nucleophilic substitution at trivalent phosphorus atom is one of the most common reactions in the synthesis of organophosphorus compounds. The substitution occurs through the formation of a pentacoordinated transition state, in which both the attacking and leaving group are in apical positions.[113]

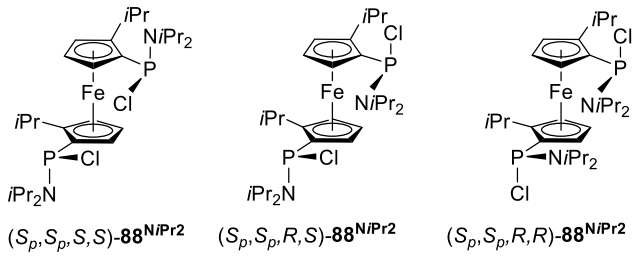

Figure 2-7. Possible diastereomers that could be generated from the reaction.

The first substitution on the upper lithiated Cp ring of (S_p,S_p)-**19**$^{\mathbf{Li}}$ can lead to 6 possible pentacoordinated transition states (Scheme 2-7). Three of the transition states generate *S*- and the other three generate *R*-isomers. Using steric reasons, one can explain why *S*-isomer is the dominant species in the mixture. Among the three transition states generating *R*-isomers (**TS1**, **TS3**, and **TS5**; Scheme 2-7), **TS1** has the lowest energy because the steric hindrance between iron and N*i*Pr$_2$ is absent. Using the same rationale, **TS2** has the lowest energy among **TS2**, **TS4**, and **TS6**. Between transition states **TS2** and **TS1**, the **TS2** has lower energy as there is no repulsion between Cl and *i*Pr group attached to Cp ring. This results in the formation of intermediate ***S*-I2**, which is the kinetic product. The nucleophilic substitution of the remaining Li atom can also be explained using the same rationale, resulting in the *S*-isomer as the dominant species. Overall, the synthesis of the 1,1'-bis(phosphanyl)ferrocene is selective, and the isolated compound (S_p,S_p,*S*,*S*)-**88**$^{\mathbf{NiPr2}}$ is also the most thermodynamically stable product based on its crystal structure.

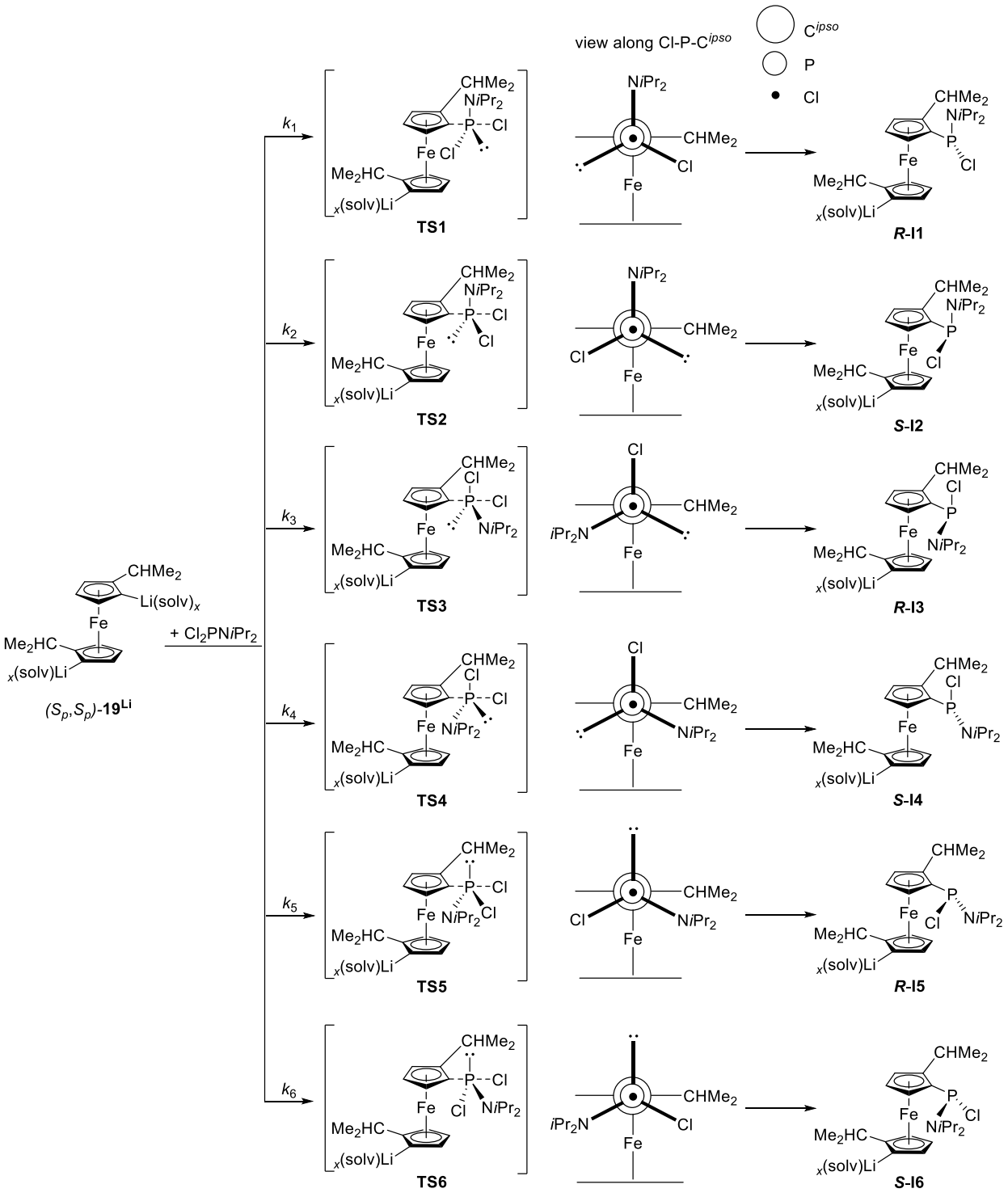

Scheme 2-7. Proposed reaction mechanism of the first substitution at phosphorus atom. Newman projection along the Cl–P–C^{ipso} bond of each transition state is shown.

Table 2-1. Crystal and structural refinement data for compound (S_p,S_p,S,S)-**88**$^{\mathbf{NiPr2}}$.

	(S_p,S_p,S,S)-**88**$^{\mathbf{NiPr2}}$
empirical formula	$C_{28}H_{48}Cl_2FeN_2P_2$
fw	601.37
cryst. size / mm^3	0.10 × 0.15 × 0.25
cryst. system	monoclinic
space group	C2
Z	2
a / Å	114871(7)
b / Å	9.9292(5)
c / Å	14.7360(9)
α / °	90
β / °	109.0810(10)
γ / °	90
volume / Å^3	1588.41(16)
ρ_{calc} / g cm^{-3}	1.257
temperature / K	173(2)
μ_{calc} / mm^{-1}	0.763
θ range / °	1.46 to 29.57
collected relections	34076
independent reflections	4470[R(int) = 0.0292]
absorption correction	multi-scan
data / restraints / params	4470/ 1 / 166
goodness-of-fit	1.195
R_1 [I > 2 σ(I)][a]	0.0258
wR_2 (all data)[a]	0.0806
largest diff. peak and hole, $\Delta\rho_{elect}$ / e Å^{-3}	0.453 and -0.467

[a] $R_1 = [\Sigma||F_o|-|F_c||]/[\Sigma|F_o|]$ for $[F_o^2 > 2\sigma(F_o^2)]$, $wR_2 = \{[\Sigma w(F_o^2-F_c^2)^2]/[\Sigma w(F_o^2)^2]\}^{1/2}$ [all data]

2.1.5 Synthesis and characterization of the chiral diphospha[2]ferrocenophanes (S_p,S_p,*R*,*R*)-90^{CH2SiMe3} and 90^{NiPr2}

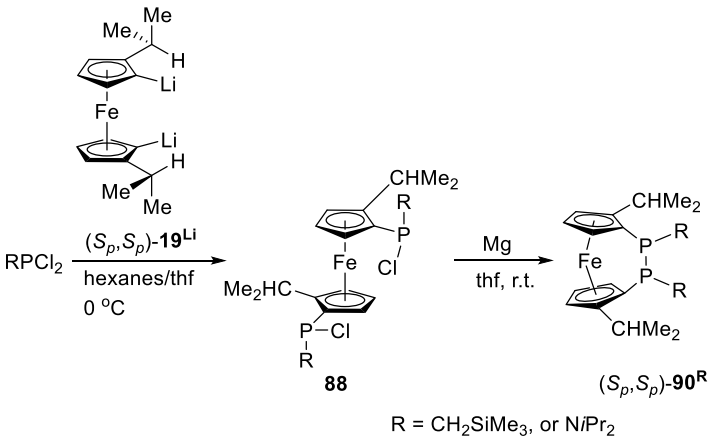

Scheme 2-8. Synthesis of the chiral diphospha[2]FCPs (S_p,S_p)-**90^{R}** (R = CH_2SiMe_3 or N*i*Pr_2).

In the first step, the same procedure as mentioned in section 2.1.4 was applied to synthesize the 1,1'-$(Me_3SiCH_2)_2fc^{iPr}$ (**88^{CH2SiMe3}**) (Scheme 2-8). The ^{31}P NMR spectrum of this reaction mixture shows that the phosphorus dihalide species $Cl_2PCH_2SiMe_3$ was completely consumed after 20 min of stirring, and signals of new compounds are detected. For example, the ^{31}P NMR spectrum shows one major signal at δ = 87.5 ppm, and one minor signal at 88.0 ppm, suggesting the presence of two diastereomers. These ^{31}P chemical shifts are quite close to those of the reported 1,1′-(*n*BuClP)$_2$fc and 1,1′-(PhClP)$_2$fc (fc = $(C_5H_4)_2Fe$) (δ = 95.2 and 77.6 ppm; respectively).[33] Attempts to isolate the diastereomeric mixture of **88^{CH2SiMe3}** by sublimation and crystallization methods were unsuccessful, thus the next step was conducted without purification. For the reductive coupling between the two phosphorus centers, a diastereomeric mixture of **88^{CH2SiMe3}** was allowed to react with magnesium turnings in thf. The ^{31}P NMR spectrum of the reaction mixture shows the presence of a new signal at δ = 2.0 ppm as the major component.

The reaction mixture was purified by FCC, then the orange fraction was collected and further purified by vacuum sublimation at 100 °C. Orange crystals were obtained from vacuum sublimation and were characterized by CHN elemental analysis, mass spectrometry, NMR spectroscopy, and single crystal X-ray diffraction analysis. The signal patterns of the ^{1}H and ^{13}C NMR spectra show that compound **90**$^{\mathbf{CH2SiMe3}}$ was successfully isolated as one single isomer, which possesses a two-fold symmetry. For example, in the ^{1}H NMR spectrum, three signals at δ = 4.94, 4.31, and 3.67 ppm are found for six Cp protons, indicating that **90**$^{\mathbf{CH2SiMe3}}$ has a two-fold symmetry with respect to the NMR time scale at ambient temperature (Figure 2-8). One of the methylene protons of the CH_2SiMe_3 group appears as a doublet of triplet (δ = 1.88 ppm; J = 13.7, 6.1 Hz), due to coupling with the other diastereotopic proton and two phosphorus atoms. Similarly, the signal of other methylene proton is a doublet of triplet (δ = 1.16 ppm; J = 13.7, 3.8 Hz). In the $^{13}C\{^{1}H\}$ NMR spectrum, Cp carbons at the *ipso* positions to phosphorus atom and *i*Pr groups are observed as two virtual triplets due to strong coupling with the two ^{31}P nuclei (δ = 72.1 and 105.4 ppm; respectively). These spectroscopic features are consistent with the formation of a P–P bond. The ^{31}P NMR spectrum shows only one signal at 2.0 ppm, indicating the formation of one single diastereomer.

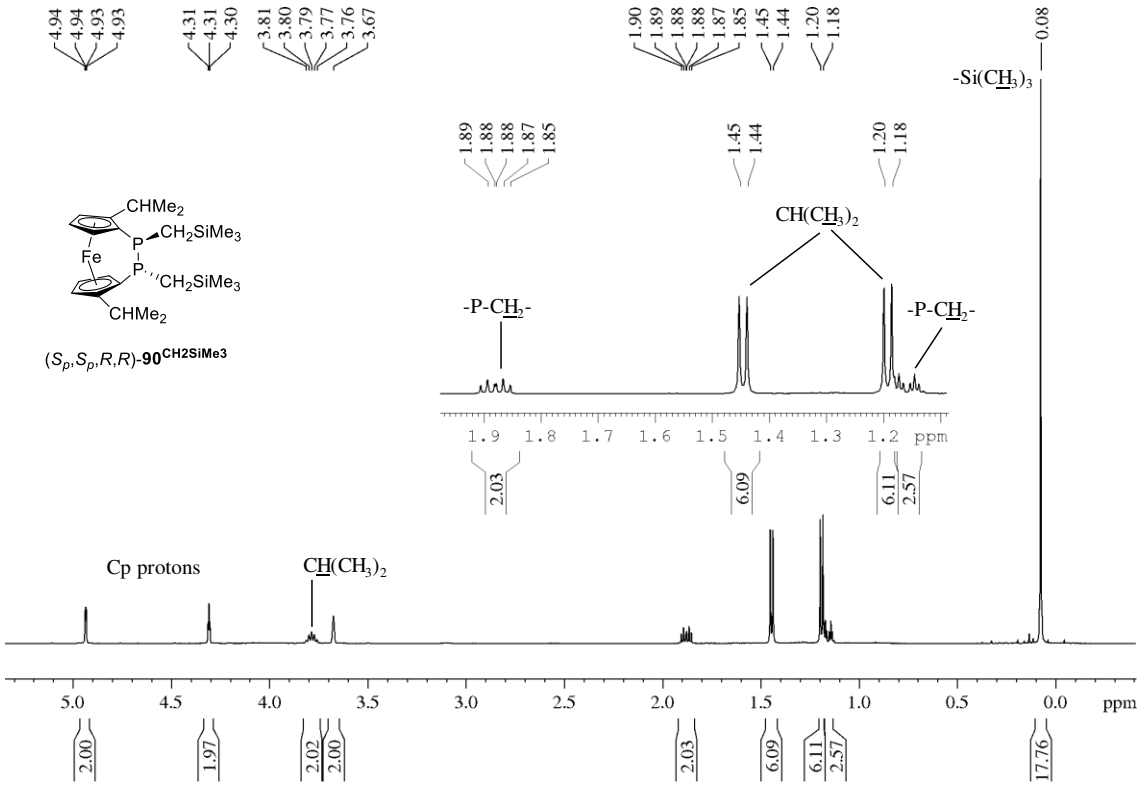

Figure 2-8. ^{1}H NMR spectrum (500 MHz) of the chiral diphospha[2]FCP (S_p,S_p,R,R)-**90**$^{\mathbf{CH2SiMe3}}$.

Species **90**$^{\mathbf{CH2SiMe3}}$ crystalizes in the orthorhombic space group $P2_12_12_1$, displaying *non*-symmetrical molecule (Figure 2-9). The two CH_2SiMe_3 groups on the phosphorus centers adopt a *trans* orientation with respect to the P–P bond, and both phosphorus atoms possess *R* configuration. This *trans* orientation was also observed for the previously reported diphospha[2]FCPs (**26**$^{t\mathbf{Bu}}$ and **26**$^{\mathbf{NEt2}}$).[33,67] By performing a density functional theory (DFT) calculation with the two configurations of $(PH)_2$-bridged [2]FCP, it was found that the *trans* configuration was more stable than the *cis* configuration.[33]

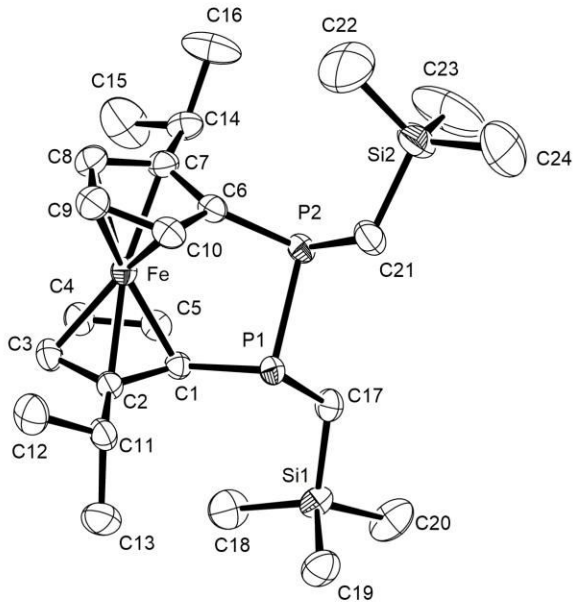

Figure 2-9. Molecular structure of (S_p,S_p,R,R)-**90**$^{\mathbf{CH2SiMe3}}$ with thermal ellipsoids at the 50% probability level. Hydrogen atom are omitted for clarity. Selected bond lengths [Å] and bond angles [°]: P1–C1 = 1.832(2); P2–C21 = 1.853(2); P1–P2 = 2.2402(8); P2–C6 = 1.828(2); C21–Si2 = 1.868(2); C21–P2–P1 = 98.71(8); C21–P2–C6 = 104.26(12); C6–P2–P1 = 97.60(7); P2–C21–Si2 = 116.73(13); C21–Si2–C24 = 110.67(19). For other bond lengths [Å] and angles [°] see Table 4–2.

The P–P bond length of (S_p,S_p,R,R)-**90**$^{\mathbf{CH2SiMe3}}$ of 2.2402(8) Å is almost identical to that of the known diphospha[2]FCPs **26**$^{\mathbf{tBu}}$ and **26**$^{\mathbf{NEt2}}$.[33,104] Despite having a relatively long P–P bond length (~ 2.1–2.3 Å) compared to the dibora[2]FCPs (~ 1.7 Å) and dicarba[2]FCPs (~ 1.3–1.9 Å),[28] diphospha[2]FCPs are still strained as the cyclopentadienyl ligands are tilted (α = 7.7–13.6°). According to the data shown in Table 2-2, the P–P bonds of diphospha[2]FCPs are shorter than the Si–Si bond of disila[2]FCP **91** (~ 2.35 Å; Table 2-2), consistent with the smaller

covalent radius of phosphorus atoms compared to silicon atoms. Shorter E–E bonds tend to make the ferrocene unit more distorted, therefore, the α angles of diphospha[2]FCP are larger than that of the disila[2]FCP **91** (around 4°).

Table 2-2. Geometry parameters of selected [2]FCPs tethered with an E–E bond.

Compound	E	E–E distance	α	Ref.
(S_p,S_p,R,R)-**90**^{CH2SiMe3}	P	2.2402(8)	12.2	This work
26^{tBu}	P	2.2502(8)	13.6	[33]
26^{NEt2}	P	2.229	12.6	[104]
24	P	2.219(1)	7.7	[66]
91	Si	2.3535(9)	4.2	[114]
92^{CH2}	C	1.539(12)	21.6	[115, 28]
92^{CMe2}	C	1.584(14)	23.3	[28, 115]

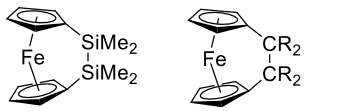

91 **92** (R = H, Me)

Figure 2-10. [2]FCPs with Si and C as bridging elements.

Table 2-3. Crystal and structural refinement data for compound (S_p,S_p,R,R)-**90**$^{\mathbf{CH2SiMe3}}$.

Compound (S_p,S_p,R,R)-**90**$^{\mathbf{CH2SiMe3}}$	
empirical formula	$C_{24}H_{42}FeP_2Si_2$
fw	504.54
cryst. size / mm^3	0.35 × 0.30 × 0.25
cryst. system	orthohombic
space group	$P2_12_12_1$
Z	4
a / Å	10.4123(5)
b / Å	12.2936(6)
c / Å	22.4168(12)
α / °	90
β / °	90
γ / °	90
volume / Å^3	2869.5(2)
ρ_{calc} / g cm^{-3}	1.168
temperature / K	173(2)
μ_{calc} / mm^{-1}	0.729
θ range / °	3.143 to 28.714
collected relections	30858
independent reflections	7405 [R(int) = 0.0262]
absorption correction	multi-scan
data / restraints / params	7405 / 0 / 273
goodness-of-fit	1.031
R_1 [I > 2 σ(I)][a]	0.0266
wR_2 (all data)[a]	0.0673
largest diff. peak and hole, $\Delta\rho_{elect}$ / e Å^{-3}	0.322 and -0.371

[a] $R_1 = [\Sigma||F_o|-|F_c||]/[\Sigma|F_o|]$ for $[F_o^2 > 2\sigma(F_o^2)]$, $wR_2 = \{[\Sigma w(F_o^2-F_c^2)^2]/[\Sigma w(F_o^2)^2]\}^{1/2}$ [all data]

The synthesis of diphospha[2]FCP **90**$^{\mathbf{NiPr2}}$ was carried out following the same method as that used for compound (S_p,S_p,*R*,*R*)-**90**$^{\mathbf{CH2SiMe3}}$. NMR spectroscopic data of the reaction mixture also show species 1,1'-(N*i*Pr$_2$)$_2$fc$^{i\mathrm{Pr}}$ (**88**$^{\mathbf{NiPr2}}$) as the major component. Without any purification, the crude mixture of **88**$^{\mathbf{NiPr2}}$ was allowed to react with magnesium turnings for the reductive coupling between the two phosphorus atoms. After stirring for 12 h, the ^{31}P{^{1}H} NMR signals of mixture of diastereomers **88**$^{\mathbf{NiPr2}}$ at δ = 123.3 ppm disappear and only a signal at δ = 11.7 ppm appears, indicating that the stereoselective formation of species **90**$^{\mathbf{NiPr2}}$ occurs. The produced diphospha[2]FCP **90**$^{\mathbf{NiPr2}}$ was obtained as an orange solid after purification by FCC and vacuum sublimation at 135 °C. Compound **90**$^{\mathbf{NiPr2}}$ was characterized by NMR spectroscopy, mass spectrometry, and CHN elemental analysis. In the ^{1}H NMR spectrum, three signals are found for six Cp protons at δ = 4.71, 4.27, and 3.99 ppm (Figure 2-11), revealing that species **90**$^{\mathbf{NiPr2}}$ has a two-fold symmetry element with respect to the NMR time scale. In the ^{13}C{^{1}H} NMR spectrum, the two *ipso*-carbon atoms attached to the *i*Pr group and phosphorus atom appear as two virtual triplets (δ = 105.0 and 67.9 ppm; respectively), owing to the two ^{31}P nuclei strongly coupling through the direct bond. This is similar to what was observed for species (S_p,S_p,*R*,*R*)-**90**$^{\mathbf{CH2SiMe3}}$. Crystal structure of species **90**$^{\mathbf{NiPr2}}$ was not obtained, thus the configuration of phosphorus atoms was not assigned. However, it was reported that the related NEt$_2$-diphospha[2]FCP **26**$^{\mathbf{NEt2}}$ had a *trans* configuration,[104] hence, the compound **90**$^{\mathbf{NiPr2}}$ might also adopt the same configuration. On the other hand, it can be assumed that the two N*i*Pr$_2$ groups on phosphorus atoms should be located away from each other, and also be away from the *i*Pr groups attached to Cp rings to avoid the steric congestion.

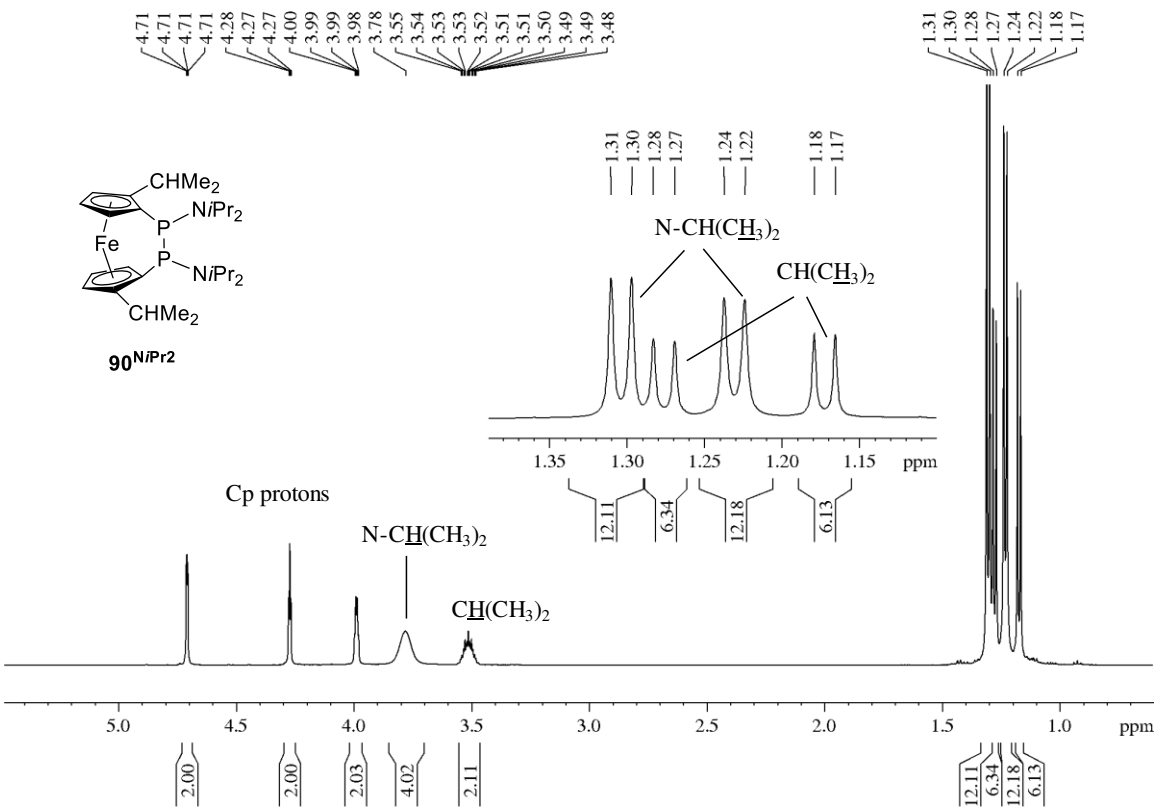

Figure 2-11. ^{1}H NMR spectrum (500 MHz) of the chiral diphospha[2]FCP **90**$^{\mathbf{NiPr2}}$.

2.2 Anionic ring-opening polymerization

As discussed in the Introduction (section 1.2.4.2), anionic ROP of strained ferrocenophanes is one of the most advanced methods to obtain well-defined metallopolymers. This type of living ROP is one of the most "painstaking" methods for polymerization. For example, it requires extremely rigorous purification of monomers, solvents, and other reagents to be used, as well as complete removal of oxygen, moisture, and other impurities from the polymerization system. In order to apply the right techniques on the polymerization of the new chiral phospha[1]FCPs, it is important to test the ability to reproduce the published data. Thus, the anionic ROP of the known phospha[1]FCP **11**$^{\mathbf{Ph}}$ was repeated following literature,[38,42] and the results were analyzed and

compared to the reported data. The same technique used for anionic ROP of the known compound **11^{Ph}** was applied to the chiral phospha[1]FCPs (S_p,S_p)-**20**.

2.2.1 Anionic ring-opening polymerization of the known phospha[1]ferrocenophane 11^{Ph}

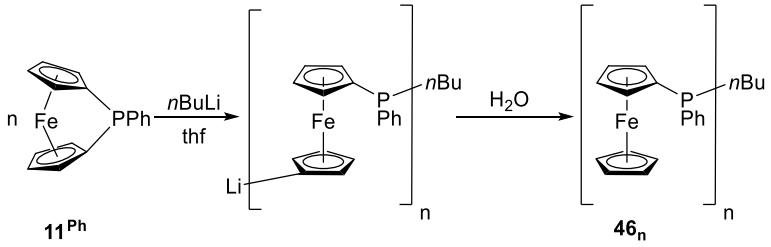

Scheme 2-9. Anionic ring-opening polymerization of the phospha[1]FCP **11^{Ph}**.

Anionic ROP of the known compound **11^{Ph}** was performed with different amounts of *n*BuLi (monomer/initiator = 1/1 to 20/1) (Scheme 2-9). The result with a monomer/initiator ratio of 11/1 is shown below as an example. After addition of *n*BuLi, the reaction mixture was stirred for 30 min at r.t., and the color of the solution slowly turned from dark-red to dark-brown while stirring. ^{31}P NMR spectrum of the reaction mixture taken after 30 min shows that all the monomer was consumed. After degassed H_2O was added to quench all the active species, the mixture was precipitated into stirred hexanes, resulting in a yellow precipitate. The ^{1}H and ^{31}P NMR spectroscopic data of the precipitates show the formation of polymeric product, and its NMR chemical shifts are similar to the reported data.[38,42] For example, the ^{1}H NMR spectrum shows broad signals in the range of δ = 4.37–4.89 ppm, corresponding to Cp rings. The ^{31}P NMR spectrum shows two sets of signals, one at δ = –29.0 ppm for the phosphorus atom attached to the *n*Bu group, and a second one in the δ range of –31.7 to –31.9 ppm for the phosphorus atoms on the main chain of the polymer. The relative intensity of these two sets of signals is ca. 1/11, which confirmed that the targeted transformation has occurred cleanly.

2.2.2 Anionic ring-opening reactions of the chiral phospha[*n*]ferrocenophanes (S_p,S_p)-**86**^{CH2SiMe3} and (S_p,S_p,*R*,*R*)-**90**^{CH2SiMe3}

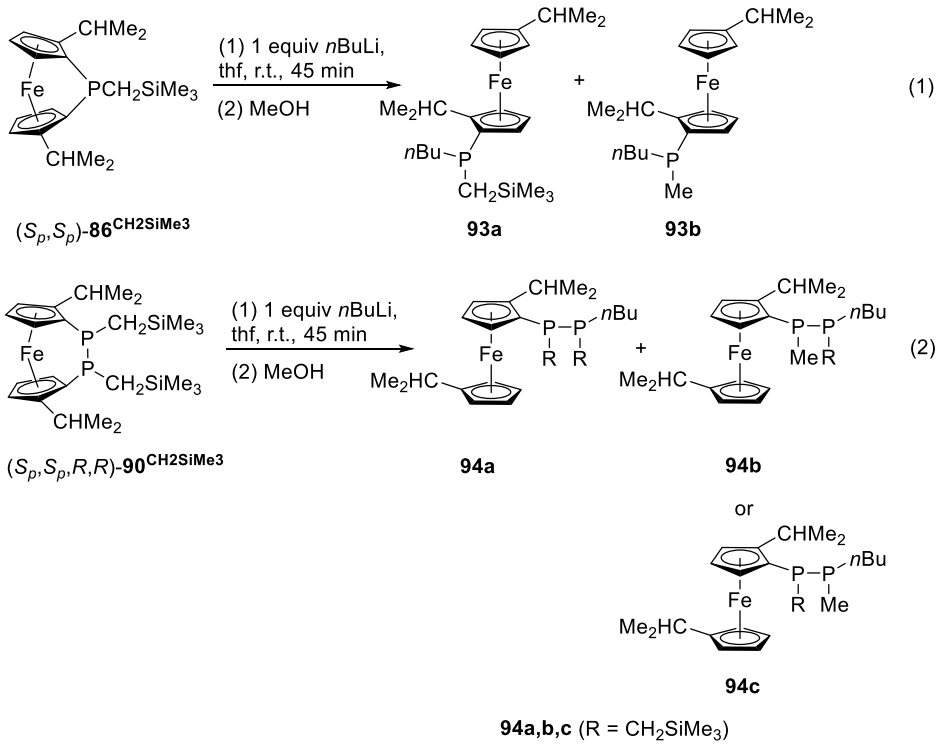

Scheme 2-10. Anionic ring-opening reactions of (S_p,S_p)-**86**^{CH2SiMe3} and (S_p,S_p,*R*,*R*)-**90**^{CH2SiMe3} with 1.0 equiv of *n*BuLi. Each of the compound **93a**, **93b**, **94a**, **94b**, and **94c** are a mixture of diastereomers.

Anionic ring-opening reactions were performed on the chiral phospha[1]FCP (S_p,S_p)-**86**^{CH2SiMe3} and diphospha[2]FCP (S_p,S_p,*R*,*R*)-**90**^{CH2SiMe3} with monomer/initiator ratio of 1/1. The reaction mixture was reacted with degassed MeOH to neutralize all the active species (Scheme 2-10). Mass spectra of the reaction mixture 1 show two major signals with molecular weights of 444.14 and 372.12, corresponding to the proposed compounds **93a** and **93b**, respectively. For reaction 2, its mass spectroscopic data shows **94a** and **94b** as the major compounds, along with the unreacted monomer (S_p,S_p,*R*,*R*)-**90**^{CH2SiMe3}. Due to phosphorus being a stereogenic centre, each compound **93a**, **93b**, **94a**, and **94b** was a diastereomeric mixture of products. It was expected to

obtain 4 diastereomers in the reaction 1, and 8 diastereomers in the reaction 2. However, the ^{31}P NMR spectrum of reaction 1 shows two signals at δ = –53.3 and –55.1 ppm, with approximate ratio of 3 to 1 (Figure 2-12). It is likely that these two ^{31}P NMR signals representing the two diastereomers of species **93a**, due to their very close ^{31}P chemical shifts (δ = –53.3 and –55.1 ppm). The absence of NMR signals from mixture **93b** was likely due to their trace amounts in the reaction mixture. Presumably, the diastereomeric mixture **93a** was generated first, and the formation of mixture **93b** was just a side reaction from **93a**. The ^{1}H NMR spectra of reaction 1 also show mainly two species with ratio of 3 to 1.

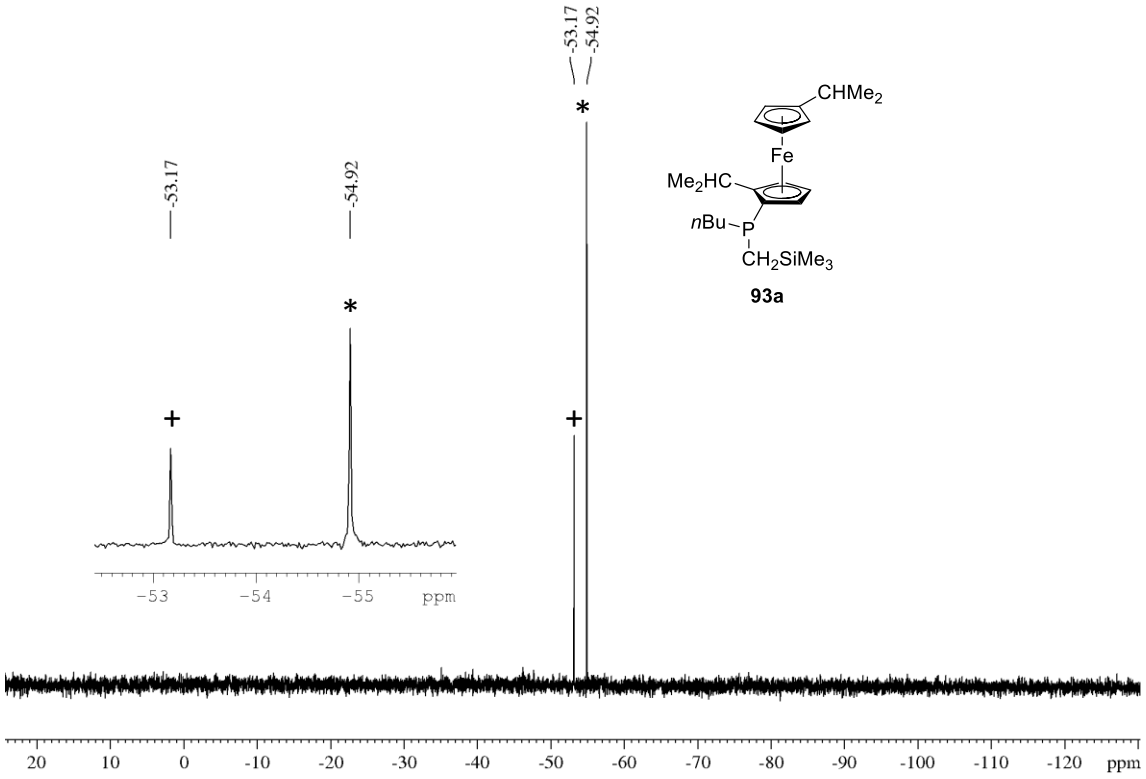

Figure 2-12. $^{31}P\{^{1}H\}$ NMR spectrum (202.5 MHz) of the reaction mixture illustrated equation 1 (Scheme 2-10). The signals of two diastereomers of **93a** are marked with * and +.

On the other hand, 7 signals were observed in the ^{31}P NMR spectra of reaction 2 (δ = 2.0, –46.8, –47.3, –60.7, –124.9, –125.2, and –141.6 ppm). Beside the signal of the unreacted

monomer (S_p,S_p,R,R)-**90**$^{\mathbf{CH2SiMe3}}$ at δ = 2.0 ppm, it can be assumed that the other signals are caused by the presence of different diastereomers of the mixture **94a** and **94b**.

Both **93a** and **94a**, respectively (reaction 1 and 2; Scheme 2-10), are the targeted compounds of the ring-opening reactions. However, the presence of other species (**93b** and **94b**, or **94c**; Scheme 2-10) indicated that the anionic ring-opening reactions are not clean. Compounds **93b** and **94b** are also the ring-opened products, but one of the $SiMe_3$ group was removed. Scheme 2-11 shows a proposed pathway for the formation of species **93b**. First, the ring-opened species **93**$^{\mathbf{Li}}$ is generated in the initiation step. Next, it is assumed that nucleophilic attack of *n*BuLi to the $SiMe_3$ group of **93**$^{\mathbf{Li}}$ leads to dissociation of the $SiMe_3$ group from the PCH_2 moiety (**93**$^{\mathbf{CH2Li}}$; Scheme 2-11). The PCH_2–Li bond of species **93**$^{\mathbf{CH2Li}}$ is then likely hydrolyzed by a proton source (MeOH) to yield compound **93b**. Following the same pathway, the formation of compound **94b** can also be similarly explained.

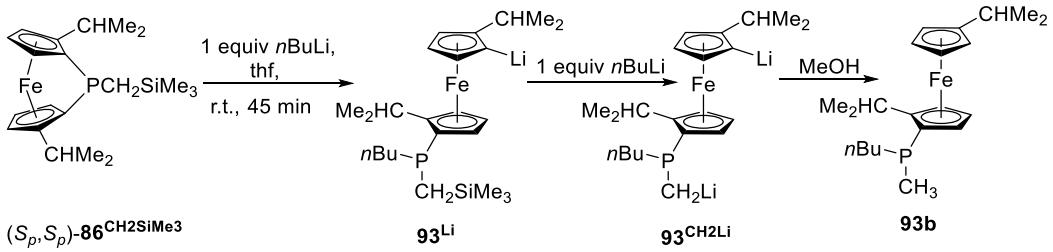

Scheme 2-11. Proposed pathway for the formation of compound **93b**.

The reaction between *n*BuLi and compounds of group 14 element is known in the literature with Li/Sn exchange as the most common one.[116,117] For example, the transmetalation reaction between $(CH_3)_2NCH_2Sn(n\text{-}C_4H_9)_3$ and *n*BuLi led to the formation of $(CH_3)_2NCH_2Li$,[116] in which the $Sn(n\text{-}C_4H_9)_3$ group was removed. However, Li/Si exchange is not quite common. Therefore, the mechanism illustrated in Scheme 2-11 is just an assumption for the formation of species **93b** and **94b**.

Anionic ROP was also attempted on the compound (S_p,S_p)-**86**$^{\mathbf{CH2SiMe3}}$. After 4 h of stirring, the ^{31}P NMR spectra of the reaction mixture of 4/1 monomer/initiator ratio shows mainly two signals at δ = –4.2 and –54.9 ppm, corresponding to the unreacted monomer (S_p,S_p)-**86**$^{\mathbf{CH2SiMe3}}$ and the ring-opened mixture **93a**. Based on the ^{31}P NMR spectrum, approximately 25% of monomer was consumed and transformed into the ring-opened mixture **93a**, along with the formation of other unidentified compounds. Similarly, the reaction at 10/1 monomer/initiator ratio shows that only 10% of monomer was reacted and converted to other unidentified species. No polymeric products could be isolated from these reactions. Presumably, there were two factors that can lead to the unsuccessful ROP of these compounds: the side reaction between the $SiMe_3$ group and *n*BuLi, and the steric repulsion between substituents of the monomer (S_p,S_p)-**86**$^{\mathbf{CH2SiMe3}}$ and the lithium species **93**$^{\mathbf{Li}}$ that hinders the propagation step.

Obviously, the phospha[*n*]FCPs (S_p,S_p)-**86**$^{\mathbf{CH2SiMe3}}$ and (S_p,S_p,*R*,*R*)-**90**$^{\mathbf{CH2SiMe3}}$ equipped with CH_2SiMe_3 groups are unsuitable for the anionic ROP initiating by *n*BuLi. To avoid these problems, ring-opening reactions of the phospha[1]FCP (S_p,S_p)-**20**$^{\mathbf{Ph}}$ were investigated and the results are discussed in the next section.

2.2.3 Investigations on anionic ring-opening reactions of chiral phospha[1]ferrocenophanes with different substituents on a phosphorus atom

2.2.3.1 Anionic ring-opening reactions of the chiral phopha[1]ferrocenophane (S_p,S_p)-20^{Ph} and identification of the ring-opened product (S_p,R)-95^{S}

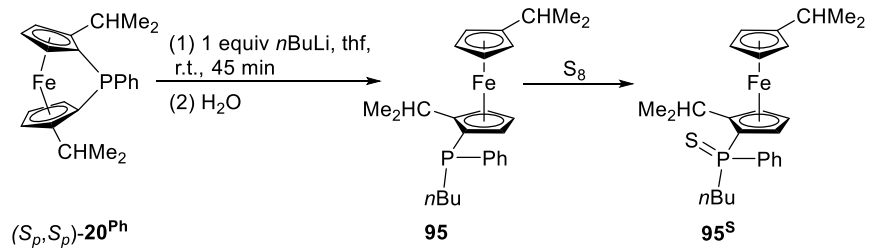

Scheme 2-12. Anionic ring-opening reaction of the chiral phospha[1]FCP (S_p,S_p)-**20^{Ph}** with 1.0 equiv of *n*BuLi.

After the addition of 1.0 equiv of *n*BuLi to the solution of (S_p,S_p)-**20^{Ph}**, the color of reaction mixture slowly turned from dark-red to orange. After 45 min of stirring, the reaction mixture was quenched with H_2O and the resulting compound was analyzed by NMR spectroscopy and mass spectrometry. Due to the presence of a P-stereogenic centre, it was expected that the reaction mixture would contain two isomers. Both ^{1}H and ^{31}P NMR spectra supported that expectation. For example, the ^{1}H NMR spectrum of the mixture **95** shows two sets of signals in the Cp range with ratio of 3 to 1, indicating two diastereomers (Figure 2-13). Both sets show seven signals each and are partially overlapping. The ^{31}P NMR spectrum also shows two distinct signals at δ = –35.7 (minor isomer) and –35.9 ppm (major isomer), and the ratio of 3 to 1 was determined by inverse gated decoupling ^{31}P NMR spectroscopy (Figure 2-14).[118]

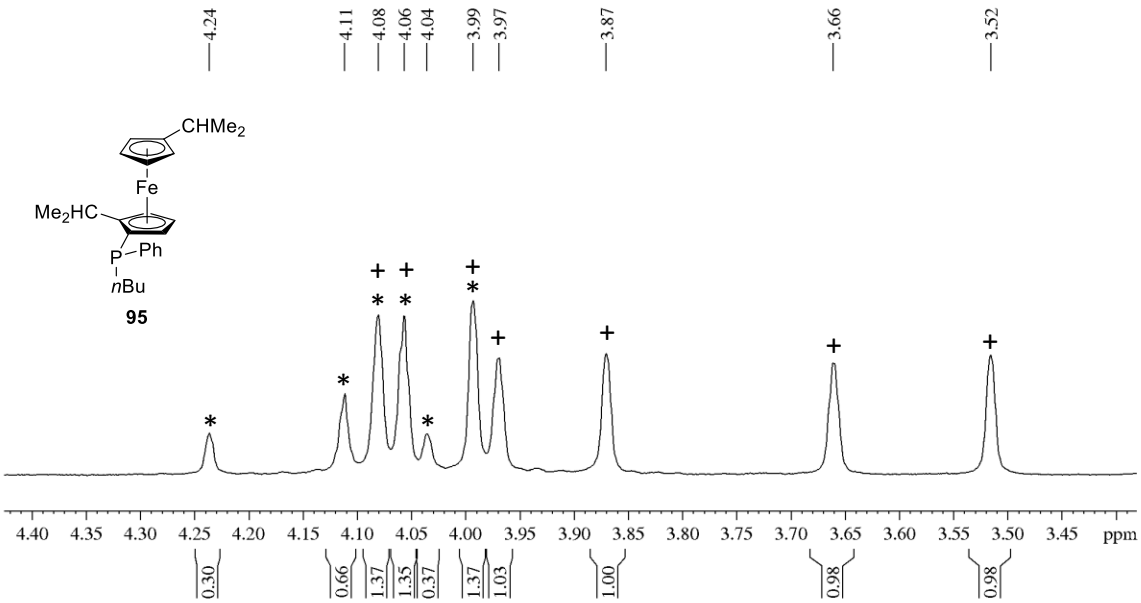

Figure 2-13. ^{1}H NMR spectrum (600 MHz) of Cp range of the mixture **95**. The two diastereomers are marked with * and +, respectively.

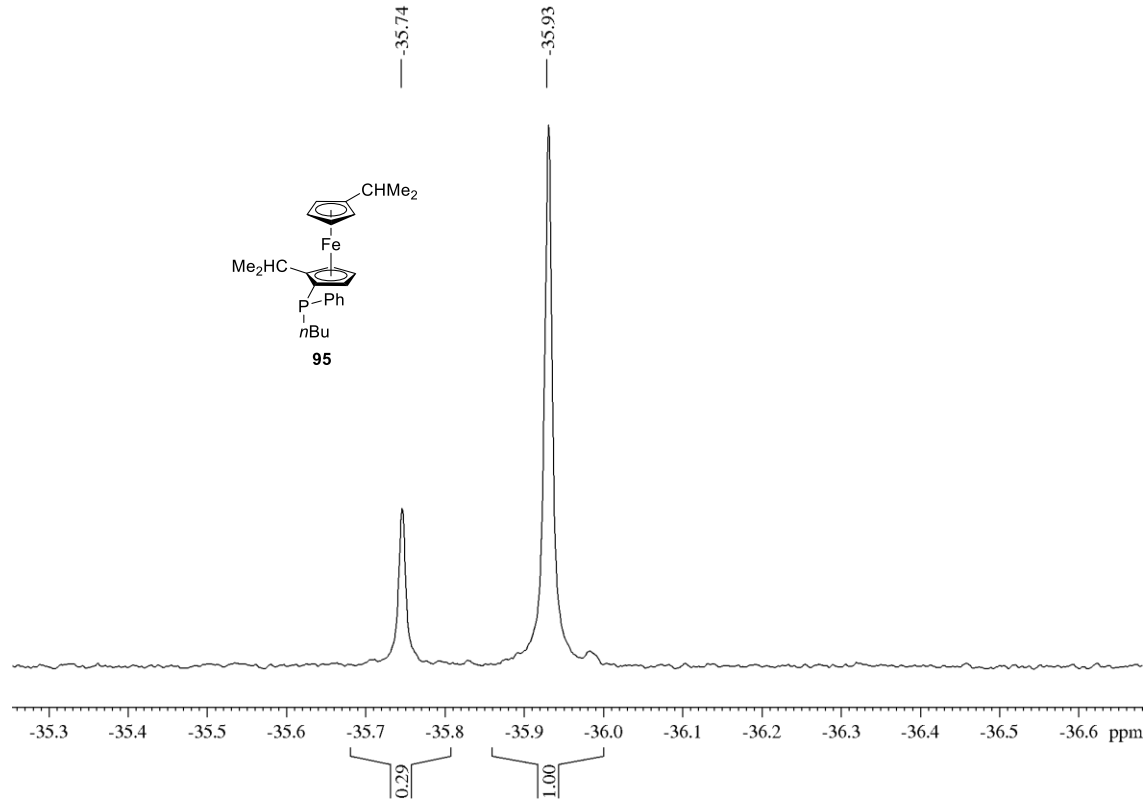

Figure 2-14. Inversed gated ^{31}P{^{1}H} NMR spectrum (243 MHz) of the mixture **95**.

Attempts to separate the two isomers from the mixture **95** by crystallization were unsuccessful. Therefore, the mixture **95** was sulfurized to obtain air-stable products, which were expected to facilitate their isolation and characterization (Scheme 2-12). ^{31}P NMR spectrum of the sulfurized mixture **95^{S}** shows two signals at δ = 42.4 and 39.9 ppm with ratio of 3 to 1, respectively (Figure 2-15).

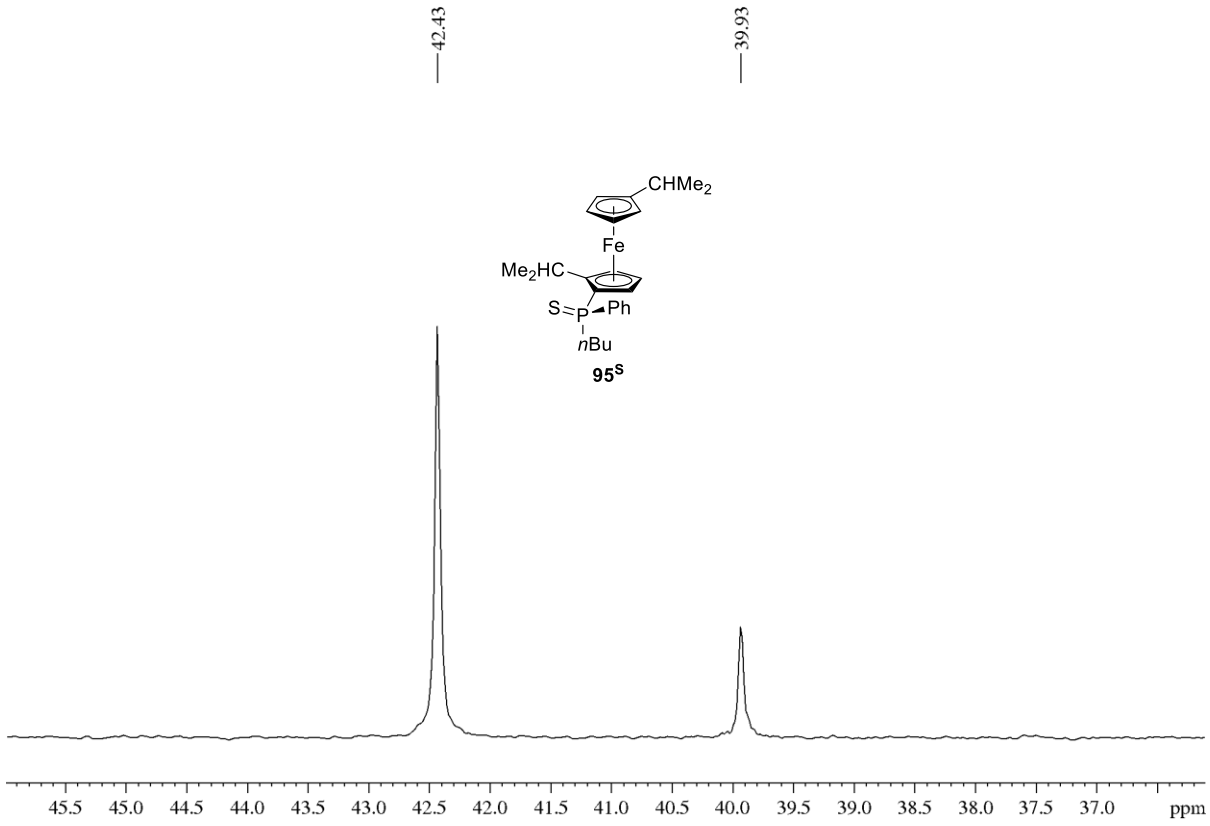

Figure 2-15. Inversed gated ^{31}P{^{1}H} NMR spectrum (243 MHz) of the sulfurized mixture **95^{S}**.

A hexanes solution of the sulfurized mixture **95^{S}** was left for crystallization, and the isolated crystals were characterized by NMR spectroscopy, mass spectroscopy and single-crystal X-ray analysis. The crystal structure shows that the isolated species is the major compound in the mixture **95^{S}** (δ = 42.4 ppm) which crystalizes in the orthorhombic space group $P2_12_12_1$, displaying a *non*-symmetrical species. According to its crystal structure, the *n*Bu group is almost

perpendicular to the Cp rings and located away from the ferrocene unit. In contrast, the phenyl group is in the close proximity of ferrocene moiety, while sulfur is pointed towards one of the *i*Pr groups attached to Cp ring. The configuration at phosphorus atom was determined as *R*.

The NMR spectroscopic data of this isolated species (S_p,*R*)-**95**$^{\mathbf{S}}$ is also in agreement with what was observed in the crystal structure. For example, the ^{1}H NMR spectrum shows 7 Cp protons (δ = 3.82, 3.91, 3.94, 3.99, 4.13, 4.41, 4.43 ppm), indicating an asymmetric species (Figure 2-16). The two methine protons of the two *i*Pr groups appear as two septets at δ = 4.10 and 2.06 ppm. The downfield signal at δ = 4.10 is likely caused by the sulfur atom, which is in close proximity with one of the *i*Pr groups. Four CH_3 groups of the two *i*Pr groups appear as four doublets at δ = 1.36, 1.25, 0.90, and 0.88 ppm. The (S_p,*R*)-**95**$^{\mathbf{S}}$ isomer shows one signal at δ = 42.3 in the ^{31}P NMR spectrum. The minor isomer, which resonates at δ = 39.9 ppm in the ^{31}P NMR spectrum, did not crystallize and remained dissolved in the mother liquor.

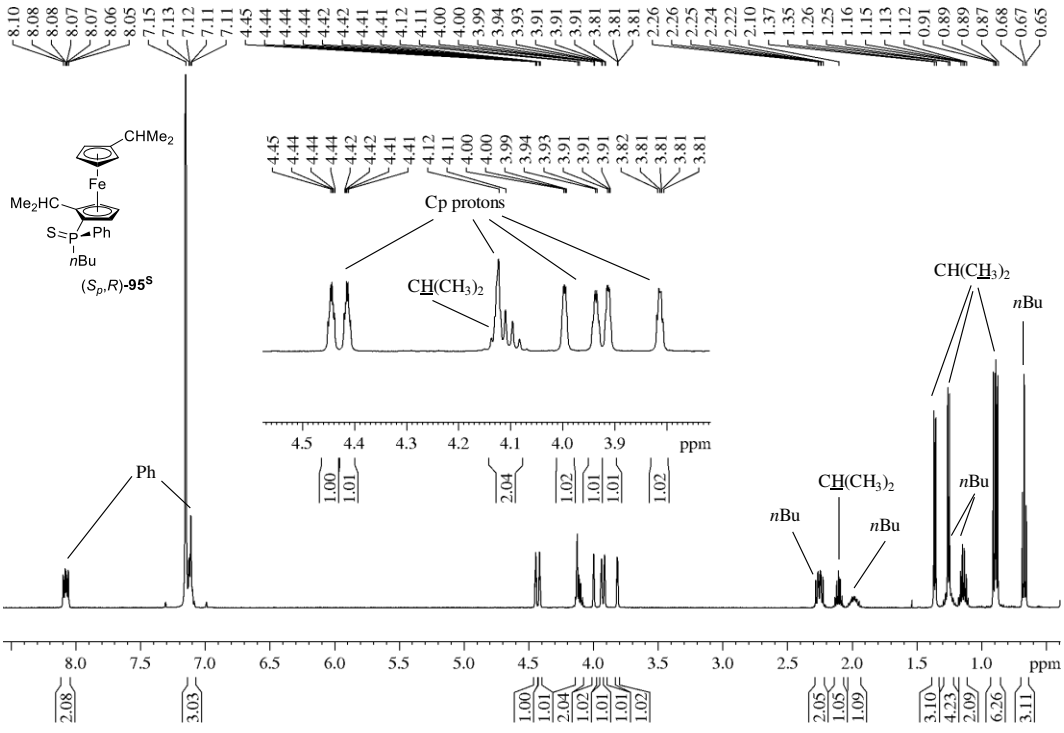

Figure 2-16. ^{1}H NMR spectrum (500 MHz) of the chiral phosphine ligand (S_p,*R*)-**95**$^{\mathbf{S}}$.

Compound (S_p,R)-**95**^{S} was the major isomer isolated from the 3 to 1 mixture. To explain this, two isomers of the non-sulfurized mixture **95** and the Newman projections of their conformers are shown in Figure 2-17.

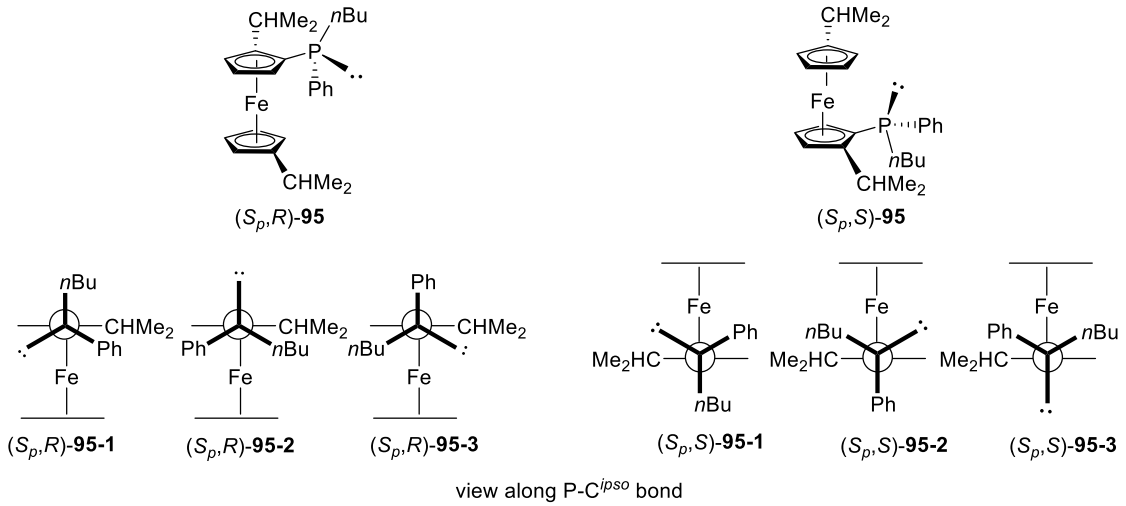

Figure 2-17. Illustration of the two resulting isomers (S_p,R)-**95** and (S_p,S)-**95**. Newman projections along P–C^{ipso} bond of conformers are shown.

Among three conformers of the (S_p,R)-**95** isomer, (S_p,R)-**95-3** is thermodynamically more stable than the others, due to the absence of steric repulsion between substituents on phosphorus with the *i*Pr group of Cp ring. Using the same rationale, (S_p,S)-**95-1** is thermodynamically more stable than other conformers of the (S_p,S)-**95** isomer. In (S_p,R)-**95-3** and (S_p,S)-**95-1**, the substituents perpendicular to Cp ring have no steric repulsion with iron, whereas the ones in close proximity of Fe can have a steric repulsion with Fe. Considering that, as the *n*Bu group has different conformers which can twist to interact with Fe, it can be assumed that the steric repulsion between *n*Bu and Fe in (S_p,R)-**95-3** is larger than that between Ph and Fe in (S_p,S)-**95-1**. Therefore, the conformer (S_p,S)-**95-1** of the *S*-isomer is thermodynamically more stable than that of the *R*-isomer. After sulfurization, the priority of the two sulfurized diastereomers change,

because the sulfur atom takes place the position of the lone pair on phosphorus atom (Scheme 2-13).

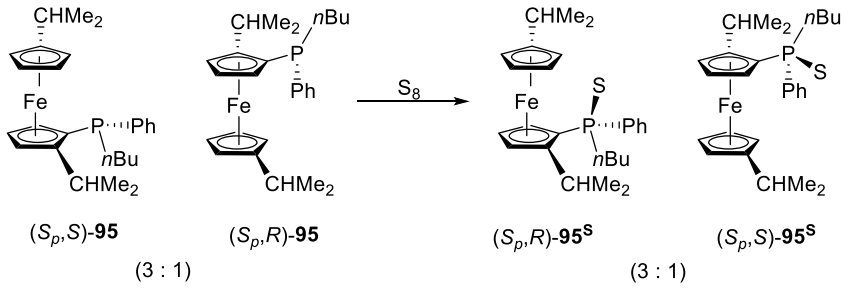

Scheme 2-13. Sulfurization of the diastereomeric mixture **95**.

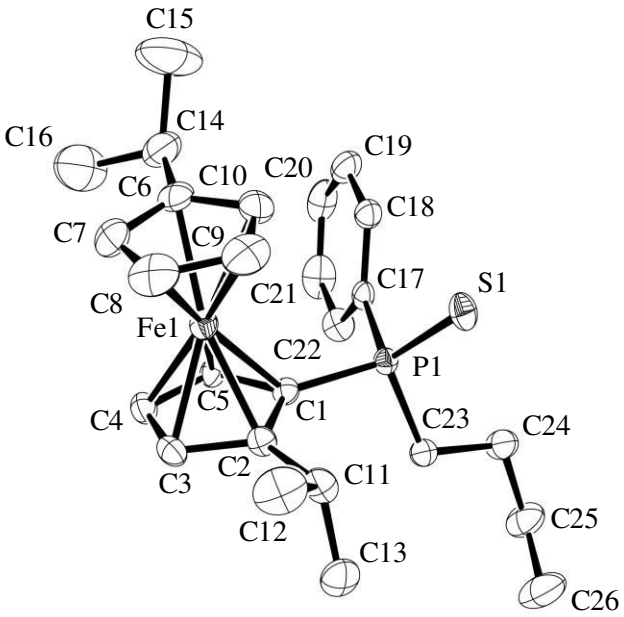

Figure 2-18. Molecular structure of (S_p,R)-**95**$^{\mathbf{S}}$ with thermal ellipsoids at the 50% probability level. Hydrogen atoms are omitted for clarity. Selected bond lengths [Å] and bond angles [°]: C1–P1 = 1.801(3); P1–S1 = 1.9569(9); P1–C18 = 1.820(2); P1–C23 = 1.819(2); C6–C14 = 1.512(4); C1–P1–C18 = 103.75(11); C18–P1–C23 = 106.28(12); C1–P1–C23 = 103.16(11); S1–P1–C23 = 113.18(9). For further bond lengths [Å] and angles [°] see Table 4–3.

Table 2-4. Crystal and structural refinement data for (S_p,*R*)-**95**$^{\mathbf{S}}$.

Compound (S_p,*R*)-**95**$^{\mathbf{S}}$	
empirical formula	$C_{26}H_{35}FePS$
fw	466.42
cryst. size / mm^3	0.60 × 0.11 × 0.07
cryst. system	orthohombic
space group	$P2_12_12_1$
Z	4
a / Å	8.4030(3)
b / Å	12.9561(4)
c / Å	22.4518(7)
α / °	90
β / °	90
γ / °	90
volume / $Å^3$	2444.33(14)
ρ_{calc} / g cm^{-3}	1.267
temperature / K	183(2)
μ_{calc} / mm^{-1}	0.778
θ range / °	3.143 to 27.378
collected reflections	33646
independent reflections	5445 [R(int) = 0.0319]
absorption correction	multi-scan
data / restraints / params	5445 / 0 / 267
goodness-of-fit	1.046
R_1 [I > 2 σ(I)][a]	0.0273
wR_2 (all data)[a]	0.0619
largest diff. peak and hole, $\Delta\rho_{elect}$ / e $Å^{-3}$	0.264 and -0.199

[a] $R_1 = [\Sigma||F_o|-|F_c||]/[\Sigma|F_o|]$ for $[F_o^2 > 2\sigma(F_o^2)]$, $wR_2 = \{[\Sigma w(F_o^2-F_c^2)^2]/[\Sigma w(F_o^2)^2]\}^{1/2}$ [all data]

Based on the successful ring-opening reaction of compound (S_p,S_p)-**20^{Ph}** with 1.0 equiv of *n*BuLi, anionic ROP with monomer/initiator ratios of 2/1 and 4/1 were attempted (Scheme 2-14). After 4 h of stirring, the crude mixture was quenched with water to neutralize all the active species.

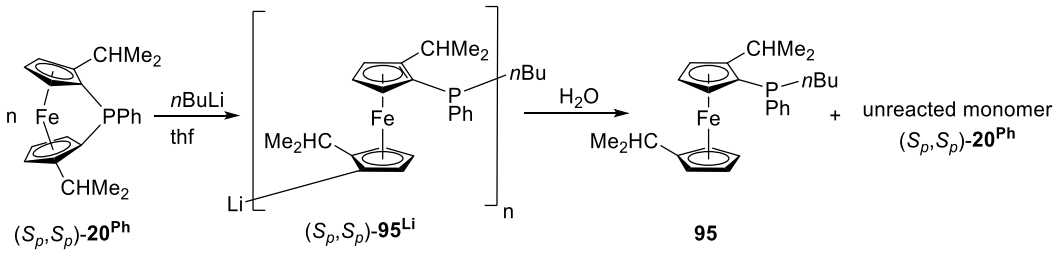

Scheme 2-14. Attempted anionic ROP of (S_p,S_p)-**20^{Ph}** with 1/n equiv of *n*BuLi.

NMR spectroscopic data showed that the reactions did not go to completion. For example, when using monomer/initiator ratio of 2/1, ^{31}P NMR spectra of the crude mixture show signals at δ = 8.3, –35.8, and –36.01 ppm, representing the unreacted monomer (S_p,S_p)-**20^{Ph}** and the diastereomeric mixture **95**, respectively. Besides these major signals, another weak signal at δ = –33.3 ppm was also observed in the ^{31}P NMR spectrum. It is assumed that this signal is from the dimer species generating in propagation step. According to ^{1}H NMR spectrum, only about 40% of the monomer was reacted and converted to the ring-opened mixture **95** (Figure 2-19). For the reaction using monomer/initiator ratio of 4/1, beside the unreacted monomer (S_p,S_p)-**20^{Ph}** and 20% of the ring-opened mixture **95**, there was no detection of other species. Obviously, in these anionic ROP reactions, the formed ring-opened species **95** could not continue to react in propagation step. This raised the question if the lithium-containing species (S_p,S_p)-**95^{Li}** is stable under the applied condition so that it could react with further monomer to start a chain-growth process. Additional work was done to get more information about the stability of lithium species (S_p,S_p)-**95^{Li}** in the reaction mixture.

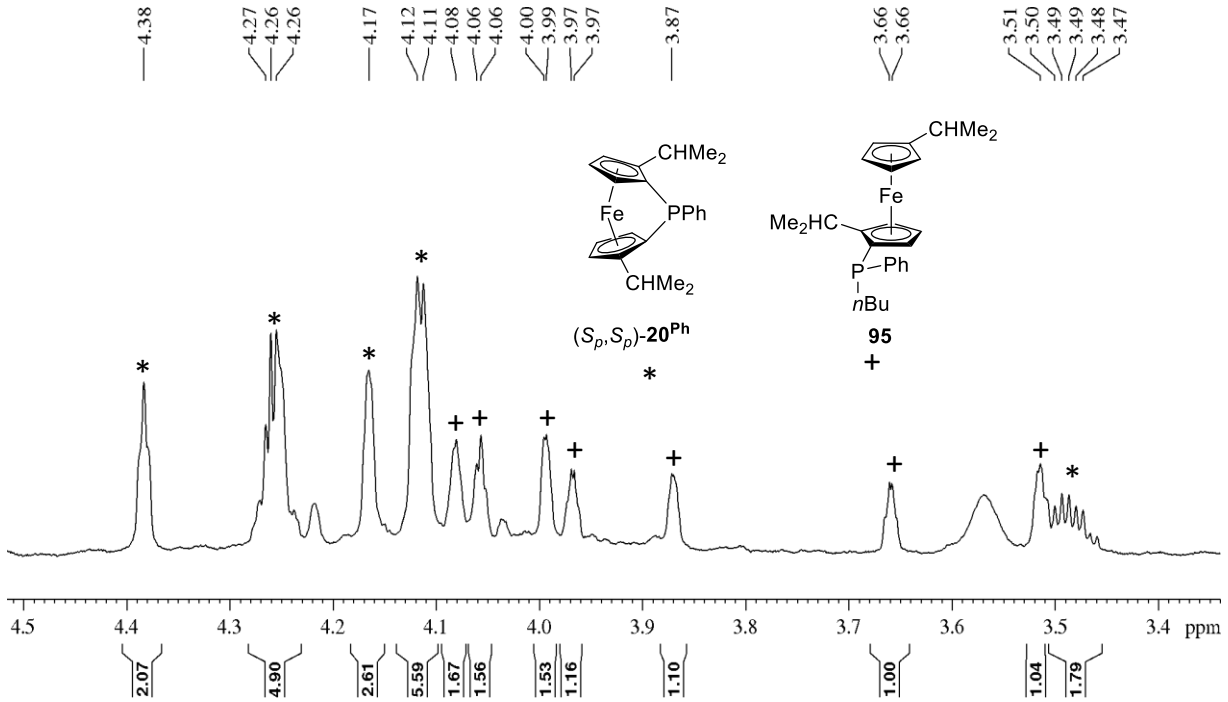

Figure 2-19. ^{1}H NMR spectrum (500 MHz) of reaction mixture with monomer/initiator ratio of 2/1. Cp signals from the monomer (S_p,S_p)-**20^{Ph}** and the ring-opened product **95** are marked with * and +, respectively.

2.2.3.2 Investigations on the stability of lithium species in thf and Et_2O

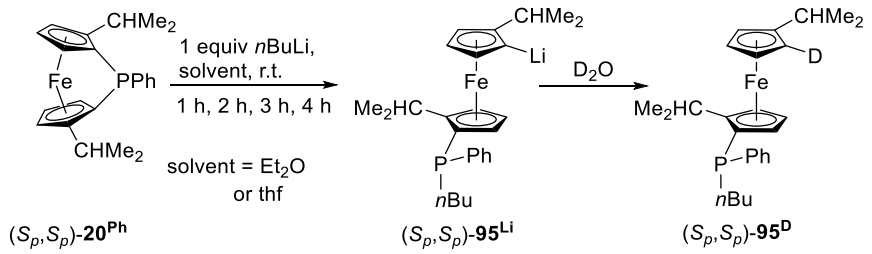

Scheme 2-15. Determination of the stability of lithium species (S_p,S_p)-**95^{Li}** in thf or Et_2O.

It was reported in the literature that ethereal solvents (like Et_2O or thf) can react with organolithium compounds in storage as well as under reaction conditions.[119,120] Therefore, side reactions could occur in which an organolithium reagent is mainly or partially consumed by the ethereal solvents instead of being available for the desired lithiation of the substrate. Based on

these investigations, it is important to see if the lithium ferrocene derivatives (S_p,S_p)-**95**$^{\mathbf{Li}}$ is long lived so that it can further react with monomers to propagate the molecule chain. Stanetty and co-workers measured half-lives of organolithium reagents in different solvents.[120] It was found that at 20 °C the half-life of *n*BuLi in Et_2O (153 h) is significantly longer than that in thf (1.73 h).[120] Therefore, the anionic ring-opening reactions of (S_p,S_p)-**20**$^{\mathbf{Ph}}$ was performed with thf and Et_2O, respectively, and the mixtures were quenched with D_2O before analysis (Scheme 2-15).

The stability of lithium species (S_p,S_p)-**95**$^{\mathbf{Li}}$ in the time frame of 1 to 4 h was monitored by ^{1}H NMR spectroscopy. If the lithium species (S_p,S_p)-**95**$^{\mathbf{Li}}$ was still present in the reaction mixture, its reaction with D_2O would form compound (S_p,S_p)-**95**$^{\mathbf{D}}$, with one deuterium atom at one of the two Cp rings. Considering the deuterium content in D_2O (99.9%), the ^{1}H NMR spectrum would show 6 signals for the two Cp rings, instead of 7 signals as being observed for the ring-opened species **95**.

Using thf as the solvent, the ^{1}H NMR spectrum of reaction mixture shows 7 signals in the Cp regions after quenching with D_2O (δ = 4.08, 4.06, 4.00, 3.97, 3.87, 3.66 ppm, and 3.52 ppm; Figure 2-20). The intensity of the signal at δ = 3.52 ppm increases gradually from 1–4 h, while the intensities of other signals of Cp rings are maintained over 4 h (δ = 4.08–3.66 ppm). After 4 h, all 7 signals in the ^{1}H NMR spectrum of Cp range appear at the same intensity. The fact that the intensity of the proton signal at δ = 3.52 ppm increased over time indicates that lithium species (S_p,S_p)-**95**$^{\mathbf{Li}}$ likely reacted with a proton source (thf) in the reaction mixture. This led to the formation of the hydrolyzed ring-opened compound **95**, instead of the deuterium species (S_p,S_p)-**95**$^{\mathbf{D}}$.

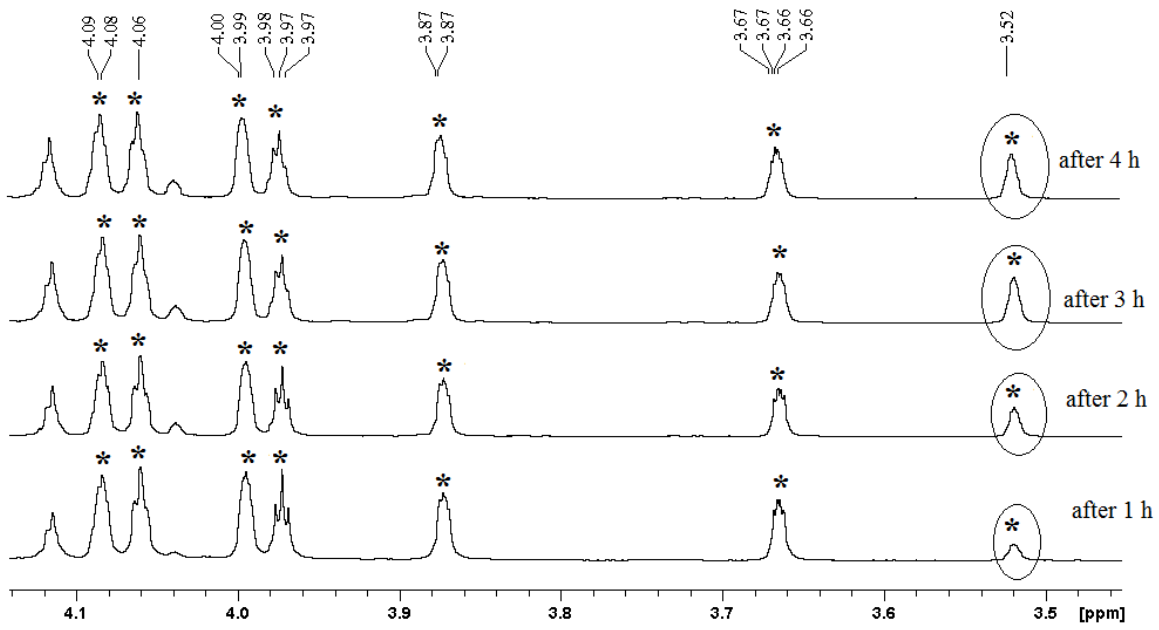

Figure 2-20. ^{1}H NMR spectrum (600 MHz) of Cp range of the reaction mixture in thf. The signals of the ring-opened species **95** are marked with *. NMR measurements were taken after different time points (1 h, 2 h, 3 h, and 4 h).

Based on the known reaction mechanisms between thf and organolithium compounds,[120,121] Scheme 2-16 shows a proposed quenching reaction for species (S_p,S_p)-**95**$^{\mathbf{Li}}$. First, the deprotonation at α-hydrogen of thf gives species (S_p,S_p)-**95**$^{\mathbf{Li\text{-}thf}}$. After that, a reverse cycloaddition of species (S_p,S_p)-**95**$^{\mathbf{Li\text{-}thf}}$ generates species **95**, plus one molecule of ethylene and one molecule of the lithium enolate of acetaldehyde **96**. Once species **95** was formed, no further reactions with another strained monomer can occur to propagate the molecule chain.

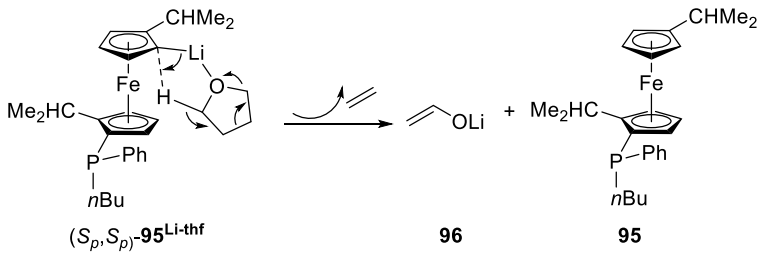

(S_p,S_p)-**95**$^{\mathbf{Li\text{-}thf}}$ **96** **95**

Scheme 2-16. Mechanism of reaction between lithium species (S_p,S_p)-**95**$^{\mathbf{Li}}$ and thf.

Based on the ^{1}H NMR spectrum (Figure 2-20), the half-life of lithium species (S_p,S_p)-**95**^{Li} in thf was quite short (within 2 h). Therefore, the same anionic ring-opening reaction was performed using Et_2O (Scheme 2-15) to see if it can improve the half-life of species (S_p,S_p)-**95**^{Li}. At different time points (1–4 h), the reaction mixture was reacted with D_2O, and analyzed by NMR spectroscopy (Figure 2-21). In the ^{1}H NMR spectrum of the mixture after 1 h, the Cp region shows almost 6 signals at δ = 4.08, 4.06, 4.00, 3.97, 3.87 and 3.66 ppm, and a very weak signal at δ = 3.52 ppm. Extending the reaction time up to 4 h made a slight increase on the intensity of the signal at 3.52 ppm. This is similar to the reaction in thf, as the lithium atom on species **95** was likely hydrolysed during the extending reaction time.

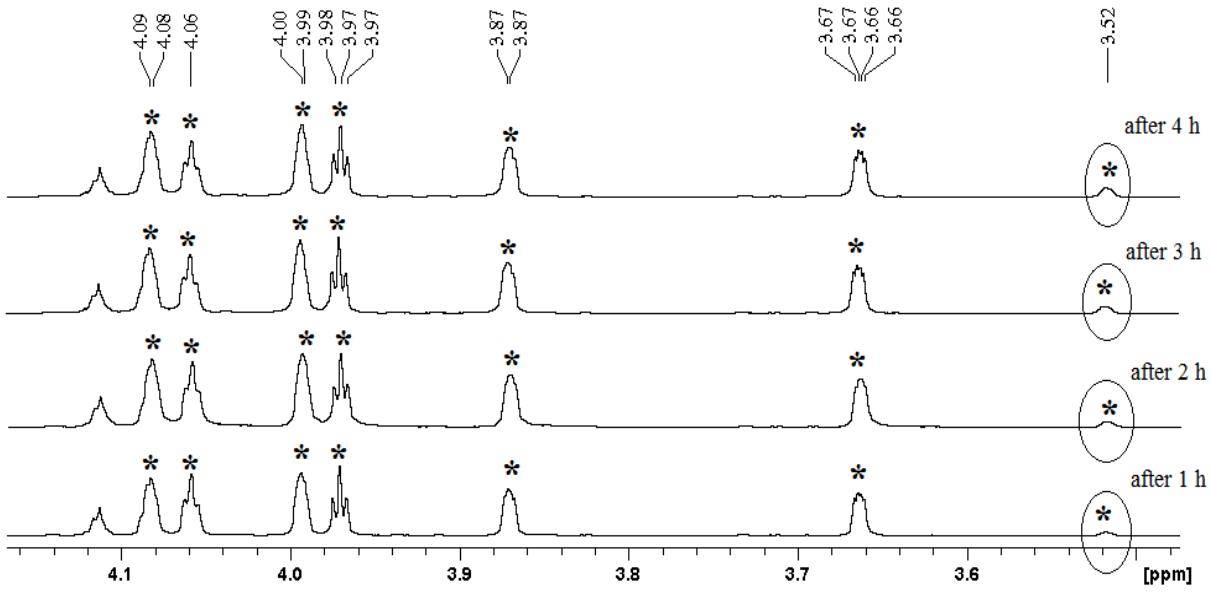

Figure 2-21. ^{1}H NMR spectrum (600 MHz) of Cp range of the reaction mixture in Et_2O. The signals of the ring-opened species **95** are marked with *. NMR measurements were taken after different time points (1 h, 2 h, 3 h, and 4 h).

The only proton source that can react with lithium species (S_p,S_p)-**95**^{Li} is the solvent Et_2O. The mechanism is similar to that of thf, and is shown in Scheme 2-17. Compared to the ring-

opening reaction which was done in thf, the lithium species (S_p,S_p)-**95**$^{\mathbf{Li}}$ in Et_2O was quite stable within 3–4 h, and converted to the hydrolyzed species **95** at a slower rate. Therefore, further anionic ring-opening reactions were performed in Et_2O.

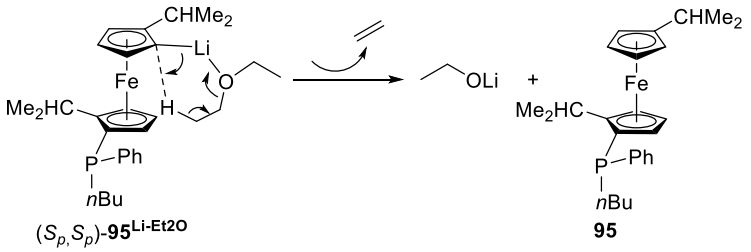

Scheme 2-17. Mechanism of the reaction between lithium species (S_p,S_p)-**95**$^{\mathbf{Li}}$ and solvent Et_2O.

2.2.3.3 Anionic ring-opening reactions in Et_2O

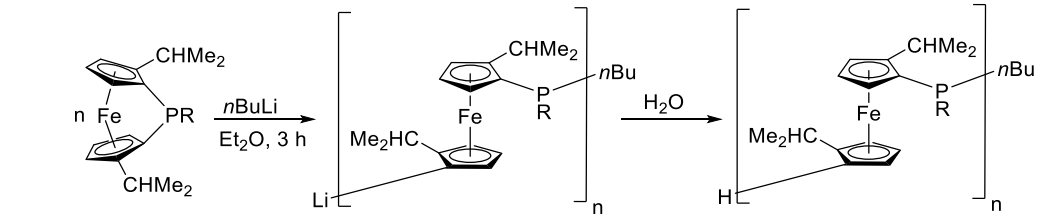

(S_p,S_p)-**20**$^{\mathbf{R}}$ (R = Ph, *t*Bu, *i*Pr)

Scheme 2-18. Anionic ring-opening reactions of chiral phospha[1]FCPs in Et_2O.

Anionic ring-opening reactions of the chiral phospha[1]FCPs (S_p,S_p)-**20**$^{\mathbf{Ph}}$, (S_p,S_p)-**20**$^{\mathbf{\textit{i}Pr}}$, and (S_p,S_p)-**20**$^{\mathbf{\textit{t}Bu}}$ were done in Et_2O. At a monomer/initiator ratio of 1/1, the monomer (S_p,S_p)-**20**$^{\mathbf{Ph}}$ was fully consumed after 1 h of stirring. ^{1}H and ^{31}P NMR spectra of the resulting product also show a 3 to 1 mixture of two diastereomers. The same reaction with *n*BuLi was applied for species (S_p,S_p)-**20**$^{\mathbf{\textit{i}Pr}}$ and (S_p,S_p)-**20**$^{\mathbf{\textit{t}Bu}}$. However, the NMR spectroscopic data of the reaction mixture did not detect any new signals, indicating that no conversion had occurred.

Attempted anionic ROP of the compound (S_p,S_p)-**20**$^{\mathbf{Ph}}$ with smaller amounts of *n*BuLi were performed in Et_2O. Using a monomer/initiator ratio of 2/1 and after quenching the mixture

with H_2O, NMR spectroscopic data detected only signals from the unreacted monomer (S_p,S_p)-**20^{Ph}** and the ring-opened species (S_p,S_p)-**95** (approximately 45%). Other attempts to extend the reaction time did not lead to further conversion. These results are similar to those done in thf (section 2.2.3.1), meaning that the attempted anionic ROP of the phospha[1]FCP (S_p,S_p)-**20^{Ph}** in Et_2O also did not occur. These results lead to the following conclusions. First, *n*BuLi reacted with the starting materials (S_p,S_p)-**20^{Ph}** and transformed it into the anionic species (S_p,S_p)-**95^{Li}**. This species is equipped with the steric bulk of two *i*Pr groups, which failed to further react with other monomers. That means that the initiation step for the attempted polymerization worked, but the ring-propagation did not occur.

However, it is obvious that the anionic ring-opening reaction of compound (S_p,S_p)-**20^{Ph}** in Et_2O generates a more stable lithium species (S_p,S_p)-**95^{Li}**. Making use of this lithium species, a new chiral phosphine ligand was synthesized, as will be discussed in the next section.

2.2.4 Synthesis of a new chiral phosphine ligand

2.2.4.1 Attempted synthesis of a new C_2-phosphine ferrocene-based ligand by substitution reaction.

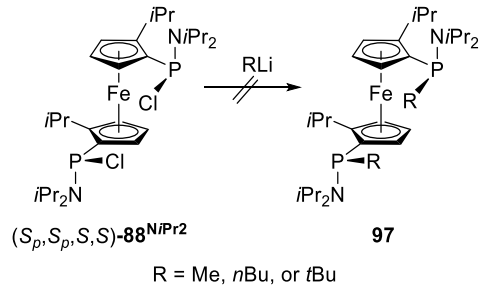

Scheme 2-19. Attempted synthesis of the C_2-phosphine ferrocene-based ligand type **97** by substitution with alkyllithium reagent.

As mentioned in section 1.3, a variety of ferrocene-based P-chiral phosphine ligands have been prepared, and the metal complexes of these phosphine ligands have been used as efficient catalysts for asymmetric reactions.[83,98,99,45] We also attempted to prepare a C_2-phosphine ligand by using substitution chemistry with the chiral 1,1'-bis(phosphanyl)ferrocene (S_p,S_p,*S*,*S*)-**88**$^{\mathbf{NiPr2}}$ species (Scheme 2-19). Compound (S_p,S_p,*S*,*S*)-**88**$^{\mathbf{NiPr2}}$ was successfully synthesized and isolated as a single diastereomer (section 2.1.4), hence, it is an advantage to start a substitution reaction with an enantiopure isomer. In addition, the two substituents on phosphorus atoms (Cl and N*i*Pr$_2$) can be substituted by alkyl groups, and these types of substitution reactions were reported in the literature.[33,98,99,122,123]

In the first attempts, compound (S_p,S_p,*S*,*S*)-**88**$^{\mathbf{NiPr2}}$ was reacted with different alkyllithium reagents (MeLi, *n*BuLi, and *t*BuLi) to replace Cl atoms by alkyl groups. ^{31}P NMR spectroscopic data show that the reaction mixture contained the unreacted starting material (S_p,S_p,*S*,*S*)-**88**$^{\mathbf{NiPr2}}$ (δ = 123.3 ppm) and other unidentified species which resonate in the range of δ = 30.8–12.0 ppm. Varying the reaction conditions, such as changing temperature, extending reaction time, or using different solvent systems, did not lead to a clean substitution. It is assumed that the synthesis was not selective, resulting in a mixture of diastereomers that could not be isolated. Thus, the desired compound **97** could not be selectively synthesized by substitutions with alkyllithium reagents.

After that, another method was applied by reacting the species (S_p,S_p,*S*,*S*)-**88**$^{\mathbf{NiPr2}}$ with HCl in order to substitute the bulky N*i*Pr$_2$ groups by Cl (Scheme 2-20).[33] The reaction was performed with 4 equiv of HCl in Et$_2$O solution. ^{31}P NMR spectroscopic data of the reaction mixture show signals at δ = 165.5, 163.2, 123.3, 121.0 and 28.7 ppm, with a signal at 123.3 which is from the unreacted (S_p,S_p,*S*,*S*)-**88**$^{\mathbf{NiPr2}}$ species. The signals at δ = 165.5 and 121.0 ppm

are assigned to the mono-substituted compound **98**$^{\text{mono-substituted}}$. Mass spectrometry data of this mixture is also in agreement with the NMR data. The presence of the unreacted compound (S_p,S_p,S,S)-**88**$^{\text{N}i\text{Pr2}}$ indicated that the conversion was not complete. Attempts to extend the reaction time or change the reaction temperature did not lead to the formation of the desired compound **98**. Considering the presence of many unidentified products, no further attempts were made.

Overall, the substitution method using 1,1'-bis(phosphanyl)ferrocene (S_p,S_p,S,S)-**88**$^{\text{N}i\text{Pr2}}$ could not generate the desired compound. Therefore, in the next part, another method was applied to synthesize a chiral phosphine ligand.

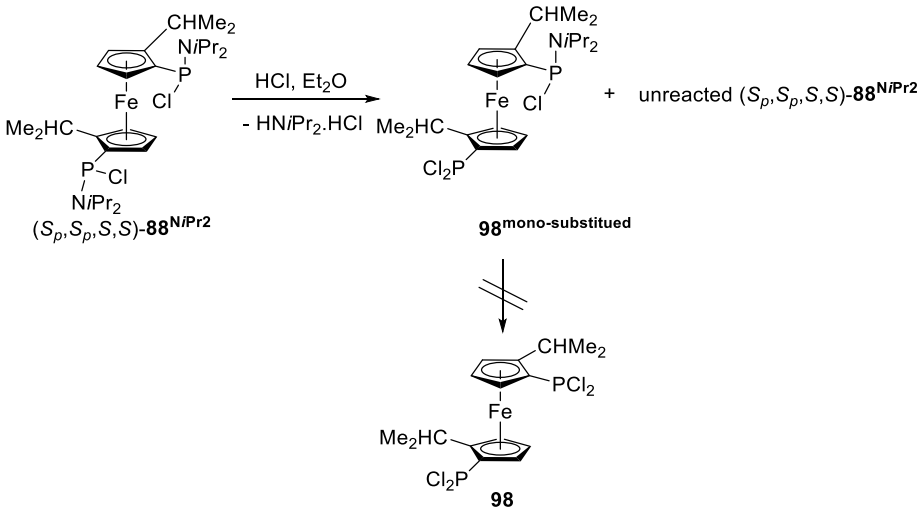

Scheme 2-20. Attempted synthesis of the C_2-phosphine ferrocene-based ligand **98** by reaction with HCl.

2.2.4.2 Synthesis of a new chiral phosphine ferrocene-based ligand (S_p,S)-99 by anionic ring-opening reaction

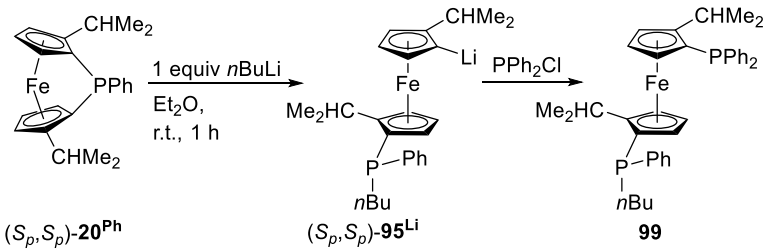

Scheme 2-21. Synthesis of the diastereomeric mixture **99**.

The preparation of 1,1′-disubstituted ferrocenes by ring-opening reaction of a non-alkylated phospha[1]FCP following by an addition of an electrophile was reported in the literature.[124,125] In section 2.2.3.2, the anionic ring-opening reaction of compound (S_p,S_p)-**20**$^{\mathbf{Ph}}$ in Et_2O was found to generate a stable lithium species (S_p,S_p)-**95**$^{\mathbf{Li}}$. Therefore, the active species (S_p,S_p)-**95**$^{\mathbf{Li}}$ could further react with another electrophile, generating a new phosphine ligand (Scheme 2-21). The phosphine reagent Ph_2PCl was chosen for this type of reaction due to its common use in ligand preparation.[99,84,124,125]

After reacting with excess amount of Ph_2PCl, the crude mixture was purified by FCC. The resulting product **99** was obtained as an orange oil in 69 % isolated yield and was analyzed by NMR spectroscopy and mass spectrometry. As expected, compound **99** is a 3 to 1 mixture of two diastereomers, and both of them are *non*-symmetrical species. For example, the ^{31}P NMR spectrum shows 2 sets of signals at δ = –24.7 and –34.2 ppm for the major isomer, and at δ = –25.2 and –36.2 ppm for the minor isomer (Figure 2-22). The ^{1}H NMR spectrum also exhibits two sets of signals in the Cp range, each caused by six overlapping Cp protons. According to NMR spectroscopic data, the diastereomeric mixture **99** was quite stable, and could be stored under normal atmosphere for at least six months without being oxidized.

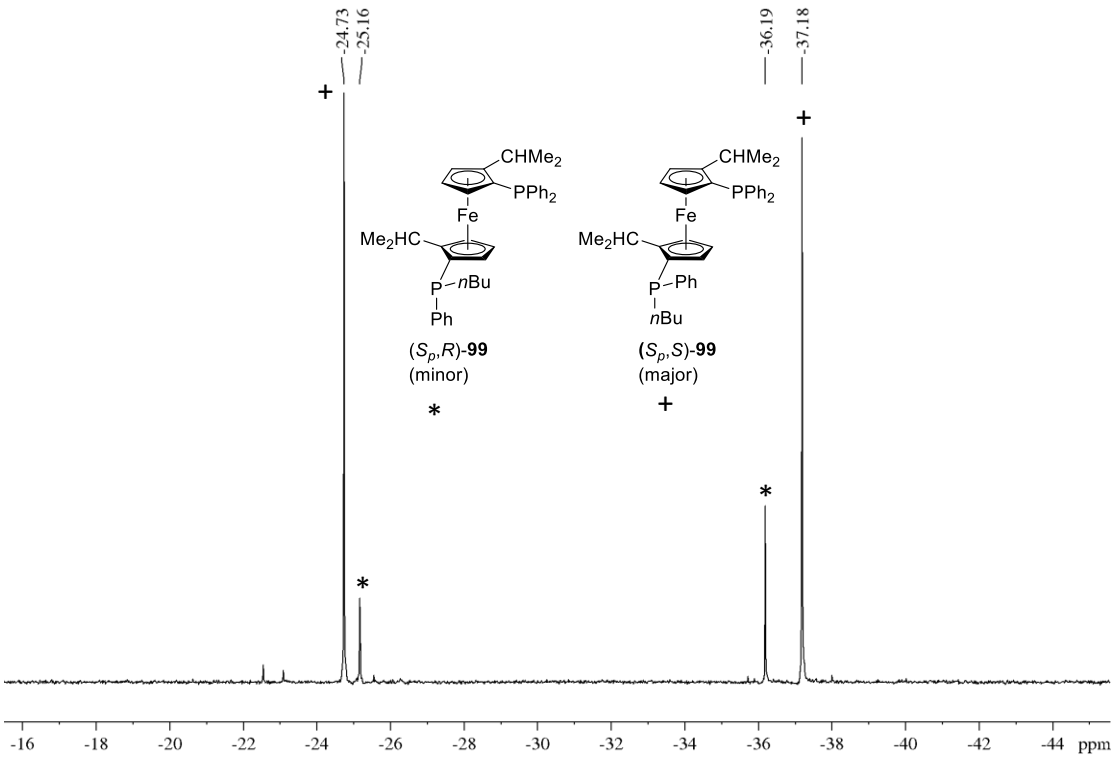

Figure 2-22. $^{31}P\{^{1}H\}$ NMR spectrum (202.5 MHz) of the mixture **99**. The signals of major and minor isomers are marked with + and *, respectively.

Attempts to separate diastereomers from the mixture **99** by FCC, PTLC, or crystallization were unsuccessful. However, following the successful separation of compound (S_p,*R*)-**95**$^{\mathbf{S}}$ (section 2.2.3.1), the diastereomeric mixture **99** was sulfurized (Scheme 2-22).

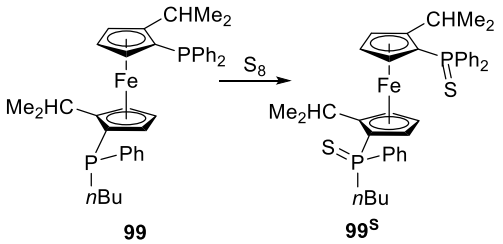

Scheme 2-22. Sulfurization of the diastereomeric mixture **99**.

After the sulfurization, the major isomer was successfully isolated from the mixture **99**$^{\mathbf{S}}$ by PTLC. ^{1}H NMR spectrum of the isolated compound shows six signals for six Cp protons at δ

= 5.59, 5.35, 4.57, 4.46, 3.59, and 3.35 ppm, indicating a *non*-symmetrical species. Its ^{31}P NMR spectrum shows two signals at δ = 41.6 and 39.6 ppm, which are shifted to the downfield region, compared to that of the non-sulfurized mixture **99** (δ = –24.7 and –37.2 ppm). Due to the structural similarity between the ring-opened compound (S_p,*R*)-**95^{S}** (section 2.2.3.1) and the isolated species **99^{S}**, it is safe to assume that the isomer **99^{S}** also possess the (S_p,*R*)-configuration.

Desulfurization was done to make compound (S_p,*R*)-**99^{S}** potentially useful as a chiral ligand (Scheme 2-23). It was reported in the literature that the treatment with $CF_3SO_3Me/P(NMe_2)_3$ was an efficient method for desulfurization, because it can retain the symmetry of the resulting product.[126,76] Therefore, the species (S_p,*R*)-**99^{S}** was allowed to react with CF_3SO_3Me, following by the addition of $P(NMe_2)_3$. After the desulfurization, the resulting product was obtained as an yellow solid, which was characterized by NMR spectroscopy and mass spectrometry.

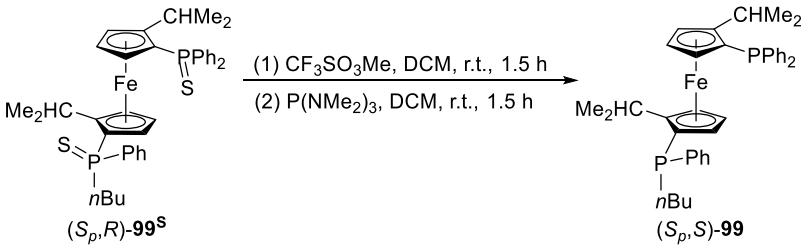

Scheme 2-23. Desulfurization of the chiral phosphine ligand (S_p,*R*)-**99^{S}**.

The most distinguishable signals in the ^{1}H NMR spectrum are the two Cp signals at δ = 2.94 and 3.33 ppm, which are shielded to the upfield region, comparing to other Cp signals. By knowing the crystal structure of the related compound (S_p,*R*)-**95^{S}**, it can be speculated that these two upfield signals are caused by the effect of phenyl groups which are in the close proximity of Cp rings (Figure 2-23). The ^{31}P NMR spectrum of the resulting product (S_p,*S*)-**99** shows 2 sharp signals at δ = –24.8 and –37.2 ppm with a relative ratio of 1:1 (Figure 2-24). This value is

comparable with the ^{31}P chemical shift of other ferrocene-based phosphine ligands (Josiphos,[84] Ferriphos,[92] Ferrophos,[94] section 1.3.2) which also showed ^{31}P chemical shift in the upfield region. Beside the isolated isomer (S_p,*S*)-**99**, ca. 3% of the other isomer (S_p,*R*)-**99** was also observed in the ^{31}P NMR spectrum (δ = –25.2 and –36.2). The presence of species (S_p,*R*)-**99** was quite surprising, as the starting material (S_p,*R*)-**99^{S}** was a single diastereomer. This suggests that isomerization must have occurred during the desulfurization.

Overall, the new phosphine ligand (S_p,*S*)-**99** was successfully synthesized via an anionic ring-opening reaction of the phospha[1]FCP (S_p,S_p)-**20^{Ph}**, followed by the addition of an appropriate electrophile. This method can be used to synthesize other compounds of the same type, which are expected to be potential ligands for catalysis reaction.

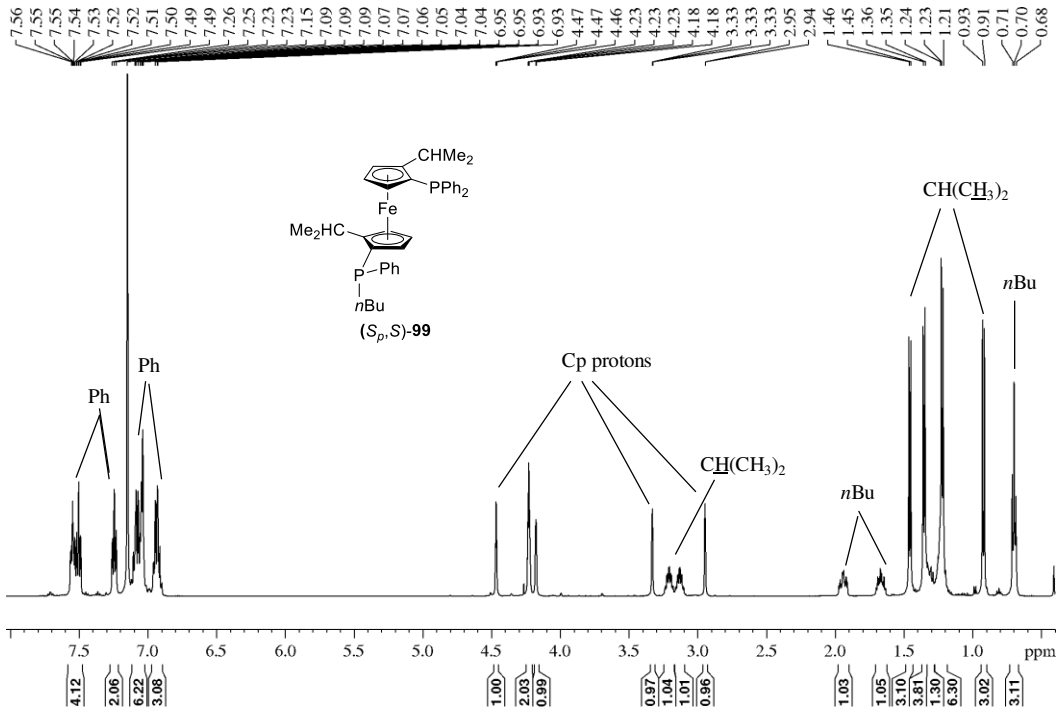

Figure 2-23. ^{1}H NMR spectrum (500 MHz) of the new chiral ferrocene-based phosphine ligand (S_p,*S*)-**99**.

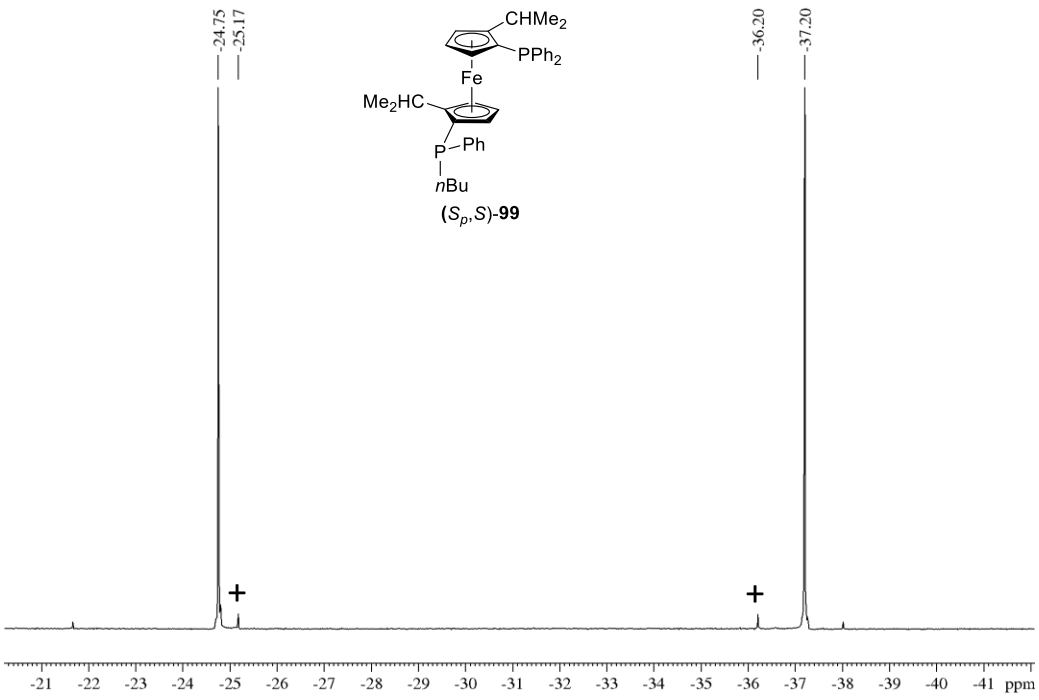

Figure 2-24. $^{31}P\{^{1}H\}$ NMR spectrum (202.5 MHz) of the new chiral ferrocene-based phosphine ligand (S_p,*S*)-**99**. The minor isomer (S_p,*R*)-**99** is marked with +.

2.3 Thermal ring-opening polymerization of phospha[1]ferrocenophanes

In this section, the thermal ROP of the chiral phospha[1]FCP (S_p,S_p)-**20**$^{\mathbf{Ph}}$ and the known compound **11**$^{\mathbf{Ph}}$ is discussed. The structures of cyclic oligomers obtained from the thermal ROP revealed that Fe–Cp bond rupture occurs during the ROP process. This is an important piece of information that provides some insight into the reaction mechanism of thermal ROP of phospha[1]FCPs.

2.3.1 Investigations of thermal properties by differential scanning calorimetry

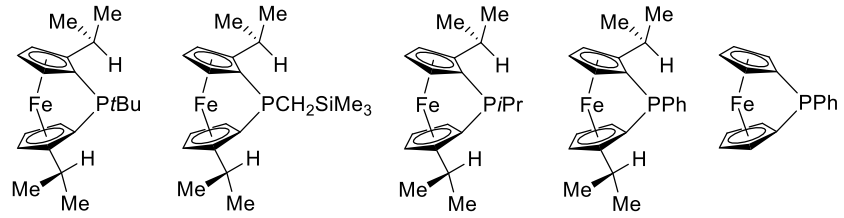

(S_p,S_p)-**20**$^{t\mathbf{Bu}}$ (S_p,S_p)-**86**$^{\mathbf{CH2SiMe3}}$ (S_p,S_p)-**20**$^{i\mathbf{Pr}}$ (S_p,S_p)-**20**$^{\mathbf{Ph}}$ **11**$^{\mathbf{Ph}}$

Figure 2-25. Phospha[1]FCPs which were investigated by differential scanning calorimetry (DSC).

In order to investigate the capability of chiral phospha[1]FCPs to undergo thermal ROP, DSC measurements were performed on the phospha[1]FCPs containing different substituents (Figure 2-25). The amount of strain in phospha[1]FCPs can also be obtained from these measurements.

Figure 2-26 shows the DSC diagrams of compounds (S_p,S_p)-**20**$^{i\mathbf{Pr}}$, (S_p,S_p)-**20**$^{\mathbf{Ph}}$ and **11**$^{\mathbf{Ph}}$. In general, the DSC curves of alkyl-substituted phospha[1]FCPs show a separation between a melting endotherm and a ROP exotherm. The average ΔH^{ROP} values for each chiral compound in Figure 2-25 were –61(±2) ((S_p,S_p)-**20**$^{t\mathbf{Bu}}$), –66(±2) ((S_p,S_p)-**20**$^{\mathbf{CH2SiMe3}}$), –77(±2) ((S_p,S_p)-**20**$^{i\mathbf{Pr}}$) and –86(±2) ((S_p,S_p)-**20**$^{\mathbf{Ph}}$) kJ mol^{-1}, respectively. It was noticed that compounds having more bulky substituents on phosphorus atom released less heat. For example, the difference in ΔH^{ROP} value of (S_p,S_p)-**20**$^{\mathbf{Ph}}$ and (S_p,S_p)-**20**$^{i\mathbf{Pr}}$ is $\Delta\Delta H^{ROP}$ = 9 kJ mol^{-1}, suggesting that species (S_p,S_p)-**20**$^{\mathbf{Ph}}$ is more strained than the (S_p,S_p)-**20**$^{i\mathbf{Pr}}$.

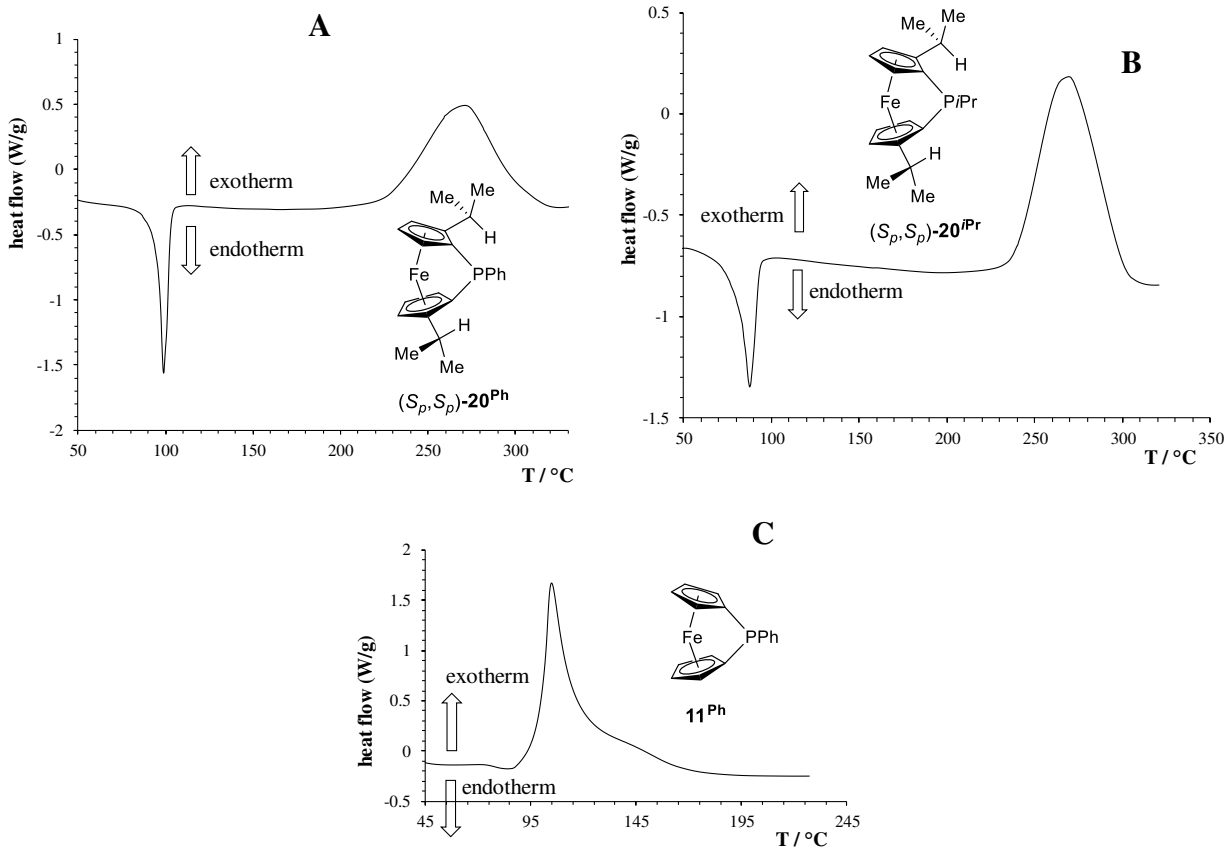

Figure 2-26. DSC diagrams of phospha[1]FCPs (S_p,S_p)-**20**$^{\mathbf{Ph}}$ (A), (S_p,S_p)-**20**$^{\mathbf{\textit{i}Pr}}$ (B) and **11**$^{\mathbf{Ph}}$ (C).

However, the sets of calculated distortion angles in (S_p,S_p)-**20**$^{\mathbf{Ph}}$ and (S_p,S_p)-**20**$^{\mathbf{\textit{i}Pr}}$ are not significantly different (Table 2-5). While the α, δ, and θ angles indicate that (S_p,S_p)-**20**$^{\mathbf{Ph}}$ is more strained than (S_p,S_p)-**20**$^{\mathbf{\textit{i}Pr}}$, the β angle indicates that it is less strained. These small geometrical differences could not lead to a difference in strain energy of 9 kJ mol^{-1}.

Table 2-5. Experimental Distortion Angles [°] in (S_p,S_p)-**20**$^{\mathbf{Ph}}$ and (S_p,S_p)-**20**$^{\mathbf{\textit{i}Pr}}$. This table is reprinted from the PhD thesis of Saeid Sadeh, 2014, University of Saskatchewan.[64]

	(S_p,S_p)-**20**$^{\mathbf{Ph}}$	(S_p,S_p)-**20**$^{\mathbf{\textit{i}Pr}}$
α[°]	26.21	25.82
β[°]	34.61(16)	36.99(31)
θ[°]	92.09(10)	92.09(10)
δ[°]	160.83(2)	160.77(47)

Probably the enthalpy difference is due to a residual of strain that is left in the resulting product.[127] To measure the amount of strain in the [1]FCPs system, Müller and co-workers applied reaction 1, which is a transformation from a strained species **100**$^{\mathbf{ERx}}$ into species **101**$^{\mathbf{ERx}}$ with parallel Cp rings (Scheme 2-24).[127] As reaction 1 is homodesmotic, it can be used to calculate the reaction enthalpies in the ROP of [1]FCPs. Two possible conformers of bis(ferrocenyl)species **101**$^{\mathbf{ERx}}$ could be obtained, namely **conf-1** and **conf-2**, which are simply illustrated in Figure 2-27.[127]

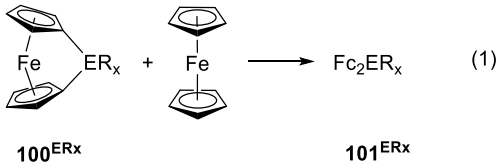

Scheme 2-24. Reaction to evaluate strain in [1]FCPs.

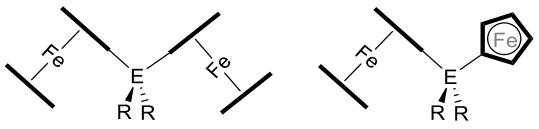

conf-1 *anti,anti* **conf-2** *anti,gauch*

Figure 2-27. Illustration of two different conformers of bis(ferrocenyl)species (**101**$^{\mathbf{ERx}}$ in Scheme 2-24): *anti*,*anti*-conformer (**conf-1**) and *anti*,*gauche*-conformer (**conf-2**).

The available space for ER_x moieties in compound **101**$^{\mathbf{ERx}}$ is less than that in the strained compound **100**$^{\mathbf{ERx}}$ due to the following reasons. First, when species **100**$^{\mathbf{ERx}}$ ring opens, the number of ferrocene moieties increases from one to two. Second, in the strained compound **100**$^{\mathbf{ERx}}$, the R groups are located away from the two Cp rings, whereas in the product **101**$^{\mathbf{ERx}}$, there can be steric hindrance between the R groups and Cp rings. With increasing size of R, less heat gets released because some residual strain remains in the resulting bis(ferrocenyl)species **101**$^{\mathbf{ERx}}$.[127] Therefore, the bulkier the group, the smaller the heat that is released in reaction 1. This speculation matched with the experimentally determined DSC value of phospha[1]FCPs in this section (Figure 2-25).

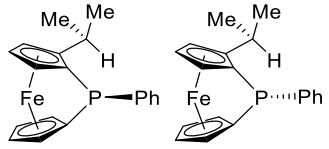

trans-**22** *cis*-**22**

Figure 2-28. *Cis* and *trans*-conformation of phospha[1]FCPs having mono-alkyl substituted on ferrocene moiety.

For the known PhP[1]FCP **11**$^{\mathbf{Ph}}$, an enthalpy for ROP of –68(±5) kJ mol^{-1} was reported in 1999.[52] We investigated the thermal properties of **11**$^{\mathbf{Ph}}$ with DSC and confirmed the published value of –68 kJ mol^{-1}.[127] However, on the DSC thermogram of **11**$^{\mathbf{Ph}}$, only an exothermic peak was observed, because melting and ROP of the monomer occurs simultaneously (Figure 2-26C).

Therefore, the value of –68 kJ mol^{-1} does not represent the intrinsic strain of **11^{Ph}**. The calculated reaction enthalpies ΔH^{378} of **11^{Ph}** were reported by Müller *et al.*, which yielded –91.9 kJ mol^{-1} for the formation of an equilibrium mixture of **conf-1** and **conf-2**.[127] The measured value for the related phospha[1]FCPs *trans*-**22** and *cis*-**22** were –89(±2) and –88(±2) kJ mol^{-1}, respectively (Figure 2-28).[51] The values of ΔH^{ROP} decreased from the non-alkylated phospha[1]FCP **11^{Ph}** ($\Delta H^{ROP}_{calculated}$ = –91.9 kJ mol^{-1}) to mono-alkylated phospha[1]FCPs *trans*-**22** and *cis*-**22** ($\Delta H^{ROP}_{measured}$ = –89 kJ mol^{-1}) and dialkylated phospha[1]FCP (S_p,S_p)-**20^{Ph}** ($\Delta H^{ROP}_{measured}$ = –85.8 kJ mol^{-1}). This tendency agrees well with previous investigation of the Müller group which involves the influence of steric hindrance on the thermal properties of strained [1]FCPs.[127] With an increased number of alkyl groups in α positions on Cp rings, less heat can get released in a ROP process as some residual strain remains in the formed polymer.

2.3.2 Thermal ring-opening polymerization of the chiral phospha[1]ferrocenophane (S_p,S_p)-20^{Ph}

2.3.2.1 Polymer synthesis and characterization

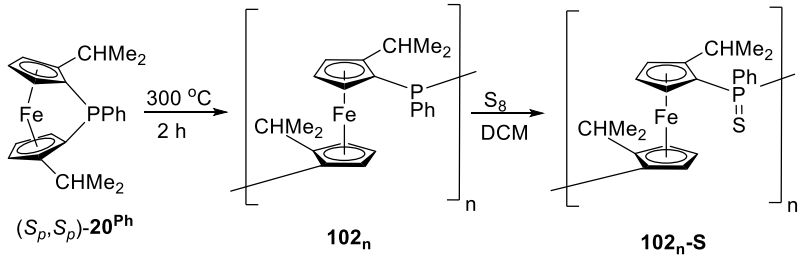

(S_p,S_p)-**20^{Ph}** **102$_n$** **102$_n$-S**

Scheme 2-25. Preparation of poly(ferrocenylphosphine)s **102$_n^S$**.

Using the DSC thermogram with an end ROP temperature of 300 °C as a guide (Figure 2-26A), compound (S_p,S_p)-**20^{Ph}** was heated for 2 h at that temperature in a sealed NMR tube (Scheme 2-25). This procedure resulted in a highly viscous melt, which solidified to a glassy solid at

ambient temperature. The crude was dissolved in thf and precipitated into hexanes which gave polymer **102$_n$** as a yellow powder (44% yield). Together with polymeric products, other gray particles were present in the reaction mixture, which were attracted toward a magnet. It is assumed that these particles are elemental iron, which were generated from the extrusion of iron at high temperature. The ^{1}H NMR spectrum of the compound **102$_n$** shows the expected broad signals for the Ph, Cp, and *i*Pr protons. For example, the Cp range appears as broad signals from 4.06 to 4.47 ppm, and the *i*Pr groups appear as broad peaks from 0.8 to 1.5 ppm.

Sulfurization was applied to make polymer **102$_n$** insensitive to oxygen and suitable for gel permeation chromatography (GPC) (Scheme 2-25).[38] The sulfurized polymer **102$_n$-S** was characterized by NMR spectroscopy and the molecular weight was determined by GPC. Similar to **102$_n$**, polymer **102$_n$-S** shows the expected broad signals in the ^{1}H NMR spectrum for the Ph, Cp, and *i*Pr protons. The ^{31}P NMR spectrum of **102$_n$-S** shows broad signals from δ = 38.2 to 42.0 ppm, which are quite close to the ^{31}P NMR chemical shifts of the published **11$_n$-S^{Ph}** that lacks the *i*Pr group (section 1.2.4.1, δ = 37.5 ppm).[37] The presence of more than one broad signals in the ^{31}P NMR spectrum (δ = 38.2 to 42.0 ppm) might indicate that the polymer **102$_n$-S** was not pure. Elemental analysis of polymer **102$_n$-S** also supports this assumption, as the value of carbon atoms in this analysis is significantly lower than expected for polymer **102$_n$-S**. As mentioned above, presumably, the impure polymer **102$_n$-S** was caused by the extrusion of iron, which gave non-iron oligomeric by-products that could not be removed. Analysis by GPC with a triple detection system revealed an absolute molecular weight of M_w = 19 kDa with a polydispersity of 1.3 for the sulfurized polymer **102$_n$-S** (Table 2-6).

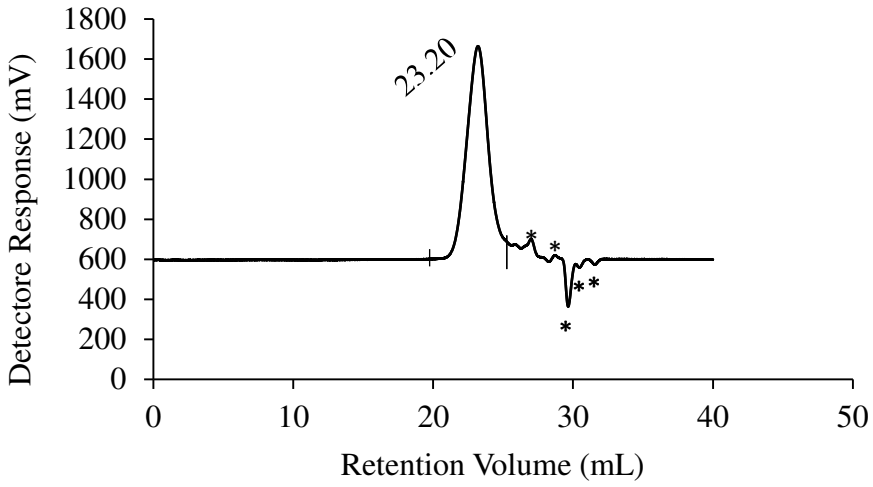

Figure 2-29. GPC trace of polymer **102_n-S** (c = 10.5 mg / 5.0 mL thf). System peaks are indicated with *.

Table 2-6. GPC analysis for polymer **102_n-S**.

	102_n-S
M_n *(Da)*	14 x 10^3
M_w *(Da)*	19 x 10^3
M_z *(Da)*	27 x 10^3
M_p *(Da)*	16 x 10^3
M_w/M_n	1.3

2.3.2.2 Identification of cyclic phosphines and proposed mechanism for thermal ring-opening polymerization

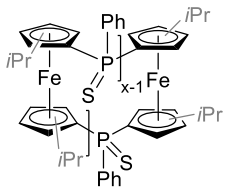

103^{S} (x = 1-7)

Figure 2-30. Cyclic oligomers present in the reaction mixture of thermal ROP of (S_p,S_p)-**20^{Ph}**.

Approximately 60% of the reaction mixture from the thermal ROP of (S_p,S_p)-**20^{Ph}** did not precipitate and stayed in the solution. This soluble part was also sulfurized, then characterized by NMR spectroscopy and mass spectrometry. The ^{31}P NMR spectrum of this mixture exhibits a series of sharp signals from δ = 34 to 42.5 ppm. Its mass spectrum shows peaks from cyclic dimers to hexamers (Figure 2-30), with signals of dimers dominating the mass diagram. Mizuta *et al*. also found the presence of cyclic oligomers, from dimers up to hexamers, while investigating the photolytic ring-opening reaction of the known phospha[1]FCP **11^{Ph}**.[126] Very recently, in a similar thermal ROP study of a PhP[1]FCP having one *i*Pr on the ferrocene moiety (*trans*-**22**), Müller and co-workers observed the formation of cyclic oligomers, from dimers up to heptamers, in the reaction mixture.[51]

In this thesis work, using preparative thin layer chromatography (PTLC), six fractions from the mixture **103^{S}** were collected. Based on ^{1}H and ^{31}P NMR spectroscopic data, five of the six fractions contained a single species with different signal patterns (fractions **103^{S}-1**, **103^{S}-2**, **103^{S}-3**, **103^{S}-4**, and **103^{S}-5**, section 4.4.2). MS data showed that all of the five fractions were dimers, meaning [1.1]ferrocenophanes ([1.1]FCPs), with the same empirical formula [{PhP(=S)C$_{10}$H$_6$(*i*Pr)$_2$}Fe]$_2$. The differences in NMR spectroscopic data of all five fractions

having the same empirical formula shows that isomeric isomers had been obtained. For example, NMR spectroscopic data of the fraction **103^{S}-1** suggests that it is a *non*-symmetrical species, which shows 12 signals for 12 Cp protons in the ^{1}H NMR spectrum, and two signals in its ^{31}P NMR spectrum (δ = 36.2 and 41.9 ppm). On the other hand, ^{1}H NMR spectra of the other fractions **103^{S}-2**, **103^{S}-3**, **103^{S}-4**, and **103^{S}-5** indicate the presence of species having a two-fold symmetry element (section 4.4.2). The ^{31}P NMR spectra these fractions show one singlet for each of them at δ =41.4 (**103^{S}-2**), 34.0 (**103^{S}-3**), 38.3 (**103^{S}-4**), and 42.6 (**103^{S}-5**) ppm. These signals are quite similar to that of the known [1.1]FCP **51** with no *i*Pr groups (δ = 40.5 and 37.7 ppm).[76]

Theoretically, many different isomers can be proposed from two ferrocene units, two PhP=S bridging units, and four *i*Pr groups. The *anti* and *syn* conformations of [1.1]FCPs are illustrated in Figure 2-31. In each structure, the α positions for the *i*Pr groups are indicated by R^1 (*exo*) and R^2 (*endo*).

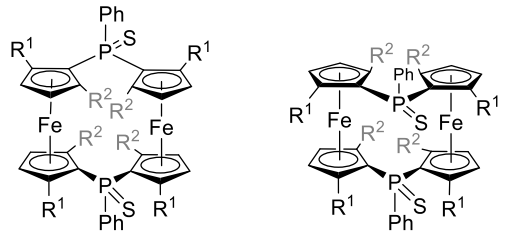

Figure 2-31. Illustration of *exo* (R^1) and *endo* (R^2) α positions in diphospha[1.1]FCPs.

For both *syn* and *anti* isomers, both phenyl groups on the two phosphorus atoms orient away from the ferrocene moieties. This is based on the structures of both *syn* and *anti* conformations of the parent [1.1]FCPs (*syn*-**51** and *anti*-**51**; section 1.2.4.3), which were isolated

by Mizuta *et al.* in the photolytic ROP of the phospha[1]FCP **11**$^{\mathbf{Ph}}$.[128] For the *syn* conformation of **103**$^{\mathbf{S}}$, there are seven possible isomers that can be formed:

(i) four *i*Pr groups in *exo* positions (R^1) results in an C_{2v}-symmetric isomer with group order h = 4.

(ii) four *i*Pr groups on *endo* positions (R^2) results in an C_{2v}-symmetric isomer with group order h = 4.

(iii) two *i*Pr groups in *exo* positions (R^1) of one ferrocene unit, and the other two *i*Pr groups in *endo* positions (R^2) results in an C_s-symmetric isomer with group order h = 2.

(iv) two *i*Pr groups in two *exo* positions (R^1) of neighboring Cp rings of two ferrocene units, and the other two *i*Pr groups in *endo* positions (R^2) of neighboring Cp rings results in an C_s-symmetric isomer with group order h = 2.

(v) two *i*Pr groups in two *exo* positions (R^1) of opposite Cp rings of two ferrocene units, and the other two *i*Pr groups in *endo* positions (R^2) of opposite Cps results in an C_2-symmetric isomer with group order h = 2.

(vi) one *i*Pr group in *endo* (R^1) and the other three *i*Pr groups in *exo* positions (R^2) results in an C_1-symmetric isomer with group order h = 1.

(vii) three *i*Pr groups in *endo* (R^1) and one *i*Pr group in *exo* positions (R^2) results in an C_1-symmetric isomer with group order h = 1.

For the *syn*-**103**$^{\mathbf{S}}$ isomer, case (ii) with all four *i*Pr groups on endo positions (R^2) is less likely occurred due to the steric congestion in the ferrocene system. Applying the same systematic approach to the *anti* isomer (*anti*-**103**$^{\mathbf{S}}$, Figure 2-31), again, seven isomers are theoretically possible.

(i) four *i*Pr groups in *exo* positions (R^1) results in an C_{2h}-symmetric isomer with group order h = 4.

(ii) four *i*Pr groups in *endo* positions (R^2) results in an C_{2h}-symmetric isomer with group order h = 4.

(iii) two *i*Pr groups in *exo* positions (R^1) of one ferrocene unit, and the other two *i*Pr groups in *endo* positions (R^2) results in an C_2-symmetric isomer, with group order h =2.

(iv) two *i*Pr groups in *exo* positions (R^1) of neighboring Cps of two ferrocene units, and the other two *i*Pr groups in *endo* positions (R^2) of neighboring Cps results in an C_s-symmetric isomer with group order h = 2.

(v) two *i*Pr groups in *exo* positions (R^1) of opposite Cps of two ferrocene units, and the other two *i*Pr groups in *endo* positions (R^2) of opposite Cps results in an C_i-symmetric isomer with group order h = 2.

(vi) one *i*Pr group in *exo* position (R^1), and three *i*Pr groups in *endo* positions (R^2) results in a *non*-symmetrical isomer (C_1-symmetry).

(vii) one *i*Pr group on *endo* position (R^2), and three *i*Pr groups in *exo* positions (R^1) results in a *non*-symmetrical isomer (C_1-symmetry).

It is expected that isomers with low steric interactions between *i*Pr groups are thermodynamically more stable and will preferably form. Crystals from one of the five fractions were obtained and its molecular structure was solved by single-crystal X-ray analysis. The structurally characterized dimer is *syn*-C_2-**103^S-3** with all four *i*Pr groups in *exo* positions (Figure 2-32), which is one of the possible seven *syn*-**103^S** isomers.

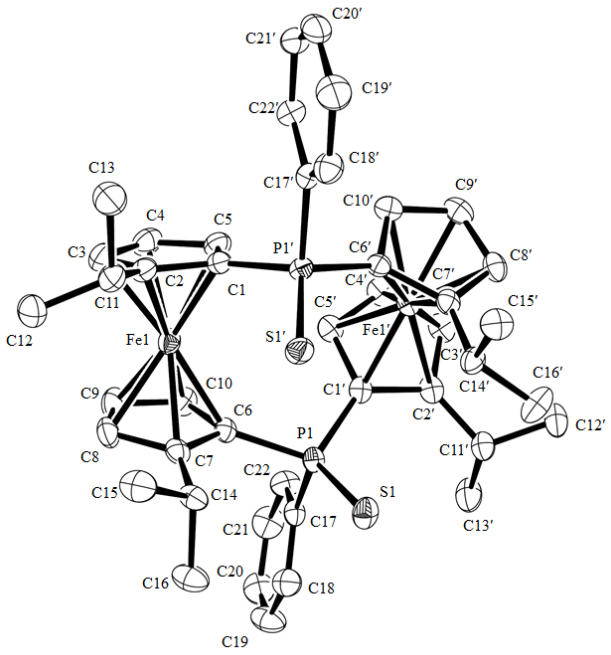

Figure 2-32. Molecular structure of *syn*-C_2-**103^{S}-3** with thermal ellipsoids at 50% probability level. Hydrogen atoms are omitted for clarity. Selected bond lengths [Å] and bond angles [°]: S1–P1 = 1.9486(11); P1–C6 = 1.823(3); P1–C1′ = 1.802(3); P1–C17 = 1.833(3); S1–P1–C6 = 117.09(11); S1–P1–C1′ = 113.32(11); C6–P1–C1′ = 109.15(14). For further bond lengths [Å] and bond angles [°] see Table 4–4.

As expected, the *syn* isomer characterized in this work is very similar to the non-alkylated compound *syn*-**51**, which was reported in 2005.[128] The P–P and Fe–Fe distances of the *syn*-C_2-**103^{S}-3** isomer are 4.701 and 4.696 Å, respectively, which are quite close to the published values of 4.632 (P–P) and 4.706 Å (Fe–Fe) in *syn*-**51**.[128]

Table 2-7. Crystal and structural refinement data for compound *syn*-C_2-**103^S-3**.

syn-C_2-**103^S-3**	
empirical formula	$C_{44}H_{55}Fe_2P_2S_2$
fw	816.64
cryst. size / mm^3	0.35 × 0.30 × 0.22
cryst. system	monoclinic
space group	$P2_1/c$
Z	4
a / Å	10.6440(4)
b / Å	19.8858(7)
c / Å	21.3131(7)
α / °	90
β / °	99.3040(10)
γ / °	90
volume / $Å^3$	4451.9(3)
ρ_{calc} / g cm^{-3}	1.472
temperature / K	173(2)
μ_{calc} / mm^{-1}	1.091
θ range / °	2.266 to 27.515
collected reflections	38400
independent reflections	10210 [R(int) = 0.0338]
absorption correction	none
data / restraints / params	10210 / 0 / 513
goodness-of-fit	1.038
R_1 [I > 2 σ(I)][a]	0.0508
wR_2 (all data)[a]	0.1300
largest diff. peak and hole, $\Delta\rho_{elect}$ / e $Å^{-3}$	1.107 and -1.163

[a] $R_1 = [\Sigma||F_o|-|F_c||]/[\Sigma|F_o|]$ for $[F_o^2 > 2\sigma(F_o^2)]$, $wR_2 = \{[\Sigma w(F_o^2-F_c^2)^2]/[\Sigma w(F_o^2)^2]\}^{1/2}$ [all data]

According to the crystal structure, the compound *syn*-C_2-**103^S-3** in a boat conformation exhibits C_2-symmetry, and one can expect that both conformers equilibrate fast on the NMR time scale, resulting in a time-averaged C_{2V} symmetrical *syn* isomer.[129,130] Such a species would give three peaks for the 12 Cp protons and two peaks for 8 methyl groups of *i*Pr moieties. However, ^{1}H NMR spectrum of this compound shows 6 signals for the 12 Cp protons (δ = 6.05, 4.84, 4.72, 4.49, 4.35, and 4.29 ppm), and 4 doublets for 8 methyl groups of *i*Pr substituents (δ = 1.45, 1.26, 1.12, and 0.04 ppm). It was speculated that at ambient temperature (24–25 °C), the molecular dynamics is slowed down with respect to NMR time scale (Scheme 2-26). Therefore, 6 signals are observed for the Cp protons. This speculation matched with what was obtained from the NMR spectroscopic data of the compound *syn*-C_2-**103^S-3**.

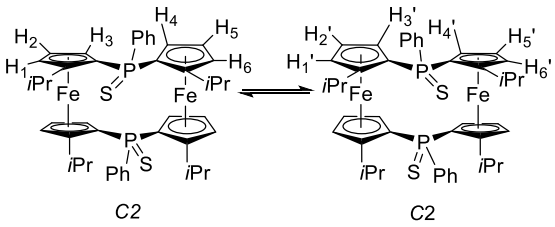

Scheme 2-26. Illustration of an equilibrium between both conformers of *syn*-C_2-**103^S-3**.

Variable temperature NMR measurements had been applied on the compound *syn*-C_2-**103^S-3** and ^{1}H NMR were recorded at high temperatures (22 to 80 °C) (Figure 2-33). The Cp proton signals get broader at higher temperature and coalescence at 80 °C. This proves that the molecule is highly dynamic in solution at higher temperature than the ambient temperature. Further NMR measurements at temperatures above 80 °C could not be done due to the instrument restriction as well as the boiling temperature of NMR solvent (toluene-d8). On the other hand, when decreasing temperature from 80 °C to 25 °C, the ^{1}H NMR of compound *syn*-C_2-**103^S-3** showed the expected number of signals for Cp protons (6 signals), which is the same

NMR pattern as before heating. This is strongly proved that the compound *syn*-C_2-**103^{S}-3** are thermally stable, and did not get decomposed when being heated at elevated temperature (80 °C).

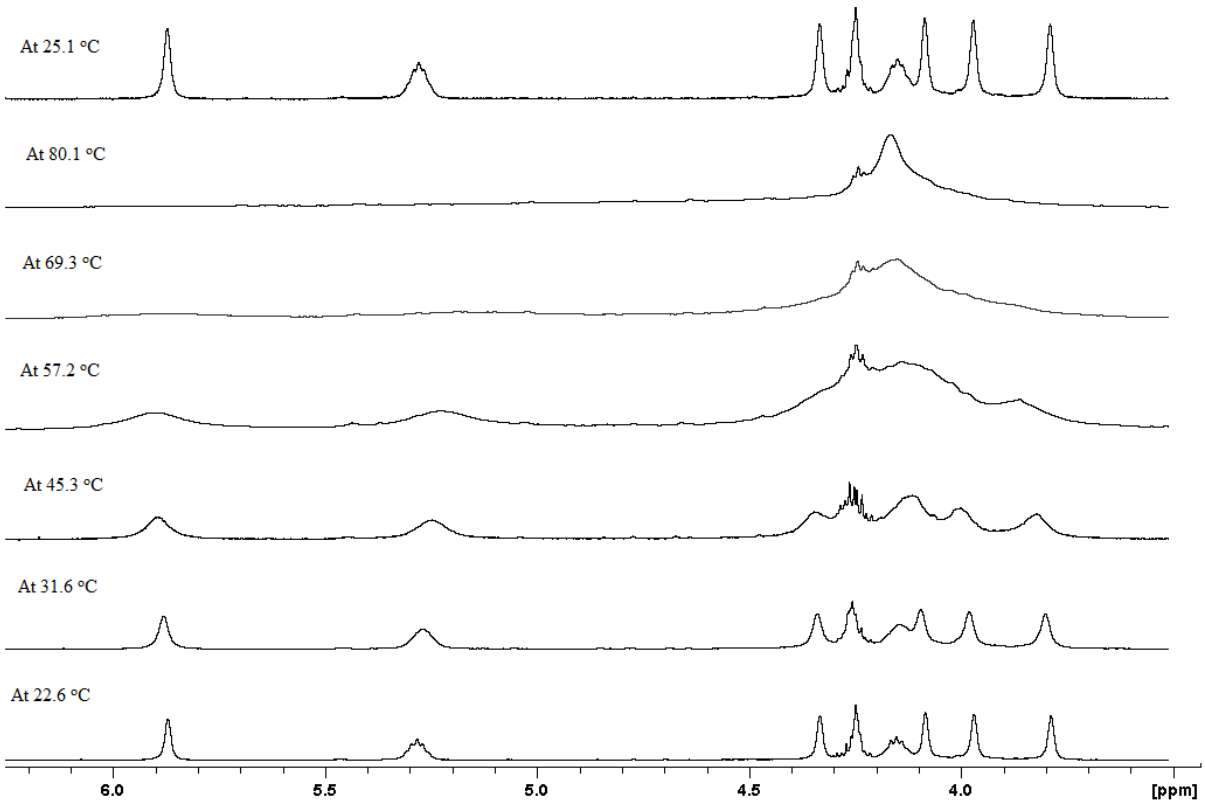

Figure 2-33. ^{1}H NMR spectra of Cp range of the compound *syn*-C_2-**103^{S}-3** recorded at variable temperatures (22–80 °C).

It is worth noticing that half of the Cp rings in *syn*-C_2-**103^{S}-3** isomer has *S* while the other half has *R* planar chirality. Compared to the starting phospha[1]FCP (S_p,S_p)-**20^{Ph}** that means that chirality has been lost (Scheme 2-27). This inversion of configuration must come from breakage of Fe–Cp bond and reformation from the other face of the Cp ring.

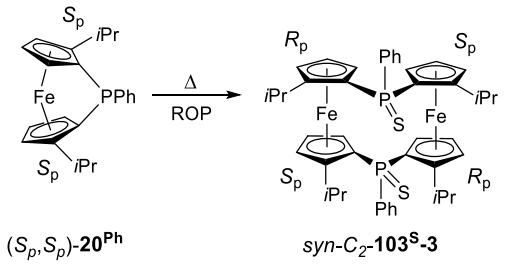

Scheme 2-27. Formation of cyclic dimer *syn*-C_2-**103^{S}-3** from the thermal ROP of phospha[1]FCP (S_p,S_p)-**20^{Ph}**.

In a similar work on the thermal ROP of phospha[1]FCP having one *i*Pr group on the ferrocene unit (*rac*-**22**), Müller and co-workers found evidence for the Fe–Cp bond rupture based on the formation of one of the cyclic dimers.[51] Based on a report about photolytic ROP from 2003,[55] and the recent report on the mechanistic investigation of thermal ROP of *trans*-**22**,[51] a similar mechanism for the thermal ROP of phospha[1]FCP (S_p,S_p)-**20^{Ph}** can be proposed (Scheme 2-28). First, monomer (S_p,S_p)-**20^{Ph}** gets transformed to the intermediate **L$_2$-20^{Ph}** through an η^5 to η^1 haptotropic shift. In this case, the loss of four electrons at iron is compensated by addition of two neutral two-electron donor molecules L. It can be assumed that the compound (S_p,S_p)-**20^{Ph}**, which is a monodentate phosphine, takes up the role of the donor molecule L. The Fe–Cp bond in **L$_2$-20^{Ph}** breaks to form **L$_3$-20^{Ph}**, which then ring-opens monomer (S_p,S_p)-**20^{Ph}** by a nucleophilic attack at iron with its Cp anion. The resulting species **L$_3$-104** is the first product of the chain growth and has two possible routes to further react. Repeated addition of monomer (S_p,S_p)-**20^{Ph}** to the key intermediate **L$_3$-104** leads to polymers **L$_3$-104$_n$** or, through backbiting, a [1.1]FCP is produced. For the case shown in Scheme 2-28, the formation of the *syn*-C_2-**103-3** is illustrated. This compound was isolated in the form of its sulfurized species *syn*-C_2-**103^{S}-3** (Figure 2-32). Obviously, at various stages of the chain-growth, cyclic species could be generated via the backbiting of species **L$_3$-104$_n$**. This explains the

formation of cyclic oligomers with general formula of [1^{x}]FCP with x = 2–6 that were detected by mass spectrometry.

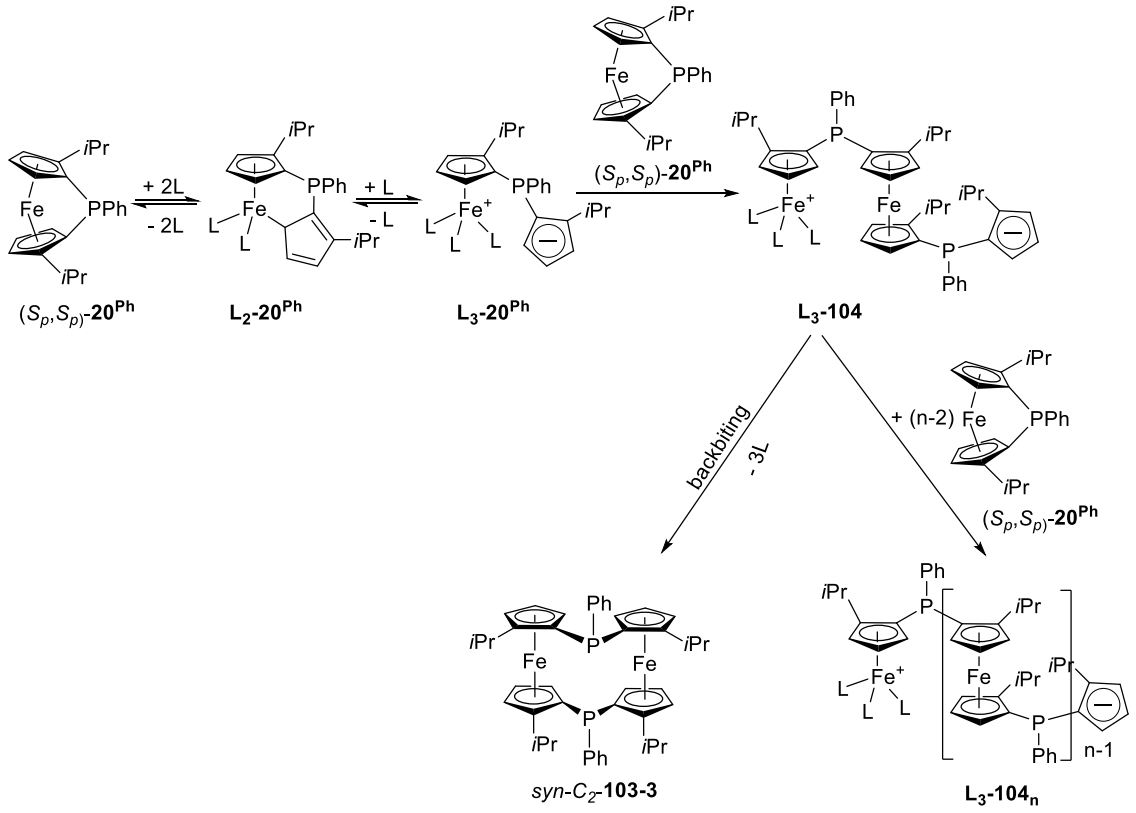

Scheme 2-28. Proposed mechanism for the thermal ROP of the chiral phospha[1]FCP (S_p,S_p)-**20^{Ph}**. Only one isomer was shown for the proposed intermediate **L$_2$-20^{Ph}**.

2.3.3 Thermal ring-opening polymerization of the known phospha[1]ferrocenophane 11^{Ph}

Thermal ROP of the known phospha[1]FCP was reported in literature,[37] however, its mechanism is still unknown. The species **11^{Ph}** was thermally polymerized at 120 °C, and this ROP temperature is significantly low compared to that of the alkylated phospha[1]FCP (S_p,S_p)-**20^{Ph}** (T = 300 °C). Therefore, it was assumed that the thermal ROP of the non-alkylated compound **11^{Ph}** might occur via a Cp–P bond rupture, which is different from that of the alkylated compound (S_p,S_p)-**20^{Ph}** (Fe–Cp bond rupture). In order to prove this, thermal ROP of the known compound **11^{Ph}** was repeated, with a focus on components of reaction mixture.

2.3.3.1 Polymer synthesis and characterization

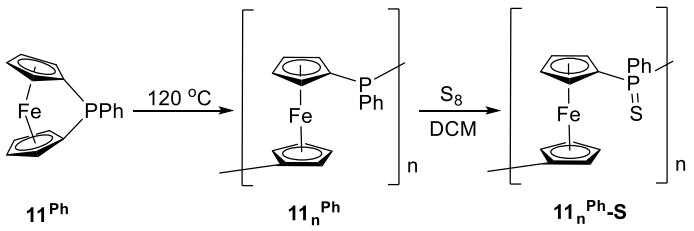

Scheme 2-29. Preparation of the known poly(ferrocenylphosphine)s.

Thermal ROP of the known phospha[1]FCP **11^{Ph}** was performed based on the published procedure,[37] followed by a sulfurization to obtain polymer **11$_n^{Ph}$-S** (Scheme 2-29). Polymer **11$_n^{Ph}$-S** was isolated from the reaction mixture by precipitation into hexanes solution, which yielded yellow powder (65% isolated yield). ^{31}P NMR spectrum of the resulting polymer shows a broad signal at δ = 37.7 ppm, which is close to the reported ^{31}P chemical shift of polymer **11$_n^{Ph}$-S** (δ = 37.5 ppm).[37] Beside the broad signal of the macromolecule, other sharp signals are present at δ = 40.0 and 37.2 ppm with a low intensity (Figure 2-34). These two peaks were assumed to be the signals of cyclic dimers *anti*-**51** and *syn*-**51**, respectively, which were reported by Mizuta and co-workers.[76]

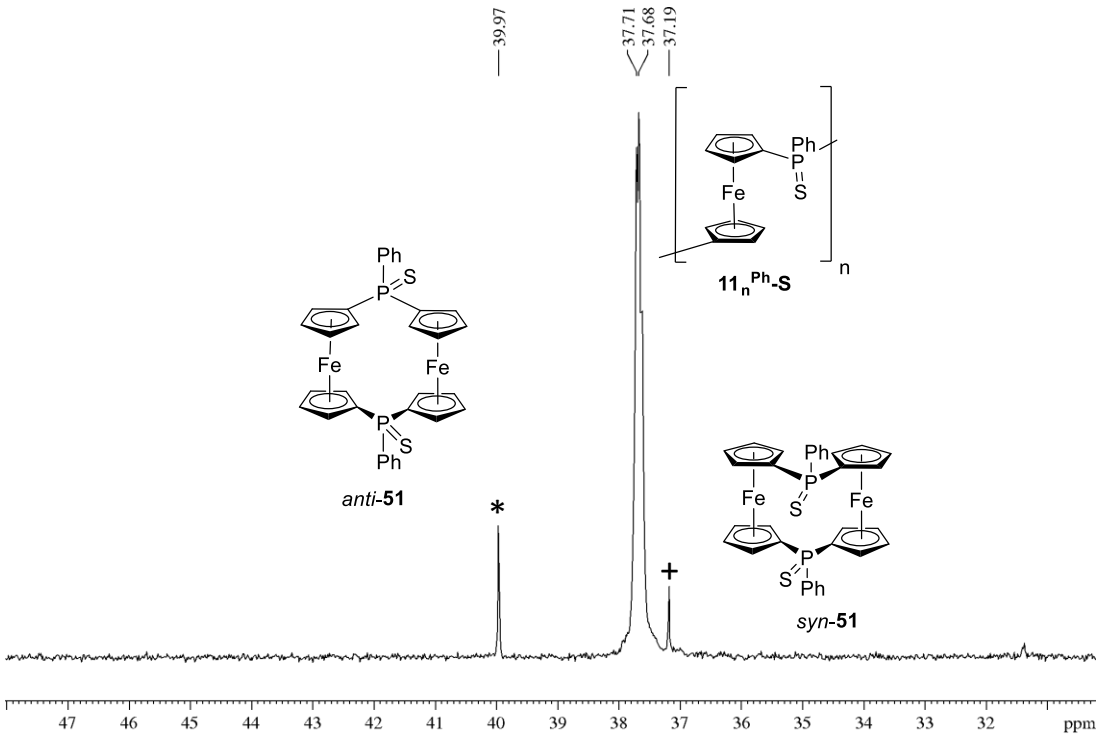

Figure 2-34. $^{31}P\{^{1}H\}$ NMR spectrum (202.5 MHz) of the sulfurized polymer $\mathbf{11_n^{Ph}}$**-S**. The signals of impurities *anti*-**51** and *syn*-**51** are marked as * and +, respectively.

The sulfurized polymer $\mathbf{11_n^{Ph}}$**-S** was analyzed by GPC with a triple detection system, which revealed an absolute molecular weight of M_w = 87 kDa and a dispersity $Đ$ = 1.6. This M_w is significantly higher compared to the published data (M_w = 18 kDa, $Đ$ = 1.52).[37] The large difference in molecular weight is due to the fact that thermal ROP is a non-living process, and it is difficult to control the molecular weight. The molecular weight distribution of polymer $\mathbf{11_n^{Ph}}$**-S** is quite broad ($Đ$ = 1.6) and the GPC curve shows tailing into the lower-molecular-weight region (high retention volume, Figure 2-34). This special GPC shape was likely caused by the contamination of two species *syn*-**51** and *anti*-**51**, which could not be separated from the resulting polymer $\mathbf{11_n^{Ph}}$**-S**.

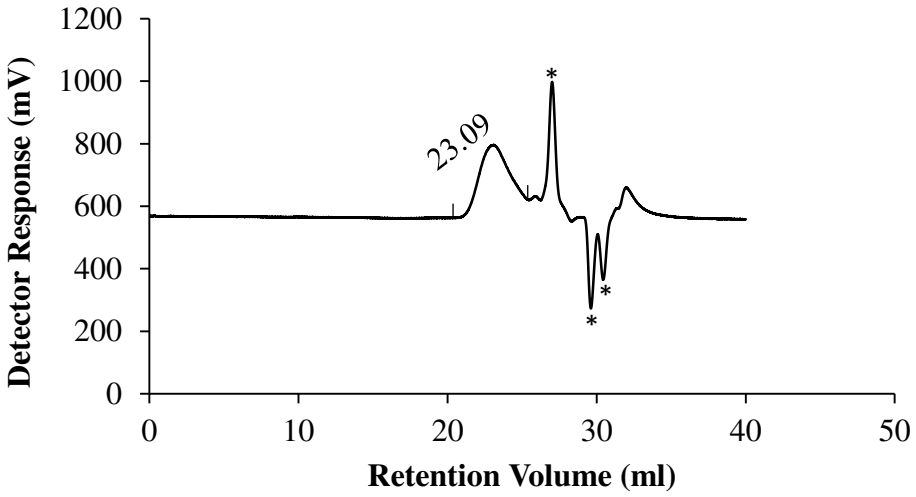

Figure 2-35. GPC trace of polymer $\mathbf{11_n^{Ph}}$**-S** (c =14.3 mg / 8.5 mL thf). System peaks are indicated with *.

Table 2-8. GPC analysis for polymer $\mathbf{11_n^{Ph}}$**-S**.

	$\mathbf{11_n^{Ph}}$**-S**
M_n *(Da)*	54 x 10^3
M_w *(Da)*	87 x 10^3
M_z *(Da)*	147 x 10^3
M_p *(Da)*	75 x 10^3
M_w/M_n	1.6

2.3.3.2 Identification of by-products and investigation of possible mechanism for the thermal ring-opening polymerization of 11^{Ph}

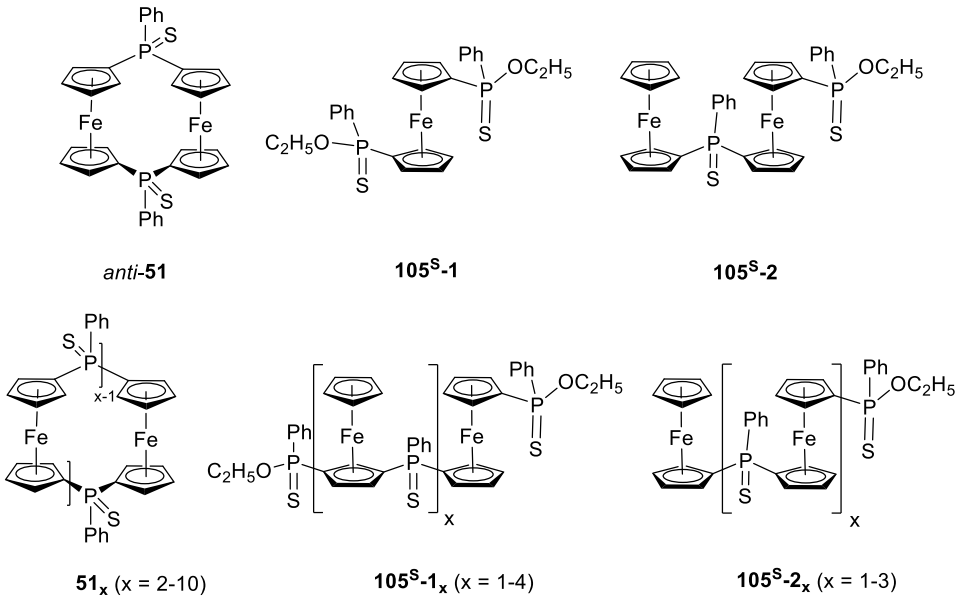

Figure 2-36. Structures of by-products in the reaction aliquots of the thermal ROP of phospha[1]FCP $\mathbf{11^{Ph}}$.

Approximately 25% of the reaction mixture from the thermal ROP of phospha[1]FCP $\mathbf{11^{Ph}}$ did not precipitate and stayed in the solution. After this soluble part was also sulfurized, the ^{31}P NMR spectrum of the mixture $\mathbf{105^S}$ exhibits a series of sharp signals from δ = 83.6 to 37.2 ppm. A mass spectrum showed peaks that referred to cyclic oligomers and linear ethoxy-containing oligomers. Using PTLC, three fractions were collected (*anti*-**51**, $\mathbf{105^S}$**-1**, and $\mathbf{105^S}$**-2**, Figure 2-36), and analyzed by NMR spectroscopy and mass spectrometry. The other cyclic and ethoxy-containing oligomers could not be isolated and identified ($\mathbf{51_x}$, $\mathbf{105^S}$**-1**$_\mathbf{x}$, and $\mathbf{105^S}$**-2**$_\mathbf{x}$), presumably due to their trace amounts in the mixture.

NMR spectroscopic data of the first isolated fraction matched with that of the known [1.1]FCP $[PhP(=S)fc]_2$ (*anti*-**51**), which was reported by Mizuta in 2005 (section 1.2.4.3).[128]

Beside this, other cyclic oligomers of type $\mathbf{51_x}$ were also detected in the mass spectrum. As mentioned above, Mizuta and co-workers also detected the presence of these cyclic oligomers (up to hexamers), while investigating the photolytic ROP of the [1]FCP $\mathbf{11^{Ph}}$.[126] However, only a cyclic trimer was isolated and characterized by NMR spectroscopy and single crystal X-ray analysis.[126] According to the authors, other cyclic oligomers existed in trace amounts and could not be isolated from the reaction mixture.[131] In another investigation, Manners and co-workers successfully isolated cyclic oligo(ferrocenylsilane)s with up to seven repeating units through a photolytic living ROP of silicon-bridged [1]FCPs.[9] It was found that in the ROP process, an intramolecular head-to-tail ring-closure likely occurred, resulting in the formation of cyclic dimers (or oligomers).[76,131,132]

NMR spectroscopic data and mass spectrometry of the other fractions show the presence of ferrocene-based phosphine compounds having ethoxy-containing group ($\mathbf{105^S}$**-1** and $\mathbf{105^S}$**-2**). Species $\mathbf{105^S}$**-1** is a mixture of two diastereomers. For example, its ^{1}H NMR spectrum shows two sets of signals in the Cp range (δ = 4.81–4.12 ppm), with ratio of 1 to 1, indicating two diastereomers. Both sets show four signals each and are partially overlapping. The ^{31}P NMR spectrum of mixture $\mathbf{105^S}$**-1** shows two signals at δ = 83.4 and 83.5 ppm, which is similar as the reported data of the sulfurized phosphine compound $Ph_2(P{=}S)OEt$ (δ = 81 ppm).[133] The compound of type $\mathbf{105^S}$**-1** has not been reported before, however, related compounds can be found in the literature.[134,133]

Species $\mathbf{105^S}$**-2** could not be cleanly isolated due to the presence of other impurities. However, both ^{1}H and ^{31}P NMR spectra detect the presence of species $\mathbf{105^S}$**-2** as the major component. For example, its ^{1}H NMR spectrum shows a sharp single signal at δ = 4.16 ppm, indicating a non-substituted Cp ring. The ^{31}P NMR spectrum shows mainly two signals at δ = 84

and 39 ppm, indicating the presence of two different phosphorus atoms. Its mass spectrum shows a major signal matched with the molecular weight of species **105^{S}-2**.

The presence of these ethoxy-containing species of type **105^{S}-1** and **105^{S}-2** is a surprise, indicating that the Cp–P bond must have been broken. Therefore, it is intriguing to figure out the source of these species. There are three possible sources that can generate ethoxy derivatives, which are contaminants of the monomer **11^{Ph}**, the solvent used to dissolve reaction mixture (in this case thf), and NMR tubes. NMR spectroscopic data of the monomer **11^{Ph}** show no trace of ethoxy-containing impurities, hence, the possibility of contaminated monomer was eliminated. Second, as thf can generate -CH_2O derivative during its decomposition, this could be considered as one possible reason for the formation of ethoxy-containing compounds. In order to prove that, the reaction crude after the thermal ROP was directly dissolved in different types of solvents, including ethereal and non-ethereal solvents (thf, *tert*-butyl methyl ether, and CH_2Cl_2) (Scheme 2-30). This mixture was then analyzed by NMR spectroscopy and mass spectrometry.

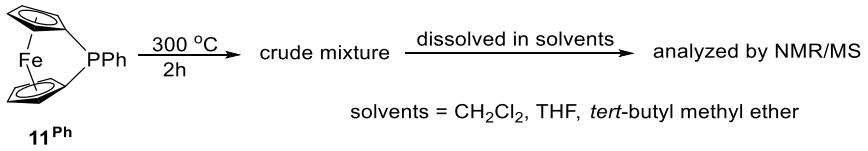

Scheme 2-30. Thermal ROP of phospha[1]FCP **11^{Ph}**. The reaction mixture was dissolved in different solvents.

The mass spectrum of the reaction mixture shows the presence of three species *anti*-**51**, **105-1** and **105-2**, even when the non-ethereal solvent was used. The ^{31}P NMR spectrum shows three sets of signals, which appear at δ =155, 106 and from –23 to –32 ppm (Figure 2-37). The signal at δ = 155 ppm is assigned to the known diethyl phenylphosphonite,[135] and multiple signals at 106 ppm are assigned to the ethoxy-containing oligomers (**105-1$_x$** and **105-2$_x$**).[136] Other signals from –23 to –32 ppm are from the cyclic oligomers (*anti*-**51$_x$**) and linear polymers

($\mathbf{11_n^{Ph}}$).[37,131] From these data, it was concluded that the choice of solvent did not affect the outcome of the thermal ROP. The ethoxy-containing species were present in the reaction mixture with or without the use of an ethereal solvent.

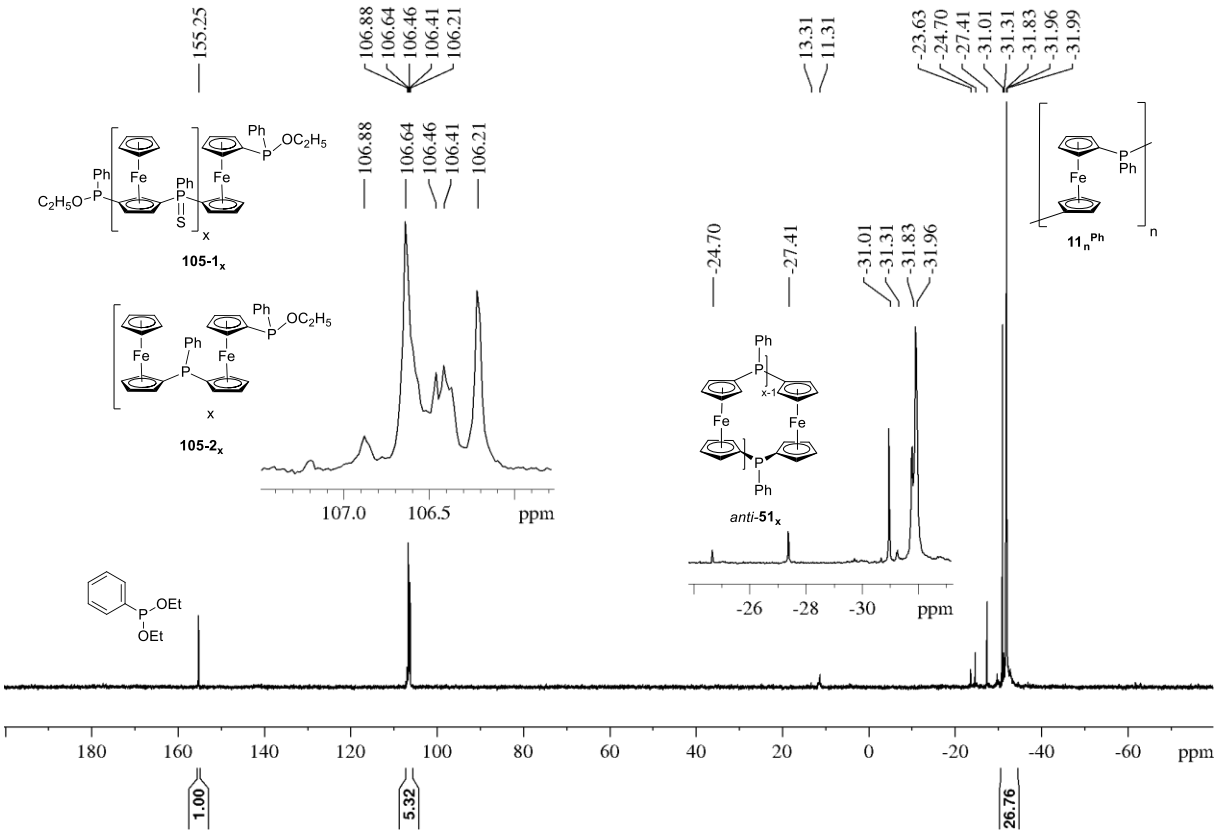

Figure 2-37. $^{31}P\{^{1}H\}$ NMR spectrum (202.5 MHz) of non-sulfurized reaction mixture from the thermal ROP of compound $\mathbf{11^{Ph}}$ using a used NMR tube. Signals of ethoxy-containing species $\mathbf{105\text{-}1_x}$ and $\mathbf{105\text{-}2_x}$ were present at 106 ppm.

Thus, the last possible source that can generate the ethoxy-containing compounds is the NMR tubes used for the thermal ROP experiments. With that idea, another thermal ROP was performed, using a new NMR tube, which comes directly from the factory and has not been used before. The reaction mixture was dissolved in CH_2Cl_2, and the resulting product was characterized by NMR spectroscopy and mass spectrometry. As expected, both ^{31}P NMR

spectroscopy and mass spectrometry did not show the presence of any ethoxy-containing ferrocene derivatives (Figure 2-38). This result confirmed that the ethoxy-containing species were generated from the side reaction between the NMR tube glass surface and reactive ferrocene compounds during the thermal ROP process. At high temperature, scratches on used NMR tubes likely allowed reactions between glass materials (SiO_2 and B_2O_3) and ferrocene species, leading to the formation of ethoxy-containing compounds of type **105-1** and **105-2**.

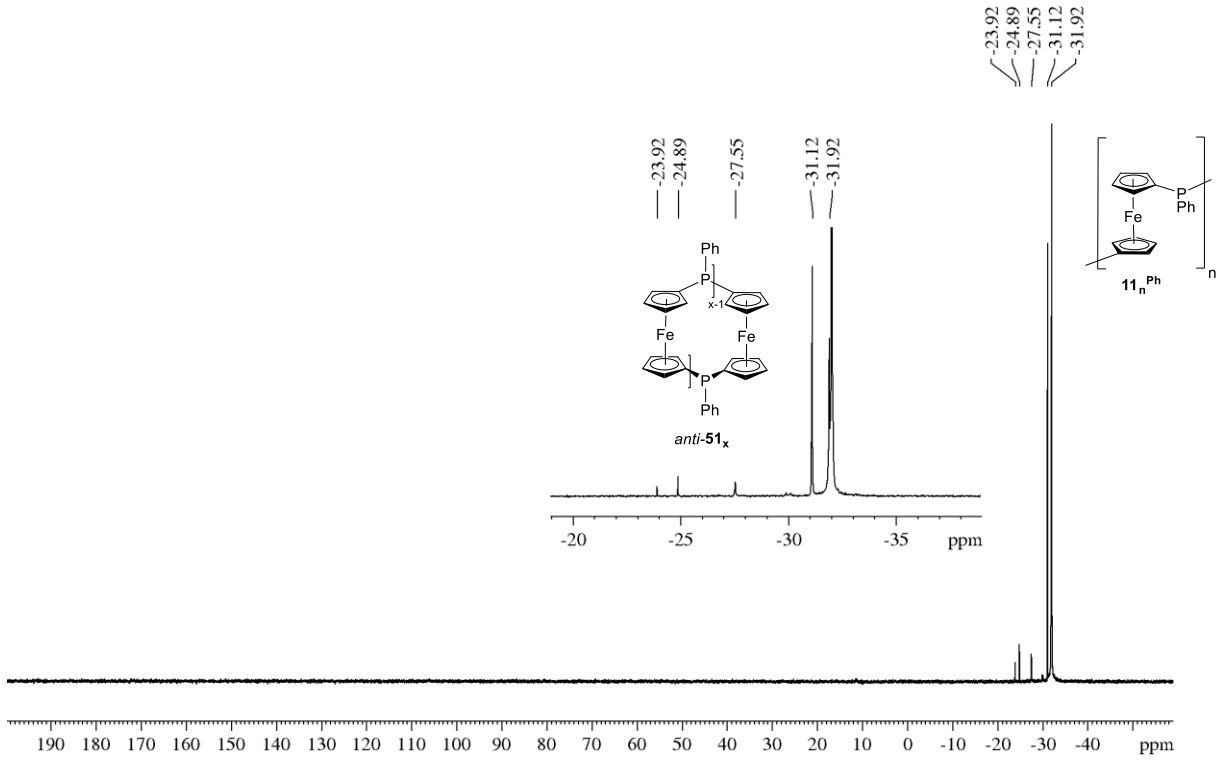

Figure 2-38. $^{31}P\{^{1}H\}$ NMR spectrum (202.5 MHz) of the non-sulfurized reaction mixture from thermal ROP of compound $\mathbf{11^{Ph}}$ using a new NMR tube. Signals of ethoxy-containing species $\mathbf{105\text{-}1_x}$ and $\mathbf{105\text{-}2_x}$ were not detected.

To conclude, the mechanism of thermal ROP of the known phospha[1]FCP $\mathbf{11^{Ph}}$ is still unknown. However, it is very important to emphasize that the quality of NMR tubes can significantly affect the outcome of this work. Therefore, one must be careful when choosing

NMR tubes for conducting experiments, especially, the experiments that are required to be conducted at high temperatures.

2.3.4 Attempted thermal ring-opening polymerization of chiral phospha[2]ferrocenophanes

The crystal structure of compound (S_p,S_p,*R*,*R*)-**90**$^{\mathbf{CH2SiMe3}}$ revealed a tilt angle α = 12.2° (section 2.1.5, Table 2-2), indicating the presence of low to moderate intrinsic strain. To date, no reactivity pathways that relates to the release of ring-strain of these compounds have been reported, perhaps due to the insufficient strain in diphospha[2]FCPs. Therefore, it would be very intriguing to see if the species (S_p,S_p,*R*,*R*)-**90**$^{\mathbf{CH2SiMe3}}$ could be thermally ring-opened.

DSC measurements were performed to investigate the thermal properties of the two compounds (S_p,S_p,*R*,*R*)-**90**$^{\mathbf{CH2SiMe3}}$ and **90**$^{\mathbf{NiPr2}}$. However, the DSC thermograms exhibit only an endothermic peak, suggesting that no ring-opening process had been occurred (Figure 2-39). In order to further support the DSC results, thermal ROP of the phospha[2]FCP (S_p,S_p,*R*,*R*)-**90**$^{\mathbf{CH2SiMe3}}$ was attempted.

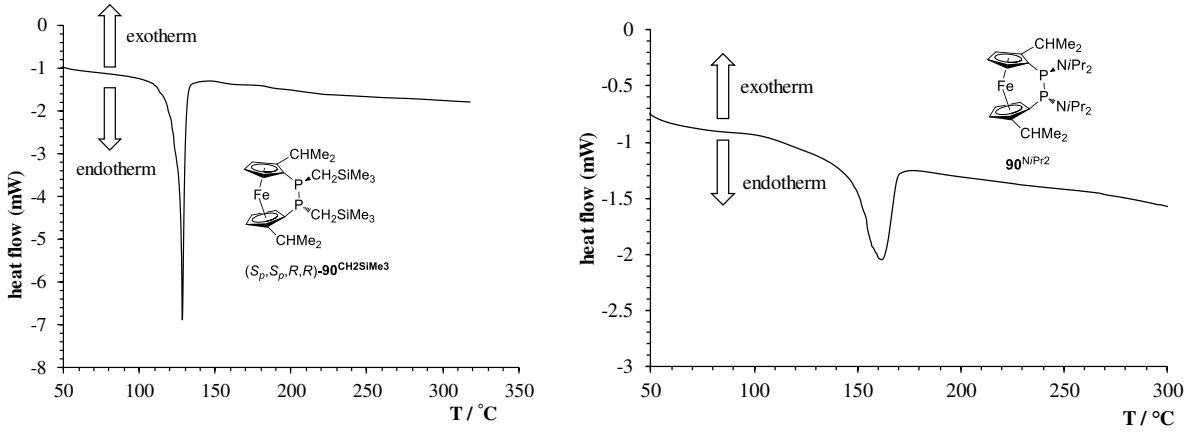

Figure 2-39. DSC measurements of the chiral phospha[2]FCPs **90**$^{\mathbf{CH2SiMe3}}$ and **90**$^{\mathbf{NiPr2}}$.

The monomer (S_p,S_p,*R*,*R*)-**90**$^{\mathbf{CH2SiMe3}}$ was heated at 300 °C for 6 h in a sealed NMR tube. During the time of heating, the color of the tube's content did not change, and the material in the NMR tube was melted. After 6 h of heating, the NMR tube was cooled down to r.t., and the melt turned into an orange solid. The tube's content was dissolved in C_6D_6 and analyzed by NMR spectroscopy. Both ^{1}H and ^{31}P NMR spectra did not detect any new signals, which are in agreement with what was observed in the DSC measurements. Although thermal ROP was not performed on the other compound, based on its DSC thermogram (Figure 2-39) and the results obtained from thermal ROP of (S_p,S_p,*R*,*R*)-**90**$^{\mathbf{CH2SiMe3}}$, compound **90**$^{\mathbf{NiPr2}}$ would likely not to be thermally ring-opened. Overall, the diphospha[2]FCPs are thermally robust and could not undergo thermal ROP. This is not surprising due to the insufficient strain in these compounds.

2.4 Attempted photolytic living anionic ring-opening polymerization of phospha[1]ferrocenophanes

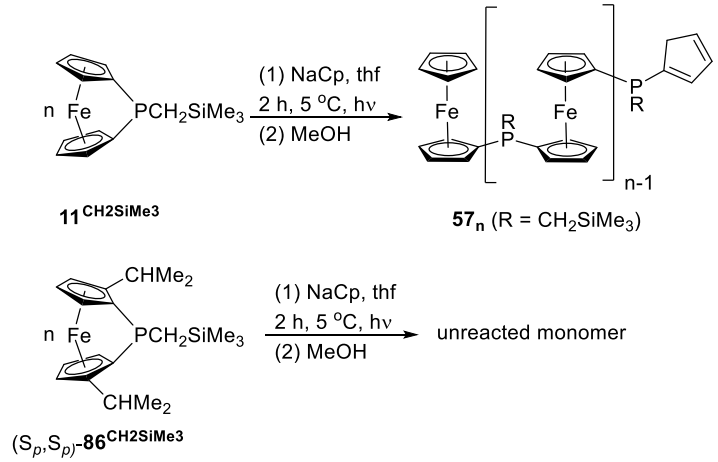

Scheme 2-31. Attempted photolytic living anionic ROP of phospha[1]FCPs **11**$^{\mathbf{CH2SiMe3}}$ and (S_p,S_p)-**86**$^{\mathbf{CH2SiMe3}}$. One of many feasible isomers of compound **57**$_{\mathbf{n}}$ is shown.

As mentioned in section 1.2.4.3, photolytic living anionic ROP is the most recent method developed to obtain well-defined metallopolymers.[39] Compared to the conventional anionic ROP

using organolithium reagents, the use of a milder initiator like NaC_5H_5 in the photolytic anionic ROP can make this polymerization method easier to perform. Preliminary results from the attempted anionic ROP of compound (S_p,S_p)-**86**^{CH2SiMe3} showed that side reactions between CH_2SiMe_3 group and *n*BuLi led to unsuccessfully polymerization (section 2.2.2). Therefore, it was hoped that using NaC_5H_5 as initiator could lead to a successful polymerization. In order to apply the right techniques on this new polymerization system, it was important to reproduce the published data. Thus, the photolytic living anionic ROP of the known phospha[1]FCP **11**^{CH2SiMe3} was repeated following literature ,[39] and the obtained results were compared with the reported data. The same technique used for the known compound **11**^{CH2SiMe3} was then applied to the chiral phospha[1]FCPs (S_p,S_p)-**86**^{CH2SiMe3}.

For the known species **11**^{CH2SiMe3}, using monomer/initiator ratio of 50/1 and after being irradiated with UV light for 2 h at 5 °C, the color of reaction mixture changed from dark-red to yellow. A few drops of degassed methanol were added to neutralize all the active species (Scheme 2-31). The reaction mixture was added to a vigorously stirred hexanes solution, resulting in yellow precipitates, which were characterized by NMR spectroscopy. The ^{1}H NMR spectrum shows broad signals from δ = 4.09–4.40 ppm for the Cp range, suggesting that the expected polymer was formed. In the ^{31}P NMR spectrum, a broad signal appears at δ = –47.5 ppm, which is very close to the reported ^{31}P chemical shift of polymer **57**$_n$ (δ = –47.1 ppm).[39] In summary, these NMR spectroscopic data are in agreement with the published data, therefore, assuring that the equipment for and the executing of the polymerization worked for the known compound **11**^{CH2SiMe3} as described in the literature.

However, using the same ROP technique for the chiral phospha[1]FCP (S_p,S_p)-**86**^{CH2SiMe3}, the color of reaction mixture did not change after 2 hours of irradiation, indicating

that the strained monomer was still the dominant species in solution. ^{1}H and ^{31}P NMR spectroscopy finally revealed that only the strained compound (S_p,S_p)-**86**$^{\mathbf{CH2SiMe3}}$ was present. Additional attempts, such as increasing reaction temperature or extending reaction time did not lead to any detectable products. Thus, the photolytic living anionic ROP of species (S_p,S_p)-**86**$^{\mathbf{CH2SiMe3}}$ did not occur. At this point, we do not have enough evidence to conclude if the initiation step could not occur, or the chain propagation failed.

CHAPTER 3. SUMMARY AND CONCLUSION

3.1 Synthesis of chiral phosphorus-bridged [*n*]ferrocenophanes

Following a reported procedure, the enantiomerically pure dibromoferrocene (S_p,S_p)-**19** was successfully prepared.[105] Through the salt-metathesis reaction of the dilithio derivative of (S_p,S_p)-**19** with dichlorophosphines, the new chiral phosphorus-bridged [1]FCPs (S_p,S_p)-**86**$^{\mathbf{CH2SiMe3}}$ and (S_p,S_p)-**86**$^{\mathbf{NiPr2}}$ were prepared (Figure 3-1). Both compounds are volatile under vacuum at elevated temperature (80 °C), and were isolated by sublimation [(S_p,S_p)-**86**$^{\mathbf{CH2SiMe3}}$] or flask-to-flask condensation [(S_p,S_p)-**86**$^{\mathbf{NiPr2}}$]. Both species possess similar NMR patterns as the previously reported chiral phospha[1]FCPs (S_p,S_p)-**20**$^{\mathbf{R}}$ and (S_p,S_p)-**21** (section 1.2.1). This supports the expectation that the two compounds (S_p,S_p)-**86**$^{\mathbf{CH2SiMe3}}$ and (S_p,S_p)-**86**$^{\mathbf{NiPr2}}$ are *non*-symmetrical species, with planar-chirality on the ferrocene moiety.

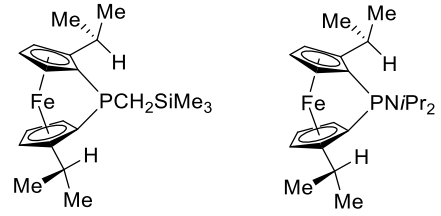

(S_p,S_p)-**86**$^{\mathbf{CH2SiMe3}}$ (S_p,S_p)-**86**$^{\mathbf{NiPr2}}$

Figure 3-1. Chiral phospha[1]FCPs (S_p,S_p)-**86**$^{\mathbf{CH2SiMe3}}$ and (S_p,S_p)-**86**$^{\mathbf{NiPr2}}$.

The enantiomerically pure diphospha[2]FCPs (S_p,S_p,*R*,*R*)-**90**$^{\mathbf{CH2SiMe3}}$ and **90**$^{\mathbf{NiPr2}}$ (Figure 3-2) were synthesized via a two-step procedure, starting from the chiral dibromoferrocene (S_p,S_p)-**19**. Both compounds were isolated via vacuum sublimation at high temperature (120 °C), and crystals of (S_p,S_p,*R*,*R*)-**90**$^{\mathbf{CH2SiMe3}}$ were subjected to single-crystal X-ray analysis. The tilt angle α of (S_p,S_p,*R*,*R*)-**90**$^{\mathbf{CH2SiMe3}}$ was determined as 12.2° (Table 2-2), which is in the range of

the known diphospha[2]FCPs (7.7–13.6°).[28,33,104] NMR spectroscopic data show that these diphospha[2]FCPs [(S_p,S_p,R,R)-**90**$^{\mathbf{CH2SiMe3}}$ and **90**$^{\mathbf{NiPr2}}$] are C_2-symmetric species. It is worth mentioning that (S_p,S_p,R,R)-**90**$^{\mathbf{CH2SiMe3}}$ and **90**$^{\mathbf{NiPr2}}$ are the first chiral diphospha[2]FCPs having both planar and central chirality.

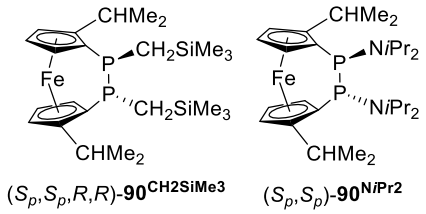

Figure 3-2. Chiral diphospha[2]FCPs (S_p,S_p,R,R)-**90**$^{\mathbf{CH2SiMe3}}$ and **90**$^{\mathbf{NiPr2}}$.

The new 1,1'-bis(phosphanyl)ferrocene (**S_p,S_p,S,S)-88**$^{\mathbf{NiPr2}}$ was synthesized via the addition of the phosphorus reagent iPr$_2$NPCl$_2$ to the lithium derivative of dibromoferrocene (S_p,S_p)-**19**. Due to phosphorus being the stereogenic atom, 3 diastereomers could possibly form in this reaction. To our surprise, the reaction was very selective. The reaction mixture mainly contained one isomer, which was isolated through vacuum sublimation at ca. 120 °C. Single-crystal X-ray analysis of the so-obtained crystals revealed that both phosphorus atoms were generated in *S* configuration.

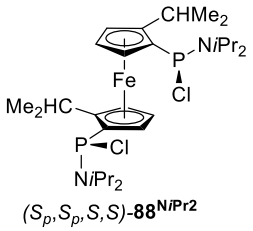

Figure 3-3. 1,1'-Bis(phosphanyl)ferrocene (S_p,S_p,S,S)-**88**$^{\mathbf{NiPr2}}$.

3.2 Attempted anionic ring-opening polymerization

3.2.1 Attempted anionic ring-opening polymerization of phospha[*n*]FCPs

A series of anionic ROPs experiments were performed with the chiral phospha[1]FCPs having different groups on phosphorus; however, no polymeric materials could be isolated. It was found that the lithium species (S_p,S_p)-**95**$^{\mathbf{Li}}$ failed to further react with other monomers, even though this species was present long enough in the reaction mixture (within 4 h in Et_2O). That means that the initiation step of the attempted anionic ROP worked, but the ring-propagation did not occur.

3.2.2 Synthesis of a new chiral ferrocene-based phosphine ligand (S_p,S)-99 via the anionic ring-opening reaction

One of the phospha[1]FCP (S_p,S_p)-**20**$^{\mathbf{Ph}}$ showed the ability to be cleanly ring-opened with 1 equiv of *n*BuLi, generating a stable lithium derivative (S_p,S_p)-**95**$^{\mathbf{Li}}$ in Et_2O (Figure 3-4). This lithium species reacted with PPh_2Cl to give the new chiral ferrocene-based phosphine ligand (S_p,S)-**99** (Figure 3-4). This new ligand possesses both planar and central chirality, and might be a useful ligand for asymmetric catalysis.

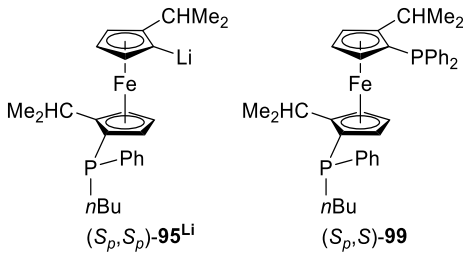

Figure 3-4. The new chiral ferrocene-based phosphine ligand (S_p,S)-**99**.

3.3 Metallopolymers through thermal ring-opening polymerization

Differential Scanning Calorimetry was performed on phospha[1]FCPs having different substituents on the phosphorus atom. Based on the DSC data, the bulkier the substituent groups on phosphorus, the smaller the heat that gets released. The alkyl groups on the ferrocene moiety of the strained monomer can increase the steric hindrance in a ferrocene system, leading to a substantial destabilization of resulting polymer. Thus, with increasing numbers of alkyl groups on Cp rings, less heat is released in the ROP process.

The thermal ROP of (S_p,S_p)-**20**$^{\mathbf{Ph}}$ at 300 °C revealed that approximately 45% of the reaction mixture contained polymeric materials, while the rest of the mixture was cyclic oligomers. Both polymeric and cyclic species were reacted with elemental sulfur, in order to get stable compounds for further characterization. Separation on the mixture of cyclic oligomers resulted in isomeric dimers, which possessed different symmetries. One of the cyclic dimers formed crystal, which was then subjected to single-crystal X-ray analysis (*syn*-C_2-**103**$^{\mathbf{S}}$-**3**). The crystal structure revealed that this dimer can only be formed via a cleavage of Fe–Cp bond in the strained monomer (S_p,S_p)-**20**$^{\mathbf{Ph}}$. Based on the recent study on thermal ROP of the phospha[1]FCP *trans*-**22**[51] and the known knowledge of photolytic ROP,[55] a mechanism for the thermal ROP of phospha[1]FCP (S_p,S_p)-**20**$^{\mathbf{Ph}}$ was proposed.

CHAPTER 4. EXPERIMENTAL SECTION

4.1 General Procedures

General Methods. If not mentioned otherwise, all syntheses were carried out using standard Schlenk and glovebox techniques. Solvents were dried using an MBraun Solvent Purification System and stored under nitrogen over 3 Å molecular sieves. All solvents for NMR spectroscopy were degassed (freeze-pump-thaw method) prior to use and stored under nitrogen over 3 Å molecular sieves. Unless otherwise noted, temperatures refer to that of the bath (e.g., dry ice/acetone bath for –78 °C). Flash chromatography was performed with neutral aluminum oxide and silica gel 60, respectively; mixed solvents eluents are reported as vol / vol solutions. For controlled addition of solution of some phosphorus reagents, a syringe pump was used (Sage Instrument, model 355).

Characterization Methods. ^{1}H, ^{13}C and ^{31}P NMR spectra were recorded on a 500 MHz Bruker Advance, 500 MHz Bruker Advance III HD, 500 MHz and 600 MHz Bruker Advance III HD NMR spectrometers at 25 ºC in C_6D_6 or $CDCl_3$, respectively. ^{1}H chemical shifts were referenced to the residual protons of the deuterated solvent [δ = 7.15 ppm (C_6D_6), 7.26 ($CDCl_3$) ppm]. ^{13}C chemical shifts were referenced to the C_6D_6 signal (δ = 128.00 ppm) and the $CDCl_3$ signal (δ = 77.00 ppm). ^{31}P NMR chemical shifts were reported relative to the external reference of 85% H_3PO_4 in D_2O. The following abbreviations are used to described NMR signals: s (singlet), d (doublet), t (triplet), pst (pseudo triplet), sept (septet), m (multiplet), br (broad), unres (unresolved). Many Cp protons appear as slightly broadened singlets, while others either appear as triplets or as an unresolved triplet. Due to limited digital resolutions in NMR spectra, reported coupling constants obtained from ^{13}C NMR spectra are rounded to integer values in Hz; those obtained from ^{1}H NMR spectra are associated with an error (the digital resolution in ^{1}H NMR

spectra is either 0.2 ((*S*$_p$,*S*$_p$,*R*,*R*)-**90**$^{\mathbf{CH2SiMe3}}$, 1,1′-(*S*$_p$,*S*$_p$,*S*,*S*)-**88**$^{\mathbf{NiPr2}}$) or 0.3 Hz). Assignments for all new compounds were supported by additional NMR experiments (DEPT, HMQC, COSY). High resolution mass data were obtained with a JEOL AccuTOF GCv 4G instrument using field desorption ionization (FDI). Elemental analyses were performed on a Perkin Elmer 2400 CHN Elemental Analyzer.

Reagents. The compounds **77**,[92] **79**,[92] **83**[92] and **85**[102] were prepared as described in the literature. The compounds **11**$^{\mathbf{Ph}}$,[37,42] **11**$^{\mathbf{CH2SiMe3}}$,[39] (*S*$_p$,*S*$_p$)-**20**$^{\mathbf{Ph}}$,[64] (*S*$_p$,*S*$_p$)-**20**$^{\mathbf{iPr}}$,[64] (*S*$_p$,*S*$_p$)-**19**,[105] Cl_2PSiMe_3 **87**,[39] Cl_2PNiPr_2 **89**[110] and the oxazaborolidine catalyst **109**,[137] were prepared according to the literature with some alterations; therefore, the synthesis of these known compounds are reported and the changes are also mentioned in the section below. The compound (*S*$_p$,*S*$_p$)-**20**$^{\mathbf{tBu}}$ was synthesized by the former member Saeid Sadeh, and used in this thesis work without any further purification.[64] *n*BuLi (2.5 M in hexanes), phenyldichlorophosphine (97%), ferrocene (98%), trimethylaluminum (2.0 M solution in hexanes), dichloroisopropylphosphine (97%), 1,2-dibromotetrachloroethane (Acros, 97%), methyl trifluoromethanesulfonate (98%), and tris(dimethylamino)phosphine (97%) were purchased from Sigma-Aldrich. N,N,N,N′-Tetramethylenediamine (Alfa Aesar, 99%), acetic anhydride (EMD, ACS grade, 99%), and magnesium turnings (99.8%) were purchased from VWR. Elemental sulfur (99%) and preparative thin layer chromatography (PTLC) plates [glass plates (20 × 20 cm) pre-coated (0.25 mm) with silica gel 60 F_{254}] were purchased from EMD. Silica gel 60 (EMD, Geduran, particle size 0.040-0.063 mm) and aluminum oxide (Sigma-Aldrich, activated, neutral, Brockmann I, 58 Å pore size) were used for flash column chromatography.

4.2 Thermal Studies

Differential Scanning Calorimetry (DSC) analyses were performed on a TA Instruments Q20 at a heating rate of 10 °C/min. Samples, sealed in hermetic aluminum pans, were tared using a balance with a repeatability of 0.1 mg (AB204-S Mettle Toledo). For each run, around 2-3 mg of a sample was measured. The known melting enthalpy of a sample of indium was used to check on the calibration of the DSC instrument. DSC data were analyzed with the TA Instruments Universal Analysis 2000 software.

4.3 Gel Permeation Chromatography (GPC) Analyses

Chromatograms were recorded on a Viscotek 350 HT-GPC system (Malvern) (column temperature of 45.1 °C; thf; flow rate = 1.0 $mL.min^{-1}$; calibrated for polystyrene standards). The instrument was equipped with the following Viscotek components: auto-sampler (Model 430 Vortex), degasser (model 7510), two pumps (model 1122), 7° and 90° light scattering detectors, refractometer, and viscometer. GPC columns cover the range of M_w of 500 to 10,000,000 $g.mol^{-1}$ (three main columns: Plgel 10 μM MIXED-B LS 300 × 7.5 mm; one guard column: 10μM GUARD 50 × 7.5 mm; Agilent Technologies). Samples were dissolved in thf and filtered through 0.45 μm syringe PTFE filters before GPC.

4.4 Syntheses

4.4.1 Syntheses of known reagents

4.4.1.1 Synthesis of oxazaborolidine (Corey-Bakshi-Shibata catalyst)

Synthesis of *(S)-N*-ethoxycarbonylproline methyl ester (**106**)

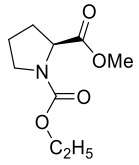

106

The known compound **106** was prepared following the described procedure[138] with the change in solvent used for work-up: ethyl acetate was used instead of chloroform. To a solution of L-proline (6.96 g, 60.4 mmol) in methanol (120 mL) was added potassium carbonate (8.35 g, 60.4 mmol). The reaction mixture was cooled down to 0 °C and ethyl chloroformate (d = 1.143 g/cm^3, 12.5 mL, 133 mmol) was added dropwise via syringe. The mixture was warmed up to r.t. and stirred overnight under atmosphere. After stirring overnight, methanol was evaporated under reduced pressure, and the residual oil was poured into a prepared beaker with distilled water (90 mL). This solution was extracted with ethyl acetate (3 x 300 mL) and the combined organic phases was washed with brine (300 mL) and then dried over Na_2SO_4. All volatiles were removed under reduced pressure, which yielded the final product as a colorless oil (12.1 g, 98%). ^{1}H NMR ($CDCl_3$, 500.1 MHz): δ 1.13 (t, 3H), 1.20 (t, 3H), 1.85–2.30 (m, 8H), 3.35–3.60 (m, 4H), 3.65 (s, 3H), 3.67 (s, 3H), 3.99–4.15 (m, 4H), 4.24 (dd, 1H), 4.30 (dd, 1H). The ^{1}H NMR data was in accordance with literature.

Synthesis of *(S)-N*-ethoxycarbonyl-*α,α*-diphenylprolinol (**107**)

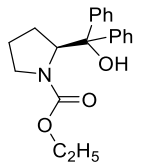

107

The known compound **107** was prepared following the described procedure[139] with detailed information about the solvent mixture used for flash column chromatography, which was not previously mentioned in the literature. Magnesium turnings (11.7 g, 480 mmol) were introduced into a 1L three-necked flask fitted with a dropping funnel and a reflux condenser, and dried under high vacuum for 3 h. Dry thf (150 mL) was added to that three-necked flask and stirred for 15 min. Bromobenzene (25.2 mL, 240 mmol) was added to another 250 mL Schlenk flask (previously prepared under vacuum and N_2) together with 50.0 mL dry thf, mixed well, and transferred to the dropping funnel. This solution of bromobenzene in thf was then added dropwise via dropping funnel to three-necked flask. First a small amount was added (ca. 15–20 drops), followed by heating the bottom of the three-necked flask in order to initiate the reaction. The addition was continued without changing the speed of dropping until bromobenzene solution was added completely, and stirred for another 30 min at r.t. to produce phenylmagnesium bromide (Note: The color turned to yellowish brown. Also, one should prepare an ice bath to cool down reaction flask if needed). During that time, *(S)-N*-ethoxycarbonylproline methyl ester (**106**) (12.1 g, 60.0 mmol) was added to another prepared 1L Schlenk flask (equipped with a stirred bar) and left on high vacuum for 30–45 min. After that, the solution of **106** with 100 mL dried thf was cooled down to 0 °C, and the solution of phenylmagnesium bromide was transferred dropwise via cannula during 30 min. After the

addition was completed, the reaction mixture was stirred at 0 °C for another 5–10 min, then warmed up to r.t. and stirred overnight under N_2. After stirring overnight, reaction mixture had turned to clear orange solution. A saturated aqueous ammonium chloride solution (130 mL) was added dropwise (vigorous gas evolution occurred) and a white precipitate formed. The mixture was extracted with CH_2Cl_2 (2 x 120 mL) and the combined organic phases were washed with brine, dried over Na_2SO_4, and concentrated under reduced pressure, which resulted in colourless oil. Flash column chromatography (hexanes / Et_2O, 1 / 1) yielded the title compound as a white solid (9.52 g, 47%, R_f = 0.31). ^{1}H NMR ($CDCl_3$, 500.1 MHz): δ 0.81 (br, 1H), 1.26 (t, 3H), 1.46–1.56 (m, 1H), 1.93–2.00 (m, 1H), 2.08–2.17 (m, 1H), 2.97 (br, 1H), 3.43 (q, 1H), 4.02–4.23 (m, 2H), 4.95 (dd, 1H), 6.11 (br, 1H), 7.28–7.44 (m, 10H). The ^{1}H NMR data was in accordance with literature.

Synthesis of *(S)-α,α*-diphenylprolinol (**108**)

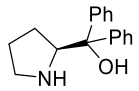

108

The known compound **107** was prepared following the described procedure[140]. The reaction temperature was 85 °C, which was not mentioned in the literature report. A mixture of **107** (9.29 g, 27.5 mmol), methanol (160 mL) and potassium hydroxide (18.5 g, 330 mmol) was added to a 500 mL r.b. flask, heated to 85 °C and stirred for 36 h under reflux. After that, volatiles were evaporated under reduced pressure which yielded white solid. Water and CH_2Cl_2 were added and the phases were separated. The mixture was extracted with CH_2Cl_2 (4 x 90 mL) and the combined organic phases were washed with brine, and dried over Na_2SO_4. After all volatiles were removed under reduced pressure to yield final product as white crystals (6.83 g, 98%) (literature report: brown crystals). ^{1}H NMR ($CDCl_3$, 500.1 MHz): δ 1.55–1.81 (m, 4H), 2.91–

3.10 (m, 2H), 4.28 (t, 1H), 7.16–7.35 (m, 6H), 7.50–7.61 (m, 4H). The ^{1}H NMR data was in accordance with literature.

Synthesis of oxazaborolidine (CBS catalyst) (**109**)

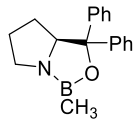

109

The known compound **108** was prepared following the described procedure[141] and used directly for the next step without any further purification. Compound **108** (7.95 g, 31.4 mmol), methylboronic acid (1.88 g, 31.4 mmol), and toluene (130 mL) were heated to 125 °C under reflux for 12 h (literature report: 3 h). Water was removed with the help of a Dean-Stark trap. The solvent was evaporated under vacuum to leave a pale-yellowish solid behind, which was directly used in the next step (8.03 g, 92%). ^{1}H NMR ($CDCl_3$, 500.1 MHz): δ 0.36 (s, 3H, B–C<u>H</u>$_3$), 0.90–0.71 (m, 1H, N–CH_2–CH_2–C<u>H</u>$_2$), 1.68–1.45 (m, 1H, N–CH_2–CH_2–C<u>H</u>$_2$), 1.90–1.70 (m, 2H, N–CH_2–C<u>H</u>$_2$–CH_2), 3.15–2.95 (m, 1H, N–C<u>H</u>$_2$–CH_2), 3.45–3.25 (m, 1H, N–C<u>H</u>$_2$–CH_2), 4.35 (dd, 1H, N–C<u>H</u>–CH_2–CH_2), 7.10–7.70 (m, 10H, Ph). The ^{1}H NMR data was in accordance with literature.

4.4.1.2 Synthesis of (S_p,S_p)-1,1′-dibromo-2,2′-di(isopropyl)ferrocene

Synthesis of (*R*,*R*)-1,1′-bis(α-hydroxyethyl)ferrocene (**77**)

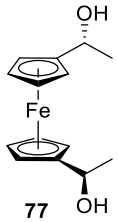

77

The known compound **77** was prepared following the described procedure[92] with changes in solvents used for work-up and flash column chromatography. Specifically, diethyl ether was used for the work-up instead of *tert*-butyl methyl ether. For flash column chromatography, a solvent mixture of hexanes / ethyl acetate (1 /1) was used instead of hexanes / *tert*-butyl methyl ether. Oxazaborolidien **109** (1.72 g, 6.20 mmol) was dissolved in dry thf (7.00 mL) and cooled down to 0 °C under nitrogen. From a syringed charged with $BH_3.SMe_2$ (2.50 mL, 1 M in thf), 20% of the final amount (0.50 mL) was added to the catalyst solution. After 5 min stirring, the remaining $BH_3.SMe_2$ and a solution of 1,1'-diacetylferrocene (11.5 mmol) in thf (24.0 mL) were added simultaneously within 20 min. The red color of the ketone turned to yellow on reduction. After 15 min at 0 °C, the excess of $BH_3.SMe_2$ was quenched by dropwise addition of methanol (10.0 mL). After the hydrolysis had ceased, the mixture was poured into saturated aqueous solution NH_4Cl (150 mL) and extracted with ether (200 mL). The organic layer was washed with water (200 mL) and brine (200 mL), dried over Na_2SO_4, and then concentrated to give an dark orange oil, which was purified by flash column chromatography (hexanes / EtOAc, 1 / 1), resulting in an orange-yellow solid (2.31 g, 74%). ^{1}H NMR ($CDCl_3$, 500.1 MHz): δ 1.39–1.40 [d, 6H, CH(C<u>H</u>$_3$)], 3.18 (br, 2H, O<u>H</u>), 4.18–4.22 (m, 8H, Cp), 4.60–4.61 [q, 2H, C<u>H</u>(CH_3)]. The ^{1}H NMR data was in accordance with literature.

Synthesis of (*R*,*R*,S_p,S_p)-1,1′-bis(α-N,N-dimethylaminoethyl)-1,1′-dibromoferrocene (**84**)

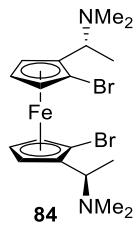

84

The known compound **84** was prepared following the described literature[105], and the crude was purified by flash column chromatography (literature report: no purification). To a stirred solution of (*R,R,S*$_p$,*S*$_p$)-1,1′-bis(α-N,N-dimethylaminoethyl)ferrocene (0.751 g, 2.29 mmol) in dry diethyl ether (8.00 mL) was added dropwise *n*BuLi (2.50 M in hexanes, 3.80 mL, 9.51 mmol) over 15 min under nitrogen at r.t. After 20 min the color of the mixture changed from orange to red. After stirring overnight, the reaction mixture was cooled down to –78 °C. A solution of 1,2-dibromotetrachloroethane (3.26 g, 10.0 mmol) in dry thf (5.00 mL) was added dropwise via syringe over 15 min. The resulting dark brown suspension was warmed up to r.t. over 90 min, stirred at r.t. for another 1 h and then quenched with saturated $Na_2S_2O_3$ solution at 0 °C. The mixture was diluted with diethyl ether (80.0 mL). The organic layer was separated and the aqueous layer was extracted with diethyl ether (2 × 30 mL). The combined organic phases were poured into a saturated aqueous NH_4Cl solution (80.0 mL), and the organic layer was extracted with NH_4Cl (5 × 50 mL). The aqueous phase was separated, neutralized with dropwise addition of 1M KOH, and extracted with diethyl ether (60.0 mL). After washing with water (30.0 mL), and saturated aqueous brine solution (30.0 mL), the combined organic layers were dried over Na_2SO_4, and concentrated to give a brown yellow solid as crude product. The crude was purified by flash column chromatography (CH_2Cl_2 / Et_3N, 95 / 5) to afford the final product as an orange solid (0.612 g, 55%). ^{1}H NMR ($CDCl_3$, 500.1 MHz): δ 1.48 [d, 6H, CH(C<u>H</u>$_3$)], 2.13 [s, 12H, N(C<u>H</u>$_3$)$_2$], 3.74 [q, 2H, C<u>H</u>(CH$_3$)], 4.13 (m, 4H, Cp), 4.27 (m, 2H, Cp). The ^{1}H NMR data was in accordance with literature.

Synthesis of (S_p,S_p)-1,1′-dibromo-2,2′-di(isopropyl)ferrocene [(S_p,S_p)-**19**]

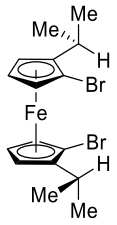

(S_p,S_p)-**19**

The known compound (S_p,S_p)-**19** was prepared following the described procedure[105], with a change in solvent used for flash column chromatography: hexanes was used instead of hexanes / EtOAc (100 / 1). To a stirred solution of (*R*,*R*,S_p,S_p)-2,2′-bis(α-acetoxymethyl)-1,1′-dibromoferrocene (0.464 g, 0.899 mmol) in dry CH_2Cl_2 (9.50 mL) was added dropwise trimethylaluminum (2.0 м in hexanes, 2.30 mL, 4.50 mmol) at –78 °C. The reaction mixture was stirred for 60 min at –78 °C, then warmed up to r.t. and stirred for additional 30 min at that temperature. After that, the mixture was transferred into the aqueous saturated $NaHCO_3$ solution (5.00 mL) at 0 °C via syringe and saturated sodium potassium tartrate solution (5.00 mL) was then added. The solvent was concentrated and the residue was dissolved in diethyl ether (10.0 mL). The resulting suspension was stirred vigorously for 20 min and then acidified with HCl 1N (5.00 mL). The organic layer was separated and the aqueous layer was extracted with diethyl ether (2 × 10 mL). The combined organic phase was washed with saturated aqueous $NaHCO_3$ solution, distilled water, brine and then dried over Na_2SO_4. All volatiles were concentrated to give orange solid, which was purified by flash column chromatography (hexanes) and followed by crystallization in hexanes at –20°C to afford orange crystal as final product (0.260 g, 62%). ^{1}H NMR ($CDCl_3$, 500.1 MHz): δ 1.05–1.06 [d, 6H, CH(C$\underline{H}_3$)$_2$], 1.31–1.32 [d, 6H, CH(C$\underline{H}_3$)$_2$],

2.80 [sept, 2H, C<u>H</u>$(CH_3)_2$], 4.02 (m, 2H, Cp), 4.07 (m, 2H, Cp), 4.23 (m, 2H, Cp). The ^{1}H NMR data was in accordance with literature.

4.4.1.3 Synthesis of phosphorus reagents

Synthesis of $Me_3SiCH_2PCl_2$ (**87**)

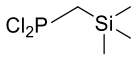

87

The known compound **87** was prepared following the described procedure,[39] and the crude mixture was purified by multi-condensation which was not mentioned in the literature. A solution of Me_3SiCH_2Cl (3.00 mL, 21.2 mmol) in dry diethyl ether (5.00 mL) was added to magnesium turnings (0.515 g, 21.2 mmol) under nitrogen flow. After the addition of half of the solution, 1,2-dibromoethane (0.05 mL) was added to the reaction mixture and was heated to reflux. When the reaction mixture started to become turbid, the remaining of (trimethylsilyl)methyl chloride solution was added. Stirring was continued at reflux temperature for 12 h. The reaction mixture was transferred to another Schlenk flask and cooled down to 0 $^\circ$C and stirred vigorously while powdered anhydrous $CdCl_2$ (1.94 g, 10.6 mmol) was added rapidly. After stirring for 2 h at 0 $^\circ$C, the salt was removed by filtration under a positive pressure of N_2. The filtrate was added dropwise to a vigorously stirred solution of PCl_3 (4.62 mL, 52.9 mmol) in dry diethyl ether (17.0 mL). After the addition was complete, the mixture was stirred at room temperature for 3 h. The white precipitate was filtered off, the filter cake was washed with dry diethyl ether (3 × 10 mL), and the combined diethyl ether solution was evaporated. Multi-condensation gave final product as a colorless oil (2.05 g, 51%). ^{1}H NMR (C_6D_6, 500.1 MHz): δ

–0.0127 [s, 9H, Si(C<u>H</u>$_3$)$_3$], 1.58–1.61 (d, 2H, C<u>H</u>$_2$). ^{31}P{^{1}H} NMR (C_6D_6, 202.5 MHz): δ 205.5 (s). The ^{1}H NMR and ^{31}P NMR data were in accordance with literature.

Synthesis of *i*Pr$_2$NPCl$_2$ (**89**)

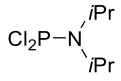

89

The known compound **87** was prepared following the described procedure,[110] with a reaction temperature at 0 °C, which was not clearly indicated in the literature. *i*Pr$_2$NH (3.96 mL, 28.3 mmol) was added dropwise to a solution of PCl_3 (1.31 mL, 15.0 mmol) in hexane (35.0 mL) under N_2 at 0 °C. The resulting white slurry was stirred at r.t. for 1 h, then it was filtered and the precipitate [(*i*Pr)$_2$NH•HCl] was washed with hexane (4 × 10 mL). Solvent was removed and the residue was distilled under reduced pressure to yield final product as a colorless liquid (1.58 g, 52%). ^{1}H NMR ($CDCl_3$, 500.1 MHz): δ 1.28 [d, 12H, CH(C<u>H</u>$_3$)$_2$], 3.92 [br, m, 2H, C<u>H</u>(CH$_3$)$_2$]. ^{31}P{^{1}H} NMR ($CDCl_3$, 202.5 MHz): δ 170.2 (s). The ^{1}H NMR and ^{31}P NMR data were in accordance with literature.

4.4.1.4 Synthesis of phosphorus-bridged [1]FCPs

Synthesis of the known phosphorus-bridged [1]FCP (**11^{Ph}**)

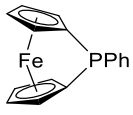

11^{Ph}

The known compound **11^{Ph}** was prepared following the described procedure,[38] and the reaction mixture was stirred for 30 min at r.t. before solvent was removed. This reaction time was not

mentioned in the literature. In addition, crystallization of the crude mixture was done at –80 °C instead of –55 °C as described in literature. To a stirred suspension of $Fe[(\eta\text{-}C_5H_4)Li]_2 \bullet ⅔tmeda$ (1.46 g, 5.31 mmol) in 12 mL of dry hexanes at –26 °C was added dropwise $PhPCl_2$ (0.77 mL, 5.68 mml) over a period of 10 min. The reaction mixture was stirred at –26 °C for a further 10 min, until the color of solution turned to dark reddish, then it was warmed up to r.t. and stirred at that temperature for another 30 min. Solvent was removed under vacuum, and the crude mixture was then filtered and extracted with dry hexanes (5 × 5 mL). The solution was concentrated to a minimum amount of hexanes and crystalized at –80 °C. The monomer was purified by three further recrystallizations in hexanes (–80 °C), resulting in dark red crystals as final product (650 mg, 41%). ^{1}H NMR ($CDCl_3$, 500.1 MHz): δ 4.43 (m, br, 2H, Cp), 4.51 (m, br, 2H, Cp), 4.69 (m, br, 4H, Cp), 7.34–7.31 (m, 1H, *p*-Ph), 7.45–7.42 (m, 2H, *m*-Ph), 7.67–7.64 (m, 2H, *o*-Ph). $^{31}P\{^1H\}$ NMR ($CDCl_3$, 202.5 MHz): δ 11.0 (s). The ^{1}H NMR and ^{31}P NMR data were in accordance with literature.

Synthesis of the known phosphorus-bridged [1]FCP (**11**$^{\mathbf{CH2SiMe3}}$)

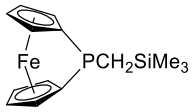

11$^{\mathbf{CH2SiMe3}}$

The known compound **11**$^{\mathbf{Ph}}$ was prepared following the described procedure,[39] with changes in the reaction temperature and reaction time. More specifically, the reaction was done at –10 °C (literature report: –30 °C), and the reaction was stirred at r.t. in 1 h (literature report: 6 h) before a filtration. A solution of $(Me_3SiCH_2)PCl_2$ (0.579 g, 3.06 mmol) in dry hexanes (30 mL) was added slowly over a period of 10 min via a syringe pump to a stirred suspension of $Fe[(\eta\text{-}C_5H_4)Li]_2 \bullet ⅔tmeda$ (0.840 g, 3.06 mmol) in dry hexanes (30 mL) at –10 °C. The reaction was

then allowed to warm up to r.t. and stirred at that temperature for another 1 h. The reaction mixture was filtered off and solvent was removed under vacuum. The crude mixture was crystallized from hexanes twice at –80 °C and further purified by vacuum sublimation at 70 °C to obtain a dark-red crystalline compound (0.55 g, 60 %). ^{1}H NMR (C_6D_6, 500.1 MHz): δ 0.17 [s, 9H, Si(C$\underline{H}_3$)$_3$], 1.13 (br, 2H, PC$\underline{H}_2$), 4.20 (m, 2H, Cp), 4.26 (m, 2H, Cp), 4.33 (m, 2H, Cp), 4.4 (m, 2H, Cp). ^{31}P{^{1}H} NMR (C_6D_6, 202.5 MHz): δ –7.8 (s). The ^{1}H NMR and ^{31}P NMR data were in accordance with literature.

Synthesis of chiral phosphorus-bridged [1]FCP [(S_p,S_p)-**20^{Ph}**]

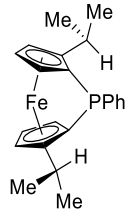

(S_p,S_p)-**20^{Ph}**

The known compound (S_p,S_p)-**20^{Ph}** was prepared following the described procedure,[64] with changes in the purification of the crude mixture. More specifically, activated Al_2O_3 was used in the flash column chromatography instead of SiO_2. The final product was obtained after a sublimation at 80 °C and crystallization in hexanes at –20 °C (literature report: only sublimation needed). *n*BuLi (2.5 M in hexanes, 1.65 mL, 4.11 mmol) was added dropwise to a cold (0 °C) solution of (S_p,S_p)-**19** (0.838 g, 1.96 mmol) in a solvent mixture (20 mL of hexanes / thf , 9 / 1). The reaction mixture was stirred at 0 °C for 30 min, resulting in an orange solution. The reaction mixture was warmed up to r.t. and $PhPCl_2$ (0.351 g, 1.96 mmol) was added dropwise within 2 min via a syringe. After the reaction mixture was stirred at r.t. for 20 min, it was transferred to a column packed with activated Al_2O_3 (hexanes / EtOAc, 9 / 1, plus 10 vol% Et_3N) under N_2

atmosphere. The dark-red fraction was collected from the column and the mixture was purified by sublimation 80 °C, and further crystallization at –20 °C resulted in dark-red crystals (0.22 g, 30%). ^{1}H NMR (C_6D_6, 500.1 MHz): δ 0.90 [d, J_{HH} = 6.6 Hz, 3H, CH(C<u>H</u>$_3$)$_2$], 1.02 [d, J_{HH} = 6.8 Hz, 3H, CH(C<u>H</u>$_3$)$_2$], 1.19 [d, J_{HH} = 6.8 Hz, 3H, CH(C<u>H</u>$_3$)$_2$], 1.31 [d, J_{HH} = 6.8 Hz, 3H, CH(C<u>H</u>$_3$)$_2$], 2.14 [sept, J_{HH} = 6.7 Hz, 1H, C<u>H</u>(CH$_3$)$_2$], 3.49 [sept/d, J_{HH} = 6.8 Hz / J_{HP} = 3.5 Hz, 1H, C<u>H</u>(CH$_3$)$_2$], 4.11 (s, br, 2H, Cp), 4.17 (s, br, 1H, Cp), 4.25 (s, br, 1H, Cp), 4.26 (pst, 1H, Cp), 4.38 (pst, unres, 1H, Cp), 7.01 (m, 1H, *p*-Ph), 7.12 (m, 2H, *m*-Ph), 7.75 (m, 2H, *o*-Ph). ^{31}P{^{1}H} NMR (C_6D_6, 202.5 MHz): δ 8.8 (s). The ^{1}H NMR and ^{31}P NMR data were in accordance with literature.

Synthesis of chiral phosphorus-bridged [1]FCP [(S_p,S_p)-**20$^{i\mathbf{Pr}}$**]

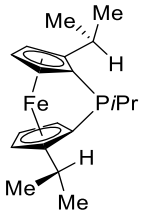

(S_p,S_p)-**20$^{i\mathbf{Pr}}$**

The known compound (S_p,S_p)-**20$^{i\mathbf{Pr}}$** was prepared following the described procedure,[64] with a change in the flash column chromatography: activated Al_2O_3 was used instead of SiO_2 as described in the literature. *n*BuLi (2.5 M in hexanes, 0.90 mL, 2.3 mmol) was added dropwise to a cold (0 °C) solution of *(S_p,S_p)*-**19** (0.460 g, 1.07 mmol) in a solvent mixture (10.3 mL of hexanes / thf , 9 / 1). The reaction mixture was stirred at 0 °C for 30 min, resulting in an orange solution. The reaction mixture was warmed up to r.t. and *i*PrPCl$_2$ (0.156 g, 1.07 mmol) was added dropwise within 2 min via a syringe. After the reaction mixture was stirred at r.t. for 20 min, it was transferred to a column packed with activated Al_2O_3 (hexanes / Et_3N, 90 / 10) under

N_2 atmosphere. The dark-red fraction was collected from the column, and the crude mixture was further purified by vacuum sublimation at 60 °C to yield in final product in form of dark-red crystals (0.182 g, 50%). ^{1}H NMR (C_6D_6, 500.1 MHz): δ 1.08 [d, J_{HH} = 6.8 Hz, 3H, CH(C<u>H</u>$_3$)$_2$], 1.16 [d, J_{HH} = 6.8 Hz, 3H, CH(C<u>H</u>$_3$)$_2$], 1.18 [d/d, J_{HP} = 18.7 Hz / J_{HH} = 6.8 Hz, 3H, PCH(C<u>H</u>$_3$)$_2$], 1.24–1.34 [m, 9H, PCH(C<u>H</u>$_3$)$_2$ and 2 x CH(C<u>H</u>$_3$)$_2$], 2.69 [sept, J_{HH} = 6.8 Hz, 1H, C<u>H</u>(CH$_3$)$_2$], 2.78 [m, 1H, PC<u>H</u>(CH$_3$)$_2$], 3.43 [sept/d, J_{HH} = 6.8 Hz / J_{HP} = 2.8 Hz, 1H, C<u>H</u>(CH$_3$)$_2$], 3.93 (s, br, 1H, Cp), 3.95 (s, br, 1H, Cp), 4.16 (s, br, 1H, Cp), 4.22 (s, br, 1H, Cp), 4.25 (pst, 1H, Cp), 4.37 (unres. pst, 1H, Cp). ^{31}P{^{1}H} NMR (C_6D_6, 202.5 MHz): δ 18.7 (s). The ^{1}H NMR and ^{31}P NMR data were in accordance with literature.

4.4.2 Synthesis of new compounds

Synthesis of chiral phosphorus-bridged [1]FCP [(S_p,S_p)-**86**$^{\mathbf{CH2SiMe3}}$]

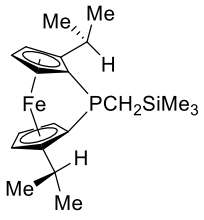

(S_p,S_p)-**86**$^{\mathbf{CH2SiMe3}}$

Species (S_p,S_p)**-19** (1.19 g, 2.79 mmol) was dissolved in a solvent mixture (27.8 mL of hexanes / thf, 9 / 1) and cooled to 0 °C. A solution of *n*BuLi (2.5 M in hexanes, 2.4 mL, 6.0 mmol) was added dropwise and the reaction was stirred at this temperature for 30 min. The reaction mixture was warmed to 50 °C, and a solution of (Me_3SiCH_2)PCl_2 (0.527 g, 2.79 mmol) in hexanes (15.0 mL) was added dropwise via syringe pump within 10 min. After 5 min, the 50 °C warm oil bath was removed and the colour of the reaction mixture changed from orange to red along with the formation of a white precipitate. After the reaction mixture was stirred at r.t. for additional 10

min, all solids were removed by flash column chromatography under N_2 flow (hexanes / Et_3N, 95 / 5; neutral Al_2O_3), and the dark-red fraction was collected. The product was further purified by vacuum sublimation at 80 °C. Crystallization in hexanes at –80 °C gave the product (S_p,S_p)-**86**$^{\mathbf{CH2SiMe3}}$ in form of dark red crystals (0.531 g, 50%). ^{1}H NMR (C_6D_6, 500.1 MHz): δ 0.23 [s, 9H, Si(C<u>H</u>$_3$)$_3$], 1.11 [d, J_{HH} = 6.8 Hz, 3H, CH(C<u>H</u>$_3$)$_2$], 1.16 [d, J_{HH} = 6.9 Hz, 3H, CH(C<u>H</u>$_3$)$_2$], 1.28 [d, J_{HH} = 6.8 Hz, 6H, CH(C<u>H</u>$_3$)$_2$], 1.36 (d/d, J_{HH} = 13.4 Hz / J_{HP} = 1.3 Hz, 1H, PC<u>H</u>$_2$), 1.92 (d, J_{HH} = 13.5 Hz, 1H, PC<u>H</u>$_2$), 3.10 [sept, J_{HH} = 6.8 Hz, 1H, C<u>H</u>(CH$_3$)$_2$], 3.43 [sept/d, J_{HH} = 6.8 Hz / J_{HP} = 3.2 Hz, 1H, C<u>H</u>(CH$_3$)$_2$], 3.96 (pst, unres, 1H, Cp), 4.04 (s, br, 1H, Cp), 4.18 (s, br, 1H, Cp), 4.22 (s, br, 1H, Cp), 4.25 (pst, 1H, Cp), 4.41 (pst, br, 1H, Cp). ^{13}C{^{1}H} NMR (C_6D_6, 125.8 MHz): δ –0.1 [d, J_{PC} = 6 Hz, Si(<u>C</u>H$_3$)$_3$], 10.7 [d, J_{PC} = 33 Hz, P<u>C</u>H$_2$Si(CH$_3$)$_3$], 19.6 (d, J_{PC} = 49 Hz, *ipso*-Cp^P), 20.4 (d, J_{PC} = 67 Hz, *ipso*-Cp^P), 21.3 [s, CH(<u>C</u>H$_3$)$_2$], 21.5 [s, CH(<u>C</u>H$_3$)$_2$], 27.2 [d, J_{PC} = 11 Hz, <u>C</u>H(CH$_3$)$_2$], 27.4 [s, CH(<u>C</u>H$_3$)$_2$], 27.8 [s, CH(<u>C</u>H$_3$)$_2$], 28.6 [s, <u>C</u>H(CH$_3$)$_2$], 73.7 (d, J_{PC} = 3 Hz, Cp), 74.1 (d, J_{PC} = 2 Hz, Cp), 74.7 (d, J_{PC} = 11 Hz, Cp), 76.0 (s, Cp), 81.4 (d, J_{PC} = 8 Hz, Cp), 83.4 (d, J_{PC} = 40 Hz, Cp), 104.7 (d, J_{PC} = 25 Hz, *ipso*-Cp$^{i\mathrm{Pr}}$), 106.7 (d, J_{PC} = 10 Hz, *ipso*-Cp$^{i\mathrm{Pr}}$). ^{31}P{^{1}H} NMR (C_6D_6, 202.5 MHz): δ –4.2. HRMS (FDI; m/z): calcd for $^{12}C_{20}{}^{1}H_{31}{}^{56}Fe^{31}P^{28}Si$, 386.1282 [$M^+$]; found 386.1281. Anal. Calcd for $C_{20}H_{31}FePSi$ (386.128): C, 62.17; H, 8.09%. Found: C, 62.04; H, 8.03%.

Synthesis of chiral phosphorus-bridged [1]FCP [(S_p,S_p)-**86**$^{\mathbf{NiPr2}}$]

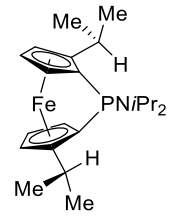

(S_p,S_p)-**86**$^{\mathbf{NiPr2}}$

Species (S_p,S_p)-**19** (0.428 g, 1.00 mmol) was dissolved in a solvent mixture (10.0 mL of hexanes / thf, 9 / 1) and cooled to 0 °C. A solution of *n*BuLi (2.5 M in hexanes, 0.90 mL, 2.25 mmol) was added dropwise and the reaction was stirred at this temperature for 30 min. A solution of (*i*Pr$_2$N)PCl$_2$ (0.219 g, 1.08 mmol) in hexanes (10.0 mL) was added dropwise via syringe pump within 10 min. The reaction mixture changed from orange to red along with the formation of a white precipitate, then it was warmed up to r.t. and stirred at that temperature for another 30 min. After that, all solids were removed by filtration under N_2 flow, and product was further purified by condensation at 80 °C, to yield the product (S_p,S_p)-**86**$^{\mathbf{NiPr2}}$ in form of dark red oil (80.0 mg, 20%). ^{1}H NMR (C_6D_6, 600 MHz): δ 1.18 [d (unres), 6H, 2 × CH(C$\underline{H}_3$)$_2$], 1.25 [d, J_{HH} = 15.4 Hz, 3H, CH(C$\underline{H}_3$)$_2$], 1.28 [d, J_{HH} = 7.0 Hz, 6H, CH(C$\underline{H}_3$)$_2$], 1.33 [d, J_{HH} = 7.0 Hz, 9H, CH(C$\underline{H}_3$)$_2$], 3.02 [sept, J_{HH} = 6.7 Hz, 1H, C$\underline{H}$(CH$_3$)$_2$], 3.57 [m, 3H, C$\underline{H}$(CH$_3$)$_2$], 3.91 (pst, unres, 1H, Cp), 4.15 (s, br, 1H, Cp), 4.22 (s, br, 3H, Cp), 4.45 (s, br, 1H, Cp). ^{13}C{^{1}H} NMR (C_6D_6, 150 MHz): δ 21.3 [s, CH(C$\underline{H}_3$)$_2$], 21.7 [s, CH(C$\underline{H}_3$]$_2$, 22.3 [s, CH(C$\underline{H}_3$)$_2$], 22.4 [s, CH(C$\underline{H}_3$)$_2$], 23.8 [s, CH(C$\underline{H}_3$)$_2$], 23.9 [s, CH(C$\underline{H}_3$)$_2$], 27.2 [s, CH(C$\underline{H}_3$)$_2$], 27.3 [s, CH(C$\underline{H}_3$)$_2$], 27.5 [s, C$\underline{H}$(CH$_3$)$_2$], 28.2 [s, C$\underline{H}$(CH$_3$)$_2$], 28.3 [s, C$\underline{H}$(CH$_3$)$_2$], 35.3 [d, J_{PC} = 76.0 Hz, *ipso*-Cp^P], 48.9 [s, N$\underline{C}$H(CH$_3$)$_2$], 49.0 [s, N$\underline{C}$H(CH$_3$)$_2$], 72.5 (br, Cp), 73.1 (s, Cp), 74.1 (d, J_{PC} = 14.0 Hz, Cp), 75.8 (s, Cp), 80.8 (s, Cp), 81.1 (s, Cp), 83.6 (d, J_{PC} = 6.0 Hz, Cp), 104.3 (d, J_{PC} = 33.0 Hz, *ipso*-Cp^{iPr}), 105.9 (d,

J_{PC} = 10.0 Hz, *ipso*-Cp^{iPr}). $^{31}P\{^{1}H\}$ NMR (C_6D_6, 243 MHz): δ 49.7. HRMS (FDI; m/z): calcd for $^{12}C_{22}{}^{1}H_{34}{}^{56}Fe^{7}N^{15}P$, 399.1778; found 399.1790. Elemental Anal. Calcd for $C_{22}H_{34}FeNP$ (399.34): C, 66.17; H, 8.58; N, 3.51%. Found: C, 66.33; H, 8.05; N, 3.32%.

Synthesis of chiral 1,1′-bis(phosphonyl)ferrocene [(S_p,S_p,*S*,*S*)-**88**^{NiPr2}]

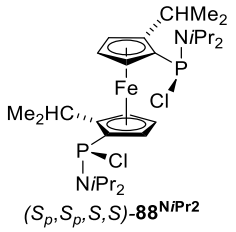

(S_p,S_p,*S*,*S*)-**88**^{NiPr2}

Species (S_p,S_p)-**19** (0.268 g, 0.626 mmol) was dissolved in a solvent mixture (6.00 mL of hexanes / thf, 9 / 1) and cooled to 0 °C. A solution of *n*BuLi (2.5 M in hexanes, 0.53 mL, 1.32 mmol) was added dropwise and the reaction was stirred at this temperature for 30 min. (*i*Pr$_2$N)PCl$_2$ (0.378 g, 1.88 mmol) was dissolved in hexanes (6.00 mL) and cooled to 0 °C. Solution of dilithio species (S_p,S_p)-**19**^{Li} was then added dropwise within 10 min via syringe pump to phosphorus reagent solution. After 5 min, the cold bath was removed, and the colour of the reaction mixture had changed to reddish orange along with formation of a white precipitate. After the reaction mixture was stirred at r.t. for another 15 min, solids were removed by filtration. After the solvent was removed under vacuum, the product was obtained by vacuum sublimation at 136 °C as a yellow solid (0.115 g, 31%). The resulting solid was dissolved in hexanes and recrystallized at –80 °C, then –20 °C, yielded yellow crystals which were suitable for single crystal analysis. ^{1}H NMR (500 MHz, C_6D_6): δ 0.59 [d, J_{HH} = 6.6 Hz, 6H, NCH(C$\underline{H}_3$)$_2$], 1.05 [d, J_{HH} = 6.6 Hz, 6H, NCH(C$\underline{H}_3$)$_2$] 1.08 [d, J_{HH} = 6.8 Hz, 6H, CH(C$\underline{H}_3$)$_2$], 1.22 [d, J_{HH} = 6.5 Hz, 6H, NCH(C$\underline{H}_3$)$_2$], 1.35 [d, J_{HH} = 6.8 Hz, 6H, CH(C$\underline{H}_3$)$_2$], 1.47 [d, J_{HH} =

6.7 Hz, 6H, NCH(C<u>H</u>$_3$)$_2$], 2.88 [sept/d, J_{HH} = 6.8 Hz / J_{HP} = 2.8 Hz, 2H, C<u>H</u>(CH$_3$)$_2$], 3.06 [m, 2H, NC<u>H</u>(CH$_3$)$_2$], 4.03 [m, 2H, NC<u>H</u>(CH$_3$)$_2$], 4.27 (m, 2H, Cp), 4.69 (pst, 2H, Cp), 5.19 (m, 2H, Cp). ^{13}C{^{1}H} NMR (125.8 MHz, C_6D_6): δ 21.2 [s, CH(<u>C</u>H$_3$)$_2$], 21.6 [s, CH(<u>C</u>H$_3$)$_2$], 23.7 [s, CH(<u>C</u>H$_3$)$_2$], 25.0 [d, J_{PC} = 3 Hz, CH(<u>C</u>H$_3$)$_2$], 25.8 [s, CH(<u>C</u>H$_3$)$_2$], 26.6 [s, CH(<u>C</u>H$_3$)$_2$], 26.7 [d, J_{PC} = 11 Hz, <u>C</u>H(CH$_3$)$_2$], 46.1 [d, J_{PC} = 23 Hz, N<u>C</u>H(CH$_3$)$_2$], 49.9 [d, J_{PC} = 10 Hz, N<u>C</u>H(CH$_3$)$_2$], 71.8 (d, J_{PC} = 3 Hz, Cp), 72.0 (d, J_{PC} = 6 Hz, Cp), 74.7 (s, Cp), 77.1 (d, J_{PC} = 23 Hz, *ipso*-Cp^{P}), 102.8 (d, J_{PC} = 28 Hz, *ipso*-Cp^{iPr}). ^{31}P{^{1}H} NMR (202.5 MHz, C_6D_6): δ 123.3. HRMS (FDI; m/z): calcd for $^{12}C_{28}{}^{1}H_{48}{}^{17}Cl_2{}^{26}Fe{}^{14}N_2{}^{31}P_2$, 600.2019 [$M^+$]; found 600.2034. Anal. Calcd for $C_{28}H_{48}Cl_2FeN_2P_2$ (601.399): C, 55.92; H, 8.05; N, 4.66%. Found: C, 55.54; H, 8.30; N, 4.46%.

Synthesis of chiral phosphorus-bridged [2]FCP [(S_p,S_p,*R*,*R*)-**90**$^{\mathbf{CH2SiMe3}}$]

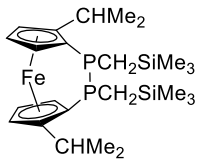

(S_p,S_p,*R*,*R*)-**90**$^{\mathbf{CH2SiMe3}}$

Species (S_p,S_p)-**19** (0.868 g, 2.03 mmol) was dissolved in a solvent mixture (20.0 mL of hexanes / thf, 9 / 1) and cooled to 0 °C. A solution of *n*BuLi (2.5 м in hexanes, 1.70 mL, 4.3 mmol) was added dropwise and the reaction was stirred at this temperature for 30 min. (Me$_3$SiCH$_2$)PCl$_2$ (1.17 g, 6.19 mmol) was dissolved in hexanes (20.0 mL) and cooled to 0 °C. Solution of dilithio species (S_p,S_p)-**19**$^{\mathbf{Li}}$ was then added dropwise within 10 min via syringe pump to phosphorus reagent solution. After 5 min, the cold bath was removed and the colour of the reaction mixture started to change to reddish orange, along with formation of a white precipitate. After the reaction mixture was stirred at r.t. for another 15 min, all solids were removed by filtration, and solvents were removed under vacuum. The reaction mixture was dissolved in thf (15.0 mL) and

the resulting solution was added dropwise via a cannula to a three-necked flask, which was charged with magnesium turnings (2.20 g, 90.5 mmol) and thf (30.0 mL). After the addition of half of the solution, 1,2-dibromoethane (0.05 mL) was added to the reaction mixture, followed by addition of the remaining solution. After the reaction mixture was stirred overnight at r.t., thf was removed under vacuum, hexanes (10 mL) was added, and the undissolved white solid was removed by filtration. After the solvents were removed under vacuum, the resulting reddish oil was purified by flash column chromatography (hexanes / Et_3N, 95 / 5; neutral Al_2O_3). The first orange fraction was collected from the column, and solvent was removed under vacuum. Vacuum sublimation at 100 °C resulted in reddish crystals (0.306 g, 30%). ^{1}H NMR (C_6D_6, 500.1 MHz): δ 0.08 [s, 18H, Si(C$\underline{H}_3$)$_3$], 1.16 (d/t, J_{HH} = 13.7 Hz / J_{HP} = 3.8 Hz, 2H, PC$\underline{H}_2$), 1.19 [d, J_{HH} = 6.8 Hz, 6H, CH(C$\underline{H}_3$)$_2$], 1.44 [d, J_{HH} = 6.9 Hz, 6H, CH(C$\underline{H}_3$)$_2$], 1.88 [d/t, J_{HH} = 13.7 Hz / J_{HP} = 6.1 Hz, 2H, PC$\underline{H}_2$], 3.67 (s, br, 2H, Cp), 3.79 [sept/tr (unres), J_{HH} = 6.8 Hz, 2H, C$\underline{H}$(CH$_3$)$_2$], 4.31 (pst, 2H, Cp), 4.94 (m, 2H, Cp). ^{13}C{^{1}H} NMR (C_6D_6, 125.8 MHz): δ 0.07 [m, Si($\underline{C}$H$_3$)$_3$], 18.2 [d, J_{PC} = 2 Hz, P$\underline{C}$H$_2$Si(CH$_3$)$_3$], 22.5 [s, CH($\underline{C}$H$_3$)$_2$], 27.1 [t, J_{PC} = 5 Hz, $\underline{C}$H(CH$_3$)$_2$], 27.2 [s, CH($\underline{C}$H$_3$)$_2$], 66.1 (t, J_{PC} = 2 Hz, Cp), 72.1 (t, J_{PC} = 14 Hz, *ipso*-Cp^{P}), 72.9 (s, Cp), 77.6 (s, Cp), 105.4 (t, J_{PC} = 14 Hz, *ipso*-Cp^{iPr}). ^{31}P{^{1}H} NMR (C_6D_6, 202.5 MHz): δ 2.0. HRMS (FDI; m/z): calcd for $^{12}C_{24}{}^{1}H_{42}{}^{56}Fe{}^{15}P_2{}^{14}Si_2$, 504.1650 [$M^+$]; found 504.1643. Anal. Calcd for $C_{24}H_{42}FeP_2Si_2$ (504.563): C, 57.13; H, 8.39%. Found: C, 57.36; H, 8.58%.

Synthesis of chiral phosphorus-bridged [2]FCP (**90**$^{\mathbf{NiPr2}}$)

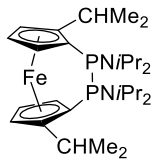

90$^{\mathbf{NiPr2}}$

Species (S_p,S_p)-**19** (0.248 g, 0.579 mmol) was dissolved in a solvent mixture (5.00 mL of hexanes / thf, 9 / 1) and cooled to 0 °C. A solution of *n*BuLi (2.5 M in hexanes, 0.49 mL, 1.22 mmol) was added dropwise and the reaction was stirred at this temperature for 30 min. (*i*Pr$_2$N)PCl$_2$ (0.357 g, 1.74 mmol) was dissolved in hexanes (5.00 ml) and cooled to 0 °C. Solution of dilithio species (S_p,S_p)-**19**$^{\mathbf{Li}}$ was then added dropwise within 10 min via a syringe pump to phosphorus reagent solution. After 5 min, the cold bath was removed and the colour of the reaction mixture had changed to reddish orange along with formation of a white precipitate. After all solids were removed by filtration, solvents were removed under vacuum. The reaction mixture was dissolved in thf (8.00 mL) and the resulting solution was added dropwise via cannula to a three-necked flask, which was charged with magnesium turnings (1.13 g, 46.4 mmol) and thf (10.0 mL). After the reaction mixture was stirred overnight at r.t., thf was removed under vacuum, hexanes (8.0 × 3 mL) was added, and the undissolved white solid was removed by filtration. After the solvent was removed under vacuum, the resulting reddish oil was purified by flash column chromatography (hexanes / Et_3N, 95 / 5; neutral Al_2O_3). The first orange fraction was collected from the column, and solvents were removed under vacuum. Vacuum sublimation at 135 °C resulted in orange solid (0.065 g, 25%). ^{1}H NMR (C_6D_6, 500 MHz): δ 1.17 [d, J_{HH} = 6.8 Hz, 6H, CH(C$\underline{H}_3$)$_2$], 1.23 [d, J_{HH} = 6.6 Hz, 12H, NCH(C$\underline{H}_3$)$_2$], 1.28 [d, J_{HH} = 6.9 Hz, 6H, CH(C$\underline{H}_3$)$_2$], 1.30 [d, J_{HH} = 6.6 Hz, 12H, NCH(C$\underline{H}_3$)$_2$], 3.51 [m, 2H,

C<u>H</u>$(CH_3)_2$], 3.78 [s, br, 4H, NC<u>H</u>$(CH_3)_2$], 3.99 (m, 2H, Cp), 4.27 (pst, 2H, Cp), 4.71 (m, 2H, Cp). $^{13}C\{^1H\}$ NMR (C_6D_6, 150.9 MHz): δ 22.9 [s, CH(<u>C</u>$H_3)_2$], 24.4 [s, NCH(<u>C</u>$H_3)_2$], 24.8 [s, NCH(<u>C</u>$H_3)_2$], 26.0 [t, J_{PC} = 7 Hz, <u>C</u>H$(CH_3)_2$], 27.3 [s, CH(<u>C</u>$H_3)_2$], 49.3 [s, N<u>C</u>H$(CH_3)_2$], 67.5 (m, unres, *ipso*-Cp^P), 67.9 (pst, unres, Cp), 73.8 (s, Cp), 77.2 (s, Cp), 105.0 (t, J_{PC} = 18 Hz, *ipso*-Cp^{iPr}), $^{31}P\{^1H\}$ NMR (C_6D_6, 202.5 MHz): δ 11.7. HRMS (FDI; m/z): calcd for $^{12}C_{28}{}^1H_{48}{}^{56}Fe^7N_2{}^{15}P_2$, 530.2642 [$M^+$]; found 530.2657. Anal. Calcd for $C_{28}H_{48}FeN_2P_2$ (530.499): C, 63.39; H, 9.12; N, 5.28%. Found: C, 63.11; H, 9.45; N, 5.20%.

Anionic ring-opening polymerization of the known phosphorus-bridged [1]FCP **11^{Ph}**

*n*BuLi (1.6 M in hexanes) was added to a solution of **10^{Ph}** in 0.5 mL of thf. The reaction was stirred at r.t. for 30 min before termination by the addition of a few drops of degassed H_2O. The mixture was precipitated into a stirred hexanes solution, yielded a yellow precipitate. The precipitate was extracted with hexanes, and solvent was removed. The polymer was dried under vacuum overnight, resulted in yellow powder. The resulting polymer was dissolved in CH_2Cl_2 (2–3 mL), then an excess amount of elemental sulfur was added and the mixture was stirred overnight under N_2 flow. After stirring, the reaction mixture was precipitated into hexanes solution, resulting in yellow precipitate. The precipitate was then extracted with hexanes and the polymer was dried under vacuum.

NMR was given for monomer/*n*BuLi ratio of 10/1. ^1H NMR (C_6D_6, 500.1 MHz): δ 2.14–0.72 (br, *n*Bu), 3.98–4.85 (br, Cp), 7.07 (br, Ph), 7.98 (br, Ph). $^{31}P\{^1H\}$ NMR (C_6D_6, 202.5 MHz): δ 37.0 [-fcPh<u>P</u>(S)fc-], 37.7 [-fc<u>P</u>(S)PhFc], 41.3 [Ph<u>P</u>(S)(*n*Bu)fc-].

Ring-opening reaction with 1 equiv *n*BuLi of (S_p,S_p)-**86**$^{\mathbf{CH2SiMe3}}$

Species (S_p,S_p)-**86**$^{\mathbf{CH2SiMe3}}$ (23.8 mg, 0.0616 mmol) was dissolved in 0.5 mL thf and stirred well. After that, *n*BuLi (1.58 M in hexanes, 40.0 μL, 0.0616 mmol) was added to the solution and stirred for 45 min. The color of solution slowly turned from dark red to orange. The reaction mixture was quenched with a few drops of degassed methanol, and the color of mixture turned to yellow. The mixture was then dissolved in a stirred hexanes solution, and solvent was removed completely to yield in a yellow oil (24.2 mg). In the following, the NMR chemical shifts with an asterisk indicate two different signals due to the presence of two diastereomers. $^{31}P\{^{1}H\}$ NMR (C_6D_6, 202.5 MHz): δ –54.9*(s) and –53.2*(s). HRMS (FDI; m/z): calcd for $^{12}C_{21}{}^{1}H_{33}{}^{56}Fe^{15}P$, 372.1669 [$M^+$]; found 372.1657; calcd for $^{12}C_{24}{}^{1}H_{41}{}^{56}Fe^{15}P^{14}Si$, 444.2065, found 444.2072.

Ring-opening reaction with 1 equiv *n*BuLi of (S_p,S_p,*R*,*R*)-**90**$^{\mathbf{CH2SiMe3}}$

Species (S_p,S_p,*R*,*R*)-**90**$^{\mathbf{CH2SiMe3}}$ (20 mg, 0.0446 mmol) was dissolved in 0.5 mL thf and stirred well. After that, *n*BuLi (1.40 M in hexanes, 32.0 μL, 0.0446 mmol) was added to the solution and stirred for 45 min. The reaction mixture was quenched with a few drops of degassed methanol, and then dissolved in a stirred hexanes solution. Solvent was removed to yield in an orange-red oil (21.5 mg). Signals from the reaction mixture could not be assigned by NMR spectrometry due to presence of many impurities and unidentified species. HRMS (FDI; m/z): calcd for $^{12}C_{28}{}^{1}H_{52}{}^{56}Fe^{15}P_2{}^{14}Si_2$, 562.2432 [$M^+$]; found 562.2442; calcd for $^{12}C_{25}{}^{1}H_{44}{}^{56}Fe^{15}P_2{}^{14}Si$, 490.2037; found 490.2049.

Ring-opening reaction with 1 equiv *n*BuLi of (S_p,S_p)-**20^{Ph}**

Species (S_p,S_p)-**20^{Ph}** (23.7 mg, 62.9 × 10^{-3} mmol) was dissolved in 0.5 mL thf and stirred until getting completely dissolved. After that, *n*BuLi (1.52 M in hexanes, 41.5 μL, 62.9 × 10^{-3} mmol) was added to the solution and stirred for 45 min. The color of solution turned from dark red to orange. The reaction mixture was quenched with a few drops of degassed H_2O, then it was dissolved into a stirred hexanes solutions (8 mL). Solvent was removed under vacuum, resulting in an orange oil (24.0 mg, 88%). The product **95** was found to be a 3 to 1 mixture of two diastereomers. In the following, the NMR chemical shifts with an asterisk indicate two different signals due to the presence of two diastereomers. $^{31}P\{^1H\}$ NMR (C_6D_6, 243 MHz): –35.8*(s) and –36.0*(s). HRMS (FDI; m/z): calcd for $^{12}C_{26}{}^1H_{35}{}^{56}Fe^{15}P$, 434.1826 [$M^+$]; found 434.1825.

Sulfurization of mixture **95** and characterization of species (S_p,R)-**95^S**

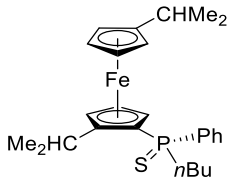

(S_p,R)-**95^S**

The 3 to 1 mixture of **95** was dissolved in dry CH_2Cl_2 (2.0 mL), then an excess amount of S_8 was added and stirred under N_2 flow for 12 h. After that, solvent was removed under vacuum, resulted in orange solid (26 mg, 88%). The product was found to be a 3 to 1 mixture of two diastereomers. In the following, the NMR chemical shifts with an asterisk indicate two different signals due to the presence of two diastereomers. ^{31}P NMR (C_6D_6, 202.5 MHz): δ 42.4* (s) and 39.9*(s). The mixture was dissolved in a minimum amount of hexanes, and was left for crystallization at –10 °C. Orange crystals was isolated and subjected to both NMR spectroscopy

and single crystal X-ray analysis. ^{1}H NMR (C_6D_6, 500.1 MHz): δ 0.67 [t, J_{HH} = 7.0 Hz, 3H, $PCH_2CH_2CH_2C\underline{H}_3$], 0.88 [d, J_{HH} = 7.0 Hz, 3H, $CH(C\underline{H}_3)_2$], 0.90 [d, J_{HH} = 7.0 Hz, 3H, $CH(C\underline{H}_3)_2$], 1.12–1.17 (m, 1H, $PCH_2CH_2C\underline{H}_2$–), 1.25 [d, J_{HH} = 7.0 Hz, 3H, $CH(C\underline{H}_3)_2$], 1.30–1.24 (m, 1H, $PCH_2C\underline{H}_2$–), 1.36 [d, J_{HH} = 7.0 Hz, 3H, $CH(C\underline{H}_3)_2$], 2.03–1.94 (m, 1H, $PC\underline{H}_2CH_2$), 2.10 [sept, J_{HH} = 6.8 Hz, 1H, $C\underline{H}(CH_3)_2$], 2.28–2.23 (m, 2H, $PC\underline{H}_2$), 3.82 (m, br, 1H, Cp), 3.91 (br, 1H, Cp), 3.94 (m, br, 1H, Cp), 3.99 (m, br, 1H, Cp), 4.08 [sept, J_{HH} = 6.8 Hz, 1H, $C\underline{H}(CH_3)_2$], 4.13 (br, 1H, Cp), 4.41 (m, br, 1H, Cp), 4.43 (m, br, 1H, Cp), 7.11 (m, 2H, Ph), 7.13 (d, 1H, Ph), 8.10–8.06 (m, 2H, Ph). ^{13}C{^{1}H} NMR (C_6D_6, 150.9 MHz): δ 13.7 (s, CH_3-*n*Bu), 23.4 [s, $CH(\underline{C}H_3)_2$], 23.5 [s, $CH(\underline{C}H_3)_2$], 23.8 [s, $CH(\underline{C}H_3)_2$], 24.1 [s, $\underline{C}H_2$-*n*Bu], 25.6 [br, $\underline{C}H(CH_3)_2$], 25.7 br, $\underline{C}H_2$-*n*Bu), 27.3 (s, $\underline{C}H_2$-*n*Bu), 27.5 [s, $\underline{C}H(CH_3)_2$], 36.3 (d, J_{PC} = 58.0 Hz, $P\underline{C}H_2$), 67.8 (s, Cp), 69.8 (s, Cp), 69.5 (d, J_{PC} = 10.0 Hz, Cp), 69.7 (d, J_{PC} = 10.0 Hz, Cp), 71.0 (s, Cp), 71.2 (s, Cp), 73.1 (d, J_{PC} = 13.0 Hz, Cp), 74.2 (d, J_{PC} = 88.0 Hz, *ipso*-Cp^{P}), 97.6 (s, *ipso*-Cp^{iPr}), 101.67 (d, J_{PC} = 13.0 Hz, *ipso*-Cp^{iPr}), 128.3–128.0 (br, Ph), 131.0 (br, Ph), 132.5 (d, J_{PC} = 9.0 Hz, Ph), 133.0 (s, *ipso*-Ph). ^{31}P{^{1}H} NMR (C_6D_6, 202.5 MHz): δ 42.4 (s).

Testing stability of lithium species in thf and Et_2O

Species (S_p,S_p)-**20^{Ph}** (18.4 mg, 49.0 × 10^{-3} mmol) was dissolved in 0.3 mL of solvent (thf or Et_2O) and stirred well. After that, *n*BuLi (1.52 м in hexanes, 32.5 μL, 49.0 × 10^{-3} mmol) was added and the solution was stirred. After 1 h, about 100 μL of reaction mixture was syringed out to a NMR tube, then 1–2 drops of D_2O was added and solvent was removed under vacuum. The procedure was repeated after 2, 3, and 4 h of reaction time. After that, all the sample was analyzed by ^{1}H NMR spectroscopy.

Synthesis of diastereomeric mixture of the chiral phosphine ligand **99**^{S}

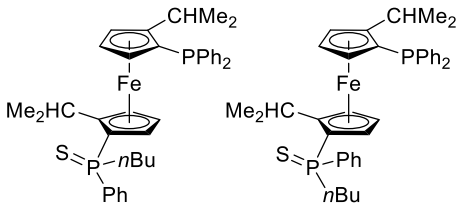

99^{S}

Species (S_p,S_p)-**20**^{Ph} (45.0 mg, 120 × 10^{-3} mmol) was dissolved in 0.5 mL Et_2O and stirred well. After that, *n*BuLi (1.52 M in hexanes, 79.0 μL, 120 × 10^{-3} mmol) was added to the solution and stirred for 1 h. The color of solution turned from dark red to orange. The reaction mixture was reacted with an excess amount of PPh_2Cl (25.0 μL, 132 × 10^{-3} mmol), and stirred for another 30 min under N_2 flow. After that, the mixture was quenched with 0.1 mL of $NaHCO_3$, and extracted with Et_2O (3 × 1 mL). Solvent was removed, and 2 mL of hexanes was added, which resulted in cloudy orange solution. The solution was filtered out via a syringe filter to afford a clear orange solution. Solvent was removed and the mixture was passed through a column packed with neutral Al_2O_3 (hexanes / EtOAc, 20 / 1, plus 5% Et_3N). The first orange fraction was collected (51 mg, 69 %) and solvent was removed under vacuum. In the following, the NMR chemical shifts with an asterisk indicate two different signals due to the presence of two diastereomers **99**. $^{31}P\{^{1}H\}$ NMR (C_6D_6, 202 MHz): –24.7 (s), –37.2*(s) and –25.2 (s), –36.2*(s). The diastereomeric mixture **99** (50 mg, 81 × 10^{-3} mmol) was dissolved in CH_2Cl_2 (2 mL), then an excess amount of elemental sulfur (15 mg) was added and stirred for 12 h under nitrogen flow. After stirring, the reaction mixture was passed through a syringe filter, and solvent was removed under vacuum, which resulted in an orange solid (58 mg, 70%). The following NMR chemical shifts with an asterisk indicate two different signals due to the presence of two diastereomers. ^{31}P NMR (C_6D_6, 202 MHz): 41.6 (s), 39.6*(s) and 39.9 (s), 39.2*(s). Preparative thin layer

chromatography (PTLC) was carried out on glass plated (20 × 20 cm) pre-coated (0.25 mm) with silica gel 60 F_{254}, solvent mixture of hexanes / ethyl acetate (5 / 1) as an eluent. Materials were detected by visualization under an ultraviolet lamp (λ = 254 nm). The corresponding strips were scraped off and washed with CH_2Cl_2 (3 × 10 mL) and filtered through a fine fritted funnel, which resulted in a orange solid (S_p,R)-**99**$^{\mathbf{S}}$. ^{1}H NMR (C_6D_6, 500.1): δ 0.63 (t, J_{HH} = 7.0 Hz, 3H, *n*Bu), 0.73 [d, J_{HH} = 7.0 Hz, 3H, CH(C$\underline{H}_3$)$_2$], 1.13–1.05 (m, 3H, *n*Bu), 1.19 [d, J_{HH} = 7.0 Hz, 3H, CH(C$\underline{H}_3$)$_2$], 1.34 [d, J_{HH} = 7.0 Hz, 3H, CH(C$\underline{H}_3$)$_2$], 1.44 [d, J_{HH} = 7.0 Hz, 3H, CH(C$\underline{H}_3$)$_2$], 1.90–1.81 (m, 1H, PC$\underline{H}_2$), 2.15–2.03 (m, 2H, *n*Bu), 3.35 (s, br, 1H, Cp), 3.59 (s, br, 1H, Cp), 3.95 [sept, J_{HP} = 6.8 Hz, 1H, C$\underline{H}$(CH$_3$)$_2$], 4.03 [sept, J_{HP} = 6.8 Hz, 1H, C$\underline{H}$(CH$_3$)$_2$], 4.46 (s, br, 1H, Cp), 4.46 (s, br, 1H, Cp), 4.57 (s, br, 1H, Cp), 5.35 (s, br, 1H, Cp), 5.59 (s, br, 1H, Cp), 6.85–6.81 (m, 2H, Ph), 6.88–6.93 (m, 7H, Ph), 7.80–7.73 (m, 6H, Ph). ^{13}C{^{1}H} NMR (C_6D_6, 125.8 MHz): δ 13.6 (s, $\underline{C}$H$_3$-*n*Bu), 23.5 [s, CH($\underline{C}$H$_3$)$_2$], 23.8 (s, $\underline{C}$H$_2$-*n*Bu), 24.0 [s, CH($\underline{C}$H$_3$)$_2$], 25.3 [br, 2× $\underline{C}$H(CH$_3$)$_2$], 25.4 (s, $\underline{C}$H$_2$-*n*Bu), 25.9 [s, CH($\underline{C}$H$_3$)$_2$], 27.2 [s, CH($\underline{C}$H$_3$)$_2$], 35.8 (d, J_{PC} = 59.0 Hz, $\underline{C}$H$_2$-*n*Bu), 72.8 (s, Cp), 72.9 (s, br, Cp), 73.0 (s, Cp), 73.1 (s, Cp), 73.2 (s, Cp), 73.6 (d, J_{PC} = 9.6 Hz, Cp), 74.4 (s, Cp), 74.5 (s, Cp), 73.9 (d, J_{PC} = 93.0 Hz, *ipso*-Cp^{P}), 75.3 (d, J_{PC} = 85.0 Hz, *ipso*-Cp^{P}), 103.3 (d, J_{PC} = 12.6 Hz, *ipso*-Cp$^{i\mathrm{Pr}}$), 103.5 (d, J_{PC} = 12.6 Hz, *ipso*-Cp$^{i\mathrm{Pr}}$), 131.1–131.0 (m, Ph), 131.8 (d, J_{PC} = 9.7 Hz, Ph), 131.7 (d, J_{PC} = 10.0 Hz, Ph), 132.3–132.1 (m, Ph), 134.1 (d, J_{PC} = 85.0 Hz, *ipso*-Ph), 136.2 (d, J_{PC} = 86.0 Hz, *ipso*-Ph). ^{31}P{^{1}H} NMR (C_6D_6, 202.5 MHz): δ 39.6, 41.6 (s).

Desulfurization of the new chiral phosphine ligand (S_p,*S*)-**99**.

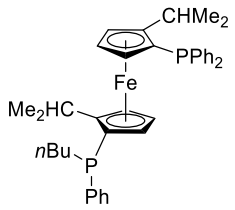

(S_p,*S*)-**99**

Species (S_p,*R*)-**99**$^{\mathbf{S}}$ (24 mg, 35.2 × 10^{-3} mmol) was dissolved in dried CH_2Cl_2 (3 mL), then CF_3SO_3Me (11.5 μL, 99.2 × 10^{-3} mmol) was added and stirred at r.t. for 1.5 h. All the volatiles were removed under vacuum. The reaction mixture was dissolved in CH_2Cl_2 (2.5 mL), then $P(NMe_2)_3$ was added and stirred at r.t. for another 1.5 h. The color of solution turned from orange to yellow while stirring. Solvent was removed under vacuum, yielded a yellow solid (20 mg). Preparative thin layer chromatography (PTLC) was carried out on glass plated (20 × 20 cm) pre-coated (0.25 mm) with silica gel 60 F_{254}, solvent mixture of hexanes /ethyl acetate (10 / 1) as an eluent. Materials were detected by visualization under an ultraviolet lamp (λ = 254 nm). The corresponding strips were scraped off and washed with CH_2Cl_2 (3 × 10 mL) and filtered through a fine fritted funnel, which resulted in a yellow solid (S_p,*S*)**-99** (15 mg, 69%). ^{1}H NMR (C_6D_6, 500.1 MHz): δ 0.70 (t, J_{HH} = 7.0 Hz, 3H, $PCH_2CH_2CH_2C\underline{H}_3$), 0.92 (d, J_{HH} = 7.0 Hz, 3H, $CH(C\underline{H}_3)_2$), 1.22 (d, J_{HH} = 7.0 Hz, 3H, $CH(C\underline{H}_3)_2$), 1.27–1.19 (m, 2H, $PCH_2CH_2C\underline{H}_2$), 1.35–1.29 (m, 2H, $PCH_2C\underline{H}_2$), 1.35 [d, J_{HH} = 7.0 Hz, 3H, $CH(C\underline{H}_3)_2$], 1.45 [d, J_{HH} = 7.0 Hz, 3H, $CH(C\underline{H}_3)_2$], 1.63–1.70 (m, 1H, $PC\underline{H}_2$), 1.91–1.96 (m, 1H, $PC\underline{H}_2$), 2.95 (s, br, 1H, Cp), 3.13 [sept/d, J_{HH} = 6.8 Hz / J_{PH} = 3.0 Hz, 1H, $C\underline{H}(CH_3)_2$], 3.20 [sept/d, J_{HH} = 6.8 Hz / J_{PH} = 2.9 Hz, 1H, $C\underline{H}(CH_3)_2$], 3.33 (s, br, 1H, Cp), 4.18 (s, br, 1H, Cp), 4.23 (m, br, 1H, Cp), 4.47 (pst, unres, 1H, Cp), 6.97–6.90 (m, 3H, Ph), 7.15–7.04 (m, 6H, Ph), 7.26–7.23 (m, 2H, Ph), 7.57–7.49 (m, 4H, Ph). ^{13}C{^{1}H} NMR (C_6D_6, 125.8 MHz): δ 13.8 (s, $\underline{C}H_3$-*n*Bu), 23.1 [s, $CH(\underline{C}H_3)_2$], 23.3 [s,

$CH(\underline{C}H_3)_2]$, 24.4 (d, J_{PC} = 12.7 Hz, CH_2-*n*Bu), 26.5 [s, $CH(\underline{C}H_3)_2]$, 26.6 [s, $CH(\underline{C}H_3)_2]$, 26.9–27.2 [m, 2 × $\underline{C}H(CH_3)_2]$, 29.2 (d, J_{PC} = 16.5 Hz, CH_2-*n*Bu), 31.0 (d, J_{PC} = 8.4 Hz, CH_2-*n*Bu), 70.2 (d, J_{PC} = 4.5 Hz, Cp), 70.6 (d, J_{PC} = 4.8 Hz, Cp), 71.0 (d, J_{PC} = 3.6 Hz, Cp), 71.2 (d, J_{PC} = 4.6 Hz, Cp), 71.3 (m, Cp), 74.1 (d, J_{PC} = 9.0 Hz, *ipso*-Cp^P), 77.4 (d, J_{PC} = 18.0 Hz, *ipso*-Cp^P), 103.4 (d, J_{PC} = 26.5 Hz, *ipso*-Cp^{iPr}), 103.4 (d, J_{PC} = 26.5 Hz, *ipso*-Cp^{iPr}), 128.4–128.3 (m, Ph), 129.1 (d, J_{PC} = 19.0 Hz, Ph), 132.8 (d, J_{PC} = 18.0 Hz, Ph), 134.3 (d, J_{PC} = 22.5 Hz, Ph), 135.8 (d, J_{PC} = 22.0 Hz, Ph), 137.6 (d, J_{PC} = 12.0 Hz, *ipso*-Ph), 138.6 (d, J_{PC} = 10.0 Hz, *ipso*-Ph), 141.4 (d, J_{PC} = 10.0 Hz, *ipso*-Ph). $^{31}P\{^1H\}$ NMR (C_6D_6, 202.5 MHz): δ –24.8 (s), –37.2 (s). HRMS (FDI; m/z): calcd for $^{12}C_{38}{}^{1}H_{44}{}^{56}Fe^{15}P_2$, 618.2268 [$M^+$]; found 618.2245.

Thermal ROP of the chiral phosphorus-bridged [1]FCP (S_p,S_p)-**20^{Ph}**

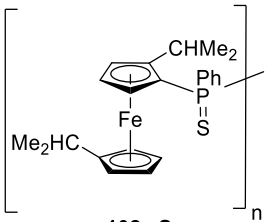

102$_n$-S

A NMR tube was charged with (S_p,S_p)-**20^{Ph}** (90.3 mg, 0.240 mmol) and sealed under vacuum. The tube was then heated to 300 °C for 2 h, after that the tube contents were dissolved in dry thf (2.00 mL) and stirred for another 15 mins to get completely dissolved. The thf solution was then filtered through 0.2 μm syringe PTFE filter into 10.0 mL stirred MeOH, yielded light yellow precipitate **102$_n$** and an orange supernatant **103**. The yellow solid was washed with MeOH (3 x 5 mL) and solvent was removed. The resultant product **102$_n$** was re-dissolved in 1.00 mL of dry thf and then precipitated again in MeOH (10.0 mL). The light yellow solid was washed with MeOH several times until the MeOH solution turned colorless. The product **102$_n$** was isolated as

a light yellow powdery material (40.1 mg, 44%). ^{1}H NMR (C_6D_6, 600 MHz): δ 1.30–0.80 [br, CH(C<u>H</u>$_3$)$_2$], 1.74 [br, C<u>H</u>(CH$_3$)$_2$], 3.01 [br, C<u>H</u>(CH$_3$)$_2$], 4.47–4.06 (br, Cp), 7.06 (br, Ph), 7.67–7.54 (br, Ph). ^{13}C{^{1}H} NMR (C_6D_6, 150.9 MHz): δ 25.9–23.1 [br, CH(<u>C</u>H$_3$)$_2$], 76.2–70.0 (<u>C</u>H of Cp and *ipso*-C^{P}), 101.4 (br, *ipso*-C$^{i\text{Pr}}$), 128.6 (br, Ph), 133.6 (br, Ph), 135.9 (br, Ph), 140.8–138.33 (br, Ph). ^{31}P{^{1}H} NMR (C_6D_6, 243 MHz): δ –25.2 to –27.4 (br), –40.1 (br), –43.2 to –47.5 (br). Polymer **102$_n$** (40.1 mg) was dissolved in CH_2Cl_2 (3 mL) and allowed to react with an excess amount of S_8 (30 mg) for 12 h. From this point on the manipulation was done under air. The CH_2Cl_2 solution was then precipitated into hexanes (10 mL) to afford a light yellow solid and a pale orange supernatant. The yellow solid was washed with hexanes (3 x 5 mL) and all the volatiles were removed. The resultant product was dissolved in a minimum amount of CH_2Cl_2, then precipitated again into hexanes (4 mL), and washed with hexanes (3 × 4 mL) until the supernatant turned clear. Solvent was removed and the product was dried under high vacuum for 12 h, which resulted in **102$_n$-S** as a yellow powder [32.5 mg, 36 % relative to monomer (S_p,S_p)-**20^{Ph}**]. A monomodal molecular weight distribution was observed by GPC. M_w = 19463, M_n = 14258, $Đ$ = 1.34. ^{1}H NMR (C_6D_6, 500 MHz): δ 1.62–0.83 [br, CH(C<u>H</u>$_3$)$_2$], 2.81[br, C<u>H</u>(CH$_3$)$_2$], 3.66 [br, C<u>H</u>(CH$_3$)$_2$], 4.70–3.96 (br, Cp), 7.40 (br, Ph). ^{13}C{^{1}H} NMR (C_6D_6, 150.9 MHz): δ 26.5–24.7 [br, CH(<u>C</u>H$_3$)$_2$ and <u>C</u>H(CH$_3$)$_2$], 75.1–72.8 (CH of Cp and *ipso*-C^{P}), 103.5–100.8 (br, *ipso*-C$^{i\text{Pr}}$), 127.6 (br, Ph), 132.7–131.4 (br, Ph), 135.6 (br, Ph). ^{31}P{^{1}H} NMR (C_6D_6, 500.1 MHz): δ 38.8 to 38.2 (br), 40.6 (br), 42.0 to 41.6 (br).

Isolation and characterization of cyclic phosphines **103**

Removal of all the volatiles from the orange supernatant of **103** resulted in an orange powdery material **103** (46.1 mg, 51%). The mass spectrum of this mixture revealed that it contained various cyclic phosphines. The mixture **103** was dissolved in CH_2Cl_2 (2 mL) and allowed to

react with an excess amount of sulfur (34.5 mg) for 12 h. From this point on the manipulation was done under air. The CH_2Cl_2 solution was then precipitated in hexanes (5 mL) to afford a light orange solid (trace amount) and an orange supernatant. All the volatiles were then removed from the orange supernatant and the resultant orange solid was dried under high vacuum. The product **103^S** was isolated as an orange material (62.6 mg). Based on ^{31}P NMR spectrum and mass spectra, resulting mixture contains several cyclic phosphine sulfides. Preparative thin layer chromatography (PTLC) was carried out on glass plated (20 × 20 cm) pre-coated (0.25 mm) with silica gel 60 F_{254}, first solvent mixture of hexanes / CH_2Cl_2 (1 / 1) as an eluent and then with the same mixture in ratio 2: 1 as an eluent. Materials were detected by visualization under an ultraviolet lamp (λ = 254 nm). The corresponding strips were scraped off and washed with CH_2Cl_2 (3 × 10 mL) and filtered through a fine fritted funnel. Overall 5 fractions (strips) were obtained and named as fractions **103^S-1**, **103^S-2**, **103^S-3**, **103^S-4**, and **103^S-5**. From each fraction approximately 3–4 mg were obtained. Suitable crystal of one of the six bands was obtained from crystallization in CH_2Cl_2 at 0 °C, which was subjected for single X-ray analysis. NMR data for the clean fractions are given below.

Characterization of **103^S-1**

^{1}H NMR ($CDCl_3$, 600 MHz): δ –0.16 [d, J_{HH} = 6.5 Hz, 3H, CH(C$\underline{H}_3$)$_2$], –0.03 [d, J_{HH} = 7.0 Hz, 3H, CH(C$\underline{H}_3$)$_2$], 0.70 [d, J_{HH} = 7.0 Hz, 3H, CH(C$\underline{H}_3$)$_2$], 0.73 [d, J_{HH} = 7.0 Hz, 3H, CH(C$\underline{H}_3$)$_2$], 1.25 [d, J_{HH} = 7.0 Hz, 3H, CH(C$\underline{H}_3$)$_2$], 1.30 [d, J_{HH} = 7.0 Hz, 3H, CH(C$\underline{H}_3$)$_2$], 1.34 [d, J_{HH} = 7.0 Hz, 3H, CH(C$\underline{H}_3$)$_2$], 1.71 [d, J_{HH} = 7.0 Hz, 3H, CH(C$\underline{H}_3$)$_2$], 2.47 [sept, J_{HH} = 6.6 Hz, 1H, C$\underline{H}$(CH$_3$)$_2$], 3.46 [sept, J_{HH} = 6.8 Hz, 1H, C$\underline{H}$(CH$_3$)$_2$], 3.73 [sept, J_{HH} = 6.8 Hz, 1H, C$\underline{H}$(CH$_3$)$_2$], 4.20 [sept, J_{HH} = 6.7 Hz, 1H, C$\underline{H}$(CH$_3$)$_2$], 4.29 (br, 1H, Cp), 4.39 (br, 1H, Cp), 4.43 (br, 1H, Cp), 4.48 (br, 1H, Cp), 4.62 (br, 2H, Cp), 4.73 (br, 1H, Cp), 5.03 (br, 1H, Cp), 5.09 (br, 1H, Cp), 5.74

(br, 1H, Cp), 6.22 (br, 1H, Cp), 6.47 (br, 1H, Cp), 7.18–7.15 (m, 2H, Ph), 7.23–7.21 (m, 4H, Ph), 7.38–7.34 (m, 2H, Ph), 7.84–7.80 (m, 2H, Ph). $^{31}P\{^{1}H\}$ NMR ($CDCl_3$, 202.5 MHz): δ 36.2 (s), 41.9 (s).

Characterization of **103^{S}-2**

^{1}H NMR ($CDCl_3$, 600 MHz): δ –0.21 [d, J_{HH} = 7.0 Hz, 6H, CH(C$\underline{H}_3$)$_2$], 0.79[d, J_{HH} = 7.0 Hz, 6H, CH(C$\underline{H}_3$)$_2$], 1.39 [d, J_{HH} = 7.0 Hz, 6H, CH(C$\underline{H}_3$)$_2$], 1.59 [d, J_{HH} = 7.0 Hz, 6H, CH(C$\underline{H}_3$)$_2$], 2.27 [sept, J_{HH} = 6.6 Hz, 2H, C$\underline{H}$(CH$_3$)$_2$], 3.61 [sept, J_{HH} = 6.7 Hz, 2H, C$\underline{H}$(CH$_3$)$_2$], 4.29 (br, 2H, Cp), 4.47 (br, 2H, Cp), 4.69 (br, 2H, Cp), 5.03 (br, 2H, Cp), 5.80 (br, 2H, Cp), 5.94 (br, 2H, Cp), 7.19–7.16 (m, 4H, Ph), 7.24–7.23 (m, 2H, Ph), 7.38–7.35 (m, 4H, Ph). $^{31}P\{^{1}H\}$ NMR ($CDCl_3$, 202.5 MHz): δ 41.4 (s).

Characterization of *syn-C_2*-**103^{S}-3**

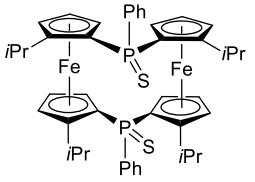

syn-C_2-**103^{S}-3**

^{1}H NMR ($CDCl_3$, 600 MHz): δ 0.04 [d, J_{HH} = 6.0 Hz, 6H, CH(C$\underline{H}_3$)$_2$], 1.12 [d, J_{HH} = 6.0 Hz, 6H, CH(C$\underline{H}_3$)$_2$], 1.26 [d, J_{HH} = 6.0 Hz, 6H, CH(C$\underline{H}_3$)$_2$], 1.45 [d, J_{HH} = 6.0 Hz, 6H, CH(C$\underline{H}_3$)$_2$], 3.86 [sept, J_{HH} = 6.5 Hz, 2H, C$\underline{H}$(CH$_3$)$_2$], 4.29 (br, 2H, Cp), 4.35 (br, 2H, Cp), 4.49 (br, 2H, Cp), 4.72 (br, 2H, Cp), 4.84 [sept, J_{HH} = 6.8 Hz, 2H, C$\underline{H}$(CH$_3$)$_2$], 6.05 (br, 2H, Cp), 7.20–7.18 (m, 6H, Ph), 7.71–7.67 (m, 4H, Ph). $^{31}P\{^{1}H\}$ NMR ($CDCl_3$, 202.5 MHz): δ 34.0 (s).

Characterization of **103^{S}-4**

^{1}H NMR ($CDCl_3$, 600 MHz): δ 0.29 [d, J_{HH} = 7.0 Hz, 12H, CH(C$\underline{H}_3$)$_2$], 1.28 [d, J_{HH} = 7.0 Hz, 12H, CH(C$\underline{H}_3$)$_2$], 3.93 [sept, J_{HH} = 6.7 Hz, 4H, C$\underline{H}$(CH$_3$)$_2$], 4.32 (br, 4H, Cp), 4.70 (br, 4H, Cp), 6.16 (br, 4H, Cp), 7.23–7.21 (m, 6H, Ph), 7.80–7.76 (m, 4H, Ph). ^{31}P{^{1}H} NMR ($CDCl_3$, 202.5 MHz): δ 38.3 (s).

Characterization of **103^{S}-5**

^{1}H NMR ($CDCl_3$, 600 MHz): δ 0.17 [d, J_{HH} = 7.0 Hz, 6H, CH(C$\underline{H}_3$)$_2$], 0.63 [d, J_{HH} = 7.0 Hz, 6H, CH(C$\underline{H}_3$)$_2$], 1.25–1.28 [m, 12H, CH(C$\underline{H}_3$)$_2$], 2.77 [sept, J_{HH} = 6.8 Hz, 2H, C$\underline{H}$(CH$_3$)$_2$], 3.43 [sept, J_{HH} = 6.7 Hz, 2H, C$\underline{H}$(CH$_3$)$_2$], 4.24 (br, 2H, Cp), 4.27–4.26 (m, 4H, Cp), 4.51 (br, 2H, Cp), 5.35 (br, 2H, Cp), 6.95 (br, 2H, Cp), 7.04 (br, 4H, Ph), 7.16 (br, 4H, Ph), 7.28 (br, 2H, Ph). ^{31}P{^{1}H} NMR ($CDCl_3$, 202.5 MHz): δ 42.6 (s).

Thermal ROP of phosphorus-bridged [1]FCP **11^{Ph}**

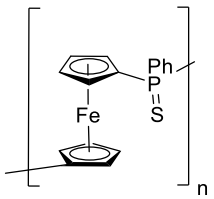

11_n^{Ph}-S

A NMR tube was charged with **11^{Ph}** (80.0 mg, 0.274 mmol) and sealed under vacuum. The tube was then heated to 120 °C for 1 h and then to 130 °C for 15 min. The tube contents were then dissolved in dry CH_2Cl_2 (2.00 mL) and stirred under N_2 flow for 1h. The reaction mixture was then added dropwise to 15.0 mL stirred hexanes that afforded a yellow solid **11_n^{Ph}** and a yellow supernatant **105**. The yellow solid **11_n^{Ph}** was washed with hexanes (3 x 5 mL) and solvent was removed. The resultant product **11_n^{Ph}** was re-dissolved in 1.00 mL of dry CH_2Cl_2 and then

precipitated again in hexanes (10.0 mL) to yield yellow solid and pale yellow supernatant. The yellow solid was washed with hexanes several times until the hexanes solution turned colorless. The product $\mathbf{11_n^{Ph}}$ was isolated as a light yellow powdery material (68.9 mg, 86%). ^{1}H NMR ($CDCl_3$, 600 MHz): δ 4.17–3.74 (br, Cp), 7.43–7.28 (br, 5H, Ph). $^{31}P\{^1H\}$ NMR ($CDCl_3$, 243 MHz): δ –26.8 (br), –31.3 to –31.5 (br). $^{13}C\{^1H\}$ NMR ($CDCl_3$, 150.9 MHz): δ 71.5 (br, Cp), 71.6 (br, Cp), 72.3 (br, Cp), 72.5 (br, Cp), 73.6–73.2 (m, Cp), 78.3 (br, Cp), 127.6 (br, Ph), 127.9 (br, Ph), 128.8 (br, Ph), 133.7 (s, Ph), 133.9 (s, Ph), 138.8 (br, Ph). Polymer $\mathbf{11_n^{Ph}}$ (68.9 mg) was dissolved in CH_2Cl_2 (3.00 mL) and allowed to react with an excess amount of S_8 (50.0 mg) for 12 h. From this point on the manipulation was done under air. The reaction mixture was precipitated into stirred hexanes (10.0 mL) to afford a yellow solid and a colorless supernatant. The yellow solid was washed with hexanes (3 x 5 mL) and then dried under high vacuum. The product $\mathbf{11_n^{Ph}}$**-S** was isolated as a yellow powdery material (52.3 mg, 65% relative to monomer $\mathbf{11^{Ph}}$). A monomodal molecular weight distribution of $\mathbf{11_n^{Ph}}$**-S** was observed by GPC. M_w = 87107, M_n = 54101, $Đ$ = 1.61. ^{1}H NMR ($CdCl_3$, 500 MHz): δ 4.67–3.88 (br, Cp, 8H), 7.76–7.43 (br, Ph, 5H). $^{13}C\{^1H\}$ NMR ($CDCl_3$, 500 MHz): δ 71.6 [d, J_{PC} = 12.3 Hz, Cp], 72.0 [d, J_{PC} = 9.8 Hz, Cp], 72.6 (br, Cp), 73.8 (br, Cp), 74.9 (br, Cp), 77.8 (s, Cp), 78.6 (s, Cp), 128.1 (br, Ph), 129.8 [d, J_{PC} = 11.7 Hz, Ph], 130.2 (s, Ph), 131.2 (br, Ph), 133.2 (s, Ph), 133.9 (s, Ph). $^{31}P\{^1H\}$ NMR ($CDCl_3$, 500.1 MHz): δ = 37.7 (br).

Isolation and characterization of phosphines by-products

Removal of all the volatiles from the yellow supernatant of **105** resulted in a yellow powdery material **105** (21.0 mg, 26%). The mass spectrum of this mixture revealed that it contained various phosphines compounds. The mixture **105** was dissolved in CH_2Cl_2 (2 mL) and allowed to react with excess amount of S_8 (15.0 mg) for 12 h. From this point on the manipulation was

done under air. The CH_2Cl_2 solution was then precipitated in hexanes (5 mL) to afford a yellow supernatant. All the volatiles were removed from the yellow supernatant and the resultant yellow solid **105^{S}** was dried under high vacuum. The product **105^{S}** was isolated as a yellow material (29.5 mg). Based on ^{31}P NMR spectrum and mass spectra, resulting mixture contains several phosphine sulfides species. Preparative thin layer chromatography (PTLC) was carried out on glass plated (20 × 20 cm) pre-coated (0.25 mm) with silica gel 60 F_{254}, first solvent mixture of hexanes / CH_2Cl_2 (1 / 1) as an eluent and then with the same mixture in ratio 2: 1 as an eluent. Materials were detected by visualization under an ultraviolet lamp (λ = 254 nm). The corresponding strips were scraped off and washed with CH_2Cl_2 (3 × 10 mL) and filtered through a fine fritted funnel. Overall 3 fractions (strips) were obtained and named as fractions *anti*-51, **105^{S}-1**, and **105^{S}-2**. From each fraction approximately 2–3 mg were obtained.

In the investigation of thermal ROP of the known compound **11^{Ph}**, the term "*used*" and "*new*" NMR tube was mentioned. A used NMR tube is defined as an NMR tube which was used for NMR measurements, then cleaned with basic and acidic solution and dried in an oven with elevated temperatures (100 °C). Therefore, these used NMR tubes contained scratches on their glass surface, which likely allow side reactions with the active ferrocene compounds. A new NMR tube comes directly from the factory and has not been used before. Hence, there are no scratches on its glass surface.

Characterization of *anti*-**51**

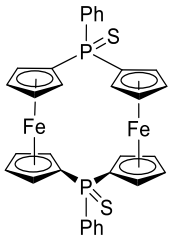

anti-**51**

^{1}H NMR ($CDCl_3$, 500.1 MHz): δ 4.54 (br, 4H, Cp), 4.79 (br, 4H, Cp), 4.92 (br, 4H, Cp), 5.55 (br, 4H, Cp), 7.23–7.16 (m, 6H, Ph), 7.48–7.43 (m, 4H, Ph). ^{31}P{^{1}H} NMR ($CDCl_3$, 202.5 MHz): δ 40.0 (s). HRMS (FDI; m/z): calcd for $^{12}C_{32}{}^{1}H_{26}{}^{56}Fe_2{}^{15}P_2{}^{32}S_2$, 647.9650 [$M^+$]; found 647.9651.

Characterization of **105^{S}-1**

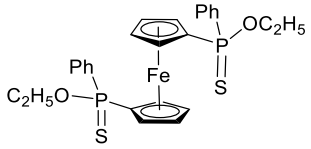

105^{S}-1

^{1}H NMR ($CDCl_3$, 500.1 MHz): δ 3.89–3.79 (m, 2H, C<u>H</u>$_2$ of OC_2H_5), 4.13–4.07 (m, 2H, C<u>H</u>$_2$ of OC_2H_5), 4.35 (br, 1H, Cp), 4.45 (br, 1H, Cp), 4.46 (br, 1H, Cp), 4.56 (br, 2H, Cp), 4.58 (br, 1H, Cp), 4.81 (br, 1H, Cp), 7.53–7.44 (m, 6H, Ph), 7.94–7.89 (m, 4H, Ph). ^{13}C{^{1}H} NMR ($CDCl_3$, 600 MHz): δ 16.3 [d, J_{PC} = 8.0 Hz, <u>C</u>H$_3$ of OC_2H_5], 60.8–60.7 (m, <u>C</u>H$_2$ of OC_2H_5), 75.2–72.8 (m, Cp), 131.8–128.2 (m, Ph). ^{31}P{^{1}H} NMR ($CDCl_3$, 202.5 MHz): δ 83.4 (s), 83.5 (s). HRMS (FDI; m/z): calcd for $^{12}C_{26}{}^{1}H_{28}{}^{56}Fe^{16}O_2{}^{15}P_2{}^{32}S_2$, 554.0355 [$M^+$]; found 554.0362.

Characterization of **105^{S}-2**

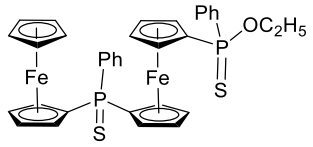

105^{S}-2

NMR spectroscopy could not solve the structure of species **105^{S}-2** due to the presence of impurities in the sample. HRMS (FDI; m/z): calcd for $^{12}C_{34}{}^{1}H_{32}{}^{56}Fe_2{}^{16}O{}^{15}P_2{}^{32}S_2$, 694.0069; found 694.0064.

Attempted thermal ROP of the chiral phosphorus-bridged [2]FCP (S_p,S_p,*R*,*R*)-**90^{CH2SiMe3}**

A NMR tube was charged with (S_p,S_p,*R*,*R*)-**90^{CH2SiMe3}** (19.5 mg, 38.6 x 10^{-3} mmol) and sealed under vacuum. The tube was then heated to 300 $^{\circ}$C for 6 h. The color of the tube content stayed as orange, and did not change during the heating time. The mixture was analyzed by NMR spectroscopy. ^{1}H and ^{31}P NMR spectra of the tube content showed the same chemical shift as the starting material. Therefore, no thermal polymerization occurred with monomer (S_p,S_p,*R*,*R*)-**90^{CH2SiMe3}**.

Photolytic living anionic ROP of known phosphorus-bridged [1]FCP **11^{CH2SiMe3}**

In the absence of light, the monomer **11^{CH2SiMe3}** (43.0 mg, 0.142 mmol) was dissolved in dried thf (1.0 mL) in a NMR tube. Na[C_5H_5] (29 μL, 2.85 × 10^{-3} mmol, 0.1 M solution in thf) was added and the mixture was photolyzed to initiate the polymerization. The reaction was maintained at 5 °C by using a thermostatically controlled acetone bath. The color of solution changed from dark-red to yellow. The polymerization was quenched with a few drops of degassed methanol. Precipitation of the solution into rapidly stirred degassed methanol (15 mL)

followed by drying overnight under vacuum afforded polymer **57$_n$** as a yellow powder (35 mg, 81%). Polymer **57$_n$** (35 mg) was dissolved in CH_2Cl_2 (2.5 mL) and allowed to with an excess amount of S_8 (12.0 mg) for 12 h. Color of solution changed from yellow to orange during stirring overnight. The solution was then precipitated into stirred hexanes (15 mL) and solvent was removed under vacuum to yield in yellow powder **57$_n^S$** as resulting product (30.0 mg, 70%). ^{1}H NMR (C_6D_6, 500 MHz): δ 0.20 [s, Si(C$\underline{H}_3$)$_2$], 1.46–1.41 (br, PC$\underline{H}_2$), 4.40–4.09 (br, Cp). ^{31}P{^{1}H} NMR (C_6D_6, 202.5 MHz): δ –47.5 (br).

Attempted photolytic living anionic ROP of chiral phosphorus-bridged [1]FCP (S_p,S_p)-**86^{CH2SiMe3}**

In the absence of light, the monomer (S_p,S_p)-**86^{CH2SiMe3}** (31.2 mg, 0.081 mmol) was dissolved in dry thf (1.0 mL) in a NMR tube. Na[C_5H_5] (16 μL, 1.6 × 10^{-3} mmol, 0.1 M solution in thf) was added and the mixture was photolyzed to initiate the polymerization. The reaction was maintained at 5 °C by using a thermostatically controlled acetone bath. The color of solution did not change during 2 h, hence, temperature was increased to 10 °C and the NMR tube was kept at this temperature for another 2 h. The tube content was analyzed by ^{1}H and ^{31}P NMR spectroscopy, and it showed the same signals as starting material. Therefore, no photolytic living anionic polymerization occurred with monomer (S_p,S_p)-**86^{CH2SiMe3}**.

APPENDIX

Table 4–1. Bond lengths [Å] and angles [deg] for 1,1′-(S_p,S_p,S,S)-**88**$^{\mathbf{NiPr2}}$ (symmetry transformations used to generate equivalent atoms ': -x+1, y, -z+1).

Fe(1)-C(5)	2.034(2)	C(1)'-Fe(1)-C(4)'	68.53(8)
Fe(1)-C(5)'	2.034(2)	C(1)-Fe(1)-C(4)'	107.85(8)
Fe(1)-C(1)'	2.0453(19)	C(5)-Fe(1)-C(4)	40.46(9)
Fe(1)-C(1)	2.0453(19)	C(5)'-Fe(1)-C(4)	129.60(9)
Fe(1)-C(4)'	2.0538(19)	C(1)'-Fe(1)-C(4)	107.84(8)
Fe(1)-C(4)	2.0538(19)	C(1)-Fe(1)-C(4)	68.53(8)
Fe(1)-C(2)'	2.0613(19)	C(4)'-Fe(1)-C(4)	168.23(14)
Fe(1)-C(2)	2.0613(19)	C(5)-Fe(1)-C(2)'	147.50(8)
Fe(1)-C(3)	2.072(2)	C(5)'-Fe(1)-C(2)'	69.19(8)
Fe(1)-C(3)'	2.072(2)	C(1)'-Fe(1)-C(2)'	41.27(8)
Cl(1)-P(1)	2.1536(7)	C(1)-Fe(1)-C(2)'	170.93(8)
P(1)-N(1)	1.6677(17)	C(4)'-Fe(1)-C(2)'	68.39(8)
P(1)-C(1)	1.809(2)	C(4)-Fe(1)-C(2)'	116.84(8)
N(1)-C(9)	1.490(3)	C(5)-Fe(1)-C(2)	69.19(8)
N(1)-C(12)	1.497(3)	C(5)'-Fe(1)-C(2)	147.50(8)
C(1)-C(5)	1.436(3)	C(1)'-Fe(1)-C(2)	170.93(8)
C(1)-C(2)	1.447(3)	C(1)-Fe(1)-C(2)	41.27(8)
C(2)-C(3)	1.428(3)	C(4)'-Fe(1)-C(2)	116.84(8)
C(2)-C(6)	1.514(3)	C(4)-Fe(1)-C(2)	68.39(8)
C(3)-C(4)	1.420(3)	C(2)'-Fe(1)-C(2)	132.13(12)
C(4)-C(5)	1.414(3)	C(5)-Fe(1)-C(3)	68.14(9)
C(6)-C(7)	1.525(3)	C(5)'-Fe(1)-C(3)	169.24(9)
C(6)-C(8)	1.533(3)	C(1)'-Fe(1)-C(3)	131.57(8)
C(9)-C(11)	1.518(3)	C(1)-Fe(1)-C(3)	68.37(8)
C(9)-C(10)	1.525(4)	C(4)'-Fe(1)-C(3)	150.12(9)
C(12)-C(13)	1.519(4)	C(4)-Fe(1)-C(3)	40.26(9)
C(12)-C(14)	1.520(4)	C(2)'-Fe(1)-C(3)	110.48(9)
C(5)-Fe(1)-C(5)'	106.04(12)	C(2)-Fe(1)-C(3)	40.42(8)
C(5)-Fe(1)-C(1)'	113.74(8)	C(5)-Fe(1)-C(3)'	169.24(9)
C(5)'-Fe(1)-C(1)'	41.21(8)	C(5)'-Fe(1)-C(3)'	68.14(9)
C(5)-Fe(1)-C(1)	41.21(8)	C(1)'-Fe(1)-C(3)'	68.37(9)
C(5)'-Fe(1)-C(1)	113.73(8)	C(1)-Fe(1)-C(3)'	131.56(8)
C(1)'-Fe(1)-C(1)	146.20(11)	C(4)'-Fe(1)-C(3)'	40.26(9)
C(5)-Fe(1)-C(4)'	129.61(9)	C(4)-Fe(1)-C(3)'	150.13(9)
C(5)'-Fe(1)-C(4)'	40.46(9)	C(2)'-Fe(1)-C(3)'	40.42(8)

C(2)-Fe(1)-C(3)'	110.48(9)	C(6)-C(2)-Fe(1)	130.20(14)
C(3)-Fe(1)-C(3)'	119.05(13)	C(4)-C(3)-C(2)	108.60(18)
N(1)-P(1)-C(1)	102.77(9)	C(4)-C(3)-Fe(1)	69.18(12)
N(1)-P(1)-Cl(1)	105.00(7)	C(2)-C(3)-Fe(1)	69.39(11)
C(1)-P(1)-Cl(1)	97.81(7)	C(5)-C(4)-C(3)	108.55(17)
C(9)-N(1)-C(12)	116.36(16)	C(5)-C(4)-Fe(1)	69.02(11)
C(9)-N(1)-P(1)	124.14(13)	C(3)-C(4)-Fe(1)	70.56(11)
C(12)-N(1)-P(1)	116.51(13)	C(4)-C(5)-C(1)	108.18(18)
C(5)-C(1)-C(2)	107.52(18)	C(4)-C(5)-Fe(1)	70.52(12)
C(5)-C(1)-P(1)	130.12(15)	C(1)-C(5)-Fe(1)	69.82(11)
C(2)-C(1)-P(1)	122.16(15)	C(2)-C(6)-C(7)	113.48(18)
C(5)-C(1)-Fe(1)	68.97(11)	C(2)-C(6)-C(8)	109.79(19)
C(2)-C(1)-Fe(1)	69.96(12)	C(7)-C(6)-C(8)	110.4(2)
P(1)-C(1)-Fe(1)	122.35(10)	N(1)-C(9)-C(11)	110.67(19)
C(3)-C(2)-C(1)	107.15(18)	N(1)-C(9)-C(10)	112.9(2)
C(3)-C(2)-C(6)	127.06(18)	C(11)-C(9)-C(10)	111.8(2)
C(1)-C(2)-C(6)	125.58(19)	N(1)-C(12)-C(13)	113.4(2)
C(3)-C(2)-Fe(1)	70.19(12)	N(1)-C(12)-C(14)	110.4(2)
C(1)-C(2)-Fe(1)	68.77(11)	C(13)-C(12)-C(14)	111.5(3)

Table 4–2. Bond lengths [Å] and angles [deg] for (S_p,S_p,*R*.*R*)-**90**^{CH2SiMe3}

Fe(1)-C(1) 2.009(2)	C(11)-C(12) 1.526(3)
Fe(1)-C(6) 2.013(2)	C(11)-C(13) 1.529(3)
Fe(1)-C(5) 2.024(2)	C(14)-C(15) 1.517(4)
Fe(1)-C(10) 2.028(2)	C(14)-C(16) 1.519(4)
Fe(1)-C(2) 2.048(2)	C(1)-Fe(1)-C(6) 99.18(8)
Fe(1)-C(7) 2.049(2)	C(1)-Fe(1)-C(5) 41.63(8)
Fe(1)-C(9) 2.061(2)	C(6)-Fe(1)-C(5) 107.36(9)
Fe(1)-C(4) 2.064(2)	C(1)-Fe(1)-C(10) 106.99(9)
Fe(1)-C(8) 2.072(2)	C(6)-Fe(1)-C(10) 41.73(8)
Fe(1)-C(3) 2.078(2)	C(5)-Fe(1)-C(10) 139.23(9)
P(1)-C(1) 1.832(2)	C(1)-Fe(1)-C(2) 41.90(8)
P(1)-C(17) 1.847(2)	C(6)-Fe(1)-C(2) 126.70(8)
P(1)-P(2) 2.2403(7)	C(5)-Fe(1)-C(2) 69.44(8)
P(2)-C(6) 1.828(2)	C(10)-Fe(1)-C(2) 105.47(9)
P(2)-C(21) 1.853(2)	C(1)-Fe(1)-C(7) 126.74(8)
Si(1)-C(19) 1.865(3)	C(6)-Fe(1)-C(7) 41.85(8)
Si(1)-C(18) 1.867(3)	C(5)-Fe(1)-C(7) 105.91(9)
Si(1)-C(17) 1.872(2)	C(10)-Fe(1)-C(7) 69.67(9)
Si(1)-C(20) 1.876(3)	C(2)-Fe(1)-C(7) 167.01(8)
Si(2)-C(23) 1.849(4)	C(1)-Fe(1)-C(9) 142.17(9)
Si(2)-C(22) 1.851(4)	C(6)-Fe(1)-C(9) 69.18(9)
Si(2)-C(21) 1.869(2)	C(5)-Fe(1)-C(9) 174.41(9)
Si(2)-C(24) 1.881(4)	C(10)-Fe(1)-C(9) 40.54(10)
C(1)-C(5) 1.433(3)	C(2)-Fe(1)-C(9) 116.12(9)
C(1)-C(2) 1.451(3)	C(7)-Fe(1)-C(9) 68.55(9)
C(2)-C(3) 1.425(3)	C(1)-Fe(1)-C(4) 69.16(9)
C(2)-C(11) 1.510(3)	C(6)-Fe(1)-C(4) 142.68(9)
C(3)-C(4) 1.417(3)	C(5)-Fe(1)-C(4) 40.56(9)
C(3)-H(3) 1.0000	C(10)-Fe(1)-C(4) 173.65(9)
C(4)-C(5) 1.418(3)	C(2)-Fe(1)-C(4) 68.24(9)
C(4)-H(4) 1.0000	C(7)-Fe(1)-C(4) 116.66(9)
C(5)-H(5) 1.0000	C(9)-Fe(1)-C(4) 140.61(10)
C(6)-C(10) 1.439(3)	C(1)-Fe(1)-C(8) 166.79(9)
C(6)-C(7) 1.451(3)	C(6)-Fe(1)-C(8) 68.85(9)
C(7)-C(8) 1.421(3)	C(5)-Fe(1)-C(8) 134.86(9)
C(7)-C(14) 1.504(3)	C(10)-Fe(1)-C(8) 68.19(9)
C(8)-C(9) 1.420(3)	C(2)-Fe(1)-C(8) 150.32(9)
C(8)-H(8) 1.0000	C(7)-Fe(1)-C(8) 40.33(9)
C(9)-C(10) 1.417(3)	C(9)-Fe(1)-C(8) 40.19(10)

C(4)-Fe(1)-C(8) 116.71(10)
C(1)-Fe(1)-C(3) 69.11(8)
C(6)-Fe(1)-C(3) 166.89(8)
C(5)-Fe(1)-C(3) 68.19(9)
C(10)-Fe(1)-C(3) 134.33(9)
C(2)-Fe(1)-C(3) 40.39(8)
C(7)-Fe(1)-C(3) 150.45(9)
C(9)-Fe(1)-C(3) 116.18(9)
C(4)-Fe(1)-C(3) 40.00(9)
C(8)-Fe(1)-C(3) 123.35(9)
C(1)-P(1)-C(17) 104.62(10)
C(1)-P(1)-P(2) 97.87(7)
C(17)-P(1)-P(2) 98.14(7)
C(6)-P(2)-C(21) 104.25(11)
C(6)-P(2)-P(1) 97.60(7)
C(21)-P(2)-P(1) 98.71(8)
C(19)-Si(1)-C(18) 110.71(14)
C(19)-Si(1)-C(17) 109.57(12)
C(18)-Si(1)-C(17) 109.59(12)
C(19)-Si(1)-C(20) 110.36(14)
C(18)-Si(1)-C(20) 110.14(15)
C(17)-Si(1)-C(20) 106.37(13)
C(23)-Si(2)-C(22) 110.5(3)
C(23)-Si(2)-C(21) 108.62(17)
C(22)-Si(2)-C(21)110.64(18)
C(23)-Si(2)-C(24) 110.7(3)
C(22)-Si(2)-C(24) 108.5(2)
C(21)-Si(2)-C(24) 107.75(17)
C(5)-C(1)-C(2) 107.08(18)
C(5)-C(1)-P(1) 127.37(16)
C(2)-C(1)-P(1) 123.34(15)
C(5)-C(1)-Fe(1) 69.75(12)
C(2)-C(1)-Fe(1) 70.52(11)
P(1)-C(1)-Fe(1) 111.74(10)
C(3)-C(2)-C(1) 107.47(18)
C(3)-C(2)-C(11) 126.08(19)
C(1)-C(2)-C(11) 126.38(18)
C(3)-C(2)-Fe(1) 70.93(12)
C(1)-C(2)-Fe(1) 67.58(11)
C(11)-C(2)-Fe(1) 129.12(15)
C(4)-C(3)-C(2) 108.56(19)
C(4)-C(3)-Fe(1) 69.46(12)
C(2)-C(3)-Fe(1) 68.68(12)
C(3)-C(4)-C(5) 108.48(19)
C(3)-C(4)-Fe(1) 70.54(12)
C(5)-C(4)-Fe(1) 68.19(12)
C(4)-C(5)-C(1) 108.40(18)
C(4)-C(5)-Fe(1) 71.24(13)
C(1)-C(5)-Fe(1) 68.62(11)
C(10)-C(6)-C(7) 107.37(18)
C(10)-C(6)-P(2) 126.62(16)
C(7)-C(6)-P(2) 123.81(15)
C(10)-C(6)-Fe(1) 69.69(11)
C(7)-C(6)-Fe(1) 70.41(11)
P(2)-C(6)-Fe(1) 112.05(10)
C(8)-C(7)-C(6) 107.10(19)
C(8)-C(7)-C(14) 126.7(2)
C(6)-C(7)-C(14) 126.1(2)
C(8)-C(7)-Fe(1) 70.73(12)
C(6)-C(7)-Fe(1) 67.74(11)
C(14)-C(7)-Fe(1) 129.76(15)
C(9)-C(8)-C(7) 109.1(2)
C(9)-C(8)-Fe(1) 69.47(13)
C(7)-C(8)-Fe(1) 68.95(12)
C(10)-C(9)-C(8) 108.2(2)
C(10)-C(9)-Fe(1) 68.48(12)
C(8)-C(9)-Fe(1) 70.35(13)
C(9)-C(10)-C(6) 108.2(2)
C(9)-C(10)-Fe(1) 70.99(13)
C(6)-C(10)-Fe(1) 68.58(11)
C(2)-C(11)-C(12) 112.61(19)
C(2)-C(11)-C(13) 109.3(2)
C(12)-C(11)-C(13) 110.44(19)
C(7)-C(14)-C(15) 113.6(2)
C(7)-C(14)-C(16) 109.4(2)
C(15)-C(14)-C(16) 109.7(3)
P(1)-C(17)-Si(1) 118.24(12)
P(2)-C(21)-Si(2) 116.75(13)

Table 4–3. Bond lengths [Å] and angles [deg] for (S_p,R)-**95**^{S}

Fe(1)-C(8)	2.031(3)	C(25)-C(26)	1.508(4)
Fe(1)-C(1)	2.032(2)	C(8)-Fe(1)-C(1)	153.27(11)
Fe(1)-C(5)	2.034(2)	C(8)-Fe(1)-C(5)	162.53(12)
Fe(1)-C(9)	2.038(3)	C(1)-Fe(1)-C(5)	41.63(9)
Fe(1)-C(7)	2.047(2)	C(8)-Fe(1)-C(9)	40.86(13)
Fe(1)-C(2)	2.049(2)	C(1)-Fe(1)-C(9)	119.93(11)
Fe(1)-C(10)	2.050(2)	C(5)-Fe(1)-C(9)	155.80(13)
Fe(1)-C(3)	2.053(2)	C(8)-Fe(1)-C(7)	40.59(12)
Fe(1)-C(4)	2.054(2)	C(1)-Fe(1)-C(7)	165.42(11)
Fe(1)-C(6)	2.067(2)	C(5)-Fe(1)-C(7)	126.36(11)
P(1)-C(1)	1.801(3)	C(9)-Fe(1)-C(7)	68.22(12)
P(1)-C(23)	1.819(2)	C(8)-Fe(1)-C(2)	117.16(11)
P(1)-C(17)	1.820(2)	C(1)-Fe(1)-C(2)	41.53(9)
P(1)-S(1)	1.9569(9)	C(5)-Fe(1)-C(2)	69.64(8)
C(1)-C(5)	1.445(3)	C(9)-Fe(1)-C(2)	106.94(10)
C(1)-C(2)	1.447(3)	C(7)-Fe(1)-C(2)	151.47(10)
C(2)-C(3)	1.426(3)	C(8)-Fe(1)-C(10)	68.24(12)
C(2)-C(11)	1.515(3)	C(1)-Fe(1)-C(10)	109.64(11)
C(3)-C(4)	1.422(4)	C(5)-Fe(1)-C(10)	121.85(11)
C(4)-C(5)	1.417(4)	C(9)-Fe(1)-C(10)	40.35(12)
C(6)-C(10)	1.418(4)	C(7)-Fe(1)-C(10)	67.90(11)
C(6)-C(7)	1.438(4)	C(2)-Fe(1)-C(10)	127.60(11)
C(6)-C(14)	1.505(4)	C(8)-Fe(1)-C(3)	105.49(11)
C(7)-C(8)	1.414(4)	C(1)-Fe(1)-C(3)	68.87(9)
C(8)-C(9)	1.420(5)	C(5)-Fe(1)-C(3)	68.43(10)
C(9)-C(10)	1.410(4)	C(9)-Fe(1)-C(3)	125.42(11)
C(11)-C(13)	1.521(3)	C(7)-Fe(1)-C(3)	117.68(10)
C(11)-C(12)	1.539(4)	C(2)-Fe(1)-C(3)	40.70(9)
C(14)-C(15)	1.512(5)	C(10)-Fe(1)-C(3)	163.90(11)
C(14)-C(16)	1.512(4)	C(8)-Fe(1)-C(4)	124.43(12)
C(17)-C(22)	1.387(3)	C(1)-Fe(1)-C(4)	69.13(9)
C(17)-C(18)	1.397(3)	C(5)-Fe(1)-C(4)	40.55(10)
C(18)-C(19)	1.386(4)	C(9)-Fe(1)-C(4)	162.35(12)
C(19)-C(20)	1.372(4)	C(7)-Fe(1)-C(4)	106.72(11)
C(20)-C(21)	1.383(4)	C(2)-Fe(1)-C(4)	68.95(9)
C(21)-C(22)	1.393(3)	C(10)-Fe(1)-C(4)	155.19(11)
C(23)-C(24)	1.527(3)	C(3)-Fe(1)-C(4)	40.53(10)
C(24)-C(25)	1.529(3)	C(8)-Fe(1)-C(6)	68.79(11)

C(1)-Fe(1)-C(6)	127.96(11)
C(5)-Fe(1)-C(6)	108.76(9)
C(9)-Fe(1)-C(6)	68.34(10)
C(7)-Fe(1)-C(6)	40.91(11)
C(2)-Fe(1)-C(6)	165.67(11)
C(10)-Fe(1)-C(6)	40.30(10)
C(3)-Fe(1)-C(6)	153.05(11)
C(4)-Fe(1)-C(6)	119.70(10)
C(1)-P(1)-C(23)	103.16(11)
C(1)-P(1)-C(17)	103.75(11)
C(23)-P(1)-C(17)	106.28(12)
C(1)-P(1)-S(1)	116.49(8)
C(23)-P(1)-S(1)	113.18(9)
C(17)-P(1)-S(1)	112.86(8)
C(5)-C(1)-C(2)	107.5(2)
C(5)-C(1)-P(1)	123.62(18)
C(2)-C(1)-P(1)	128.85(17)
C(5)-C(1)-Fe(1)	69.29(12)
C(2)-C(1)-Fe(1)	69.89(12)
P(1)-C(1)-Fe(1)	127.71(12)
C(3)-C(2)-C(1)	106.99(19)
C(3)-C(2)-C(11)	124.9(2)
C(1)-C(2)-C(11)	127.9(2)
C(3)-C(2)-Fe(1)	69.77(12)
C(1)-C(2)-Fe(1)	68.58(11)
C(11)-C(2)-Fe(1)	130.95(16)
C(4)-C(3)-C(2)	109.2(2)
C(4)-C(3)-Fe(1)	69.79(13)
C(2)-C(3)-Fe(1)	69.53(12)
C(4)-C(3)-H(3)	125.4
C(2)-C(3)-H(3)	125.4
Fe(1)-C(3)-H(3)	125.4
C(5)-C(4)-C(3)	108.1(2)
C(5)-C(4)-Fe(1)	68.99(13)
C(3)-C(4)-Fe(1)	69.69(13)
C(4)-C(5)-C(1)	108.2(2)
C(4)-C(5)-Fe(1)	70.46(14)
C(1)-C(5)-Fe(1)	69.08(12)
C(10)-C(6)-C(7)	106.5(2)
C(10)-C(6)-C(14)	125.6(3)
C(7)-C(6)-C(14)	127.8(3)
C(10)-C(6)-Fe(1)	69.19(14)
C(7)-C(6)-Fe(1)	68.79(14)
C(14)-C(6)-Fe(1)	129.92(17)
C(8)-C(7)-C(6)	108.5(3)
C(8)-C(7)-Fe(1)	69.08(15)
C(6)-C(7)-Fe(1)	70.30(14)
C(7)-C(8)-C(9)	107.8(3)
C(7)-C(8)-Fe(1)	70.34(14)
C(9)-C(8)-Fe(1)	69.86(16)
C(10)-C(9)-C(8)	107.9(3)
C(10)-C(9)-Fe(1)	70.27(14)
C(8)-C(9)-Fe(1)	69.28(16)
C(9)-C(10)-C(6)	109.2(3)
C(9)-C(10)-Fe(1)	69.38(15)
C(6)-C(10)-Fe(1)	70.51(15)
C(2)-C(11)-C(13)	110.3(2)
C(2)-C(11)-C(12)	112.1(2)
C(13)-C(11)-C(12)	108.5(2)
C(22)-C(17)-C(18)	118.6(2)
C(22)-C(17)-P(1)	119.81(18)
C(18)-C(17)-P(1)	121.52(19)
C(19)-C(18)-C(17)	120.4(2)
C(20)-C(19)-C(18)	120.4(3)
C(19)-C(20)-C(21)	120.2(2)
C(20)-C(21)-C(22)	119.6(2)
C(17)-C(22)-C(21)	120.8(2)
C(24)-C(23)-P(1)	116.06(17)
C(23)-C(24)-C(25)	112.5(2)
C(26)-C(25)-C(24)	114.6(2)
C(6)-C(14)-C(15)	112.6(3)
C(6)-C(14)-C(16)	109.9(3)
C(15)-C(14)-C(16)	109.8(3)

Table 4–4. Bond lengths [Å] and angles [deg] for *syn*-C_2-**103^S-3**

Fe(1)-C(10)	2.048(3)	C(8)-C(9)	1.411(5)
Fe(1)-C(4)	2.051(3)	C(8)-H(8)	1.0000
Fe(1)-C(9)	2.054(3)	C(9)-C(10)	1.411(5)
Fe(1)-C(5)	2.057(3)	C(11)-C(12)	1.526(4)
Fe(1)-C(3)	2.061(3)	C(11)-C(13)	1.529(5)
Fe(1)-C(8)	2.069(3)	C(14)-C(16)	1.516(4)
Fe(1)-C(1)	2.069(3)	C(14)-C(15)	1.540(4)
Fe(1)-C(6)	2.079(3)	C(17)-C(22)	1.387(4)
Fe(1)-C(2)	2.104(3)	C(17)-C(18)	1.388(4)
Fe(1)-C(7)	2.113(3)	C(18)-C(19)	1.393(5)
Fe(1')-C(10')	2.044(3)	C(18)-H(18)	0.9500
Fe(1')-C(9')	2.048(3)	C(19)-C(20)	1.373(6)
Fe(1')-C(5')	2.059(3)	C(20)-C(21)	1.382(5)
Fe(1')-C(4')	2.060(3)	C(21)-C(22)	1.382(5)
Fe(1')-C(3')	2.065(3)	C(1')-C(5')	1.435(4)
Fe(1')-C(1')	2.065(3)	C(10)-Fe(1)-C(4)	106.95(13)
Fe(1')-C(8')	2.068(3)	C(10)-Fe(1)-C(9)	40.25(13)
Fe(1')-C(6')	2.085(3)	C(4)-Fe(1)-C(9)	104.04(13)
Fe(1')-C(2')	2.092(3)	C(10)-Fe(1)-C(5)	110.96(13)
Fe(1')-C(7')	2.118(3)	C(4)-Fe(1)-C(5)	40.18(13)
S(1)-P(1)	1.9486(11)	C(9)-Fe(1)-C(5)	133.95(13)
S(1')-P(1')	1.9515(11)	C(10)-Fe(1)-C(3)	133.01(13)
P(1)-C(1')	1.802(3)	C(4)-Fe(1)-C(3)	39.98(13)
P(1)-C(6)	1.823(3)	C(9)-Fe(1)-C(3)	104.89(13)
P(1)-C(17)	1.833(3)	C(5)-Fe(1)-C(3)	67.43(13)
P(1')-C(1)	1.793(3)	C(10)-Fe(1)-C(8)	67.47(13)
P(1')-C(6')	1.815(3)	C(4)-Fe(1)-C(8)	132.24(13)
P(1')-C(17')	1.835(3)	C(9)-Fe(1)-C(8)	40.03(13)
C(1)-C(5)	1.439(4)	C(5)-Fe(1)-C(8)	172.20(13)
C(1)-C(2)	1.451(4)	C(3)-Fe(1)-C(8)	107.68(13)
C(2)-C(3)	1.421(5)	C(10)-Fe(1)-C(1)	142.67(13)
C(2)-C(11)	1.508(5)	C(4)-Fe(1)-C(1)	68.07(13)
C(3)-C(4)	1.406(5)	C(9)-Fe(1)-C(1)	171.79(12)
C(4)-C(5)	1.411(5)	C(5)-Fe(1)-C(1)	40.82(12)
C(6)-C(10)	1.447(4)	C(3)-Fe(1)-C(1)	67.74(12)
C(6)-C(7)	1.452(4)	C(8)-Fe(1)-C(1)	144.21(13)
C(7)-C(8)	1.421(4)	C(10)-Fe(1)-C(6)	41.05(12)
C(7)-C(14)	1.509(4)	C(4)-Fe(1)-C(6)	139.47(13)

C(9)-Fe(1)-C(6)	68.23(12)	C(3')-Fe(1')-C(8')	106.77(14)
C(5)-Fe(1)-C(6)	116.63(12)	C(1')-Fe(1')-C(8')	145.07(13)
C(3)-Fe(1)-C(6)	173.10(12)	C(10')-Fe(1')-C(6')	40.88(12)
C(8)-Fe(1)-C(6)	67.64(12)	C(9')-Fe(1')-C(6')	67.97(13)
C(1)-Fe(1)-C(6)	119.08(11)	C(5')-Fe(1')-C(6')	117.73(12)
C(10)-Fe(1)-C(2)	172.89(12)	C(4')-Fe(1')-C(6')	140.42(13)
C(4)-Fe(1)-C(2)	67.51(13)	C(3')-Fe(1')-C(6')	172.57(12)
C(9)-Fe(1)-C(2)	135.24(13)	C(1')-Fe(1')-C(6')	119.53(12)
C(5)-Fe(1)-C(2)	68.04(13)	C(8')-Fe(1')-C(6')	67.42(12)
C(3)-Fe(1)-C(2)	39.88(13)	C(10')-Fe(1')-C(2')	173.63(13)
C(8)-Fe(1)-C(2)	112.49(13)	C(9')-Fe(1')-C(2')	135.63(14)
C(1)-Fe(1)-C(2)	40.67(12)	C(5')-Fe(1')-C(2')	68.19(13)
C(6)-Fe(1)-C(2)	145.99(12)	C(4')-Fe(1')-C(2')	67.79(13)
C(10)-Fe(1)-C(7)	68.05(12)	C(3')-Fe(1')-C(2')	40.31(13)
C(4)-Fe(1)-C(7)	171.28(13)	C(1')-Fe(1')-C(2')	40.77(12)
C(9)-Fe(1)-C(7)	67.45(12)	C(8')-Fe(1')-C(2')	112.36(13)
C(5)-Fe(1)-C(7)	147.65(12)	C(6')-Fe(1')-C(2')	145.38(12)
C(3)-Fe(1)-C(7)	138.41(13)	C(10')-Fe(1')-C(7')	67.86(13)
C(8)-Fe(1)-C(7)	39.70(12)	C(9')-Fe(1')-C(7')	67.38(13)
C(1)-Fe(1)-C(7)	120.34(12)	C(5')-Fe(1')-C(7')	148.97(12)
C(6)-Fe(1)-C(7)	40.53(12)	C(4')-Fe(1')-C(7')	170.36(13)
C(2)-Fe(1)-C(7)	116.81(12)	C(3')-Fe(1')-C(7')	137.42(13)
C(10')-Fe(1')-C(9')	40.12(14)	C(1')-Fe(1')-C(7')	121.15(12)
C(10')-Fe(1')-C(5')	111.03(14)	C(8')-Fe(1')-C(7')	39.73(12)
C(9')-Fe(1')-C(5')	133.03(14)	C(6')-Fe(1')-C(7')	40.35(11)
C(10')-Fe(1')-C(4')	107.34(14)	C(2')-Fe(1')-C(7')	116.28(12)
C(9')-Fe(1')-C(4')	103.43(15)	C(1')-P(1)-C(6)	109.15(14)
C(5')-Fe(1')-C(4')	40.01(13)	C(1')-P(1)-C(17)	103.33(14)
C(10')-Fe(1')-C(3')	133.34(13)	C(6)-P(1)-C(17)	100.99(14)
C(9')-Fe(1')-C(3')	104.61(14)	C(1')-P(1)-S(1)	113.32(11)
C(5')-Fe(1')-C(3')	67.38(13)	C(6)-P(1)-S(1)	117.09(11)
C(4')-Fe(1')-C(3')	39.94(14)	C(17)-P(1)-S(1)	111.42(11)
C(10')-Fe(1')-C(1')	142.33(13)	C(1)-P(1')-C(6')	108.72(14)
C(9')-Fe(1')-C(1')	171.21(14)	C(1)-P(1')-C(17')	103.26(14)
C(5')-Fe(1')-C(1')	40.72(12)	C(6')-P(1')-C(17')	98.91(13)
C(4')-Fe(1')-C(1')	67.92(13)	C(1)-P(1')-S(1')	114.36(11)
C(3')-Fe(1')-C(1')	67.90(13)	C(6')-P(1')-S(1')	118.18(10)
C(10')-Fe(1')-C(8')	67.32(14)	C(17')-P(1')-S(1')	111.36(11)
C(9')-Fe(1')-C(8')	40.00(14)	C(5)-C(1)-C(2)	107.4(3)
C(5')-Fe(1')-C(8')	170.84(13)	C(5)-C(1)-P(1')	124.9(2)
C(4')-Fe(1')-C(8')	131.07(14)	C(2)-C(1)-P(1')	127.3(2)

C(5)-C(1)-Fe(1)	69.11(17)	C(12)-C(11)-C(13)	108.9(3)
C(2)-C(1)-Fe(1)	70.96(17)	C(7)-C(14)-C(16)	112.8(3)
P(1')-C(1)-Fe(1)	131.09(16)	C(7)-C(14)-C(15)	109.6(3)
C(3)-C(2)-C(1)	106.6(3)	C(16)-C(14)-C(15)	108.8(3)
C(3)-C(2)-C(11)	124.7(3)	C(22)-C(17)-C(18)	118.9(3)
C(1)-C(2)-C(11)	128.3(3)	C(22)-C(17)-P(1)	121.2(2)
C(3)-C(2)-Fe(1)	68.43(18)	C(18)-C(17)-P(1)	119.8(2)
C(1)-C(2)-Fe(1)	68.37(17)	C(17)-C(18)-C(19)	120.2(3)
C(11)-C(2)-Fe(1)	133.9(2)	C(20)-C(19)-C(18)	120.2(3)
C(4)-C(3)-C(2)	109.5(3)	C(19)-C(20)-C(21)	119.7(3)
C(4)-C(3)-Fe(1)	69.61(18)	C(22)-C(21)-C(20)	120.3(3)
C(2)-C(3)-Fe(1)	71.69(17)	C(21)-C(22)-C(17)	120.5(3)
C(3)-C(4)-C(5)	108.5(3)	C(5')-C(1')-C(2')	107.6(3)
C(3)-C(4)-Fe(1)	70.40(18)	C(5')-C(1')-P(1)	125.6(2)
C(5)-C(4)-Fe(1)	70.12(17)	C(2')-C(1')-P(1)	126.6(2)
C(4)-C(5)-C(1)	108.0(3)	C(5')-C(1')-Fe(1')	69.41(18)
C(4)-C(5)-Fe(1)	69.70(18)	C(2')-C(1')-Fe(1')	70.62(17)
C(1)-C(5)-Fe(1)	70.06(17)	P(1)-C(1')-Fe(1')	128.89(16)
C(10)-C(6)-C(7)	106.8(3)	C(3')-C(2')-C(1')	106.4(3)
C(10)-C(6)-P(1)	123.2(2)	C(3')-C(2')-C(11')	124.1(3)
C(7)-C(6)-P(1)	127.2(2)	C(1')-C(2')-C(11')	128.9(3)
C(10)-C(6)-Fe(1)	68.29(17)	C(3')-C(2')-Fe(1')	68.81(18)
C(7)-C(6)-Fe(1)	70.97(16)	C(1')-C(2')-Fe(1')	68.61(17)
P(1)-C(6)-Fe(1)	140.26(16)	C(11')-C(2')-Fe(1')	134.3(2)
C(8)-C(7)-C(6)	107.0(3)	C(4')-C(3')-C(2')	109.2(3)
C(8)-C(7)-C(14)	123.9(3)	C(4')-C(3')-Fe(1')	69.85(19)
C(6)-C(7)-C(14)	128.6(3)	C(2')-C(3')-Fe(1')	70.88(18)
C(8)-C(7)-Fe(1)	68.49(17)	Fe(1')-C(3')-H(3')	125.4
C(6)-C(7)-Fe(1)	68.50(16)	C(3')-C(4')-C(5')	108.5(3)
C(14)-C(7)-Fe(1)	134.8(2)	C(3')-C(4')-Fe(1')	70.2(2)
C(9)-C(8)-C(7)	109.6(3)	C(5')-C(4')-Fe(1')	69.96(19)
C(9)-C(8)-Fe(1)	69.42(18)	C(4')-C(5')-C(1')	108.3(3)
C(7)-C(8)-Fe(1)	71.81(17)	C(4')-C(5')-Fe(1')	70.03(19)
C(10)-C(9)-C(8)	108.2(3)	C(1')-C(5')-Fe(1')	69.88(18)
C(10)-C(9)-Fe(1)	69.62(18)	C(10')-C(6')-C(7')	106.9(3)
C(8)-C(9)-Fe(1)	70.55(18)	C(10')-C(6')-P(1')	121.6(2)
C(9)-C(10)-C(6)	108.4(3)	C(7')-C(6')-P(1')	128.3(2)
C(9)-C(10)-Fe(1)	70.13(19)	C(10')-C(6')-Fe(1')	68.04(18)
C(6)-C(10)-Fe(1)	70.66(17)	C(7')-C(6')-Fe(1')	71.06(17)
C(2)-C(11)-C(12)	112.4(3)	P(1')-C(6')-Fe(1')	141.37(16)
C(2)-C(11)-C(13)	109.3(3)	C(8')-C(7')-C(6')	106.7(3)

C(8')-C(7')-C(14')	124.4(3)
C(6')-C(7')-C(14')	128.1(3)
C(8')-C(7')-Fe(1')	68.24(19)
C(6')-C(7')-Fe(1')	68.59(17)
C(14')-C(7')-Fe(1')	135.9(2)
C(9')-C(8')-C(7')	109.5(3)
C(9')-C(8')-Fe(1')	69.25(19)
C(7')-C(8')-Fe(1')	72.03(18)
C(10')-C(9')-C(8')	108.3(3)
C(10')-C(9')-Fe(1')	69.77(18)
C(8')-C(9')-Fe(1')	70.75(19)
C(9')-C(10')-C(6')	108.5(3)
C(9')-C(10')-Fe(1')	70.10(19)
C(6')-C(10')-Fe(1')	71.08(17)
C(2')-C(11')-C(12')	112.3(3)
C(2')-C(11')-C(13')	109.2(3)
C(12')-C(11')-C(13')	109.2(3)
C(7')-C(14')-C(16')	113.5(3)
C(7')-C(14')-C(15')	108.7(3)
C(16')-C(14')-C(15')	108.7(3)
C(18')-C(17')-C(22')	118.8(3)
C(18')-C(17')-P(1')	120.2(2)
C(22')-C(17')-P(1')	120.9(2)
C(17')-C(18')-C(19')	120.5(3)
C(20')-C(19')-C(18')	120.3(4)
C(19')-C(20')-C(21')	120.2(3)
C(20')-C(21')-C(22')	120.1(3)
C(21')-C(22')-C(17')	120.1(3)
Cl(2S)-C(1S)-Cl(1S)	111.4(3)
Cl(4S)-C(2S)-Cl(3S)	110.5(3)

REFERENCES

1. MacDiarmid, A. G. *Angew. Chem., Int. Ed.* **2001**, *40*, 2581–2590.
2. Mayes, A. G.; Whitcombe, M. J. *Adv. Drug Deliv. Rev.* **2005**, *57*, 1742–1778.
3. Galli, P.; Haylock, J. C. *Prog. Polym. Sci.* **1991**, *16*, 443–462.
4. Bellas, V.; Rehahn, M. *Angew. Chem., Int. Ed.* **2007**, *46*, 5082–5104.
5. Eloi, J. C.; Chabanne, L.; Whittell, G. R.; Manners, I. *Mater. Today* **2008**, *11*, 28–36.
6. Chan, W. Y.; Clendenning, S. B.; Berenbaum, A.; Lough, A. J.; Aouba, S.; Ruda, H. E.; Manners, I. *J. Am. Chem. Soc.* **2005**, *127*, 1765–1772.
7. Masson, G.; Beyer, P.; Cyr, P. W.; Lougv, A. J.; Manners, L. *Macromolecules* **2006**, *39*, 3720–3730.
8. Schachner, J. A.; Tockner, S.; Lund, C. L.; Quail, J. W.; Rehahn, M.; Müller, J. *Organometallics* **2007**, *26*, 4658–4662.
9. Herbert, D. E.; Gilroy, J. B.; Chan, W. Y.; Chabanne, L.; Staubitz, A.; Lough, A. J.; Manners, I. *J. Am. Chem. Soc.* **2009**, *131*, 14958–14968.
10. Whittell, G. R.; Manners, I. *Adv. Mater.* **2007**, *19*, 3439–3468.
11. Herbert, D. E.; Mayer, U. F. J.; Manners, I. *Angew. Chem., Int. Ed.* **2007**, *46*, 5060–5081.
12. Elschenbroich, C.; Hurley, J.; Metz, B.; Massa, W.; Baum, G. *Organometallics* **1990**, *9*, 889–897.
13. Braunschweig, H.; Breher, F.; Capper, S.; Dück, K.; Fuß, M.; Jimenez-Halla, J. O. C.; Krummenacher, I.; Kupfer, T.; Nied, D.; Radacki, K. *Chem. Eur. J.* **2013**, *19*, 270–281.
14. Braunschweig, H.; Friedrich, M.; Kupfer, T.; Radacki, K. *Chem. Commun.* **2011**, *47*, 3998–4000.
15. Braunschweig, H.; Kupfer, T.; Radacki, K. *Angew. Chem., Int. Ed.* **2007**, *46*, 1630–1633.

16. Tamm, M.; Kunst, A.; Bannenberg, T.; Herdtweck, E.; Sirsch, P.; Elsevier, C. J.; Ernsting, J. M. *Angew. Chem., Int. Ed.* **2004**, *43*, 5530–5534.

17. Elschenbroich, C.; Paganelli, F.; Nowotny, M.; Neumüller, B.; Burghaus, O. *Z. Anorg. Allg. Chem.* **2004**, *630*, 1599–1606.

18. Rinehart, K. L.; Curby, R. J. *J. Am. Chem. Soc.* **1957**, *79*, 3290–3291.

19. Rinehart, K. L.; Frerichs, A. K.; Kittle, P. A.; Westman, L. F.; Gustafson, D. H.; Pruett, R. L.; McMahon, J. E. *J. Am. Chem. Soc.* **1960**, *82*, 4111–4112.

20. Osborne, A. G.; Whiteley, R. H. *J. Organomet. Chem.* **1975**, *101*, C27–C28.

21. Bhattacharjee, H.; Müller, J. *Coord. Chem. Rev.* **2016**, *314*, 114–133.

22. Withers, H. P.; Seyferth, D.; Fellmann, J. D.; Garrou, P. E.; Martin, S. *Organometallics* **1982**, *1*, 1283–1288.

23. Seyferth, D.; Withers, H. P. *Organometallics* **1982**, *1*, 1275–1282.

24. Brunner, H.; Klankkermayer, J.; Zabel, M. *J. Organomet. Chem.* **2000**, *601*, 211–219.

25. Herberhold, M.; Hertel, F.; Milius, W.; Wrackmeyer, B. *J. Organomet. Chem.* **1999**, *582*, 352–357.

26. Herberhold, M. *Angew. Chem., Int. Ed.* **1995**, *34*, 1837–1839.

27. Bellas, V.; Rehahn, M. *Angew. Chem., Int. Ed.* **2007**, *46*, 5082–5104.

28. Musgrave, R. a.; Russell, A. D.; Manners, I. *Organometallics* **2013**, *32*, 5654–5667.

29. Fischer, A. B.; Kinney, J. B.; Staley, R. H.; Wrighton, M. S. *J. Am. Chem. Soc.* **1979**, *101*, 6501–6506.

30. Blake, A. J.; Mayers, F. R.; Osborne, A. G.; Rosseinsky, D. R. *Dalton Trans.* **1982**, *12*, 2379–2383.

31. Berenbaum, A.; Braunschweig, H.; Dirk, R.; Englert, U.; Green, J. C.; Jäkle, F.; Lough,

A. J.; Manners, I. *J. Am. Chem. Soc.* **2000**, *122*, 5765–5774.

32. Butler, I. R.; Cuilen, W. R.; Frederick, W. B.; Willis, A. J.; Rettig, S. J. *Organometallics* **1983**, *1*, 128–135.

33. Tanimoto, Y.; Ishizu, Y.; Kubo, K.; Miyoshi, K.; Mizuta, T. *J. Organomet. Chem.* **2012**, *713*, 80–88.

34. Arimoto, F. S.; Haven, A. C. *J. Am. Chem. Soc.* **1955**, *77*, 6295–6297.

35. Foucher, D. A.; Tang, B.-Z.; Manners, I. *J. Am. Chem. Soc.* **1992**, *114*, 6246–6248.

36. Rulkens, R.; Ni, Y.; Manners, I. *J. Am. Chem. Soc.* **1994**, *116*, 12121–12122.

37. Honeyman, C. H.; Foucher, D. A.; Dahmen, F. Y.; Rulkens, R.; Lough, A. J.; Manners, I. *Organometallics* **1995**, *14*, 5503–5512.

38. Peckham, T. J.; Massey, J. A.; Honeyman, C. H.; Manners, I. *Macromolecules* **1999**, *32*, 2830–2837.

39. Patra, S. K.; Whittell, G. R.; Nagiah, S.; Ho, C. L.; Wong, W. Y.; Manners, I. *Chem. Eur. J.* **2010**, *16*, 3240–3250.

40. Bagh, B.; Gilroy, J. B.; Staubitz, A.; Müller, J. *J. Am. Chem. Soc.* **2010**, *132*, 1794–1795.

41. Bagh, B.; Schatte, G.; Green, J. C.; Müller, J. *J. Am. Chem. Soc.* **2012**, *134*, 7924–7936.

42. Honeyman, C. H.; Peckham, T. J.; Massey, J. A.; Manners, I. *Chem. Commun.* **1996**, 2589–2590.

43. Monti, C.; Gennari, C.; Steele, R. M.; Piarulli, U. *Eur. J. Org. Chem.* **2004**, 3557–3565.

44. Bates, J. I.; Dugal-Tessier, J.; Gates, D. P. *Dalton Trans.* **2010**, *39*, 3151–3159.

45. Dutartre, M.; Bayardon, J.; Jugé, S. *Chem. Soc. Rev.* **2016**, *45*, 5771–5794.

46. Noonan, K. J. T.; Gillon, B. H.; Cappello, V.; Gates, D. P. *J. Am. Chem. Soc.* **2008**, *130*, 12876–12877.

47. Soto, A. P.; Manners, I. *Macromolecules* **2009**, *42*, 40–42.

48. Mark, J. E.; Allcock, H. R.; West, R. *Inorganic Polymers, Second Edition*; 2005.

49. Baumgartner, T.; Réau, R. *Chem. Rev.* **2006**, *106*, 4681–4727.

50. Monge, S.; Canniccioni, B.; Graillot, A.; Robin, J.-J. *Biomacromolecules* **2011**, *12*, 1973–1982.

51. Khozeimeh Sarbisheh, E.; Esteban Flores, J.; Zhu, J.; Müller, J. *Chem. Eur. J.* **2016**, *22*, 16838–16849.

52. Peckham, T. J.; Lough, A. J.; Manners, I. *Organometallics* **1999**, *18*, 1030–1040.

53. Mizuta, T.; Onishi, M.; Miyoshi, K. *Organometallics* **2000**, *19*, 5005–5009.

54. Resendes, R.; Nelson, J. M.; Fischer, A.; Jäkle, F.; Bartole, A.; Lough, A. J.; Manners, I. *J. Am. Chem. Soc.* **2001**, *123*, 2116–2126.

55. Mizuta, T.; Imamura, Y.; Miyoshi, K. *J. Am. Chem. Soc.* **2003**, *125*, 2068–2069.

56. Cao, L.; Manners, I.; Winnik, M. A. *Macromolecules* **2001**, *34*, 3353–3360.

57. Paquet, C.; Cyr, P. W.; Kumacheva, E.; Manners, I. *Chem. Commun.* **2004**, *2*, 234–235.

58. Paquet, C.; Cyr, P. W.; Kumacheva, E.; Manners, I. *Chem. Mater.* **2004**, *16*, 5205–5211.

59. Massey, J. A.; Winnik, M. A.; Manners, I.; Chan, V. Z.-H.; Ostermann, J. M.; Enchelmaier, R.; Spatz, J. P.; Möller, M. *J. Am. Chem. Soc.* **2001**, *123*, 3147–3148.

60. MacLachlan, M. J.; Ginzburg, M.; Coombs, N.; Coyle, T. W.; Raju, N. P.; Greedan, J. E.; Ozin, G. A.; Manners, I. *Science* **2000**, *287*, 1460–1463.

61. Osborne, A. G.; Whiteley, R. H.; Meads, R. E. *J. Organomet. Chem.* **1980**, *193*, 345–357.

62. Seyferth, D.; Withers, H. P. *J. Organomet. Chem.* **1980**, *185*, C1–C5.

63. Khozeimeh Sarbisheh, E.; Green, J. C.; Müller, J. *Organometallics* **2014**, *33*, 3508–3513.

64. Sadeh, S. ; Ph.D. Thesis, University of Saskatchewan, 2014.

65. Allcock, H. R.; Lavin, K. D.; Riding, G. H.; Suszko, P. R.; Whittle, R. R. *J. Am. Chem. Soc.* **1984**, *106*, 2337–2347.

66. Moser, C.; Belaj, F.; Pietschnig, R. *Chem. Eur. J.* **2009**, *15*, 12589–12591.

67. Maeno, Y.; Ishizu, Y.; Kubo, K.; Kume, S.; Mizuta, T. *Dalton Trans.* **2016**, *2*, 19034–19044.

68. Dey, S.; Sun, W.; Müller, J. *Inorg. Chem.* **2016**, *55*, 3630–3639.

69. Höcher, T.; Cinquantini, A.; Zanello, P.; Hey-Hawkins, E. *Polyhedron* **2005**, *24*, 1340–1346.

70. Moser, C.; Belaj, F.; Pietschnig, R. *Phosphorus, Sulfur Silicon Relat. Elem.* **2015**, *190*, 837–844.

71. Kargin, D.; Kelemen, Z.; Krekic, K.; Maurer, M.; Bruhn, C.; Nyulaszi, L.; Pietschnig, R. *Dalton Trans.* **2016**, *45*, 2180–2189.

72. Voituriez, A.; Panossian, A.; Fleury-Brégeot, N.; Retailleau, P.; Marinetti, A. *Adv. Synth. Catal.* **2009**, *351*, 1968–1976.

73. Fleury-Brégeot, N.; Panossian, A.; Chiaroni, A.; Marinetti, A. *Eur. J. Inorg. Chem.* **2007**, *2007*, 3853–3862.

74. Osborne, A. G.; Pain, H. M.; Hursthouse, M. B.; Mazid, M. A. *J. Organomet. Chem.* **1993**, *453*, 117–120.

75. Borucki, S.; Kelemen, Z.; Maurer, M.; Bruhn, C.; Nyulászi, L.; Pietschnig, R. *Chem. Eur. J.* **2017**, *23*, 10438–10450.

76. Mizuta, T.; Imamura, Y.; Miyoshi, K.; Yorimitsu, H.; Oshima, K. *Organometallics* **2005**, *24*, 990–996.

77. Evans, C. E. B.; Lough, A. J.; Grondey, H.; Manners, I. *New J. Chem.* **2000**, *24*, 447–453.

78. Schlogl, K. *Top. Stereochem.* **1967**, *1*, 39–91.

79. Blaser, H.-U.; Brieden, W.; Pugin, B.; Spindler, F.; Martin, S.; Togni, A. *Top. Catal.* **2002**, 3–16.

80. Hayashi, T.; Yamamoto, K.; Kumada, M. *Tetrahedron Lett.* **1974**, *15*, 4405–4408.

81. Hayashi, T. *Ferrocenes: Homogeneous Catalysis, Organic Synthesis, Materials Science*; Togni, A., Hayashi, T., Eds.; VCH: Weinheim, 1995.

82. Tang, W.; Zhang, X. *Chem. Rev.* **2003**, *103*, 3029–3069.

83. Gómez Arrayás, R.; Adrio, J.; Carretero, J. C. *Angew. Chem., Int. Ed.* **2006**, *45*, 7674–7715.

84. Togni, A.; Breutel, C.; Schnyder, A.; Spindler, F.; Landert, H.; Tijani, A. *J. Am. Chem. Soc.* **1994**, *116*, 4062–4066.

85. Spindler, F.; Malan, C.; Lotz, M.; Kesselgruber, M.; Pittelkow, U.; Rivas-Nass, A.; Briel, O.; Blaser, H.-U. *Tetrahedron: Asymmetry* **2004**, *15*, 2299–2306.

86. Ireland, T.; Tappe, K.; Grossheimann, G.; Knochel, P. *Chem. Eur. J.* **2002**, *8*, 843–852.

87. Sturm, T.; Weissensteiner, W.; Spindler, F. *Adv. Synth. Catal.* **2003**, *345*, 160–164.

88. Barbaro, P.; Togni, A. *Organometallics* **1995**, *14*, 3570–3573.

89. Cabrera, S.; Gómez Arrayás, R.; Carretero, J. C. *Angew. Chem., Int. Ed.* **2004**, *116*, 4034–4037.

90. Cabrera, S.; Arrayás, R. G.; Alonso, I.; Carretero, J. C. *J. Am. Chem. Soc.* **2005**, *127*, 17938–17947.

91. Lotz, M.; Polborn, K.; Knochel, P. *Angew. Chem., Int. Ed.* **2002**, *41*, 4708–4711.

92. Schwink, L.; Knochel, P. *Chem. Eur. J.* **1998**, *4*, 950–968.

93. Colacot, T. J. *Chem. Rev.* **2003**, *103*, 3101–3118.

94. Kang, J.; Lee, J. H.; Ahn, S. H.; Choi, J. S. *Tetrahedron Lett.* **1998**, *39*, 5523–5526.

95. Berens, U.; Burk, M. J.; Gerlach, A.; Hems, W. *Angew. Chem., Int. Ed.* **2000**, *39*, 1981–1984.

96. Marinetti, A.; Labrue, F.; Pons, B.; Jus, S.; Ricard, L.; Genêt, J.-P. *Eur. J. Inorg. Chem.* **2003**, 2583–2590.

97. Marinetti, A.; Labrue, F.; Genêt, J.-P. *Synlett* **1999**, 1975–1977.

98. Chen, W.; McCormack, P. J.; Mohammed, K.; Mbafor, W.; Roberts, S. M.; Whittall, J. *Angew. Chem., Int. Ed.* **2007**, *46*, 4141–4144.

99. Chen, W.; Spindler, F.; Pugin, B.; Nettekoven, U. *Angew. Chem., Int. Ed.* **2013**, *52*, 8652–8656.

100. Togni, A. *Angew. Chem., Int. Ed.* **1996**, *35*, 1475–1477.

101. Ikemoto, T.; Nagata, T.; Yamano, M.; Ito, T.; Mizuno, Y.; Tomimatsu, K. *Tetrahedron Lett.* **2004**, *45*, 7757–7760.

102. Kang, J.; Lee, J. H.; Im, K. S. *J. Mol. Catal. A Chem.* **2003**, *196*, 55–63.

103. Ireland, T.; Großheimann, G.; Wieser-Jeunesse, C.; Knochel, P. *Angew. Chem., Int. Ed.* **1999**, *111*, 3397–3400.

104. Maeno, Y.; Ishizu, Y.; Kubo, K.; Kume, S.; Mizuta, T. *Dalton Trans.* **2016**, *45*, 19034–19044.

105. Sadeh, S.; Schatte, G.; Müller, J. *Chem. Eur. J.* **2013**, *19*, 13408–13417.

106. Bhattacharjee, H.; Martell, J. D.; Khozeimeh Sarbisheh, E.; Sadeh, S.; Quail, J. W.; Müller, J. *Organometallics* **2016**, *35*, 2156–2164.

107. Sadeh, S.; Cao, M. P. T.; Wilson Quail, J.; Zhu, J.; Muller, J. *Under Rev.* **2018**.

108. Hierso, J. C. *Chem. Rev.* **2014**, *114*, 4838–4867.

109. Khozeimeh Sarbisheh, E.; Green, J. C.; Müller, J. *Organometallics* **2014**, *33*, 3508–3513.

110. Nurminen, E. J.; Mattinen, J. K.; Lönnberg, H. *J. Chem. Soc. Perkin Trans. 2* **1998**, *7*, 1621–1628.

111. Kolodiazhnyi, O. *Tetrahedron: Asymmetry* **1998**, *9*, 1279–1332.

112. Kolodiazhnyi, O. I.; Kolodiazhna, A. O. *Phosphorus, Sulfur Silicon Relat. Elem.* **2017**, *192*, 621–633.

113. Kolodiazhnyi, O. I.; Kolodiazhna, A. *Tetrahedron: Asymmetry* **2017**, *28*, 1651–1674.

114. Dement'ev, V. V; Cervantes-Lee, F.; Parkanyi, L.; Sharma, H.; Pannell, K. H.; Nguyen, M. T.; Diaz, A. *Organometallics* **1993**, *12*, 1983–1987.

115. Nelson, J. M.; Nguyen, P.; Petersen, R.; Rengel, H.; Macdonald, P. M.; Lough, A. J.; Manners, I.; Raju, N. P.; Greedan, J. E.; Barlow, S.; O'Hare, D. *Chem. Eur. J.* **1997**, *3*, 573–584.

116. Peterson, D. J. *J. Am. Chem. Soc.* **1971**, *93*, 4027–4031.

117. Meyer, N.; Seebach, D. *Chem. Ber.* **1980**, *113*, 1290–1303.

118. McGill, N. W. *Application of Quantitative Phosphorous Nuclear Magnetic Resonance Spectroscopy to Chemical Warfare Agents*; Internal Defence Science and Technology Organization Report, 2012.

119. Bates, R. B.; Kroposki, L. M.; Potter, D. E. *J. Org. Chem.* **1972**, *37*, 560–562.

120. Stanetty, P.; Mihovilovic, M. D. *J. Org. Chem.* **1997**, *62*, 1514–1515.

121. Schlosser, M. *Organometallics in synthesis: A manual*, Ed.; Wiley: London, 1994.

122. Chen, W.; Mbafor, W.; Roberts, S. M.; Whittall, J. *J. Am. Chem. Soc.* **2006**, *128*, 3922–3923.

123. Nie, H.; Yao, L.; Li, B.; Zhang, S.; Chen, W. *Organometallics* **2014**, 10–15.

124. Butler, I. R.; Cullen, W. R.; Kim, T.-J.; Rettig, S. J.; Trotter, J. *Organometallics* **1985**, *4*, 972–980.

125. Butler, I. R. *Eur. J. Inorg. Chem.* **2012**, *28*, 4387–4406.

126. Mizuta, T.; Aotani, T.; Imamura, Y.; Kubo, K.; Miyoshi, K. *Organometallics* **2008**, *27*, 2457–2463.

127. Khozeimeh Sarbisheh, E.; Bhattacharjee, H.; Cao, M. P. T.; Zhu, J.; Müller, J. *Organometallics* **2017**, *36*, 614–621.

128. Mizuta, T.; Imamura, Y.; Miyoshi, K.; Yorimitsu, H.; Oshima, K. *Organometallics* **2005**, *24*, 990–996.

129. Schachner, J. A.; Lund, C. L.; Burgess, I. J.; Quail, J. W.; Schatte, G.; Müller, J. *Organometallics* **2008**, *27*, 4703–4710.

130. Lund, C. L.; Schachner, A.; Burgess, I. J.; Quail, J. W.; Schatte, G.; Müller, J. *Inorg. Chem.* **2008**, *47*, 5992–6000.

131. Mizuta, T.; Aotani, T.; Imamura, Y.; Kubo, K. *Organometallics* **2008**, *23*, 2457–2463.

132. Herbert, D. E.; Mayer, U. F. J.; Gilrov, J. B.; López-Gómez, M. J.; Lough, A. J.; Charmant, J. P. H.; Manners, I. *Chem. Eur. J.* **2009**, *15*, 12234–12246.

133. Kenny, N. P.; Rajendran, K. V; Gilheany, D. G. *Chem. Commun.* **2015**, *51*, 16561–16564.

134. Oms, O.; Bideau, J. Le; Vioux, A.; Leclercq, D. *J. Organomet. Chem.* **2005**, *690*, 363–370.

135. Petneházy, I.; Jászay, Z. M.; Szabó, A.; Everaert, K. *Synth. Commun.* **2003**, *33*, 1665–1674.

136. Colle, K. S.; Lewis, E. S. *J. Org. Chem.* **1978**, *43*, 571–574.

137. Corey, E. J.; Bakshi, R. K.; Shibata, S.; Chen, C. P.; Singh, V. K. *J. Am. Chem. Soc.* **1987**,

109, 7925–7926.

138. Gautier, F.-M.; Jones, S.; Martin, S. J. *Org. Biomol. Chem.* **2009**, *7*, 229–231.

139. Gibson, C. L. *Tetrahedron: Asymmetry* **1999**, *10*, 1551–1561.

140. Corey, E. J.; Bakshi, R. K.; Shibata, S.; Chen, C. P.; Singh, V. K. *J. Am. Chem. Soc.* **1987**, *109*, 7925–7926.

141. Mathre, D. J.; Jones, T. K.; Xavier, L. C.; Blacklock, T. J.; Reamer, R. A.; Mohan, J. J.; Jones, E. T. T.; Hoogsteen, K.; Baum, M. W.; Grabowski, E. J. J. *J. Org. Chem.* **1991**, *56*, 751–762.